INVESTIGATIONS ON TWO-LEVEL MASER OSCILLATIONS

Ian Mason Firth

A Thesis Submitted for the Degree of PhD
at the
University of St Andrews

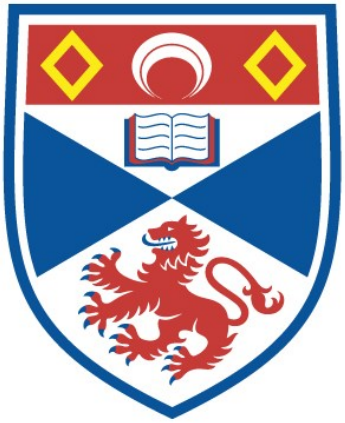

1962

INVESTIGATIONS ON TWO-LEVEL MASER OSCILLATIONS

A Thesis

presented by

Ian Mason Firth, B.Sc.

to the

University of St. Andrews

in application for the Degree

of Doctor of Philosophy

ProQuest LLC.
789 East Eisenhower Parkway
P.O. Box 1346
Ann Arbor, MI 48106 – 1346

Th 5054

DECLARATION

I hereby declare that the following Thesis is based on the results of experiments carried out by me, that the Thesis is my own composition, and that it has not previously been presented for a Higher Degree.

CERTIFICATE

I certify that Ian Mason Firth, B.Sc., has spent nine terms as a research student in the Physical Laboratory of the United College of St. Salvator and St. Leonard in the University of St. Andrews, that he has fulfilled the conditions of Ordinance No. 16 of the University Court of St. Andrews and that he is qualified to submit the accompanying Thesis in application for the Degree of Doctor of Philosophy.

Research Supervisor

CAREER

I matriculated in the United College of St. Salvator and St. Leonard in the University of St. Andrews in October 1955 and followed a course leading to graduation in 1959 with the degree of Bachelor of Science with Second Class Honours in Natural Philosophy. In October 1959, I was admitted by the Senatus Academicus of the University of St. Andrews as a research student in the Department of Natural Philosophy in the same College, since which time I have been engaged in the research which is the topic of this Thesis. I was appointed to the Madras College Postgraduate Scholarship in 1959, retaining this until my appointment as Assistant in the Department of Natural Philosophy in October 1961.

ACKNOWLEDGEMENTS

The author wishes to express his appreciation for the assistance and encouragement given by friends and colleagues. To Professor J.F. Allen he is especially indebted for the use of facilities in the experimental laboratory; to Dr. D. Bijl, he is grateful for critical supervision throughout the studies; to Messrs. J. McNab, T. Marshall and M. Bird, for excellent workmanship on the apparatus; to Mr. R. Mitchell for the necessary supply of liquid helium; to Mr. J. Gerrard for expert advice on many problems and for the preparation of the photographs contained in this Thesis; to Mr. H. Cairns for the loan of many items of equipment and advice on electronic problems; and to Mr. A.W.O. Firth for many stimulating discussions on the problems of analogue computation. Discussions with Dr. C.K. Campbell in the initial stages of this work were of great value, and subsequently, discussions with members of the School of Natural Philosophy, especially those with Professor R.B. Dingle and Dr. C.G. Kuper, are much appreciated. The Award of a Postgraduate Scholarship by the Trustees of the Madras College Endowment is gratefully acknowledged. Finally, the author wishes to thank Mrs. C. Evans for the expert typing of this Thesis.

C O N T E N T S

LIST OF ILLUSTRATIONS

LIST OF TABLES

CHAPTER 1

INTRODUCTION

1.1 Maser Amplifiers

The development of maser amplifiers and oscillators has been rapid since the first discussion by Weber (1953)[1] into the feasibility of maser action in an excited molecular system. Proposals for maser action in two-level molecular systems were made about the same time by Gordon, Zeiger and Townes (1954)[2] and by Basov and Prokhorov (1954)[3]. Bloembergen (1956)[4] introduced the 3-level maser scheme which, in the development of maser techniques, has been shown to be a more effective design than two-level maser proposals. Nevertheless, both two-level and 3-level masers have the advantage over conventional electronic devices that, amplification with a very much lower overall noise temperature is attained, and oscillation of coherent radiation with high spectral purity is obtained at reasonable powers. The most serious drawback is the small gain-bandwidth product and gain saturation in cavity masers.

The name maser, coined by Gordon et al[2], describes the main operation of the device and is an acronym for 'Microwave Amplification by Stimulated Emission of Radiation'. The word is now used very loosely and may be used to describe any device in which the strength of an electromagnetic field is increased by stimulated emission of radiation from a molecular system maintained in, or transiently placed in an excited state by some external means. Most solid state masers use

magnetic dipole transitions between spin states of a paramagnetic crystal, the splitting between the states being due largely to an applied magnetic field which may be augmented by a generally small crystalline electric field interaction acting through spin-orbit coupling.

In the case that only two energy levels of the molecular system are of importance, e.g. magnetic dipoles with $S = \frac{1}{2}$ only, maser action can be described in the following simple manner. Interaction between the molecular system and a radiation field occurs when the frequency of the field satisfies Planck's radiation condition,

$$\hbar\omega = (E_2 - E_1) \qquad 1.1$$

where E_2, E_1 $(E_2 > E_1)$ are the energies of the two levels. The interaction takes the form of absorption of energy for an upwards induced transition $E_1 \rightarrow E_2$, or emission by a downwards induced transition $E_2 \rightarrow E_1$, where the quantum mechanical transition probabilities are proportional to the populations of the lower and upper levels respectively A net absorption of energy occurs because the initial thermal equilibrium populations are governed by a Boltzmann distribution, so that the lower level is more densely populated. A net emissive state will occur when the populations are inverted from the equilibrium state; the level E_2 being more populated than the level E_1. Spontaneous emission has been neglected in this discussion, for in comparison the probability of a spontaneous transition occuring is very small at the micro-wave frequencies generally used in maser operation. The lower noise limit is generally considered to be set by spontaneous emission in the maser

amplifier, but in practice external thermal noise is the limiting factor.

Methods of activation used to obtain the requisite population inversion in the energy levels for maser action fall into three groups. Firstly, where the molecular system is gaseous, molecules in the upper level can be physically separated from a molecular beam of the gas and directed into a microwave structure: this method is used in the ammonia beam maser. However, where the molecular system is embedded in a solid the actual populations of the levels must be changed, for physical separation of the excited molecules is, of course, impossible: the other techniques pertain to this case. In the second type inversion may be accomplished by controlled application of a large pulse of radiant energy at the transition frequency (180° pulse technique) or by executing an adiabatic fast passage (A.F.P.) through the molecular transition. The third method makes use of another energy level as an intermediate step to inverting the populations of the two maser working levels: this method is used in the 3-level maser proposed by Bloembergen[4].

Amplification of the stimulating radiation field will generally occur after activation, but if the energy stored in the molecular system is sufficient to overcome the energy losses of the microwave structure in which the system is mounted, energy will be spontaneously released as microwave oscillations. These microwave oscillations are coherent because of the interaction of the molecular system and the microwave structure, and occur either by the stimulating influence of components

of external thermal noise close to the transition frequency, or by an avalanche of induced transitions caused by spontaneous emission from the system. Two-level maser oscillators can be operated either in a steady applied magnetic field at the resonance value, or in a magnetic field swept through the resonance value. In practice the latter type is the more common.

1.2 Two-Level Maser Oscillators

The work contained in this Thesis is concerned with the mode of oscillation of two-level, solid state, masers. It is interesting, therefore, to trace the history of such devices. Combrisson, Honig and Townes (1956)[5] performed the first two-level maser experiment utilising the favourable paramagnetic properties of donor electrons in crystalline silicon. Stimulated emission was observed but maser oscillations were not achieved, possibly because of the low spin density used in the experiment. The first successful two-level maser resulting in oscillation was performed by Feher et al (1958)[6] using phosphorous doped silicon (pure to 99.88%). Inversion was effected by A.F.P., oscillations being observed as the magnetic field was swept through the transition value at a later time. More sophisticated techniques developed by Chester, Wagner and Castle (1958)[7] allowed oscillations to be observed in the steady magnetic field case and also the swept case. These workers noted output powers up to a maximum of 80 mw from the maser material, colour centres in neutron-irradiated quartz. In this laboratory maser oscillations, in a swept magnetic field, were observed by Campbell[8] using F-centres in neutron-irradiated MgO.

These experiments have shown that useful amounts of microwave power, in pulsed form, can be generated in two-level masers and have further suggested that it should be possible to extract microwave energy at a frequency higher than the frequency of activation of the maser material. The question of the mechanism of oscillation of two-level masers was forcibly raised in these experiments, however, because it was found that oscillations were unexpectedly accompanied by periodic amplitude modulation of the output power.

The initial explanation of the phenomenon, given independently by Feher and Chester, was of interference between different spin packets within the paramagnetic resonance line. This tentative theory which, nevertheless, must contribute in some way to the amplitude modulation, has been superseded by another picture which takes into account the interaction of the spin system and the microwave structure. The interaction that exists can be described in terms of radiation damping effects due to the coupling between the spin system and its own radiation field within the cavity. In any description of the behaviour of a two-level maser oscillator an analysis of the steady-field type may be regarded as basic to an understanding of the more complex, but more usual, field-swept case.

1.3 Contents of Thesis

The work contained in this Thesis falls, naturally, into

two parts; theoretical studies and experimental studies on two-level maser oscillators, and will be presented in the following manner. The theory of paramagnetic resonance is discussed in Chapter 2 and points pertaining to maser operation are stressed: the classical explanation of paramagnetic resonance which leads to the well known Bloch equations, is discussed. In Chapter 3 the circuit relations for a two-level maser are developed and the problem of the oscillator is formulated in Chapter 4 on classical lines. The solutions of the resulting equations, obtained by an analogue computer, are presented. Various conclusions are reached from the solutions, i.e. on the interrelation of certain measurable variables, on the comparison of the solutions to observable data and on the validity of classical equations to describe maser action. The maser instrumentation is described in Chapter 5, and in Chapter 6, details are given of the paramagnetic material, neutron-irradiated MgO, used in the experimental studies. In Chapters 7 and 8, experimental results are considered, and concluding remarks, criticism and indications for future research are made in Chapter 9.

1.4 Units

The set of units that will be used consistently in this Thesis will be Gaussian. However, where it is essential to use MKS units this will be stated explicitly. A synopsis of Gaussian units is contained in Reitz and Milford, 'Foundations of Electro-magnetic Theory'[9], and reference is made to Von Hipple, 'Dielectrics and Waves'[10] in connection with MKS units.

CHAPTER 2

PARAMAGNETIC RESONANCE

2.1 Introduction

Of the four main types of magnetism found in matter, diamagnetism, paramagnetism, ferromagnetism and antiferromagnetism, only diamagnetism and paramagnetism are properties of the atom. The distinguishing feature of the latter is the occurrence of permanent magnetic dipoles originating in the electronic motion of the atom. As opposed to ferromagnetics, in which there is strong interaction, or co-operation between large groups of atoms with permanent magnetic dipoles, paramagnetism is a magnetic property of substances in which the magnetic dipoles are relatively independent of each other. With the advent of quantum theory the presence of atomic magnetic moments was properly ascribed to atoms which contained partially filled electron shells. The dipole magnetic fields of electronic orbital motion together with electronic spin can be described by a term $\mu_\beta \mathbf{H}' (\mathbf{L} + g\mathbf{S})$ in the Hamiltonian of the free atom, where $\mathbf{H}$ is the externally applied magnetic field and μ_β the Bohr magneton. The spectroscopic factor, or g-factor, is exactly 2.0023 for the free electron, but is usually taken as 2.0. Most atoms do not exhibit paramagnetism, for the orbital angular momentum is largely quenched, but the principle groups of elements whose ions are paramagnetic in the ground state are the transition elements and the rare earths.

One of the first complete treatments of static paramagnetism, by Van Vleck (1932)[11], placed the theory on a firm basis and is still of great importance in the field. The full theoretical treatment of paramagnetic resonance given by Bleaney and Stevens (1953)[12] is of fundamental importance and a subsequent report by Bowers and Owen (1955)[13], also of the Oxford Group, details magnetic properties of various compounds and lists paramagnetic resonance data. Further data has been compiled by Orton[14]. A work edited by Grivet[15], connects theory with experimental practice in spin resonance spectroscopy, while the recent text by Abragam[16], is very important in the field of nuclear magnetic resonance. The classic works of Bloch[17] and Bloembergen, Purcell and Pound[18], as well as the two French authors mentioned, are concerned with nuclear magnetic resonance (N.M.R.) but the treatments of spin dynamics and other related topics is similar to those in electron spin resonance (E.S.R.). In fact the circuit relationships in microwave circuits of E.S.R. are almost identical with those of rf structures in N.M.R. in so far as microwave circuits can be treated by lumped parameters.

2.2 General Properties of Interaction with a Radiation Field

In Chapter 1 the three independent radiative processes which make up the interaction between an atomic system of discrete energy levels with an electromagnetic field were cursorily introduced. The processes are, (a) induced absorption, (b) induced emission, and (c) spontaneous emission. The relative importance of these processes with

regard to maser action will be described.

The process of spontaneous emission can be likened to the decay of a radioactive substance where the decay probability is independent of factors outside the atom. The probability of finding an atom in an excited state in the absence of a radiation field decreases exponentially with a lifetime 1/W (Heitler[19]) where

$$W = \frac{\mu^2 \nu^3}{\hbar c^3}$$

At optical frequencies, $\nu = 10^{15}$ cs, $W = 10^8$ sec^{-1} but at microwave frequencies where the dipole moment μ is 137 times smaller than in the usual optical transitions, $W = 10^{-11}$ sec^{-1}. This latter figure must be altered [20] somewhat in taking into account the finite extent of the paramagnetic material and the possibility of induced emission caused by background thermal radiation. However, a more realistic probability is found to be $W = 10^{-5} - 10^{-3}$ sec^{-1} which is very small. As spontaneous emission is independent of circumstances outside the atom, radiation produced by this transition will be incoherent with respect to any incident radiation.

By a quantum statistical mechanical treatment of the energy density of 'black body' radiation, Einstein[21] showed that for a two-level atomic system the quantum mechanical probabilities of induced absorption and induced emission are equal. It is possible to infer from the analysis that energy absorbed or emitted as a result of induced transitions takes place coherently with the inducing radiation field.

The relation between the probability B_{12} of induced transitions and the probability A_{21} of spontaneous emission between two energy levels E_2, E_1 is given by

$$A_{21} = \frac{8\pi h\nu^3}{c^3} B_{12} \qquad 2.1$$

where exact expressions for the probabilities can be obtained from quantum mechanical treatments. Equation 2.1 shows the over-riding importance of induced transitions at microwave frequencies, $\nu = 10^{10}$ cs, for here

$$A_{21} = 10^{-27} B_{12}$$

The Einstein probabilities have been stressed to show that spontaneous (incoherent) emission at microwave frequencies is insignificantly small in comparison to coherent stimulated emission. By acting upon the Boltzmann distribution of spins in the levels in a spin-only system a net emissive state can be obtained if a surplus of unpaired spins is made to occur in the upper state E_2. Under certain circumstances coherent emission may be made proportional to the stimulating radiation field intensity resulting in linear amplifier operation.

2.3 Quantum Mechanical Treatment

Generally the energy levels of paramagnetic ions in solids depend in complicated ways upon the crystalline fields, spin-orbit coupling and interaction with other electrons and nuclei, and although these mechanisms are often unknown quantitively, the interaction can

be described in a simple way by the Spin Hamiltonian. By means of this Hamiltonian, the complicated structure of the lowest energy levels of an ion in a magnetic field, that group of levels between which transitions at microwave frequencies can be made, is related in a simple manner to parameters of observed spectra. The details of this treatment will not be discussed here, for this subject does not bear directly on the main work of this Thesis. One aspect of quantum mechanical treatments will, however, be discussed in the next section.

2.4 Equivalence of Quantum Mechanical and Classical Treatments

A basic problem in paramagnetic resonance is the behaviour of a free spin in a uniform magnetic field. Quantum mechanically this can be described by the equations of motion of the magnetic momentum operator $\underline{\mu}$ which, in the Heisenberg representation, are

$$(-\hbar/j)\, d\underline{\mu}/dt = [\mathcal{H}, \underline{\mu}] \qquad 2.2$$

where $\mathcal{H} = -\underline{\mu}.\underline{H}$ is the Hamiltonian of the magnetic interaction with the applied field $\underline{H}$ and $j = \sqrt{-1}$. Further, $\underline{\mu}$ is related to the spin operator $\hbar\,\underline{\sigma}/2$ by the ratio γ

$$\underline{\mu} = \gamma \hbar \underline{\sigma}/2$$

where γ is the electronic magnetogyric ratio. Equation 2.2 becomes

$$\begin{aligned} d\underline{\mu}/dt &= (-j/\hbar)(\gamma^2\hbar^2/4)\ [\underline{\sigma}.\underline{H}, \underline{\sigma}] \\ &= (-j/\hbar)(\gamma^2\hbar^2/4)\ (\underline{\sigma} \times \underline{H}) \qquad 2.3 \\ &= (-j/\hbar)(\gamma\hbar/2)\, 2j\, (\underline{\mu} \times \underline{H}) \\ &= \gamma\, (\underline{\mu} \times \underline{H}) \end{aligned}$$

by a well known commutation relationship.

In a system containing paramagnetic atoms or ions, all of which have the same magnetogyric ratio, a property of the system is that it can be characterized classically by a macroscopic magnetization $\underline{M}$. Corresponding to $\underline{M}$ the system has a macroscopic angular momentum $\underline{A}$ and between $\underline{M}$ and $\underline{A}$ there exists the same relation as between the magnetic moment and the spin angular momentum of individual atoms

$$\underline{M} = \gamma \underline{A}$$

The macroscopic behaviour of the system in an applied field can be described classically by the equation of motion, in a stationary co-ordinate system

$$d\underline{A}/dt = (\underline{M} \times \underline{H})$$

so that

$$d\underline{M}/dt = \gamma (\underline{M} \times \underline{H}) \qquad 2.4$$

This equation has the same form as the quantum mechanical equation, Equation 2.3.

This identity implies that the expectation value $\langle \underline{\mu} \rangle$ taken over the wave function of the free spin $\underline{\mu}$ also obeys the classical equation, so that the magnetization of a system of spins, N per unit volume, is given by

$$\underline{M} = N \langle \underline{\mu} \rangle$$

It has been stated by Rabi, Ramsey and Schwinger[22] that the behaviour of a paramagnetic quantum system may be equally described by classical equations.

In addition to the interaction with applied fields the spin system is subject, however, to relaxation mechanisms. Although these can be treated in detail by quantum mechanical methods it generally suffices to place additional terms in Equation 2.4. The macroscopic picture that has been presented in this section will be elaborated, and further theoretical discussions will use classical rather than quantum equations for a description of the behaviour of the spin magnetisation.

2.5 Relaxation Processes

The steady state solution of Equation 2.4 for a constant applied field H_o in the z direction, gives a Larmor precession of $\underline{M}$ about the z direction. In this simple case the orientation of the magnetic dipole is dependent only on the applied field, being quite independent either of any interaction with matter nearby, or of interaction among the individual spins of the system. It is necessary, therefore, to focus attention on these two interections in order to obtain a full description of the spin dynamics.

Considering a system of 'spin-only' magnetism, where the spin angular momentum $S = \frac{1}{2}$, there will be two states in an applied field, the energy separation of the levels being determined by Equation 1.1. The sudden application of a uniform field leads only to a Larmor precession about the field direction of all individual elemental dipoles which does not affect the initial equal distribution of the dipoles between the two levels. In this situation the spin system is

not in equilibrium with its surroundings, the spin populations of the levels being greatly unequal to the Boltzmann distribution at the temperature of the whole sample. For thermal equilibrium

$$N_2/N_1 = e^{-\Delta E/kT} = e^{-\hbar\omega_o/kT} \qquad 2.5$$

should hold, where N_2, N_1 are the number of spins in the upper and lower energy levels respectively and T is the temperature of the sample. In practice this distribution is established by energy exchange between the spin system and the remainder of the sample through the action of time varying electric fields caused by thermal molecular movement or crystalline lattice vibrations.

Although a single time constant does not always describe the trend of spins to equilibrium with the lattice, such a constant is usually introduced. In terms of the longitudinal magnetization M_z, where

$$M_z = \mu_\beta (N_1 - N_2) \quad (S = \tfrac{1}{2}) \qquad 2.6$$

thermal equilibrium is approached as

$$M_z = M_o (1 - e^{-t/T_1})$$

or expressed in differential form

$$dM_z/dt = -(M_z - M_o)/T_1 \qquad 2.7$$

T_1 is called the longitudinal, or more commonly the spin-lattice relaxation time and M_o is the thermal equilibrium value of M_z,

$$M_o = N \mu_\beta^2 \frac{H_o}{kT} \qquad 2.8$$

When $S = \frac{1}{2}$, for the usual case $kT \rangle \mu_\beta H_o$

There exists another type of relaxation process which affects the transverse magnetization. The thermal equilibrium state is one of maximum entropy so that no phase coherence can exist between elemental magnets in the plane transverse to the applied field H_o. Relaxation processes that tend to destroy the coherence of transverse moments act generally through spin-spin coupling so that energy is exchanged within the system although the total energy of the system need not depart from its equilibrium value. The process is often described by the equations

$$dM_{x,y}/dt = - M_{x,y}/T_2 \qquad 2.9$$

where again a single relaxation time T_2 is used to describe the decay. T_2 is called the transverse, or spin-spin relaxation time.

By adding Equations 2.7 and 2.9 to the right hand side of Equation 2.4 the behaviour of the spin system in the presence of an applied field, usually made up of steady and time varying components, and relaxation mechanisms is described. Equation 2.4 modified in this way forms the well known Bloch equations[17].

2.6 The Bloch Equations

In stationary co-ordinates the Bloch equations are

$$\dot{M}_x = -|\gamma|\,(M_y H_o - M_z H_y) - M_x/T_2 \qquad (a)$$

$$\dot{M}_y = |\gamma|\,(M_x H_o - M_z H_x) - M_y/T_2 \qquad (b) \qquad 2.10$$

$$\dot{M}_z = -|\gamma|\,(M_x H_y - M_y H_x) - (M_z - M_o)/T_1 \qquad (c)$$

and in complex notation where

$$M^+ = M_x + jM_y$$

$$H^+ = H_x + jH_y$$

Equation 2.10 becomes

$$\dot{M}^+ = +j\omega_o M^+ - j|\gamma| M_z H^+ - M^+/T_2$$

$$\dot{M}_z = -|\gamma|\ \mathrm{Im}\,(M^+ H^{+*}) - (M_z - M_o)/T_1$$

where $\gamma = -|\gamma|$ is the electronic magnetogyric ratio and the variables are expressed in Gaussian units. In order to excite transitions between the states of the system it is necessary to supply radiation with the magnetic vector circularly polarised in the transverse plane, rotating at or near the transitional frequency $\omega_o = |\gamma| H_o$. In practice the generation of linear magnetic fields, of the form

$$H_{rf} = 2H_1 \cos\omega t$$

is more usual but this field can be resolved into two counter-rotating fields

$$H_{rf} = H_1\, e^{j\omega t} + H_1\, e^{-j\omega t}$$

using complex notation. The resonance interaction is caused by the term $H_1\, e^{j\omega t}$ acting in synchronism with the precessing magnetization whereas the contra-rotating field $H_1\, e^{-j\omega t}$ acts as a small perturbing

term to the resonance and can be shown to have negligible effect[23].

It is convenient to express the Bloch equations in a co-ordinate system that is rotating with the synchronous component of the radiation field. The transformation

$$M^{+} = M' \, e^{+j\omega t}$$
$$H^{+} = H' \, e^{+j\omega t} \qquad 2.11$$

where

$$M' = M_u + jM_v$$
$$H' = H_u + jH_v$$

in the rotating frame, gives the Bloch equations as

$$\dot{M}' = -M' (1/T_2 - j\Delta\omega) - j|\gamma| M_z H'$$
$$\dot{M}_z = -|\gamma| \mathrm{Im} (M'^{*} H') - (M_z - M_o)/T_1 \qquad 2.12$$

$\Delta\omega = (\omega_o - \omega)$ and M'^{*} is the complex conjugate of M'. When the perturbing field H_{rf} is included, the equations become

$$\dot{M}_u = \Delta\omega M_v - M_u/T_2 \qquad (a)$$
$$\dot{M}_v = \Delta\omega M_u - \omega_1 M_z - M_v/T_2 \qquad (b) \qquad 2.13$$
$$\dot{M}_z = \omega_1 M_v - (M_z - M_o)/T_1 \qquad (c)$$

Solutions of Equations 2.13 are particularly useful in the steady state, e.g. slow passage or transient state, e.g. rapid passage. In the case of slow passage through the resonance value, the rate of change of H_o is small compared to T_1, T_2, and a time independent solution is

possible. Experimentally this is of importance in the search for, and measurement of, unknown spin transitions. With

$$\dot{M}_u = \dot{M}_v = \dot{M}_z = 0$$

the resulting components are

$$M_u = M_o \frac{\omega_1 T_2^2 \Delta\omega}{S + T_2^2 \Delta\omega^2} \qquad (a)$$

$$M_v = -M_o \frac{\omega_1 T_2}{S + T_2^2 \Delta\omega^2} \qquad (b) \qquad 2.14$$

$$M_z = M_o \frac{1 + T_2^2 \Delta\omega^2}{S + T_2^2 \Delta\omega^2} \qquad (c)$$

where $S = 1 + \omega_1^2 T_1 T_2$, $\omega_1 = |\gamma| H_1$: the term $\omega_1^2 T_1 T_2$ in S is called the saturation factor. The components of the magnetization in the stationary frame are, from Equation 2.11, functions of time, and can induce voltages in an electronic structure, usually a microwave cavity, at frequency ω. Hence, the motion of $\underline{M}$ during slow passage is detected experimentally by measuring the components M_u, M_v.

The power flow between the radiation field and the paramagnetic system per unit volume can be obtained from the total Zeeman energy of the system

$$W_z = -M_z H_o$$

The power flow is, therefore, from Equation 2.13

$$P = \dot{W}_z = -\dot{M}_z H_o$$

$$= - \omega \, {}_{o}H_1 M_v + H_o \, (M_z - M_o)/T_1 \qquad 2.15$$

where the first term represents the power absorbed from the rf field and the second, the power transferred to the lattice by T_1 mechanisms. In the steady state these terms are equal. The power absorbed by the spin system is

$$P_{spin} = - \omega \, {}_{o}H_1 M_v \qquad 2.16$$

$$= \frac{M_o H_o \omega_1 T_2}{S + T_2^2 \, \Delta\omega^2}$$

whence the name absorption is given to the component M_v. P_{spin} has its maximum at $\Delta\omega = 0$ and for large H_1, that is large saturation factor, P_{spin} grows to

$$(P_{spin})^{max} = M_o H_o / T_1$$

This expresses the maximum rate of transfer of energy from spins to the lattice through the mechanisms of T_1 and describes complete saturation of the system, i.e. the two levels of the spin system are equally populated. It should be noted, as will be shown later, that the signal available for detection is proportional to M_v and not to P, the absorbed power.

Equation 2.16 demonstrates the feasibility of maser action in an excited spin system. When M_o is negative, corresponding to an inversion of the spin populations of the two energy levels, P_{spin} is negative indicating that energy is released by the spin system. For weak signals, $S = 1$, the power emitted is proportional to the perturbing

power.

For negligible saturation, $S = 1$, M_v is

$$M_v = - M_o \frac{\omega_1 T_2}{1 + T_2^2 \Delta\omega^2}$$

This curve has a Lorentz shape, with width at half intensity

$$\Delta\omega_L = \frac{2}{T_2}$$

When saturation is considerable $\omega_1^2 T_1 T_2 \gg 1$, the shape of M_v is changed somewhat due to the influence of the high intensity perturbing field, the natural width being increased to

$$\Delta\omega_L = \frac{2}{T_2}\sqrt{1 + \omega_1^2 T_1 T_2}$$

$$= 2\omega_1 \sqrt{T_1/T_2} \qquad (\omega_1^2 T_1 T_2 \gg 1)$$

The increase is termed saturation broadening.

The value of M_v is maximum at resonance $\Delta\omega = 0$, being equal to

$$M_v^{max} = - M_o \frac{\omega_1 T_2}{S}$$

When $S = 1$, a linear relationship holds between M_v^{max} and H_1, but a maximum is reached at $S = 2$ followed by a decrease to zero as S becomes large. A similar discussion can be followed for the in phase component of the magnetization, M_u, called, in analogy to forced harmonic oscillations, the dispersive component.

It should be remarked here that the magnitude of the saturation

term can be calculated by observing the deviation of maximum absorption from linearity as a function of microwave power incident at the spin system. Further calculations on the saturation term can yield a value for the spin-lattice relaxation time T_1, or more exactly, T_1 T_2.

Slow passage takes place experimentally in a cavity resonator which provides the perturbing field and the reaction of M_u, M_v on the structure allows paramagnetic resonance to be observed. In discussing this interaction it will suffice to treat the microwave cavity as a series L C R electrical circuit tuned to the cavity resonant frequency ω.

The incident radiation at the sample will be augmented by the radiation field of the transverse moment of the spin system. The total magnetic field can be expressed as

$$H'_{total} = 2H_1 + 4\pi M'$$

$$= 2H_1 [1 + 4\pi\chi]$$

where the rf susceptibility is expressed as a complex function

$$\chi = M' / 2H_1 = \chi' - j\chi''$$

the real and imaginary parts being evaluated by reference to Equation 2.13. Taking into account that the sample may not completely fill the microwave cavity, the cavity field is

$$H'_{total} = 2H_1 [1 + 4\pi\eta\chi] \qquad 2.17$$

where $\eta = \dfrac{\int_{V_s} H \cdot dV_s}{\int_{V_c} H \cdot dV_c}$, is defined as the filling factor of the cavity, V_s and V_c being the sample and cavity volumes respectively, and is about equal to V_s/V_c if H is fairly uniform over V_c. To show the effect of the additional resonance field, the impedance of the circuit will be considered. The impedance of the cavity

$$Z_c = R + j(\omega L - 1/\omega C)$$

is changed by the additional field which acts through the inductance of the circuit. The total impedance is

$$Z_{total} = R + j(\omega L(1 + 4\pi\eta\chi) - 1/\omega C)$$

$$= (R + 4\pi\chi''\eta\omega L) + j(\omega L(1 + 4\pi\chi'\eta) - 1/\omega C)$$

Spin resonance increases, therefore, the resistive losses of the cavity through absorption and changes the reactance due to dispersion. The increase in resistive losses corresponds to transfer of energy from the electrical circuit to the spin system, being dissipated in the sample through spin lattice relaxation mechanisms. To record absorption or dispersion the detecting circuit element should be tuned to be sensitive to power level in the circuit or to changes in the resonant frequency of the circuit respectively. The signal detected in each case is, however, proportional to M_v and M_u respectively.

2.7 Spin Lattice Relaxation

A spin system disturbed from the equilibrium Boltzmann distribution is assumed to reach thermal equilibrium with some

characteristic time constant. The spin-lattice relaxation time, T_1, introduced and defined in Equation 2.7 assumes that, for at least a large part of the paramagnetic sample, the exchange of energy between the spin system and the lattice of the crystal proceeds with the same rate for all spins. The exchange is effected through some mechanism able to change the magnetic moment component of some spins along the applied field direction. In classical terms, the lattice ions which are in thermal motion must have some way of exerting torques on the spins to reverse them in order to re-establish equilibrium. Purely electrostatic forces, exerted by the lattice ions on a paramagnetic ion cannot produce such torques by acting directly on the spins; indirect action through spin-orbit coupling does, however, give such torques.

Two types of coupling have been suggested. One is modulation of the spin-spin interactions by lattice vibrations, introduced by Waller[24]; the second, now recognised to be the more significant, is modulation of the spin-orbit coupling by lattice vibrations, originally discussed by Kronig[25] and later by Van Vleck[26]. In the latter mechanism for an ion whose orbital momentum is nearly quenched, the electrostatic field associated with lattice vibrations can cause mixing of higher orbitals with the lowest crystalline orbital in which most electrons reside at low temperatures. It is probable, therefore, that a net orbital angular momentum component in the plane transverse to the applied field may appear momentarily, allowing transitions to

occur between the spin states. For this mechanism to be resonant the frequency of the lattice vibrations must be close to the Zeeman frequency of the transition. This process predominates at low temperatures and is often called the 'direct process', for spins absorb or emit a single phonon at the Zeeman frequency. At low temperatures the density of lattice modes with the Zeeman frequency is inversely proportional to the temperature, T: hence a T^{-1} dependence for the spin-lattice relaxation time is expected. At higher temperatures, in the liquid air range and above, a scattering or Raman process occurs in which a phonon is absorbed and another emitted with frequency differing by the Zeeman frequency. The Raman process leads to a much stronger dependence on temperature[25].

The theory of spin-lattice interaction is not well established and those predictions that have been made on T_1 dependence, such as those of Kronig[25] and Van Vleck[26], have not been thoroughly verified. In fact the predicted decrease of T_1 with increased H_o, an H_o^{-4} variation, has not been carefully checked and in some cases, discussed by Cooke[27], and also in the pulsed field maser reported by Foner[28], the predictions seem to be incorrect. Furthermore, for example, the inverse variation with temperature seems, in some cases, to be stronger for T as low as 1.3°K.[29].

The experimental determination of the true T_1 may be affected by the spin temperature (a concept defined for the distribution of spins in the levels directly from the Boltzmann relation $N_2/N_1 =$

$e^{-\hbar\omega/kT_{spin}}$[30]), for a phonon emitted by a spin has a high probability of being absorbed by some other spin before ultimately reaching the crystal boundary and giving up its energy to the bath. The re-establishment of thermal equilibrium can conceivably be determined by the rate at which phonons can escape from the crystal. This phenomenon is often called 'phonon-bath bottleneck' and has caused considerable controversy since its introduction by Giordmaine et al[31]. One interesting aspect of this 'bottleneck' is spin-lattice relaxation from the inverted state. Castle et al[29] have indicated that spin-lattice relaxation may proceed with two relaxation times. In the inverted state, a phonon interacting with a spin may stimulate the emission of a phonon so that the relaxation rate will be accelerated, but as soon as a positive spin temperature occurs, the recovery is retarded because of the 'bottleneck'. Various criticisms of Giordmaine's conclusions have been made by Anderson[32] and Bloembergen[33] has given alternative explanations of the results from the standpoint of experimental maser operation. In Chapter 7, the appearence of a bottleneck in colour centres in MgO will be discussed.

2.8 Spin-Spin Relaxation

In addition to spin-lattice interactions which serve to maintain the spin system at the lattice temperature, there are others acting within the spin system which serve to destroy internal coherence among the magnetic dipoles. The main mechanism of the latter is normally dipolar interaction but exchange interaction may

be important in paramagnetically concentrated systems.

The interaction energy of two neighbouring dipoles, μ^2/r^3 where the separation is r, is capable of inducing transitions through the oscillating field produced by the rotating component of the dipole moment in the transverse plane. Transitions are of the form of mutual spin-flips so that the z component of the magnetisation is generally not changed in the process; the total Zeeman energy, therefore, remains constant. Spin-flips of this nature decrease the normal life time of the energy state so that any coherence in the transverse magnetization is gradually destroyed with a characteristic decay time, T_2; the spin-spin relaxation time.

A very clear discussion on the basis of energy transfer by spin-spin contact has been given by Bloembergen et al[33]. These authors discuss transfer of energy between spins in different, although partly overlapping, lines (cross-relaxation) and consider cases of multiple spin-flips involving more than two spins. The rapidity of cross-relaxation processes depends upon the degree to which the Zeeman, together with the zero field splitting energy is conserved, and on the proximity of spins participating in the spin-flips. The characteristic time of cross-relaxation processes lies typically between T_1 and T_2.

Another topic in spin-spin relaxation is spin diffusion, discussed by Portis[34]. This process describes transfer of energy by

a series of spin-flips through a distribution of spins where in each step the Zeeman energy is not quite conserved. In this case the z component of the magnetization is not conserved.

2.9 Structure and Intensity of E.S.R. Spectra

It is very rare that the spectra of a $S = \frac{1}{2}$ transition consists of a single line, the single spectra being changed rather by complex interactions which may be described by terms in the Spin Hamiltonian. Some causes of structure, other than that due to chemical impurities, are enumerated.

(1) Fine Structure. For a spin transition $S > \frac{1}{2}$, the zero field splitting term of the Spin Hamiltonian is non-zero. This leads to unequal splitting of the energy levels so that a fine structure in the spectra is observed. In all 2S lines will appear.

(2) Non-Equivalent Crystalline Sites. If the symmetry axes of the crystalline electric field are oriented differently for spins at different sites in the crystal, the spin states of the paramagnetic centres at these sites will be non-equivalent. Hence the g-factor depends upon the direction and type of nearest neighbours and the presence of isotopes in the crystal lattice can contribute to this type of structure. This is often the cause of structure in the case of colour centres.

(3) Hyperfine Structure. The presence of a nuclear magnetic moment in a paramagnetic ion causes a magnetic interaction with the

electronic magnetic moment. Each electronic level is thus split into $(2I + 1)$ levels, where I is the nuclear spin quantum number, corresponding to the $(2I + 1)$ orientations, each of different Zeeman energy, of the nuclear moment. The selection rule for transitions is here $\Delta M_I = 0$ for the nuclear spin states do not change during the transition.

(4) Nuclear Quadrupole Interaction. If the nucleus has an electronic quadrupole moment, then in the presence of an electric field gradient, different orientations of the nucleus have varying interaction energies with the electric field. Any field gradient at the nucleus is caused principally by the electronic charge distribution which is in turn determined by the symmetry of the orbital spin states in the presence of the crystalline electric field. An electrostatic interaction can exist, therefore, between electrons and the nucleus, the energy of the interaction changing the resonance spectrum. The effect is similar in many ways to hyperfine structure, but is of second order.

In Section 2.6 the intensity of an $S = \frac{1}{2}$ resonance absorption line was shown to be proportional to $\chi'' H_1^2$; that is, proportional to the concentration of spins in the sample; inversely proportional to the line width; and proportional to the rf field strength. However, for $S > \frac{1}{2}$ transitions, the rf field interactions for different allowed transitions, $\Delta M_s = \pm 1$, are in general unequal. The relative magnitudes of the absorption lines can, however, be calculated from

quantum mechanical transition probabilities. Intensities of the so-called forbidden transitions in more complex spectra, $\Delta M_s \neq \pm 1$, are usually smaller than those of allowed transitions but can be theoretically estimated only if orbital wave functions of the electron configuration are known.

2.10 Broadening Mechanisms in Spin Resonance

Considering for simplicity a spin-only magnetic system, split by an applied magnetic field, the two spin states are not, however, perfectly defined in energy because of the action of various line broadening mechanisms. Generally the mechanisms can be grouped under the headings: Homogeneous and Inhomogeneous Broadening[35].

Homogeneous Broadening. Broadening is here due to mechanisms confined within the spin system and arises from dipolar interactions between like-spins, that is, spins with the same Zeeman frequency or interactions with an applied radiation field. In this way thermal equilibrium of the spin system is preserved during resonant absorption, for energy absorbed from the radiation field is spread uniformly throughout the whole system. This mechanism is just the spin-spin interaction described in Section 2.8 where the phase of the rotating component of a magnetic dipole is defined for a time T_2. Together with dipolar interaction between like-spins the phase life time may be limited by two other interactions: (1) spin-lattice relaxation which if short enough can make $T_2 = T_1$, and (2) random time variation in local magnetic fields due to thermal motion of nearby nuclei. Often these

three processes, assumed to be purely random, are lumped together into a single relaxation time, T_2, for the transverse magnetization component and the system assumed to obey the Bloch equations.

Inhomogeneous Broadening. Any line broadening mechanism which does not tend to equalise the energies of the paramagnetic spins leads to inhomogeneous broadening. Portis[35] has introduced the concept of the spin packet, the line shape of which is due to homogeneous broadening, for the discussion of this case. The overall line shape is then the envelope of a number of spin packets due to a distribution of local magnetic fields causing different spin packets to 'see' different fields. The inverse line width, T_2^x, of inhomogeneously broadened lines is, therefore, less than T_2, the inverse line width of the spin packets. There are three main causes of the spatial distribution of the splitting field:

(a) inhomogeneity of the applied field across the paramagnetic sample. With care this can be made insignificantly small for small samples. It is clear that any hyperfine structure with splittings less than the inhomogeneity of the applied field cannot be resolved by E.S.R.;

(b) unresolved hyperfine structure can produce different fields at different spins. The field seen at an electron spin due to a nearby nucleus shows a continuous distribution because the distribution of the nuclei in the nuclei states, M_I, is essentially random; all of the M_I states being about equally populated at helium temperatures;

(c) dipolar interactions between unlike spins cannot cause complete mutual spin-spin flips[34]. This interaction has the property of producing a local field at the site of a spin which is continuously distributed, just as in the case of unresolved hyperfine structure.

Experimentally the presence of either type of broadening can be determined generally either by the hole burning method[29] or by studying the way the paramagnetic system saturates at high microwave fields[35]. Evidence is presented in Chapter 7 to show that the colour centre line in $M_g O$ is inhomogeneously broadened.

CHAPTER 3

CIRCUIT PROPERTIES OF THE MASER

3.1 Introduction

The interaction of a 'spin only' magnetic system with an electromagnetic field was discussed in Chapter 2 and it was shown that maser action would be obtained if the Boltzmann populations of the levels were inverted. Activation may be brought about by using the techniques particularly familiar in transient nuclear resonance experiments:[36-39] (a) A.F.P., (b) 180° pulse, (c) non-adiabatic field reversal. One of these, A.F.P., shown to be the most effective and most easily performed method[40] and used consistantly in the experimental work, will be discussed.

It was shown, furthermore, that radiative absorption or emission of energy was proportional to H_{rf}. By placing the paramagnetic sample in a microwave resonant cavity this field can be conveniently increased at a given power level. Interaction of this field with the paramagnetic system can be expressed as a circuit parameter of the cavity. For a reflection cavity maser, the circuit properties are studied in Section 3.3 to ascertain the requisite conditions for maser amplification and oscillation.

3.2 Adiabatic Fast Passage Inversion

Inversion of the spin populations by a fast passage through resonance was first introduced by Bloch[17]. A detailed solution of

Equation 2.13 shows that when the time of passage is long compared to $(|\gamma| H_1)^{-1}$ yet short compared to T_1 and T_2 a reversal of the spin magnetization occurs. The condition on the time of passage, ΔT, has been shown by Redfield[41] to be less stringent on T_2 than was originally thought, provided H_1 is greater than the value required for complete saturation of the spin system.

During A.F.P. the spin system is taken through a series of quasi-steady states leading to inversion of the spin populations. The phenomenon can be most simply described macroscopically by considering the motion of the magnetization about the effective magnetic field in the rotating frame,

$$\underline{H}_{eff} = [\, \underline{H}_0 - \underline{\omega}/|\gamma| \,] - \underline{H}_1$$

where the precession of $\underline{M}$ takes place about $\underline{H}_{eff}$ with angular frequency

$$\Omega = |\gamma| H_{eff}$$

When $\underline{H}_0$ is well below the resonance value, $\omega = \omega_0 = |\gamma| H_0$, $\underline{M}$ will have just the thermal equilibrium value M_0 and be parallel to $\underline{H}_0$. As $\underline{H}_0$ is swept through resonance H_{eff} decreases to zero and finally becomes negative, approaching an orientation anti-parallel to $\underline{H}_0$. If $\underline{H}_{eff}$ changes by only small fractional amounts in one Larmor period, the magnetization can follow the change in $\underline{H}_{eff}$ (adiabatically), so that as a result of the passage the magnetization is orientated anti-parallel to $\underline{H}_0$. A 'nutation' of $\underline{M}$ from the normal to the inverted state takes place. The adiabatic condition can be expressed as

$$\Delta T \gg (|\gamma| H_1)^{-1}$$

where ΔT is the time to sweep through the resonance width $\Delta \omega_L$, and $(2\pi / |\gamma| H_1)$ is the Larmor period at resonance about $\underline{H}_{eff}$. It is to be noted that A.F.P. can be carried out either by sweeping the frequency, ω, of the radiation field or the applied magnetic field, H_o, the direction of sweep being unimportant.

The other restriction on ΔT is that $\Delta T \ll T_1$ so that during A.F.P. the magnitude of $\underline{M}$ will not change appreciably from its equilibrium value M_o and nearly perfect inversion can be achieved. It is obvious that inversion is made easier for long T_2 because spin dephasing will then be small during the passage through the line.

There is, however, a mechanism that opposes inversion of the spin system: radiation damping occurs due to the coupling of the spin system to the microwave cavity. The precessing magnetization produces its own coherent radiation field, $\underline{H}_r$, that is out of phase with the inverting cavity field $\underline{H}_1$. There exists, therefore, a reactionary effect whereby $\underline{M}$ tends to precess about $\underline{H}_r$ and so nutate back to its initial orientation parallel to $\underline{H}_o$. It is possible to estimate the magnitude of $\underline{H}_r$ by considering the precession of the transverse moment M_T in the absence of other cavity fields. Zeeman energy is radiated at the rate $\omega_o H_r M_T V_s$, where V_s is the sample volume, and is dissipated in the cavity losses, the transfer being governed by the equation

$$\omega_o H_r H_T V_s = \omega_o V_c H_r^2 / 2\pi Q_L$$

so that

$$H_r = 2\pi Q_L H_T V_s / V_c \qquad 3.1$$

$$\propto 2\pi Q_L H_T \eta$$

where Q_L is the loaded cavity quality factor and V_c the cavity volume. When $\underline{M}$ is totally in the transverse plane H_r has the maximum value

$$H_r^{max} = 2\pi Q_L M_o \eta \qquad 3.2$$

To defeat the opposing effects of the radiation damping field H_r, three choices are open. (a) Make $H_1 \gg H_r^{max}$ so that radiation damping is a negligible effect compared to A.F.P., (b) lower Q_L during inversion, making use of the differential dependence of H_r and H_1 on Q_L, that is, $H_r \propto Q_L$ and $H_1 \propto Q_L^{\frac{1}{2}}$, and (c) temporarily inhomogenise the applied field H_o over the sample volume during inversion so that the number of spins undergoing inversion at any one time is reduced and, therefore, the effective M_o in Equation 3.2 is also reduced.

A comparison[40] of the two methods of A.F.P., (a) frequency sweep with constant H_o, (b) field sweep with constant ω_o, shows that the latter method can be used with fewer experimental limitations. The main advantage of field sweep A.F.P. is that no special precautions are required to suppress spontaneous re-radiation of the stored energy which may be brought about by some remnant transverse moment after inversion has been effected. The reason is that on completion of the

inverting sweep the Larmor frequency of the spin system is removed from the cavity frequency so that little energy is radiated from the spin system. Furthermore, by employing a sufficiently large sweep, the whole resonance line can be traversed regardless of the relative values of the paramagnetic line width and the cavity bandwidth so that all spins in the resonant distribution can be inverted. On the other hand, in frequency sweep only those spins having a Larmor frequency within the cavity bandwidth will be inverted.

3.3 Circuit Relations: Conditions for Maser Amplification and Oscillation

The reflection type resonant cavity maser has been used throughout the experimental work. Notwithstanding its simplicity of construction from the standpoint of cryogenics and cavity coupling problems, it has been shown to be the superior design as far as gain-bandwidth and noise figures are concerned[42]. Operation characteristics of the reflection cavity maser can be expressed most satisfactorily in terms of the quality factors of the composite parts of the maser.

The well known definition of the quality factor of a resonator is

$$Q_L = \omega_o W/P$$

where Q_L = loaded cavity Q

$W = 1/2\pi \int_{V_c} H_1^2 dV_c$ = energy stored in the cavity fields

P = total power dissipated

The term, P, is made up of losses due to the cavity alone, P_o, and losses introduced where the cavity is coupled to a transmission waveguide, P_c, so that

$$P = P_o + P_c$$

Defining the unloaded quality factor of the cavity, Q_o, and the coupling quality factor, Q_c, as

$$Q_o = \omega_o W/P_o$$

$$Q_c = \omega_o W/P_c$$

the familiar expression is obtained

$$1/Q_L = 1/Q_o + 1/Q_c \qquad 3.3$$

The degree of coupling that exists between cavity and waveguide can be expressed in terms of Q_o and Q_c[43]. The three types of coupling are

Overcoupled cavity	$Q_o/Q_c > 1$	
Critically coupled	$Q_o/Q_c = 1$	3.4
Undercoupled cavity	$Q_o/Q_c < 1$	

so that Q_L may have any value between Q_o and zero depending upon the coupling, although in experimental work operation near match, $Q_L = \frac{1}{2}Q_o$ is more usual. From the foregoing definitions it is seen that tighter coupling may be obtained by an increase of the coupling losses, say, by increasing the coupling iris area.

The effect of a paramagnetic sample within a resonant cavity can be expressed, in a similar notation, by defining a magnetic quality

factor, Q_m,

$$Q_m = \omega_o W/P_{spin}$$

where P_{spin} is either the power dissipated or emitted by the spin system in the presence of a weak radiation field. P_{spin}, already evaluated in Equation 2.16 on a per unit volume basis, can be expressed in terms of the imaginary susceptibility

$$P_{spin} = \tfrac{1}{2} \omega_o (2H_1)^2 \chi''$$

generalising this expression to the case when $(2H_1)$ is not uniform over the sample value V_s, gives

$$P_{spin} = \tfrac{1}{2} \omega_o \chi'' \int_{V_s} (2H_1)^2 dV_s \qquad 3.5$$

The stored energy in the cavity volume V_c is expressed as

$$W = 1/8\pi \int_{V_c} (2H_1)^2 dV_c \qquad 3.6$$

so that the magnetic Q is

$$Q_m = 1/4\pi \chi'' \eta \qquad 3.7$$

where the filling factor η has been defined before, and χ'' is evaluated for negligible saturation ($S = 1$). The value of Q_m depends upon the magnitude of $\underline{M}$ in the z direction so that Q_m is positive when the spin system is in thermal equilibrium but becomes negative after inversion of the magnetization.

The total quality factor, Q_t, is given, therefore, by

$$1/Q_t = 1/Q_o + 1/Q_c + 1/Q_m \qquad 3.8$$

$$= 1/Q_L + 1/Q_m$$

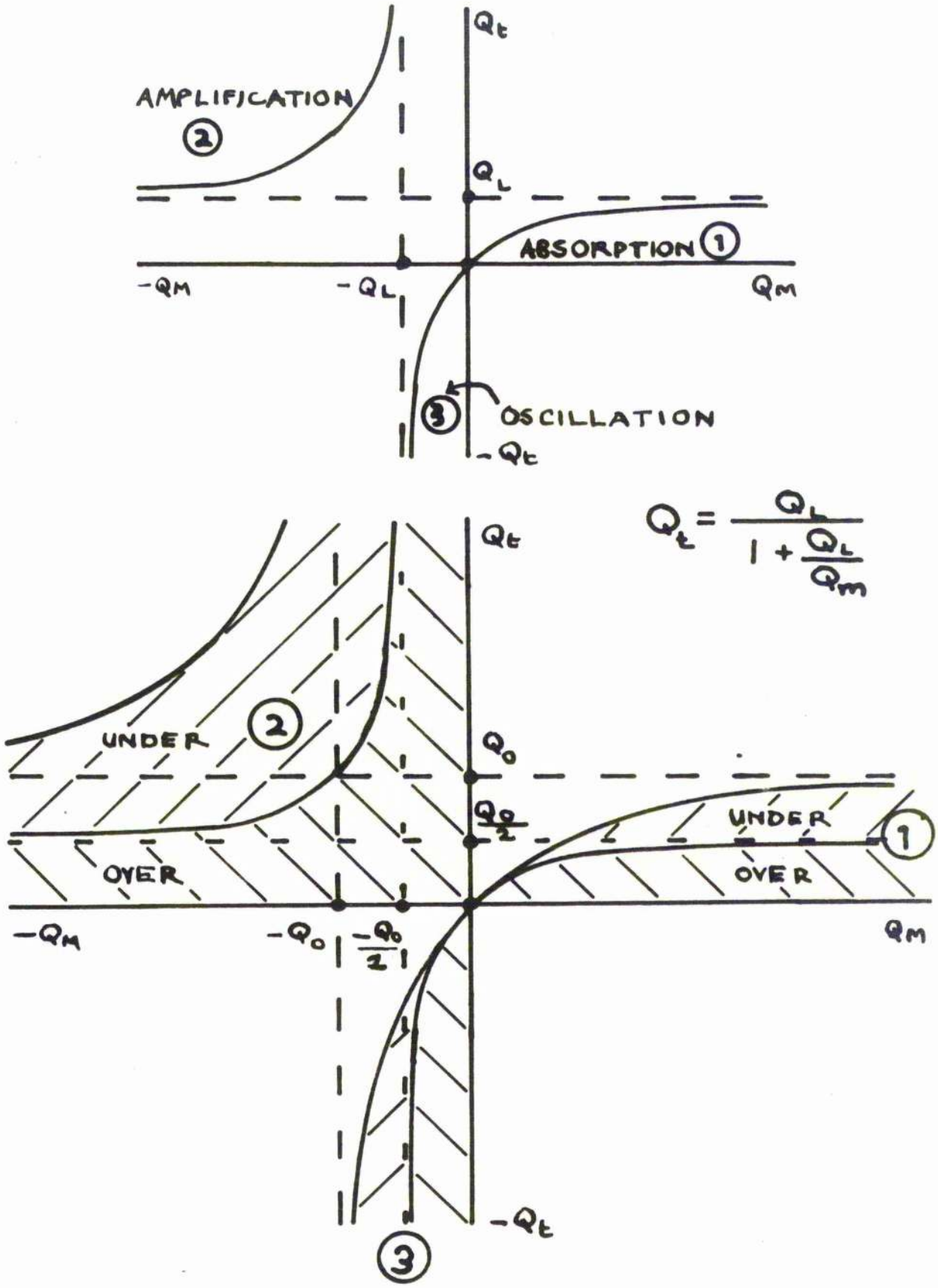

Figure 3.1 Q_m, Q_t Plotted for the cases of Under and Over-Coupling.

Equation 3.8 expresses the hyperbolic relationship between Q_t and Q_m and is plotted as a series of curves in Figure 3.1 for the cases of under and overcoupling. The axes of the hyperbolae occur at $Q_t = Q_L$ and $Q_m = -Q_L$. Figure 3.1 will be studied to disclose some of the conditions of operation of the maser.

The operating point moves on a particular curve corresponding to a given Q_L and its position at any time is determined by the value of Q_m and hence the magnitude of $\underline{M}$ in the z direction. In region (1) where there is no inversion, M_z positive, the cavity losses are increased by Q_m, the additional paramagnetic losses decreasing asymptotically to zero as saturation is approached. At the point of saturation, $M_z = 0$, $Q_m \longrightarrow \pm\infty$ and $Q_t = Q_L$, the paramagnetic system does not alter the cavity resistive properties and so appears transparent to incident radiation. When the spin system is inverted, M_z negative, but $-Q_m \rangle Q_L$, Figure 3.1 shows, in region (2) that Q_t is positive and becomes greater than Q_L. This implies that power supplied by the paramagnetic sample overcomes the cavity losses and amplification is possible.

In region (3) where $-Q_m \langle Q_L$, Q_t is negative so that the maser is super-regenerative. Oscillations can only be maintained, however, as long as $-Q_m \langle Q_L$ a self-quenching action occuring when an amount of energy sufficient to reduce Q_m below $-Q_L$ has been released from the sample. For an experimental system with varying coupling, that is varying Q_L, the conditions on oscillation are not

so strict as would be supposed from the above requirements. Figure 3.1 shows that oscillations are more easily obtained for an undercoupled cavity for $-Q_L$ is smaller than in the overcoupled case. This can be an important factor in experimental adjustments when oscillation conditions are not strongly established due either to the small density of spins present or to imperfect inversion. In fact, to be certain of obtaining maser oscillations, it is better to have

$$-Q_m < Q_o/2$$

so as to operate near critical coupling.

The oscillation condition may be expressed in terms of the number of spins in the paramagnetic sample. Q_m evaluated at resonance can be expressed as

$$Q_m = 1/4\pi \chi'' \eta$$

$$= 1/2\pi M_z T_2 \eta |\gamma|$$

For perfect inversion, $M_z = -M_o$, the oscillation condition is

$$M_o > 1/2\pi T_2 Q_L \eta |\gamma| \qquad 3.9$$

so that by Equation 2.10

$$N > kT/2\pi T_2 Q_L \omega_o \mu_\beta^2 \eta$$

$$N > kT \Delta\omega_L/4\pi Q_L \mu_\beta^2 \eta \qquad 3.10$$

where the line width $\Delta\omega_L = 2/T_2$ and N is the number of spins per c.c. This relation agrees with that evaluated by Combrisson, Honig and Townes[5].

A further point may be made about the self-quenching action of the maser oscillator by reference to the asymptotic behaviour of Q_t in the region $Q_m = -Q_L$. In an oscillator for which $-Q_m < Q_L$ is only just satisfied, the emission of very little microwave energy will change the value of Q_t by orders of magnitude so that rapid quenching of oscillation occurs. It is to be expected, therefore, that if in experimental work Q_m is made to approach the threshold of oscillation value from the region where oscillation conditions are well established, there should appear a sudden cessation of oscillation as the threshold is reached. This situation obtains in practice (Section 8.5) and will be further referred to in Chapter 4.

The transient nature of the two-level maser has been implied up to now, but from the foregoing discussions it is obvious that in the absence of any stimulating field, Q_m can remain negative only for a time of the order of the spin-lattice relaxation time, T_1, because thermalising mechanisms act on the disturbed spin system to re-establish the Boltzmann distribution. Maser amplification or oscillation must occur, therefore, within a time of the order of T_1 following activation. In order that reproducible maser operation is obtained the spin system must be returned to the distribution it had prior to inversion, so that a thermalising period of a few times T_1 must follow the period of useful operation before activation can be reinitiated. The cycle repetition period is, therefore, never less than a few T_1 in order to obtain complete re-establishment of

the Boltzmann distribution, and minimum ($-Q_m$) (maximum efficiency). If, however, the cycling period is shortened, the equilibrium distribution will not be obtained, so that $(-Q_m) > (-Q_m)^{min}$ and the maser will operate on a less efficient part of its characteristic. This can serve as a useful experimental means of altering the operating point in Figure 3.1.

CHAPTER 4

THEORY OF TWO-LEVEL MASER OSCILLATORS

4.1 Introduction

Maser oscillations can only commence in a perfectly inverted spin system, $\underline{M} = -\underline{M}_0$, in the presence of a radiative field. This is apparent from the macroscopic torque equation, $\underline{T} = \underline{M} \times \underline{H}$, which requires some transverse magnetic field to force $\underline{M}$ to nutate away from the -z direction, an unstable equilibrium position. Such fields are always present, however, through spontaneous emission transitions and external thermal radiation, or in the case of imperfect inversion, i.e. $\underline{M}$ has a small component in the transverse plane, through the radiation field of some transverse moment. As $\underline{M}$ nutates from the -z direction a transverse component appears in the magnetization vector of the spin system. The reaction field of the transverse component lags behind the magnetization, to first order, by 90° [44], and so supplements the initial stimulating field. $\underline{M}$ is consequently forced to precess further and further from the -z direction, the process being one of mutual positive feedback.

In enquiring into the possibility of coherent emission arising through the reaction of $\underline{M}$ to its own radiation field, it would seem at first sight that dephasing effects of spin-spin relaxation seriously hinder coherent build-up of the cavity radiation field. Two possibilities arise, however: (1) the transverse

magnetization is destroyed too rapidly to be compensated by nutation of $\underline{M}$ further away from the -z direction under the influence of the initial stimulating field. Therefore, the stimulating field does not grow and $\underline{M}$ remains essentially in the -z direction, and (2) the reaction field grows by sufficiently rapid nutation of $\underline{M}$ to overcome losses of the transverse magnetization and may in short times become quite large. Dicke[45] has shown that in the presence of a coherent radiation field, coherence among individual dipoles of the system is produced so that, in the presence of a cavity field, the transverse magnetization should remain defined for times longer than T_2. In formulating a description of the behaviour of a spin system under the conditions of maser oscillation the work of Dicke[45] shows that the description should be possible on classical lines. If this were not possible, any description would entail the use of quantum mechanics; an interesting study in this direction has been made by Stevens and Josephson[46] but could not be concluded only because of the mathematical difficulties involved. This treatment suggests, however, that during oscillations in a two-level maser, the microwave cavity output power should show amplitude modulated structure after an initial rapid build-up.

Of the two types of two-level maser oscillator, the field-swept type is by far the more common; in two-level schemes, other than that utilising a Q-switch with inversion by A.F.P. frequency sweep[47], magnetic field sweep is present to some degree. Although

this type is more common, an understanding of the simpler steady-field maser can be considered as basic to full comprehension of the field-swept case. It is likely that detailed studies of the behaviour of the steady-field maser will give pertinent information to the operation of the field-swept type.

In this work the behaviour of a two-level maser oscillator (steady-field case) is formulated on classical lines. In any analytical description, it would be impossible to include all interactions of the spin system, but if the line width of the sample is assumed to be sufficiently narrow, most inhomogeneous broadening mechanisms can be neglected, and single, constant spin-spin and spin-lattice relaxation times can be defined. The magnetic system is then assumed to obey the Bloch equations. Supplementary equations are required to describe the interaction between the spin system and the microwave field of the cavity containing the sample.

The results of this theoretical study will be compared in Chapter 8 to experimental results obtained from a two-level maser oscillator using neutron-irradiated MgO as the maser material.

4.2 Formalism

In the maser oscillator any radiant field that arises in the microwave cavity is produced by the spin system as an induction field in the electrical circuit. The microwave cavity will be represented here as two coils, at right angles to each other, with

axes in the transverse plane each being a series L C R resonant circuit tuned to the cavity resonant frequency ω with loaded quality factor Q_L. By this representation rotating fields can be produced. The Kirchoff equation describing the behaviour of one of the coils, say with axis in the x direction, is

$$L di/dt + Ri + (1/C)\int_0^t i\,dt = 0 \qquad 4.1$$

$$di/dt + \omega/Q_L i + \omega^2 \int_0^t i\,dt = 0 \qquad 4.2$$

in terms of the circuit current i and in the absence of an applied voltage. If a spin system, with point magnetic moment per unit volume $\underline{m}$, is placed in the coil a further term has to be added to Equation 4.2 to express the induction effects of the spin system. The derivation of this term will be considered in detail.

The magnetic field $\underline{h}$ at a point $\underline{r}$ in the coil is some function of $\underline{r}$ and time t

$$\underline{h}(\underline{r}, t) = \underline{f}(\underline{r})\, i(t)$$

where $\underline{f}(\underline{r})$ is a geometrical function expressing the field configuration in the coil. The energy stored inside the coil is

$$E_c = \int_{V_c} \underline{h}^2/8\pi \, dt$$

where V_c is the coil volume, so that the self induced voltage in the coil (1st term of Equation 4.2) is

$$v_c(t) = (dE_c/dt)/i(t) = 1/4\pi \; (di/dt) \int_{V_c} \underline{f}^2 dV_c$$

Similarly the stored energy in the spin system, per unit current in the coil, is

$$E_s = \int_{V_s} \mathbf{f}\cdot\mathbf{m}\, dV_s$$

where V_s is the sample volume, and the voltage induced by the spin system in the coil is

$$v_s(t) = \int_{V_s} \mathbf{f}\cdot\dot{\mathbf{m}}\, dV_s \qquad [\, i(t) = 1 \,]$$

v_s supplements the self induced voltage of the coil v_c and the effect of the spin system can be described by modifying the first term in Equation 4.1 to

$$\frac{di}{dt}\,\frac{\int_{V_c} \mathbf{f}^2\, dV_c}{4\pi} + \frac{d}{dt}\int_{V_s} \mathbf{f}\cdot\mathbf{m}\, dV_s$$

and, therefore, in Equation 4.2 to

$$\frac{d}{dt}\left[i + 4\pi \frac{\int_{V_s} \mathbf{f}\cdot\mathbf{m}\, dV_s}{\int_{V_c} \mathbf{f}^2\, dV_c} \right] \qquad 4.3$$

If the coil is cylindrical $\mathbf{f}$ can be taken to be uniform over samples which are small in comparison to the coil dimensions and is also directed along the coil axis. The average field over the sample may be defined by

$$H_x = \frac{1}{V_s}\int_{V_s} h\, dV_s = \frac{i(t)}{V_s}\int_{V_s} f\, dV_s \qquad 4.4$$

Equation 4.2 becomes, using Equation 4.3 and 4.4

$$\ddot{H}_x + \omega/Q\,\dot{H}_x + \omega^2 H_x + 4\pi\eta \frac{d^2}{dt^2}\left[\frac{\int_{V_s} f\,dV_s \int_{V_s} f\cdot M\,dV_s}{\int_{V_c} f^2\,dV_c}\right] = 0$$

The component M_x of the average magnetization of the sample in the x direction is

$$M_x = \frac{1}{V_s}\int_{V_s} M\,dV_s$$

where only the x component of $\underline{M}$ is integrated, so that Equation 4.2 reduces to

$$\ddot{H}_x + \omega/Q\,\dot{H}_x + \omega^2 H_x + 4\pi\eta\,\ddot{H}_x = 0 \qquad 4.5$$

where the filling factor η has been defined in Section 2.6.

An identical treatment for the other coil with axis along the y direction yields an exactly similar expression to Equation 4.5 and the two can be combined by using complex notation as

$$\ddot{H}^+ + \omega/Q\,\dot{H}^+ + \omega^2 H^+ + 4\pi\eta\,\ddot{H}^+ = 0 \qquad 4.6$$

Using the transformation of Equation 2.11, this equation in the rotating frame becomes

$$\ddot{H}' + \dot{H}'(\omega/Q + 2j\omega) + j\omega^2/Q\,H' + 4\pi\eta(\ddot{M}' + 2j\omega\dot{M}' - \omega^2 M') = 0 \qquad 4.7$$

Equation 4.7 becomes

$$T/\omega\,\ddot{H}' + \dot{H}/\omega + 2jT\dot{H}' + jH' + (2/T_r|\gamma M_o|)(\ddot{M}'/\omega^2 + 2j\dot{M}'/\omega - M') = 0 \qquad 4.8$$

When expressed in terms of characteristic times of the maser system: $T = Q_L/\omega$, the cavity ringing time and $T_r = (2\pi\eta\,Q_L|\gamma M_o|)^{-1}$, the radiation damping time first defined by Bloembergen and Pound[44] for

a single coil.

The relative importance of terms in Equation 4.8 can be determined by a simple numerical calculation on the torque equation $\dot{\underline{M}} = -|\gamma|(\underline{M} \times \underline{H})$. In rotating co-ordinates the torque equation transforms to $\dot{\underline{M}} = -|\gamma|(\underline{M} \times (\underline{H} - \underline{\omega}/|\gamma|))$, Section 3.2, so that at resonance, $\underline{\omega} = -|\gamma|\underline{H}_0$, the effective magnetic field is in the transverse plane. The rates of change of M' and H' can be compared to the microwave frequency by considering a simple nutation of $\underline{M}$ to take place from the -z direction to the +z direction within one period of the microwave frequency ($\omega \simeq 2\pi\ 10^{10}\ \text{sec}^{-1}$). If the perturbing field is H_u the nutation takes place in the vz plane so that

$$H_u = -\dot{M}_v/|\gamma|M_z$$

Assuming that the initial growth of M_v is linear, then $\dot{M}_v = 2M_o\ 10^{10}$ where $M_z = -M_o$ so that the field required to give this rate of nutation is

$$H_u = 10^3 \text{ gauss}$$

where $|\gamma| = 1.76\ 10^7\ \text{gauss}^{-1}\ \text{sec}^{-1}$. This field is to be compared with the radiation damping field of the spin system, given by Equation 3.2 which, for obtainable magnetizations, say, $N \simeq 10^{18}$ spins at 4.2°K, has the maximum value ($\eta = 1$), where Q_L is for example $5\ 10^3$

$$H_r = 2\pi Q_L M_o \eta$$

$$\simeq 15 \text{ gauss}$$

It is concluded, therefore, that M_v, H_u, and likewise M_u, H_v, change only by small fractional amounts in one microwave cycle. Terms of the order $1/\omega$ and $1/\omega^2$ are neglected henceforth in Equation 4.8 to give

$$j2M'/T_2|M_0\gamma| + 2\dot{H}' + H' = 0 \qquad 4.9$$

Equation 4.9 together with Equation 2.12 are taken as the general equations which describe a two-level maser oscillator. In terms of the components of the average field and average magnetization in the u, v, z directions, they are

$$\begin{aligned}
\dot{H}_u &= +2\pi\omega\eta M_v - \omega/2Q_L H_u && 1\\
\dot{H}_v &= -2\pi\omega\eta M_u - \omega/2Q_L H_v && 2\\
\dot{M}_u &= |\gamma| M_z H_v - M_u/T_2 && 3 \qquad 4.10\\
\dot{M}_v &= -|\gamma| M_z H_u - M_v/T_2 && 4\\
\dot{M}_z &= |\gamma|(M_v H_u - M_u H_v) - (M_z - M_0)/T_1 && 5
\end{aligned}$$

A further simplification is possible: experimental work is consistent in that the duration of maser oscillations is short compared with T_1. $1/T_1$ is, therefore, assumed to be zero and is neglected as a damping factor.

4.3 Study of the Maser Equations

Equations 4.10 are clearly nonlinear, the nonlinearities appearing as simple products of two variables in three of the component equations. The form of the equations indicates that

a longhand solution would be tedious but it was felt, nevertheless, that in this Thesis Equations 4.10 should be investigated fully in order to obtain a full understanding of the behaviour of $\underline{M}$ during the period of maser oscillations. In previously reported work[48, 49, 50, 51] on this subject, the overall validity of the relevant equations has not been checked, attention being focussed rather on obtaining reasonable agreement with experiment in only one aspect of solutions. In order to accomplish a comprehensive study, the equations have been programmed for an analogue computer (Radic System, Messrs. Redifon Ltd., Crawley, Sussex.) and have been solved for values of the coefficients likely to be encountered in experimental work and for varying initial conditions of the variables that lead to maser oscillation.

A review of the aims of this detailed study is indicated, before considering the techniques of computing and the various computed solutions. The aims are:

(1) to discover the general behaviour of $\underline{M}$ and the microwave power, represented by $(H_u^2 + H_v^2)$, during oscillation,

(2) to look for interrelations and dependences between measurable variables with a view to experimental verification,

(3) to investigate fully the discrepancies that have appeared in previous calculations[48, 49, 50, 51] when compared to observed data, and to attempt to indicate the cause,

(4) to evaluate the overall success of a purely classical description

of the maser oscillator, e.g. to show the nature of the threshold of oscillation, and

(5) to provide information pertinent to the design of a pulsed-field maser that is at present under construction in this laboratory.

4.4 Initial Conditions

The initial value of the longitudinal magnetization $M_z(o)$ required for maser oscillations has been discussed in Section 3.3. In addition to $M_z(o)$ a perturbing field must be included in Equation 4.10 to trigger the oscillation, and for simplicity this perturbation has been represented by $H_u(o)$ alone, the initial values of the other variables $M_u(o)$, $M_v(o)$, $H_v(o)$, being made equal to zero. The magnitude of $H_u(o)$ depends upon either the value of the cavity field due to thermal noise, or the radiation field of some non-decayed transverse moment and a realistic value should be chosen with reference to these. Considering the latter, a residual transverse magnetization of only 10^{-6} M_o would give a radiation damping field, from Equation 3.2, of $H_r \simeq 5\ 10^{-5}$ gauss for reasonable spin densities (say $N = 10^{18}$ spins cm^{-3}, $T = 4.2^{\circ}K$, $Q_L = 5\ 10^3$, $\eta = 1$). A perturbing field of this value, $H_u(o) = 5\ 10^{-5}$ gauss, has been used in all solutions.

These initial conditions lead to an interesting approximation of Equation 4.10 in the region of $t = 0$. The torque equations indicate that $\dot{M}_z = 0$ in this region so that the maser equations become linear with $M_z = M_z(o)$. Solutions may easily be obtained, by

use of the Laplace transform for instance, and for each of H_u, H_v, M_u, M_v, the solution may be expressed as

$$H_{u,v},\ M_{u,v} = AH_u(o)\ (Be^{-at} + Ce^{-bt}) \qquad 4.11$$

where A, B, C are constants and a and b are the sum and difference of

$$(1/2T_2 + \omega/4Q_L) \pm \sqrt{(1/2T_2 + \omega/4Q_L) - \omega/2Q_LT_2 - 2\pi\omega\eta M_z(o)}$$

When $M_z(o) = -M_o$, the exponents of Equation 4.11 are

$$(1/2T_2 + \omega/4Q_L) \pm \sqrt{(1/2T_2 + \omega/4Q_L) - \omega/2Q_LT_2 + \omega/Q_LT_r}$$

where $T_r = (2\pi\eta Q_L|M_o\gamma|)^{-1}$ is the radiation damping time for a single coil[44]. An expression similar to Equation 4.11, but differing only in the constant part, is obtained when all the variables are non-zero at $t = 0$. Hence under all initial conditions the variables are exponentially increasing when

$$T_r/2 < T_2 \qquad 4.12$$

This condition governs, therefore, the presence of maser oscillations in Equation 4.10, and the condition $T_r/2 = T_2$ determines the threshold of oscillation.

A comparison of this condition for maser oscillations to that of Equation 3.9 suggests that a discrepancy of a factor 2 exists between the present formalism and circuit relationships discussed previously. The expression that has been developed here takes into account only that field that is rotating in the same sense as the

spin precession, whereas in evaluating the energy stored in a microwave cavity in Section 3.3, this field together with the counter-rotating field are used. Hence the energy stored in the microwave cavity is apparently twice that stored in the crossed coils. In this connection Bloembergen and Pound[44] have indicated that the radiation damping time of a crossed coil system is one half that of a single coil. It is clear, therefore, that the motion of $\underline{M}$ is correctly described by Equation 4.10, but the computed rf field must be multiplied by a factor two to obtain a valid comparison with observations on cavity masers.

The circuit constants that make up the coefficients of Equation 4.10 have been chosen so as to simulate possible experimental conditions. Two values for each of Q_L, η and T_2, (where for a homogeneously broadened line $T_2 = 2/\Delta\omega_L = 2/(\gamma\Delta H_L)$ have been chosen and are listed in Table 4.1; the choice fixes the threshold value of $M_z(o)$. Solutions over the eight permutations of the constants have been undertaken for varying $M_z(o)$ and constant $M_u(o)$. Table 4.2 lists input data for the complete set of solutions. A detailed investigation into one case for each of the Q_L's would indicate that fewer solutions were required for the other cases.

4.5 Computer Programme

In the choice of the type of computer to be used to solve Equation 4.10, for the input data of Table 4.2, certain factors have been considered. Firstly, previous calculations have indicated

CONSTANT	FIRST	SECOND
Q_L	10^4	$5\ 10^3$
η	10^{-1}	1
T_2	10^{-7}	sec
$\lvert\gamma\rvert$	$1.76\ 10^7$ gauss^{-1} sec^{-1}	
ω	$2\pi\ 10^{10}$ sec^{-1}	

Table 4.1 Constants used in Computation

Q_L	10^4				$5\ 10^3$			
η	10^{-1}		1		10^{-1}		1	
T_2	10^{-7}	∞	10^{-7}	∞	10^{-7}	∞	10^{-7}	∞
$-M_z(o)$	5.010^{-3}				5.010^{-3}			
	2.510^{-3}	2.510^{-3}	3.510^{-3}	2.510^{-3}	2.510^{-3}	2.510^{-3}	2.510^{-3}	2.510^{-3}
	1.010^{-3}				1.010^{-3}			
	5.010^{-4}	5.010^{-4}	5.010^{-4}	5.010^{-4}	5.010^{-4}	5.010^{-4}	5.010^{-4}	5.010^{-4}
	3.010^{-4}				4.010^{-4}			
	1.010^{-4}	1.010^{-4}	1.010^{-4}	1.010^{-4}	3.010^{-4}			
	8.010^{-5}				2.010^{-4}	2.010^{-4}	2.010^{-4}	2.010^{-4}
	7.010^{-5}				1.510^{-4}			
	5.010^{-5}	5.010^{-5}	5.010^{-5}	5.010^{-5}	1.010^{-4}	1.010^{-4}	1.010^{-4}	1.010^{-4}
$-M_z(o)$ Thres.	4.510^{-5}	0	4.510^{-6}	0	9.010^{-5}	0	9.010^{-6}	0
	1	2	3	4	5	6	7	8

Table 4.2 List of Computer Solutions

that the mathematical model used in the formalism fits the physical system only approximately and hence it would seem that too much faith cannot be put into computed results of this study. Secondly, in any practical maser observed data (Q_L, M_o, T_2 in particular) may not be known to an accuracy better than about 10%, so that calculations using observations as input data, taken to eight or ten digits would be wasteful of time, and in any case may give an erroneous picture of the physical situation. The third factor considered is the time that would be required to carry out the forty calculations that have been chosen.

These factors indicated that the most expedient method of computation would be by analogue computer. An electronic analogue computer is suited to problems of this nature where the input data is not known to an accuracy better than that of the computation, about 1%. Furthermore, an analogue computer is a very fast machine, its operations being performed continuously and in parallel. The Radio analogue computer was utilised for the study because of its high precision specification of electrical components, .01%, and also because of its availability to the Author.

The computation accuracy of the Radio analogue computer was thought to be better than 1% when all factors of the computation, input data setting, recording etc., were taken into account. This figure was confirmed in a test computation of an equation of the form $\ddot{y} = -a^2 y$ for which the solution is well known. The accuracy

was thence assumed constant for all calculations.

In electronic analogue computers the dependent variables of equations are represented by D.C. voltages and time is usually used as the independent variable. The principal computing elements are D.C. amplifiers with near infinite gain and input impedance, almost zero output impedance and wide frequency response. These amplifiers act as summers with resistive feedback and with capacitive feedback act as integrators, the initial condition of the integration being inserted as an initial voltage across the feedback condenser. Multiplication is generally carried out by servo-mechanical devices. The method of programming a problem for an analogue computer is to connect the various elements together in an analogous way to flow diagrams. Coefficients of the equations and initial conditions of the integrals are inserted in the programme through variable potentiometers. The computer is made to compute the problem by activating a series of relays, which also enter the initial conditions before the actual computation commences. The results may be displayed on an oscilloscope or recorded permanently on paper as pen traces. With regard to computing techniques, reference has been made to the texts of Jackson[52] and Korn and Korn[53], and to the specification handbook of the Radic computer.

The computer programme for Equation 4.10 is shown in Figure 4.1. The programme is shown as a block diagram of the computer

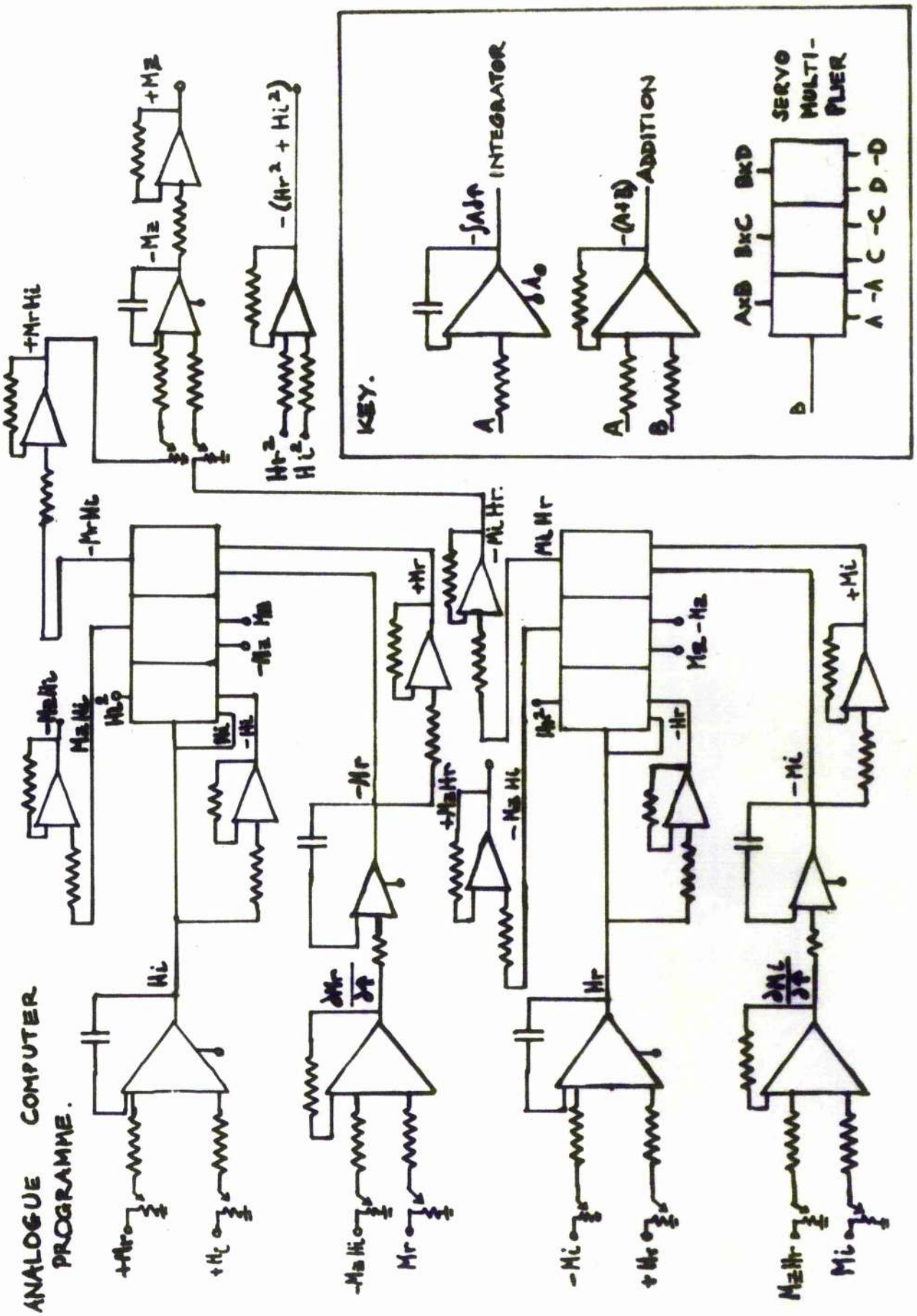

Figure 4.1 Analogue Computer Programme.

elements utilised in the problem, and describes the relation between voltages (computer variables) and computer elements (computer operators). All potentiometers were set automatically by a servo-mechanism; this arrangement ensured that minimum time was spent in entering the coefficients and initial conditions of the cases of Table 4.2. The five variables, together with $(H_u^2 + H_v^2)$, and $\int_0^\infty (H_u^2 + H_v^2)dt$ were recorded on teledetos paper by a standardised pen recorder. The complete computer schedule was carried out by the Author.

The scaling of variables follows the discussions on this topic in References 52 and 53. The variable scale factors were set to make maximum use of the computer range by a process of trial and error. The problem was slowed down in time by a factor 10^7, or 10^8 in some cases, so that the frequency of the problem came within the frequency response of all computing elements: the slowest element is the servo-multiplier with a maximum response of one cycle per second.

4.6 General Discussion of Solutions

The time dependent behaviour of some solutions is shown in Figures 4.2, 4.3, 4.4 and 4.5. Figure 4.2 illustrates the general behaviour of the solutions under varying strengths of oscillation, for the circuit parameters $Q_L = 10^4$, $\eta = 10^{-1}$,

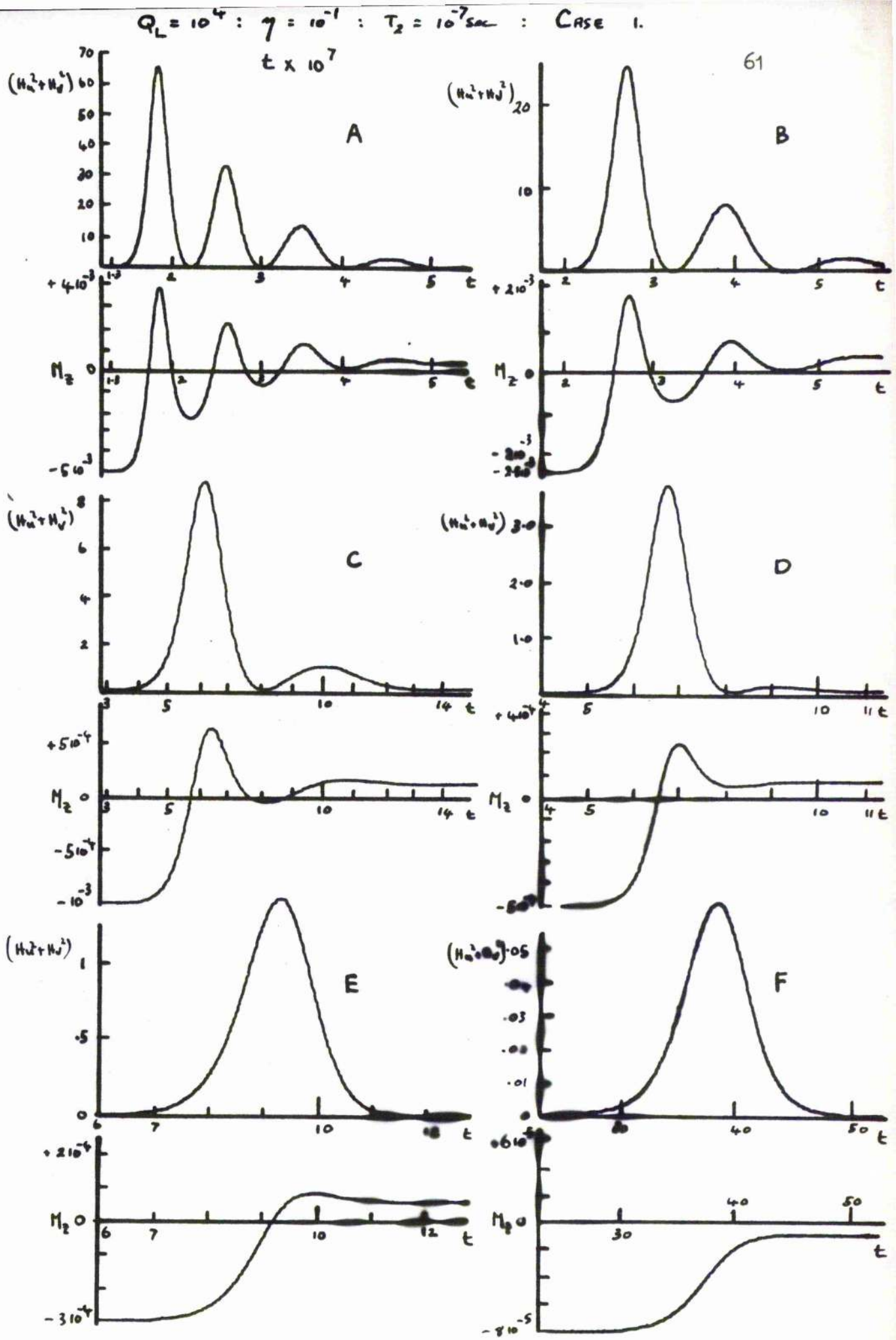

Figure 4.2 Series of Computer Solutions.

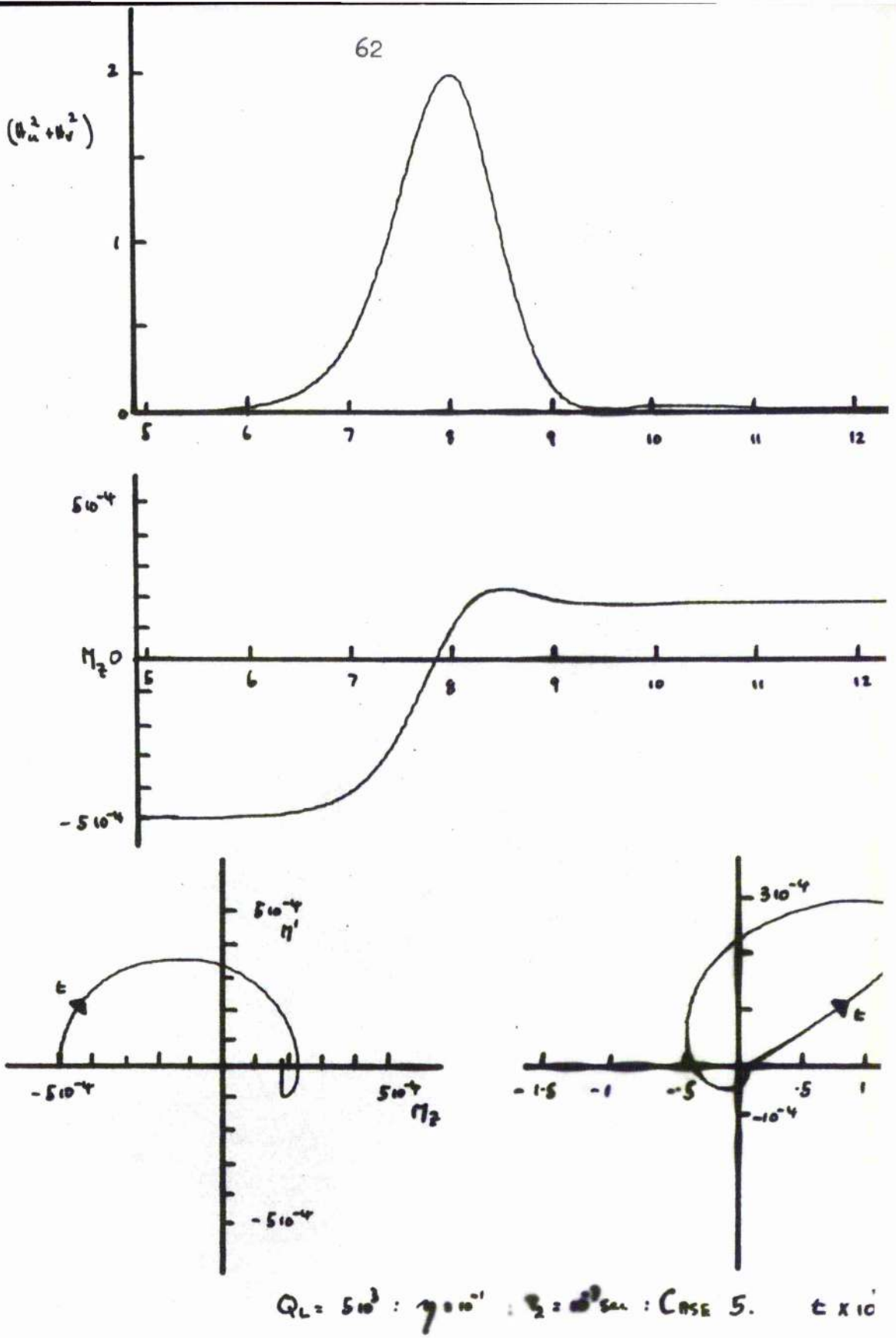

Figure 4.3 Computer Solution.

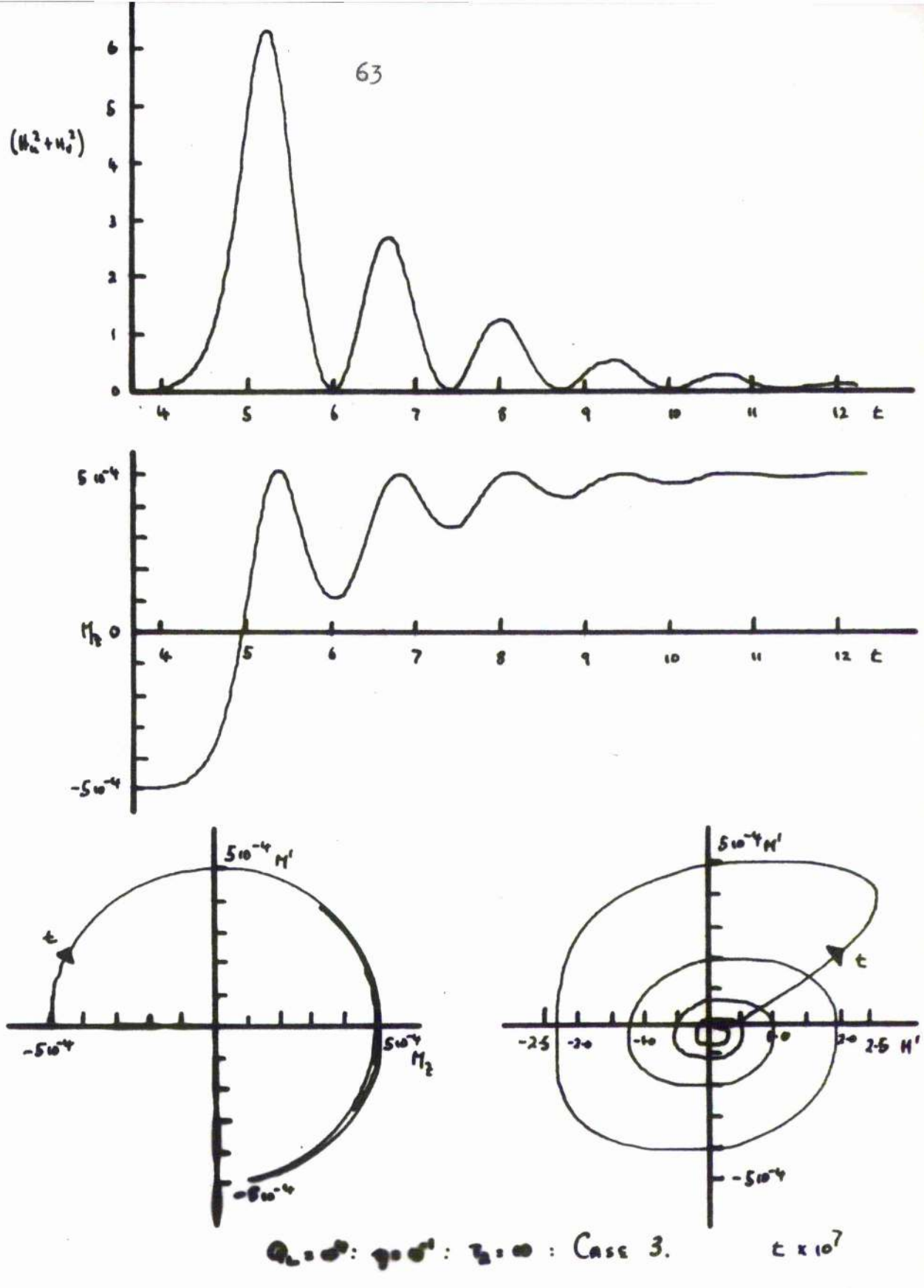

$Q_x = \infty$: $\gamma = \sigma'$: $T_2 = \infty$: Case 3.

Figure 4.4 **Computer** Solution.

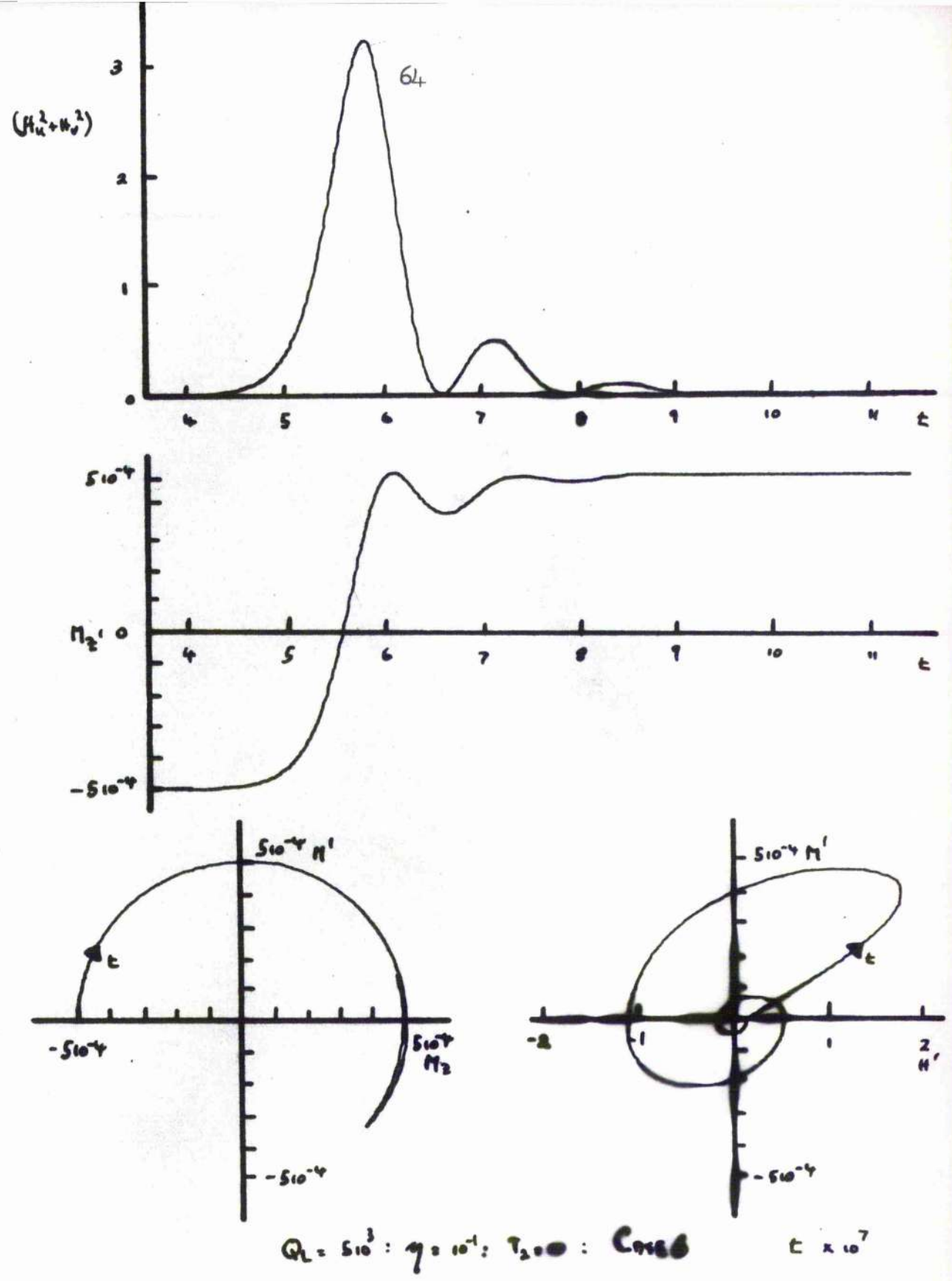

Figure 4.5 Computer Solution.

$T_2 = 10^{-7}$ sec (case 1)*. The series of recordings demonstrates that in solutions where oscillatory conditions are well established $T_r/2 \ll T_2$ (Figure 4.2, (1),(2),(3)) amplitude modulation of the cavity power occurs and is accompanied by damped oscillatory motion of M_z. However, in solutions that are near the threshold of oscillation $T_r/2 \simeq T_2$ (Figure 4.2, (6)) emission is a simple growth and decay that is more delayed and spread out than in the former cases. Where amplitude modulation is present, it is complete and occurs at frequencies less, by about a factor 10^3, than the microwave frequency.

The motion of M_z, representing the energy stored in the spin system, is correlated to the instantaneous cavity energy, represented by $(H_u^2 + H_v^2)$; an oscillatory transfer of energy takes place between the sample and the cavity radiation field and maximum cavity energy generally occurs near minimum sample energy. The positive maxima of M_z lag behind the peaks of $(H_u^2 + H_v^2)$ indicating that as M_z approaches a maximum, the rate of release of energy from the sample becomes less than the rate at which energy is dissipated in cavity losses. Hence, modulated emission may be viewed as a relaxation oscillator, in which, after a period of

---

* Footnote: M_z and $(H_u^2 + H_v^2)$ are plotted for they represent respectively the energy stored in the spin system and the energy stored in the electrical circuit. Of the variables in the problem, it should be possible to detect these two experimentally.

oscillation, that is $(M_u^2 + M_v^2)$ increasing, there is a dead time in which the oscillator recovers nearly to its initial state, M_z decreasing towards $M_z(o)$, followed by a further period of oscillation and so on. Oscillations decrease in magnitude with time due to system losses.

One difference is noted immediately between cases of finite and infinite T_2 (Figures 4.2, 4.3, 4.4 and 4.5). When $T_2 = \infty$ the magnitude of $\underline{M}$ remains equal to M_o throughout the period of oscillation because spin-spin dephasing is absent, so that finally $\underline{M}$ returns to its ground state, $M_z(\infty) = +M_o$. In general, for finite T_2, emission terminates when M_z reaches some value, either positive or negative, at which oscillation conditions are no longer fulfilled so that some residual magnetization is present after oscillations have ceased. In practice, however, $M_z(\infty)$ decays to the thermal equilibrium value $+M_o$ in a time of the order of T_1.

Phase Relations

The motion of $\underline{M}$ in the rotating frame is shown in Figure 4.6 for the cases of Figure 4.2, and in Figures 4.3, 4.4, 4.5; M_z is plotted against the transverse moment M', where M' has magnitude $\sqrt{M_u^2 + M_v^2}$. Solutions show that $M' \simeq M_v$, an equality that is expected for two reasons: firstly, the cavity is tuned to the Zeeman frequency of the spin system so that the rf susceptibility is purely imaginary, and, secondly, the perturbing field $H_u(o)$ acts

$Q_L = 10^4$: $\eta = 10^{-1}$: $T_2 = 10^{-7}$ sec : Case 1.

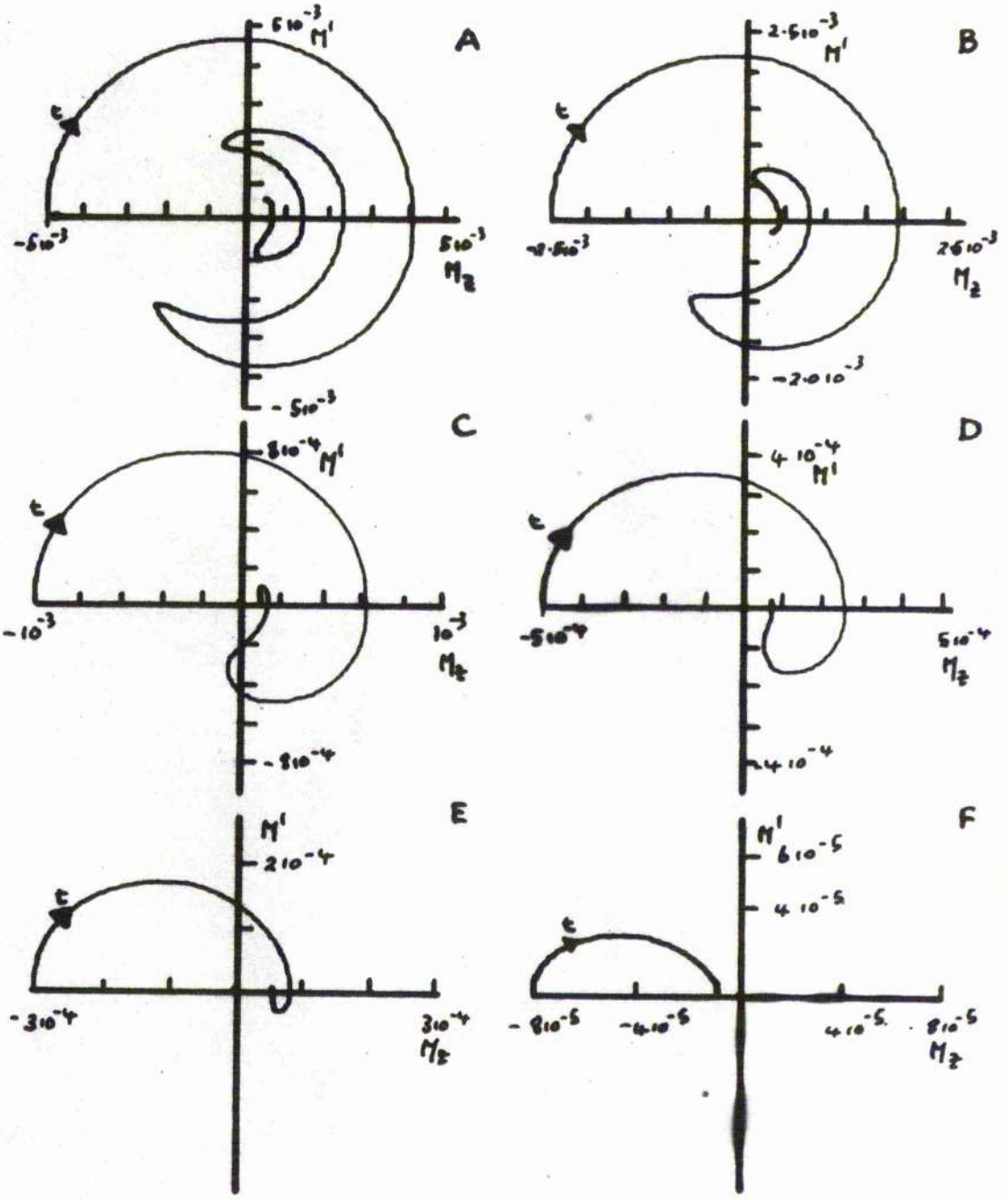

Figure 4.6 Computer Solution.

Plot of M_z against M'.

primarily to produce a transverse moment in the v direction.

For cases of finite T_2, Figures 4.3 and 4.6, $\underline{M}$ exhibits a pendulum-like motion for strong oscillations. The length of $\underline{M}$ decreases in the emissive period due to progressive loss of energy from the spin system. In the region of threshold $T_r/2 \simeq T_2$ the motion of $\underline{M}$ in the transverse plane is severely damped by spin-spin dephasing, so that $\underline{M}$ tips only slightly from the z direction. On the other hand, when $T_2 = \infty$, Figures 4.4 and 4.5, $\underline{M}$ is conserved and, therefore, moves on a circular trajectory. Some oscillatory motion of $\underline{M}$ is present here in all solutions investigated, for strong oscillation conditions prevail for the range of $M_z(o)$ used; the threshold condition is here $T_r = \infty$.

A simple phase relation should exist between M' and H' because the rf susceptibility is imaginary. Solutions confirm that the cavity field H' is orthogonal to the transverse magnetization M' and, as shown in Figures 4.3, 4.4, 4.5 and 4.7, M' leads H' for periods of emission of energy from the spin system and M' lags behind H' when energy is absorbed by the spin system. The time lag that has been mentioned in connection with maxima of $(H_u^2 + H_v^2)$ and M_z, is evident in these diagrams as a phase different between maxima of H' and minima of M' and vice versa.

The general behaviour of the two-level maser oscillator may be summarised by remarking that there are many similarities between

$Q_L = 10^4$: $\eta = 10^{-1}$: $T_2 = 10^{-7}$ Sec. CASE 1.

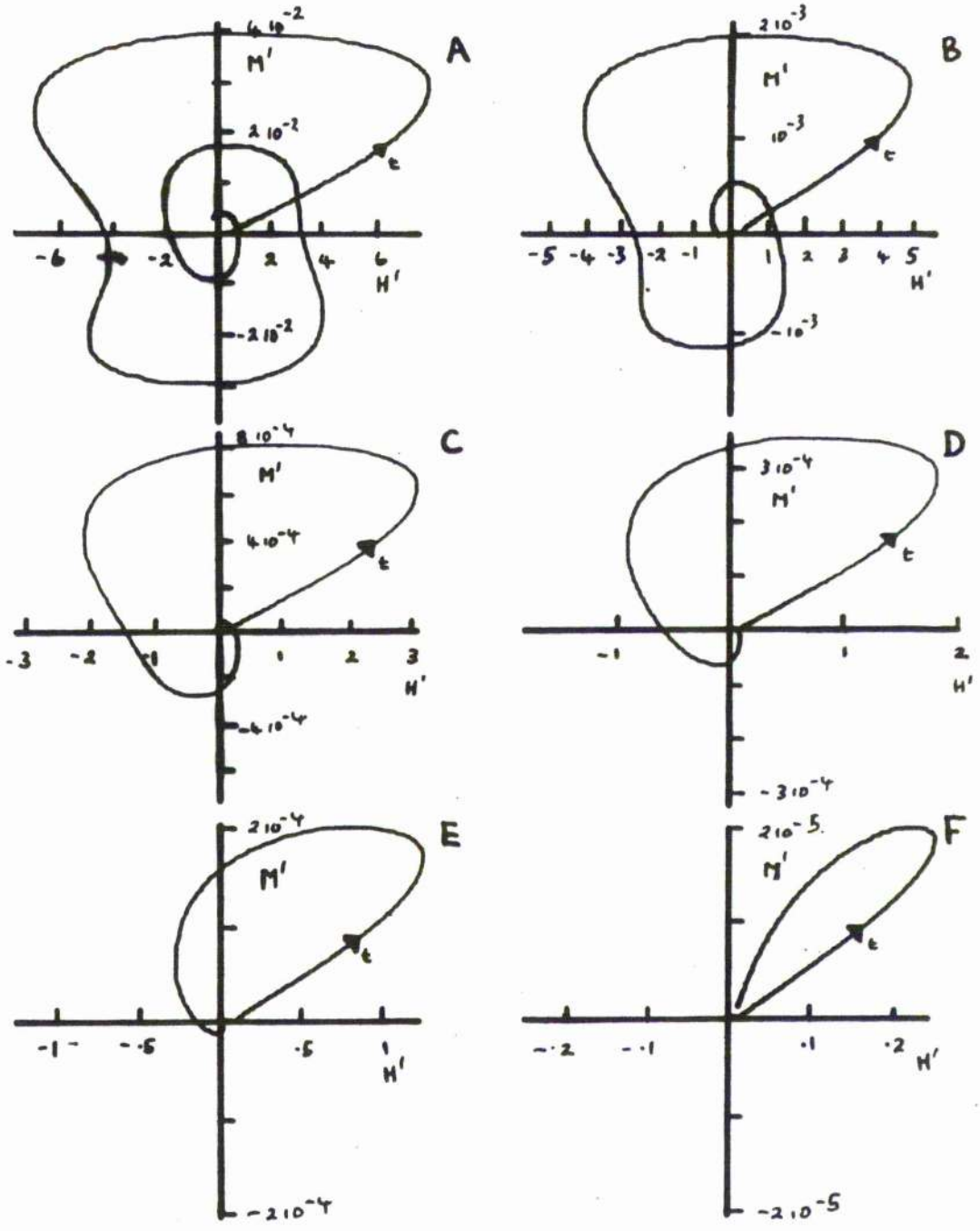

Figure 4.7 Computer Solution.

Plot of H' against M'.

its behaviour and that of two coupled pendulums. In the analogy, one of the degrees of freedom is the microwave cavity and the other the spin system. Energy is periodically transferred between the two degrees of freedom, giving rise to modulation of the energy stored in each. In the maser oscillator only one degree of freedom is easily monitored, the cavity energy, so that although amplitude modulation of the cavity power has been observed by many workers[6,7,8,47], the nutating character of $\underline{M}$ has not been detected experimentally. In this connection Stevens and Josephson[46] have suggested that an instructive test of the theoretical explanations of modulated maser oscillations would be to monitor $\underline{M}$ simultaneously with the cavity power. In Chapter 8 evidence supporting the nutating character of $\underline{M}$ during oscillations will be presented, the variation in the relatively slow moving component M_z has been detected directly.

Frequency of Modulation

The dependence of the modulation frequency β on $M_z(o)$ has been checked in some detail. For finite T_2, β could only be measured for cases of strong oscillation where appreciable modulation of $(M_u^2 + M_v^2)$ occurs. A slight increase of β is noted as the oscillation progresses and β is, to first approximation, proportional to time. In the limit $1/Q_L = 1/T_2 = 0$, β seems to follow the law

$$\beta \propto M_z(o)^{0.4} \qquad 4.14$$

and the exact relationships that hold for the eight cases are given

in Table 4.3, where β is evaluated for the second cycle of modulation. The dependence of β on $N_z(o)$ is weak in all cases but there is a definite tendency for the dependence to become weaker for decreased T_r (increased strength of oscillation). The following general variation of β is seen to occur in Figure 4.8, where β is plotted against $N_z(o)$ for the data of Table 4.3:

η constant: T_2 finite ; increase of Q_L decreases β

T_2 infinite ; " " " increases β

T_2, Q_L constant: increase of η increases β

η, Q_L constant: " " T_2 " β

Wang and Singer[49] have studied the problem of the two-level maser oscillator for a completely lossless system, $1/Q_L = 1/T_2 = 0$, and have found the modulation frequency to be given by

$$\beta = (4\pi\eta\omega|\gamma|)^{\frac{1}{2}} N_z(o)^{\frac{1}{2}} \qquad 4.15$$

where the constant of proportionality has to be modified to $(2\pi\eta\omega|\gamma|)^{\frac{1}{2}}$ to apply to this treatment. This factor is compared in Table 4.3 to the constant of proportionality obtained in this study and in all cases the constant is slightly less than $(2\pi\eta\omega|\gamma|)^{\frac{1}{2}}$. The dependence of β in the full nonlinear treatment is, nevertheless, close to Equation 4.15.

4.7 Envelope of the Cavity Energy

The parameter $(H_u^2 + H_v^2)$ represents the instantaneous cavity

Q_L	10^4				$5\ 10^3$			
η	10^{-1}		1		10^{-1}		1	
T_2	10^{-7}	∞	10^{-7}	∞	10^{-7}	∞	10^{-7}	∞
β [x 10^8]	3.3 $M_z^{.63}$	3.0 $M_z^{.53}$	5.1 $M_z^{.48}$	3.9 $M_z^{.4}$	3.7 $M_z^{.6}$	2.7 $M_z^{.55}$	6.2 $M_z^{.51}$	6.3 $M_z^{.45}$
$(2\pi\eta\omega\lvert\gamma\rvert)^{\frac{1}{2}}$ [x10^8]	8.34	8.34	26.3	26.3	8.34	8.34	26.3	26.3
T_{Decay}	10^{-7}	$1.7\ 10^{-7}$	$1.1\ 10^{-7}$	$1.9\ 10^{-7}$	$5.0\ 10^{-8}$	$8.2\ 10^{-8}$	$4.3\ 10^{-8}$	$6.5\ 10^{-8}$
$\frac{Q_L}{\omega}$	$1.6\ 10^{-7}$	$1.6\ 10^{-7}$	$1.6\ 10^{-7}$	$1.6\ 10^{-7}$	$1.6\ 10^{-7}$	$8.0\ 10^{-8}$	$8.0\ 10^{-8}$	$8.0\ 10^{-8}$
	1	2	3	4	5	6	7	8

Table 4.3 Variation of β and T_{Decay}

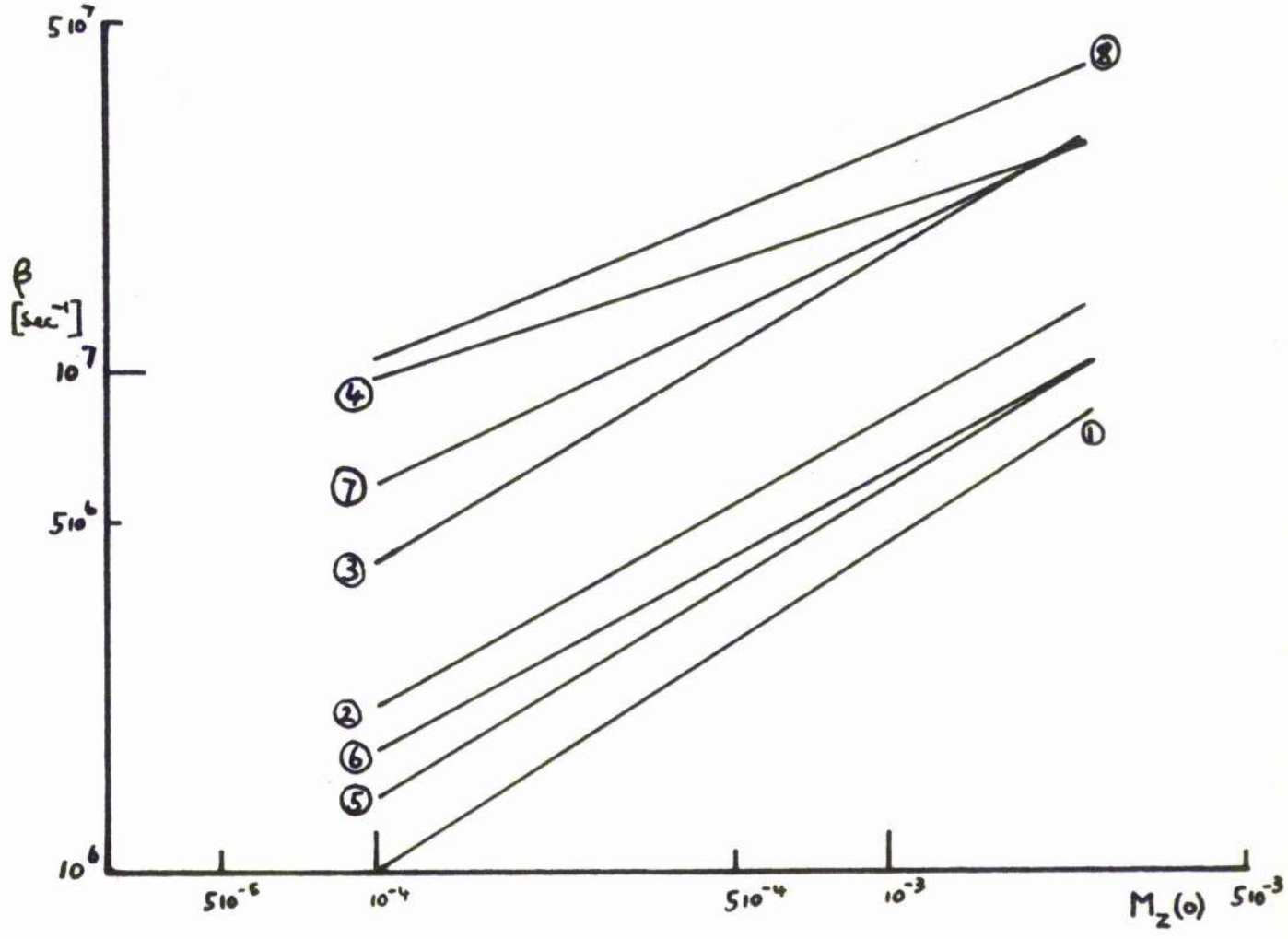

Figure 4.8 Frequency of Modulation β plotted against $M_z(0)$.

energy, but it is noted that in practice only part of $(H_u^2 + H_v^2)$ could be detected, the exact fractional amount being determined by the coupling condition of the cavity. Four main observations may be made on the envelope of $(H_u^2 + H_v^2)$.

Incubation Time

The time that elapses from the start of oscillation (t = 0) to the first peak of $(H_u^2 + H_v^2)$, called the "incubation time", is found to be shortened for increased $H_u(o)$. This feature of the computation is expected, for the exponential increase of variables near the origin, described by Equation 4.11, depends directly upon $H_u(o)$. To first order approximation, that is assuming $M_z = M_z(o)$ up to the first peak of $(H_u^2 + H_v^2)$[n], the incubation time can be written in terms of the circuit parameters. Under strong oscillation conditions the decreasing term of Equation 4.11 can be neglected and the solution for H_u is

$$H_u = D\, H_u(o)\, e^{-bt}$$

where b is negative. The incubation time, T_I, defined as the time

---

n Footnote: This is reasonably correct for strong oscillations, because M_z is constant for a large proportion of the incubation time. The approximation does not hold, however, near the threshold.

taken for $H_u = H_{peak}$ is, therefore

$$T_I = 1/b \ln (H_p/D) - 1/b \ln (H_u(o))$$

$$= X - Y \ln (H_u(o))$$

where X and Y are constants depending upon the circuit parameters, so long as H_p is independent of $H_u(o)$. Hence T_I is related to the cavity power P present at t = 0 by

$$T_I \propto -\ln P \quad (P \propto H_u(o)^2) \qquad 4.16$$

The logarithmic dependence on $(H_u(o))$ was checked in solutions for one case ($Q_L = 10^4$, $\eta = 10^{-1}$, $T_2 = 10^{-7}$ sec, $H_z(o) = -5\ 10^{-4}$ gauss) for a hundred fold increase in $H_u(o)$, and was found to be correct. Furthermore, increased $H_u(o)$ did not alter the shape of the emission but simply triggered the emission at an earlier time. The experimental work of Chester et al[47] in verification of Equation 4.16 is noted, but no further check has been possible in these experimental studies (see Chapter 8).

A similar treatment to the above shows that

$$T_I \propto H_z(o)^{-\frac{1}{2}}$$

$$\propto T_r^{\frac{1}{2}} \qquad 4.17$$

when $T_r/2 \ll T_2$, that is when the term $\omega/Q_L T_r$ dominates the root of the exponential. A plot of T_I versus $H_z(o)$ in all solutions shows Equation 4.17 to hold. A sharp increase of T_I near the threshold is noted, however, indicating the onset of the threshold

and the breakdown of the approximation used here, $M_z = M_z(o)$. In experiment this relation has been checked by relating the incubation time to the degree of inversion and details are given in Chapter 8. The significance of Equation 4.17 in connection with pulsed-field masers is explained in Section 4.11.

Rate of Decay

For strong oscillations the decay of peaks of $(H_u^2 + H_v^2)$ is exponential, the characteristic times of decay being listed in Table 4.3. These are to be compared with the ringing time of the cavity Q_L/ω and the spin-spin relaxation time T_2. When spin-spin dephasing is absent ($T_2 = \infty$) the decay is that of the cavity. When T_2 is finite, however, the decay is more rapid than that of the cavity; this would seem impossible at first sight. Bloembergen and Pound[44] have indicate, however, that when $T_2 \simeq Q_L/\omega$, the case here, the decay is due to a mixture of spin-spin and cavity damping neither of which is predominant.

The rate of decay of $(H_u^2 + H_v^2)$ for cases near threshold is long and is determined by neither T_2 nor Q_L/ω, but rather by the rate at which M_z approaches its final value. At times after the peak of $(H_u^2 + H_v^2)$ the rate at which energy is supplied by the spin system to the cavity is not great enough to overcome cavity losses, but is sufficient to maintain the cavity field for times much longer than the cavity ringing time.

Maximum Power

The magnitude of the first peaks of $(H_u^2 + H_v^2)$ is plotted in Figure 4.9 for the cases investigated. The family of curves falls into two groups, $\eta = 1$ and $\eta = 10^{-1}$ each with an upper limit when $T_2 = \infty$, $Q_L = 10^4$. In all curves, when oscillations are well established,

$$(H_u^2 + H_v^2) = M_z(o)$$

Maximum cavity energy or cavity power output, occurs in the most favourable case, $Q_L = 10^4$, $\eta = 1$, $T_2 = \infty$ curve 4, the upper portion of this curve would seem to give in reality an impossible maser system for apart from the difficulties that would be encountered in inverting the system the output power is large, about 10 watts when $(H_u^2 + H_v^2) = 400$ gauss^2. Apart from this unrealistic situation some useful information can be taken from Figure 4.9.

Firstly, for cases of finite T_2, the output power tends sharply to zero near the threshold value of $M_z(o)$, whereas for $T_2 = \infty$ the relation between the two parameters remains linear. Secondly, the output power varies for changes of Q_L, η, T_2 at constant $M_z(o)$ such that

η	increases from	10^{-1}	to	1,	$(H_u^2 + H_v^2)$	increases by a factor	15
Q_L	"	" $5\,10^3$	"	10^4,	"	" " " "	2
T_2	"	" 10^{-7}	"	∞,	"	" " " "	1.2

These tendencies are consistent with an increase in the strength of

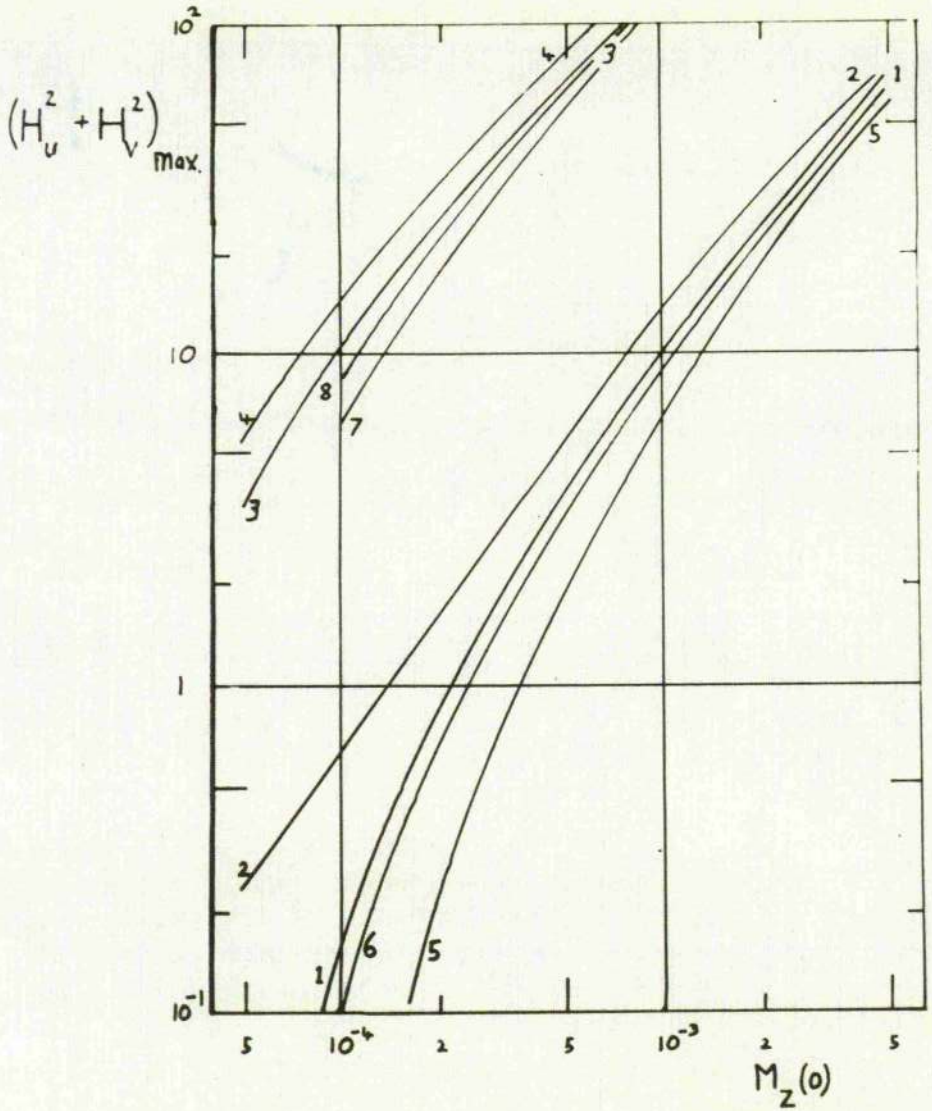

FIGURE 4·9 $(H_u^2+H_v^2)_{max}$: $M_z(0)$

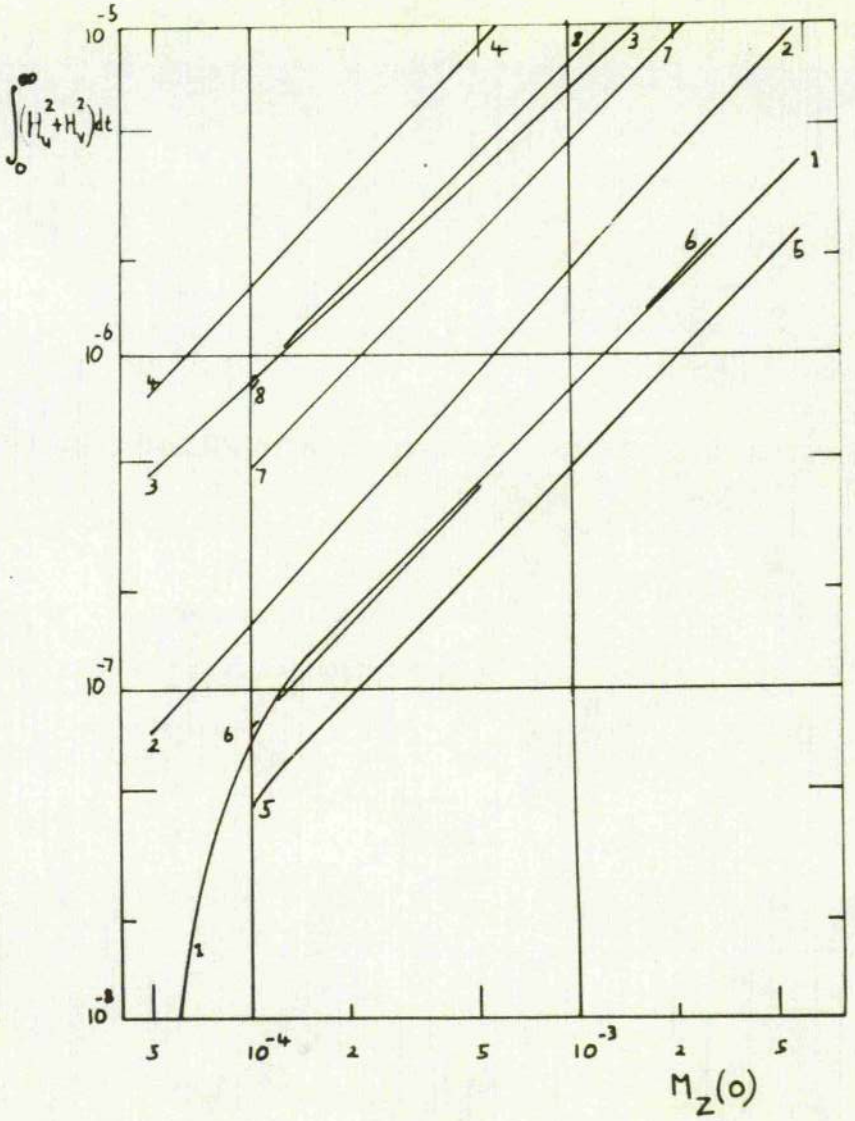

FIGURE 4·10 $\int_0^\infty (H_u^2+H_v^2)\,dt$: $M_z(0)$

oscillation. Hence, it would be experimentally more favourable to use an increased filling factor to increase the output power than it would be to increase the cavity Q_L or to decrease the line width of the maser sample. Furthermore, it is technically easier to increase the filling factor than to change either Q_L or T_2 by an appreciable amount.

Energy Output

The total energy output of the oscillator is given by the expression

$$E_{osc} = \omega/4\pi\, Q_L \int_{V_c} \int_0^\infty (H_u^2 + H_v^2)\,dt\,dV_c \qquad 4.18$$

$$= \omega V_c/4\pi\, Q_L \int_0^\infty (H_u^2 + H_v^2)\,dt$$

the time integral being evaluated in the computation. The theoretical output from a cavity maser is $4E_{osc}$ because E_{osc} represents only the energy associated with the synchronous rotating component of the microwave cavity. $\int_0^\infty (H_u^2 + H_v^2)\,dt$ is plotted for the cases of computation in Figure 4.10. A similar increase in E_{osc} for increased Q_L, η, T_2 is noted as that for maximum $(H_u^2 + H_v^2)$ and also a rapid decrease of output energy occurs near the threshold of oscillation. When oscillations are well established

$$E_{osc} \propto N_s(o)$$

As T_1 relaxation processes are ignored in this treatment conservation of energy for the whole system demands that the area

of the envelope of $(H_u^2 + H_v^2)$ is equivalent to the energy lost by the spin system. The energy balance is governed by

$$\omega/4\pi Q_L \int_0^\infty (H_u^2 + H_v^2)dt = \eta H_0 (|M_z(0) - M_z(\infty)|) \qquad 4.19$$

This relation is found to be satisfied in all solutions of the computation.

4.8 Threshold of Oscillation

An observed characteristic of any two-level maser oscillator (see Chapter 8) is the sharp fall in the output power as the threshold of oscillator $T_r/2 = T_2$ is approached. The treatment of Stevens and Josephson[46] of the coupling of a spin system to the cavity mode, indicates that a sharp threshold of oscillation should be present on theoretical grounds. However, reported semi-classical treatments[48,49,50] have given no indication as to the behaviour of the pertinent equations in this region.

The behaviour of solutions near the threshold have already been indicated; the emission occurs at a later time, is more spread out and is less energetic. To indicate most effectively the behaviour of $\underline{M}$ in this region, $M_z(\infty)/M_z(0)$ is plotted against $M_z(0)$ in Figure 4.11 (b) for the case $Q_L = 10^4$, $\eta = 10^{-1}$, $T_2 = 10^{-7}$ sec. For $T_r/2 \ll T_2$ the change in $M_z(\infty)/M_z(0)$ is very small but as threshold is approached a rapid change to the sub-threshold value +1 occurs. The microwave energy output undergoes an associated rapid decrease to zero as threshold is reached; this

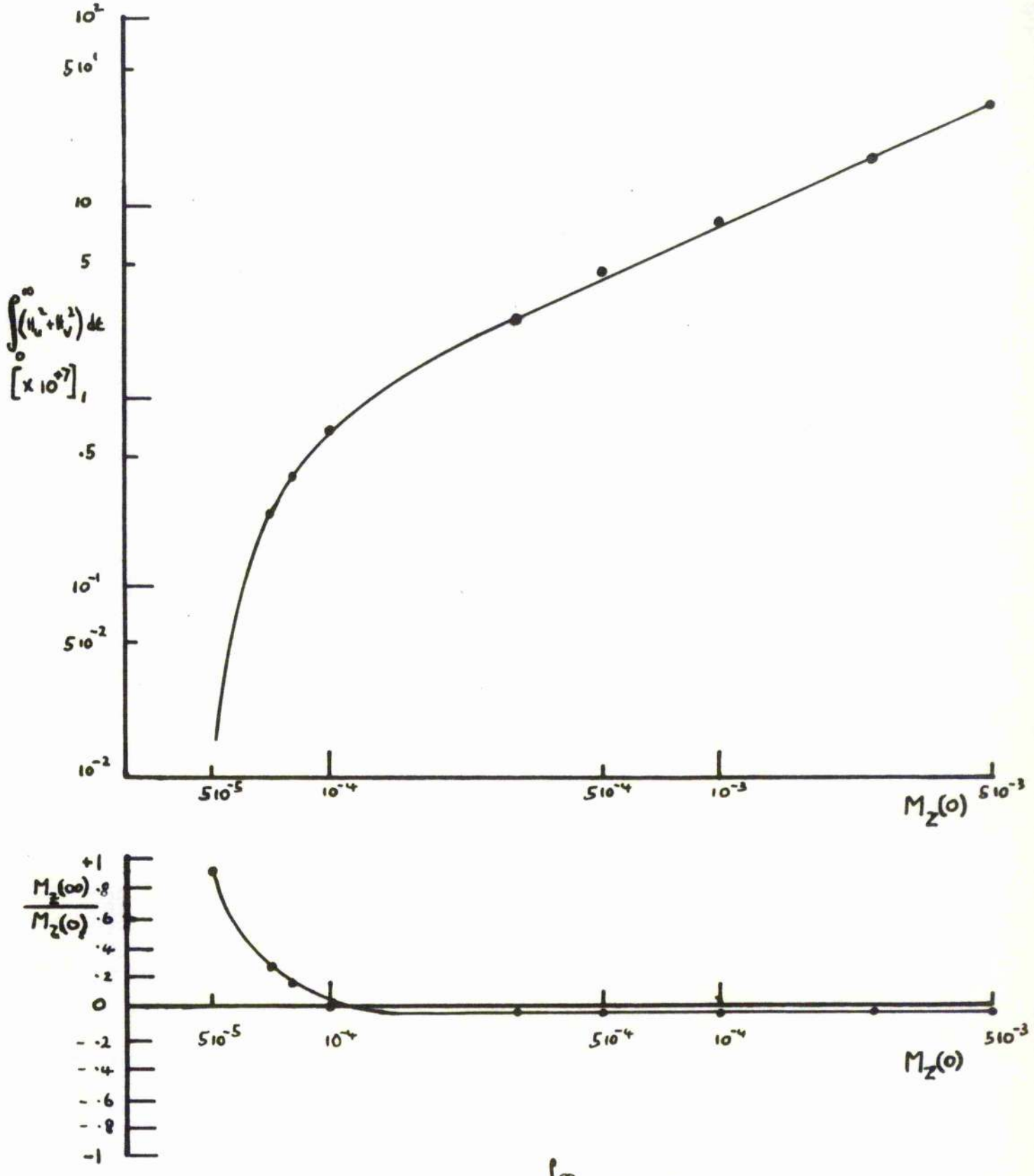

Figure 4.11 $\int_0^\infty (H_u^2 + H_v^2)dt$ and $M_z(\infty)/M_z(0)$

Plotted against $M_z(0)$.

is shown in Figure 4.11 (a) for the same parameters as Figure 4.11 (b). These results are to be compared with the predictions of Section 3.3 from circuit considerations. Further comparisons to Figure 4.11 will be made with experimental results in Chapter 8.

4.9 Comparison with Experiment

A comparison between computed curves and observed data on maser oscillators operated in a steady magnetic field is hampered by a serious lack of observations. A comparison with the one reported case, that of Chester et al[47], is useful. It is admitted that only one comparison may not show shortcomings of this formulation of the problem.

In Chester's work A.F.P. was carried out by the frequency sweep method using a Q-switch, and oscillations were triggered by re-activating the Q-switch at a later time. The trigger was not sharp, however, as seen from Figure 4.12.

Figure 4.12 shows the oscillogram* of maser oscillation for the parameters detailed in Table 4.4 and, in comparison, the

---

* Footnote: Permission to reproduce this figure has been kindly given by Dr. P.F. Chester. The original figure is contained in Westinghouse Research Laboratories Scientific Paper 6-94439-8-P4, "Amplification and Oscillation in Two-Level Spin System", P.F. Chester, E.E. Wagner and J.C. Castle, Jr., December 8, 1958.

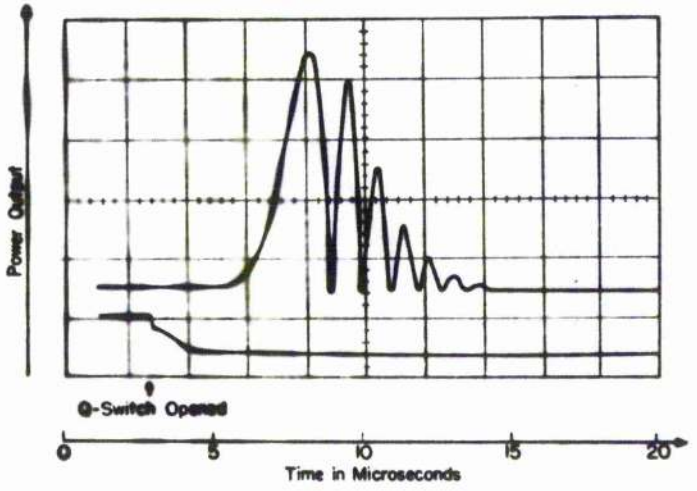

Experimental Recording of Chester et al.

Maser Oscillations in Neutron-Irradiated Quartz.

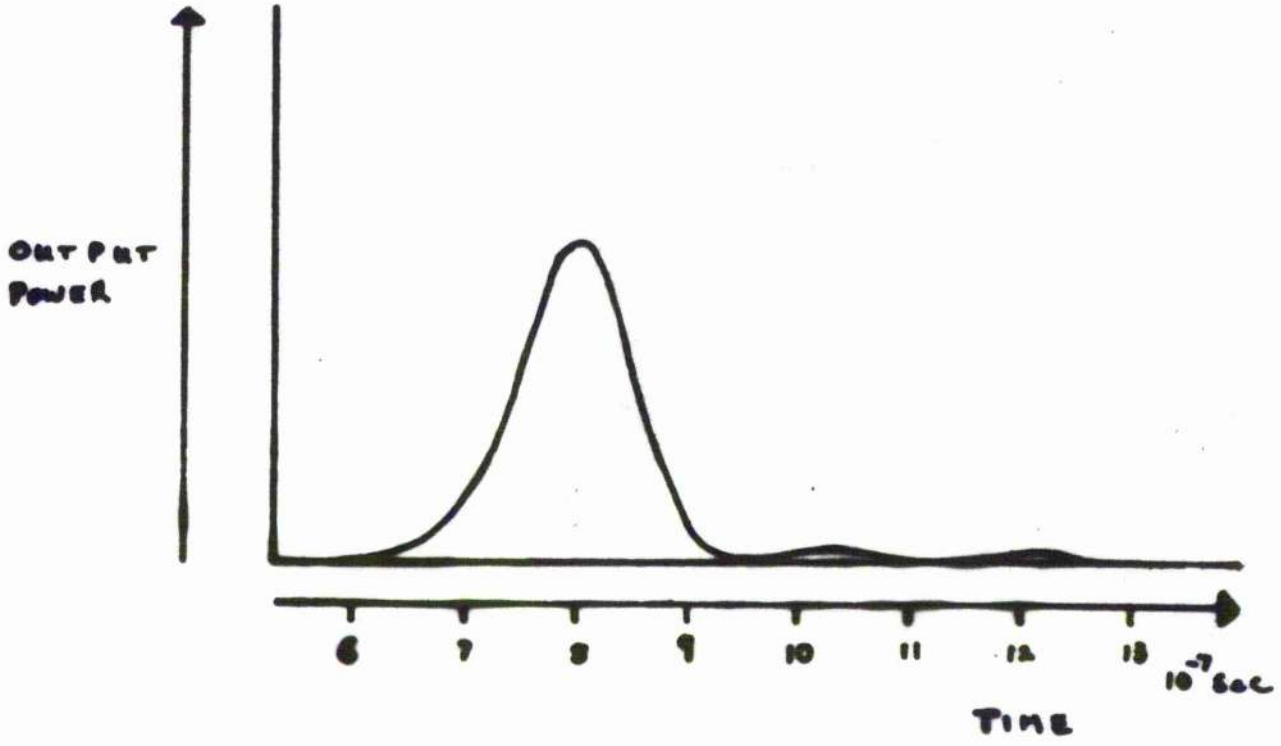

Calculated Oscillation Output for input data similar to

the above Recording.

Figure 4.12 Comparison of Experimental to Computed Oscillation Output Powers.

PARAMETER	CHESTER ET AL	CALCULATION
Q_L	6000	5000
γ		10^{-1}
$\triangle H_L$	0.5 gauss	
T_2		10^{-7} sec
T	$4.2^{o}K$	
$M_z(o)$	10^{18} spins	$5.0\ 10^{-4}$ gauss
β	$1.1\ 10^{6}$	$1.9\ 10^{6}$ sec^{-1}
T_I	5.010^{-6}	$8.0\ 10^{-7}$ sec
T_{Decay}	$9.0\ 10^{-7}$	$1.5\ 10^{-7}$ sec
MAX. CAVITY FIELD	$\sim$ 0.7	2.8 gauss
TOTAL ENERGY OUTPUT	$\sim$ 0.5	4.4 erg

[MATERIAL : NEUTRON IRRADIATED QUARTZ]

Table 4.4 Comparison of Observed and Computed Data

computed curve for nearly identical parameters. Detailed measurements from these curves are listed in Table 4.4: the maximum cavity field and the total output energy for the observed case have been computed from the maximum reported power of 10 mw assuming the microwave cavity to be operated close to match. The agreement of observed and computed data is within an order of magnitude.

Although the general agreement between observed and computed data is reasonably good, discrepancies occur. At the beginning of this study, it was realised that the mathematical model would only fit the physical situation loosely, so that now the question is raised, can the discrepancies be removed by a better choice of coefficients in Equation 4.10? For changes of coefficients to have any significance, only η or T_2 can be varied for these are not specified in detail by Chester.

From the general discussion in Section 4.7 on the effect of η and T_2 on the emission, it would seem that by utilising a smaller value of η or of T_2 in Equation 4.10, β, $(H_u^2 + H_v^2)$ and $\int_0^\infty (H_u^2 + H_v^2)dt$ would become smaller and T_1 larger so tending to reduce the discrepancies. There are, however, two opposing features of this favourable explanation. Firstly, a decrease in T_2 would weaken the strength of oscillation so that modulation of the solution would tend to disappear and, secondly, decreased T_2 would

shorten the decay time of the emission.

The difficulties of the comparison remain, therefore, by simple variation of the coefficients of Equation 4.10. It is necessary to look further into the properties of the paramagnetic transition used in the oscillator to obtain a possible explanation of the discrepancies of the comparison.

4.10 Inhomogeneously Broadened Line

Equations 4.10 were developed on the assumptions that the Bloch equations held for the maser material. This implies that the paramagnetic resonance line is homogeneously broadened and that a single spin-spin relaxation time applies. However, Chester reports that the maser material used in his work, neutron irradiated quartz, had a line width of 0.5 gauss whereas studies on the material by Weeks[54] show a line width of 0.1 gauss. The sample used by Chester seems, therefore, to be inhomogeneously broadened; this is generally the case for colour centres.

The problem of the maser oscillator has to be reconsidered and the presence of a distribution of spin packets taken into account. The broadening of the spin packets is characterised by a distribution function $g(\omega - \omega_o)$, normalised so that

$$\int_0^\infty g(\omega - \omega_o)d\omega = 1$$

which has an homogeneous inverse line width $T_2 = \pi g(0)$. The

homogeneous T_2 may be measured by spin-echo techniques[55] and may be typically of the order of microseconds for colour centres.

In the inhomogeneous case, the spin packets are assembled under the envelope of the distribution in local fields $h(\omega - \omega_o)$ a similarly normalised function, which has an inverse line width T_2^x, given here from measurements of the paramagnetic line width. The assembly may be written as

$$\int_o^\infty g(\omega - \omega')\ h(\omega' - \omega_o)d\omega'$$
$$= h(\omega - \omega_o) \int_o^\infty g(\omega - \omega')d\omega'$$
$$= h(\omega - \omega_o)$$

where $h(\omega' - \omega_o)$ is slowly varying compared to $g(\omega - \omega')$ in the region of ω'. It should be remembered that individual spin packets are essentially independent, each having a separate transition frequency and that energy is not easily transferred between packets.

If the bandwidth of the microwave cavity $\Delta\omega_c = \omega/Q_L$ is comparable with the overall width of the paramagnetic line $\Delta\omega_L = 2/T_2^x$, as is the case in Chester's work ($\Delta\omega_L = 2\ 10^7$ sec^{-1}, $\Delta\omega_c = 1.26\ 10^7$, $0.63\ 10^7$ sec^{-1} for $Q_L = 5\ 10^3$, 10^4 respectively), the greater proportion of the line will be able to undergo transitions during oscillation. The equation of motion of a single spin packet in the rotating frame is, therefore, from Equation 2.12

$$\dot{M}' = M'(j\Delta\omega - 1/T_2) - j|\gamma| M_z H' \qquad 4.20$$
$$\dot{M}_z = -|\gamma| \mathrm{Im}(M'^x H')$$

where $M' = M'(\Delta\omega, t)$, $M_z = M_z(\Delta\omega, t)$, $\Delta\omega$ being the departure of the Zeeman frequency from the line centre frequency, and $H' = H'(t)$ the total cavity field. The homogeneous line shape of the spin packets is included in Equation 4.20 but the equations may be simplified by considering the spin packet as a dela function, $1/T_2 = 0$. The oscillation condition thus implies that $T_r/2 < T_2^x$ and $T_r/2 < T_2$, the latter condition generally being satisfied because $T_2 > T_2^x$ for most inhomogeneously broadened lines.

The basic circuit equation, Equation 4.9, in the presence of an inhomogeneously broadened line becomes, therefore,

$$H' + \omega/2Q_L H' + 2\pi\omega\eta j \int_0^\infty M' h(\Delta\omega)\, d\omega = 0 \qquad 4.21$$

which gives the total cavity field in terms of the total magnetization $\int_0^\infty M'(\Delta\omega, t)\, h(\Delta\omega)\, d\omega$. The most common inhomogeneous line shape encountered is the Lorentz shape, $h(\Delta\omega) = T_2^x/\pi\,(1 + (\Delta\omega\, T_2^x)^2)^{-1}$ where T_2^x is defined in the general case by $(T_2^x)^{-2} = \int_0^\infty \Delta\omega^2\, g(\Delta\omega)\, d\omega$, which is the second moment of the spin distribution.

The integral in Equation 4.21 would seem at first sight to mean that the emission from each individual spin packet is superimposed to give the total cavity field. If this is so an approximate idea of the solution of Equations 4.20 and 4.21 can be obtained from data already computed. In the inhomogeneously broadened line the magnetization, and consequently T_r of each

packet is determined by the line shape function. Hence, for a spin packet with a particular T_r, the cavity field can be computed and assuming the frequency response of the cavity to be approximately uniform across the paramagnetic line, the cavity fields of all spin packets can be superimposed to give the total oscillator emission. Taking for instance the case $Q_L = 10^4$, $\eta = 10^{-1}$, $T_2 = 10^{-7}$ sec with peak magnetization $5\ 10^{-4}$ gauss, the line width can be divided into approximately six equal parts, see Figure 4.13, each part containing an equal number of spin packets. The computed curves for the emission of the six sub-lines are superimposed in Figure 4.13 and it is seen that although the incubation time still remains short, the emission has a slow decay. If a finer division of the linewidth were undertaken, essentially no modulation of the envelope occurs.

Reference to Equation 4.21 shows that this method of superimposition of individual solutions does not take into account the fact that the whole cavity field interacts with each individual spin packet; the ordering effect of the cavity field over all spins in the line is lost, therefore, in this approximate method of solution. The effect of the same driving field on all spins in the line would reduce inhomogeneous dephasing effects by keeping all spins 'in step', so that there would be a tendency of the spins to return to coherence periodically: H' would go through zero and the cavity power would be modulated to full depth. Kemp[56] has

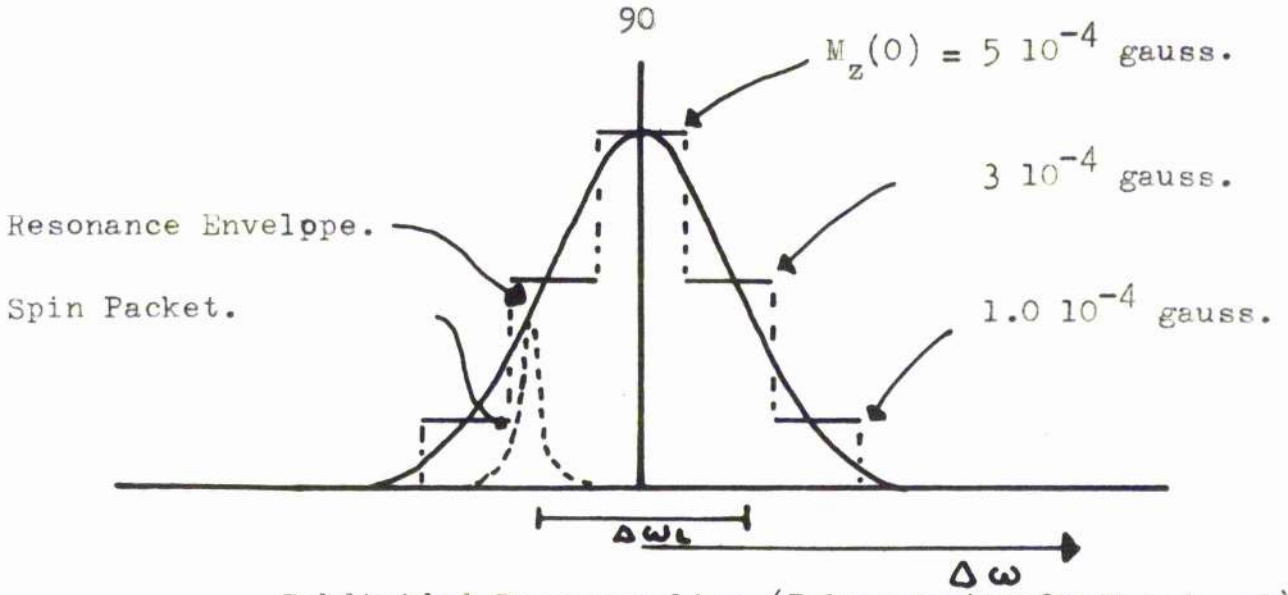

Subdivided Resonace Line (Inhomogeniously Broadened)

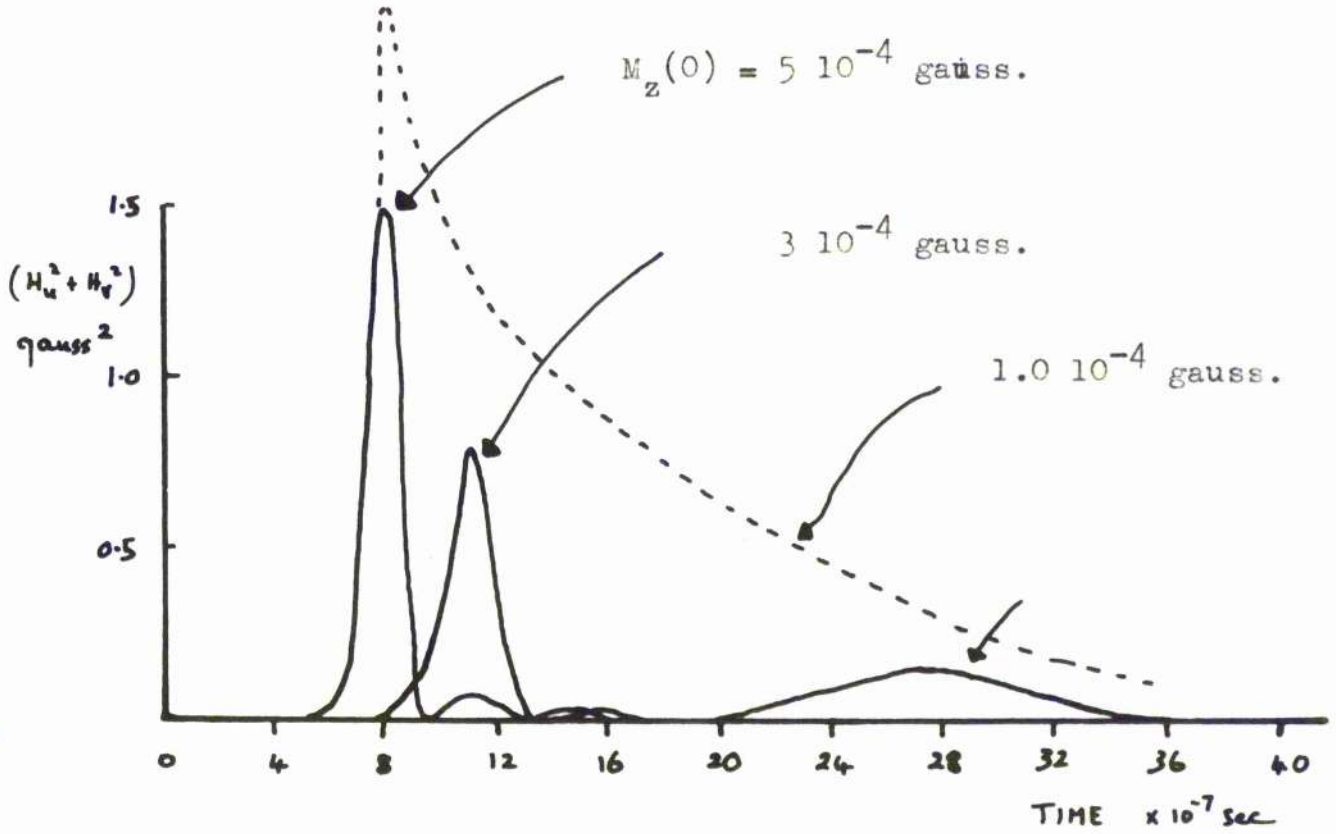

Computer Emission for Subdivisions of Resonance Line.

Figure 4.13 Superposition of Computed Emission for Division of Spin Resonance Line.

treated this problem analytically and has shown this type of coherence to be present. Kemp also suggests that a judicious choice of T_r and T_2^x should allow theoretical solutions of the general equations of motion to be adjusted to fit observed wave forms. The findings of the present study are consistent with this suggestion.

4.11 Pulsed-Field Maser

Equations describing the field-swept maser oscillator can be developed from Equations 4.20 and 4.21 by replacing the term $\Delta\omega$ by $(\Delta\omega + \Delta\omega_s)$ where $\Delta\omega_s$ is time varying and represents the difference between the cavity frequency and the Zeeman frequency so allowing variation of the magnetic field to be present in the problem. In connection with the solution of the field-swept maser equations, reference is made to the work carried out by Kemp[30]. A few comments on the operation of the pulsed-field maser[28], a limiting case of the field-swept type, based upon the findings of the present study are, however, in order.

In the pulsed-field maser (two-level scheme) the spin system is activated at one frequency (X-band) and the magnetic field is then immediately pulsed to a high value. As the Zeeman frequency is swept through the higher resonant modes of the cavity, maser oscillation may occur if the cavity radiation field of one mode can grow sufficiently.

The cavity field will grow, where maser oscillation conditions are satisfied, when the Zeeman frequency of the wing of the spin distribution coincides with the cavity frequency. As the sweep progresses, the cavity field will continue to increase under maser action but as the sweep of the line through the cavity mode is completed maser action ceases and the cavity field decays. The oscillation pulse duration would seem, therefore, to be determined by the time of sweep through the resonance line. If the sweep time is less than the incubation time of the maser oscillator operating in that particular mode, oscillations are clearly inhibited. This consideration fixes an upper limit to the rate of field sweep through the resonance line (see Chapter 8).

In order to be sure of obtaining maser oscillations in the practical pulsed-field maser, the incubation time should be as short as possible so that the rate of field sweep is not too critical. Reference to Section 4.7 shows that an increase in any of Q_L, η, N_o, T_2 will decrease T_r, and so T_I giving a more favourable situation for oscillations at the higher frequency. Experimentally, of these parameters, η is probably the most easily increased so that as a general rule, η should be as close to unity as is possible.

CHAPTER 5

EXPERIMENTAL APPARATUS

5.1 Equipment Layout

Four frontal views of the equipment used in the experimental studies are shown in Figures 5.1, 5.2, 5.3 and 5.4. The electromagnet, in many ways the heart of the apparatus, seen in Figure 5.1, is mounted on rails which run the length of the E.S.R. laboratory. The stabilized current for the magnet is supplied by the large power supply to the right of the magnet in Figure 5.2. The cryostat is mounted centrally above the rails at a height to clear the magnet yoke, and to the right of the cryostat, in Figure 5.1, the helium gas return valves are mounted together with manometers for monitoring the cryostat pressure: the gas valves are separated from the rest of the apparatus for ease and speed of operation. To the immediate left of the cryostat head, Figure 5.1, is placed the power amplifier used to drive the magnetic field-sweep coils.

The waveguide from the cryostat head is coupled to the main waveguide system; this is mounted on a table under which the electronic racks are placed. The microwave system is shown in detail in Figure 5.3. In this photograph, the power klystron (Varian X-13) is seen near the front edge of the table area and the local oscillator and monitor klystron (English Electric K.311's) are seen in the centre and at the right edge of the table respectively.

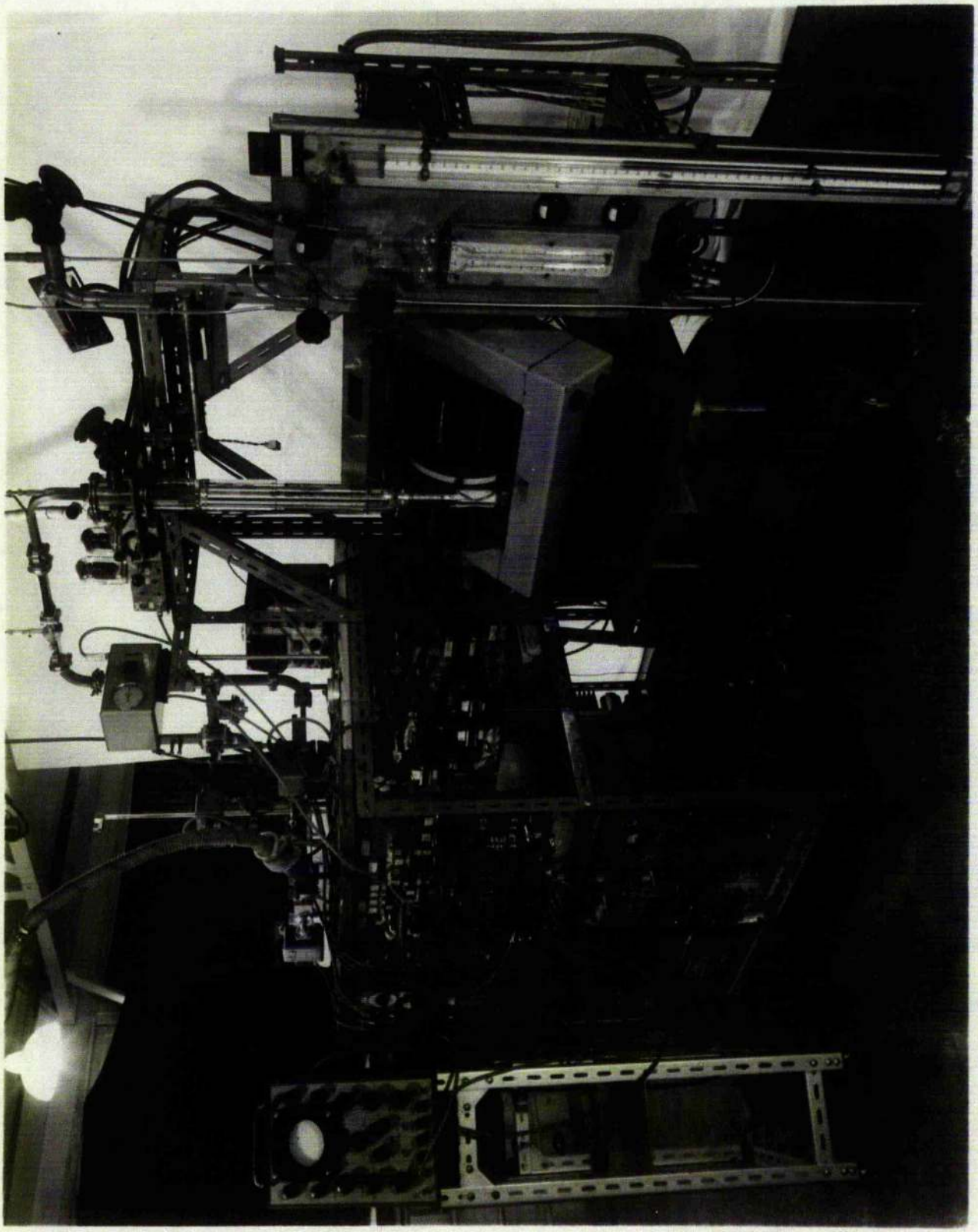

Figure 5.1 View of the Apparatus from the Right

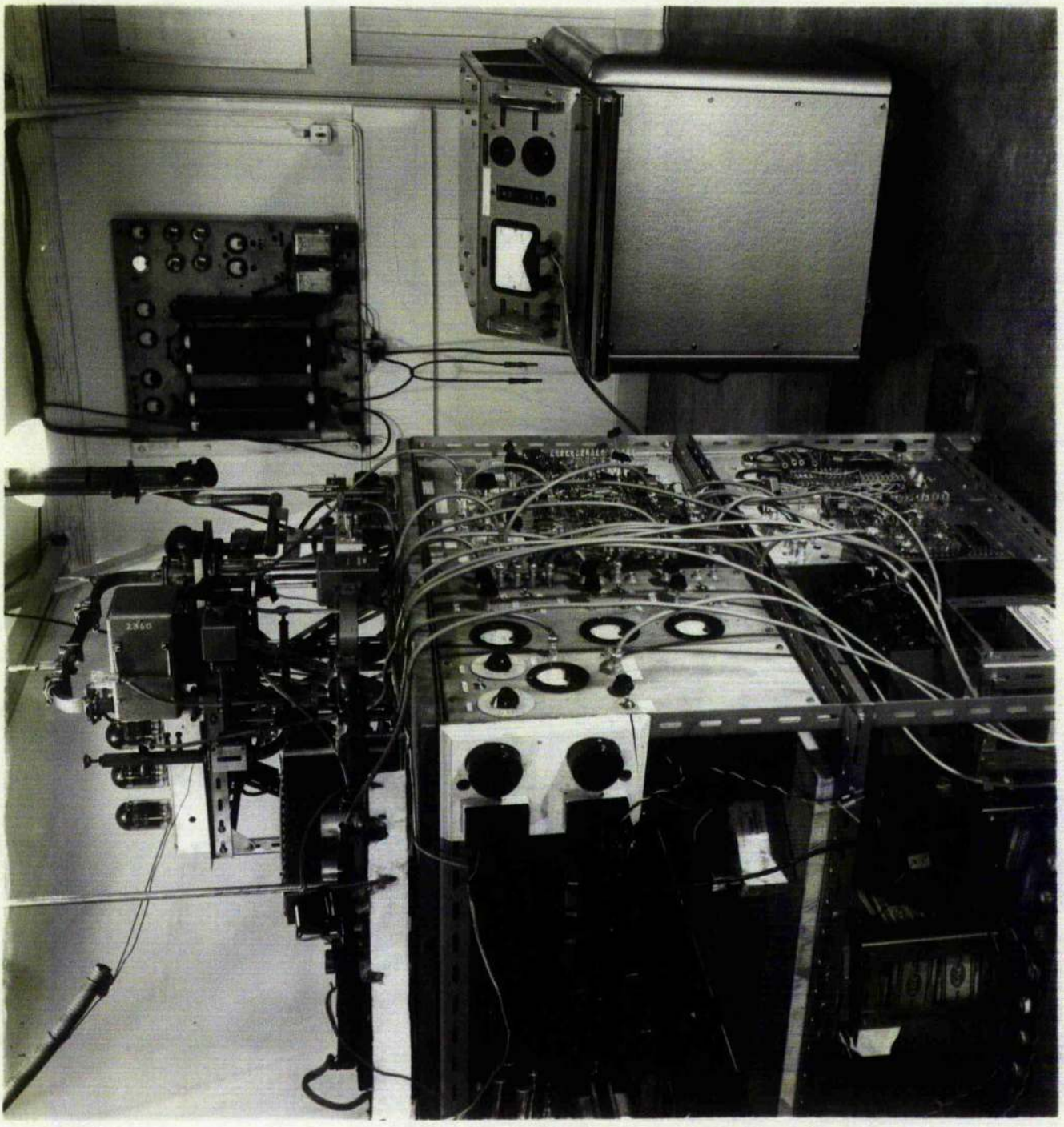

Figure 5.2 View of the Apparatus from the Left
The electronic racks are in the foreground
and to the right is the Magnet Power
Supply Unit

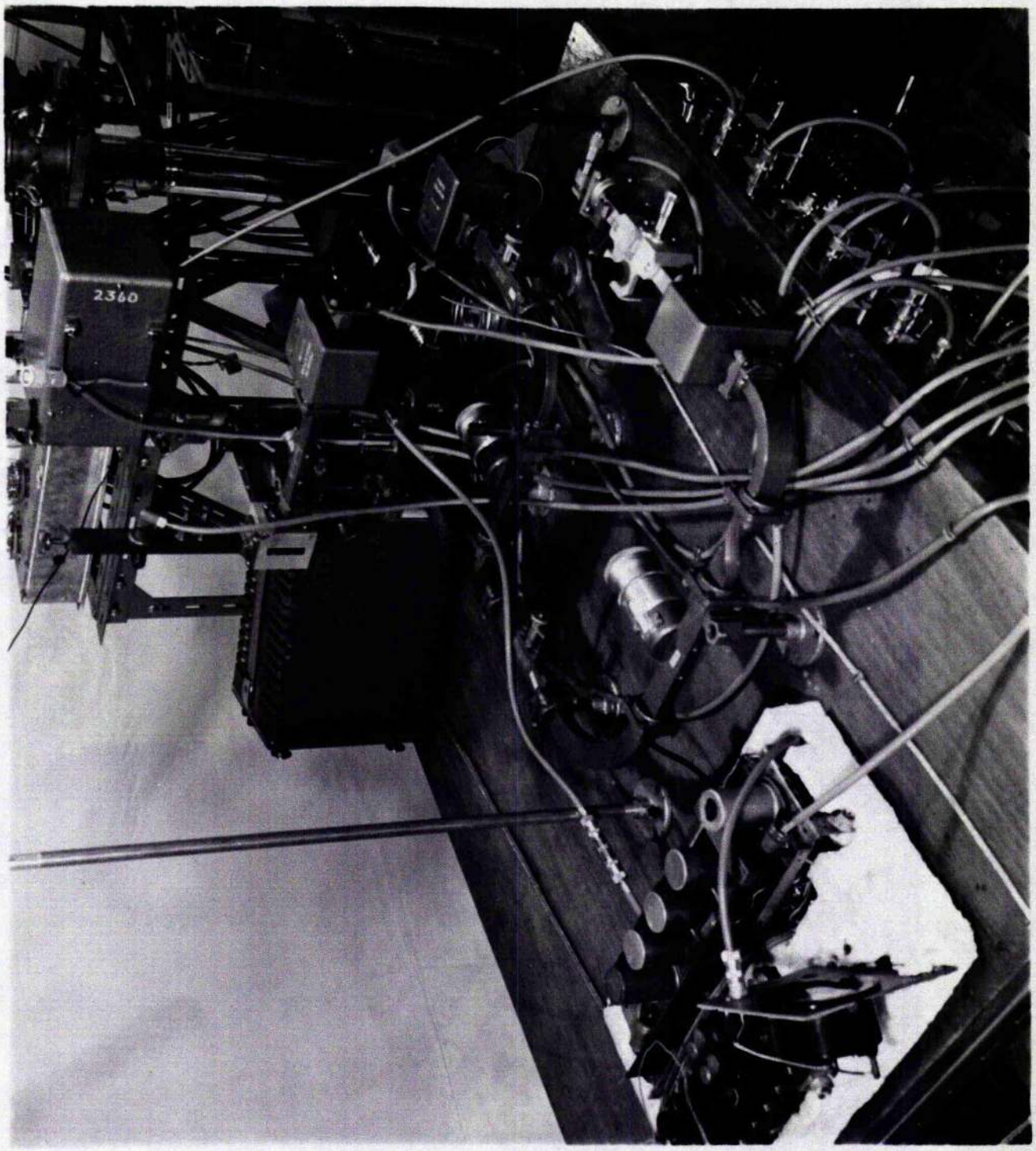

Figure 5.3 View of the Apparatus from the Left

The microwave circuit is shown in detail

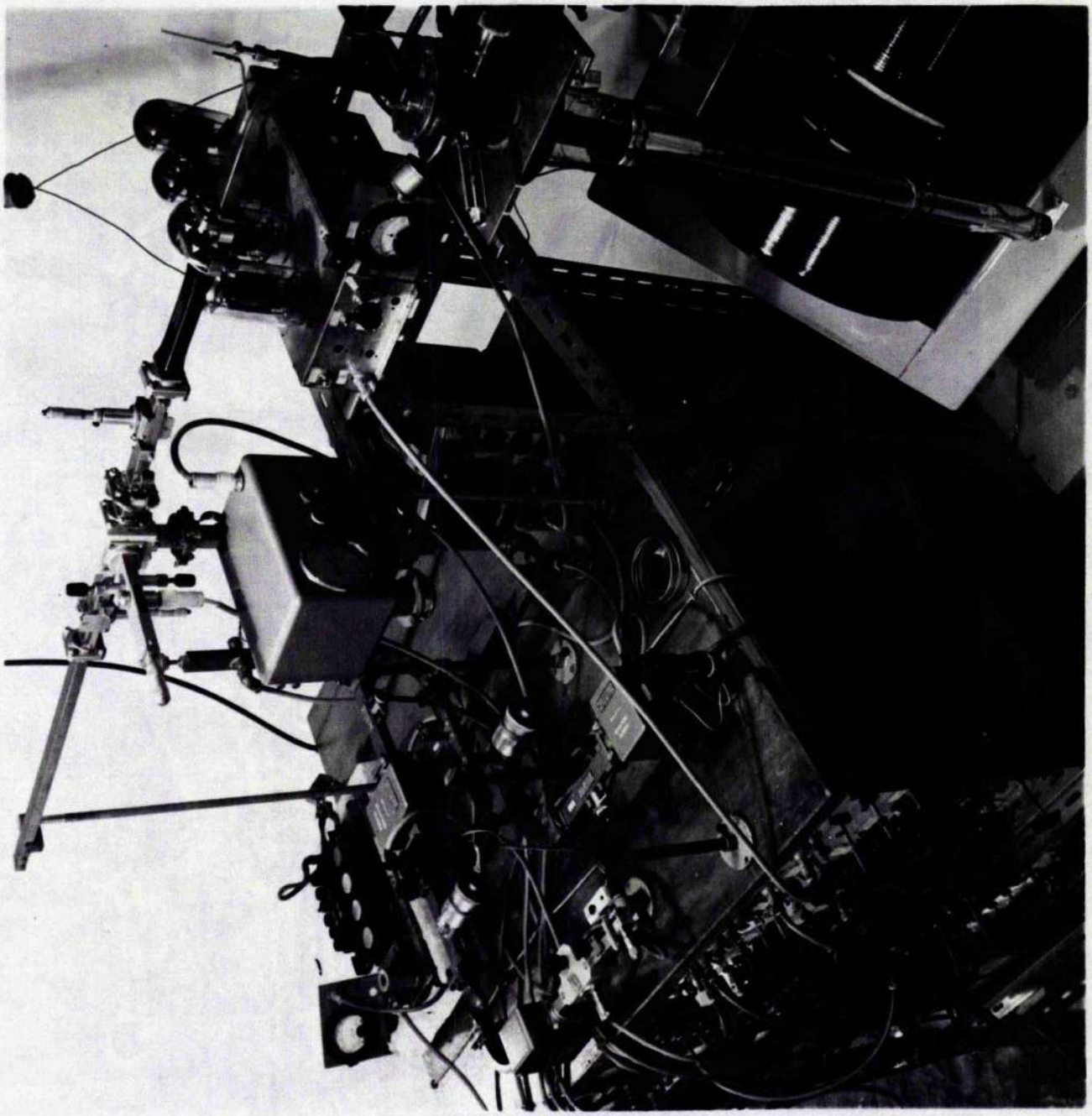

Figure 5.4 View of the Apparatus from the Right

The additional bridge for Q measurements

is shown

A ferrite, three-port circulator is incorporated in the microwave system, background of Figure 5.3, and the receiving arm of the circulator directs reflected power from the cavity to a magic-tee mixer and crystal detectors, upper portion of Figure 5.3: directly above the circulator is the wavemeter and the I.F. amplifier of the detection system is also seen in the foreground of this Figure. In Figure 5.4 the additional tee bridge required for cavity Q measurements is shown in place: the bridge is inserted in place of an E-plane bend in the transmission arm of the circulator of Figure 5.1.

The electronic racks in the foreground of Figure 5.2 are fed by power supplies placed in a similar position to the rear of the apparatus; klystron control panels are placed to the left of the electronic racks. Oscilloscopes used for display and recording are mounted on trolleys and are used in the space in front of the apparatus.

5.2. Design Considerations : General Instrumental Problems

The general design of the apparatus follows the lines already described by Campbell[8]. Many alterations to the original apparatus were incorporated when the apparatus was rebuilt during removal to the present E.S.R. laboratory and the design has been further developed on lines necessary for the present maser studies. In this chapter the equipment will be described and new developments

will be described, but first the general design criterion for the two-level maser will be reviewed.

The programme of maser investigations has been carried out using the F-centre line of neutron-irradiated MgO. Details of this material and the reasons for its choice for these studies are given in Chapter 6. It is concluded from the discussion in Chapter 3 that prior knowledge of T_1 and H_L is required before the design of a maser can proceed. The likely values of these parameters for any sample of neutron-irradiated MgO are $T_1 = 4$ msec and $H_L = 0.7 - 1.8$ gauss[8,47,57]. These figures determine, therefore, the rate of field or frequency sweep in A.F.P. inversion and the cycling rate for maser operation. The choice of technique to be used for activation of the maser sample is limited to A.F.P. by field sweep or A.F.P. by frequency sweep in the presence of some field inhomogeneity because the development of a Q-switch[47] is not sufficiently advanced to be easily incorporated into the apparatus. Both of these methods of activation have been achieved and will be discussed in Chapters 7 and 8.

Before proceeding to a detailed description of the apparatus a few remarks will be made on the general problems encountered with particular equipment. The stability of the magnetic field is established by a high stability current power supply. Hysteresis in the iron yoke is present, of course, making

it impossible to return the field to a previously adjusted value, after having changed the field by some large amount, by merely adjusting the magnet current to its former value. This is not too troublesome because the field is generally adjusted by observing the oscilloscope display of the phenomenon under study, but it implies that a calibration of the field with current is only rough. Precise measurements of the magnetic field have been carried out by an N.M.R. magnetometer.

A difficulty arises in the frequency stability of the klystrons but here the requirements on stability are only stringent when the apparatus is operated as an E.S.R. spectrometer. As the primary design is for transient spin resonance experiments, stability is only required for short durations: no electronic stabilisation has, therefore, been employed.

The eddy currents induced in the magnet pole tips and the microwave cavity, by rapid variations of the applied field present other problems. Eddy currents in the pole tips and the cavity react on the sweep coils, through Lenz's law, opposing the variation of the field, while the heating effects in the cavity may cause local raising of the helium bath temperature and, furthermore, curtail the length of an experimental helium run. These problems are discussed further in this chapter.

Lastly, cryogenic problems may be mentioned. All experiments have been carried out in the range 4.2°K - 1.5°K and for simplicity of cavity design, liquid helium has been allowed to fill the cavity and the associated cryostat waveguide section. The change in the cavity frequency upon cooling to this temperature is due mainly to the dielectric effect of helium in the cavity[58]; this change must be taken into account in the cavity design. Random bubbling in the cavity has not proved troublesome but, in general, the effect is absent because operation is mainly below the λ point.

5.3 The Magnet System

The magnet used in these studies is a Newport magnet, Type 'E', with plane pole tips, designed by the E.S.R. group of this department; a detailed description has already been given by I.M. Brown[59] who was partly instrumental in its design. The magnet is of low impedance and is air cooled: the pole diameter is 7", pole gap 5.85 cms, with parallelism of the pole tips better than 0.004". Two sweep coils are mounted for 50 cs field modulation.

The stabilized current for the magnet is provided by a Newport Magnet Power Supply Unit Type 'B' (Mark 2). In this unit the current is stabilized by a feedback amplifier which controls a saturable core reactor and additional stability is given by a mains stabilized transformer. Working into the Type 'E'

magnet, the following performance data is specified:-

Mean output current stability : 1 part in 10^4

Field ripple : 0.5 gauss

Overall time constant of unit : 0.2 sec.

The stability has been satisfactory in all the experiments, but the field ripple proved troublesome in transient resonance experiments. For example, with a repetitive linear field sweep through a paramagnetic resonance line, the exact time of sweep through the line centre shows random fluctuations because the magnetic field is constant in time to only $\pm$ 0.25 gauss.

An N.M.R. magnetometer has been built to measure the magnetic field, and has been used to plot the field homogeneity of the electromagnet. The circuit of the magnetometer is that proposed by Lowe[60] and is shown in Figure 5.5, the inset showing a diagram of the field probe. The basic circuit is a Hopkins autodyne, modified to give greater amplitude stability at very low levels by means of a feedback loop, and the unit acts as a marginal oscillator detector for N.M.R. absorption signals. The oscillator has a high af gain and its output is further amplified and displayed. The unit is shown in Figure 5.6.

The specimen coil is mounted at the end of a probe, a length of brass piping, and the dimensions of the coil have been kept as small as possible, consistent with the requirements for coil inductance and high coil Q. The use of glycerine, of

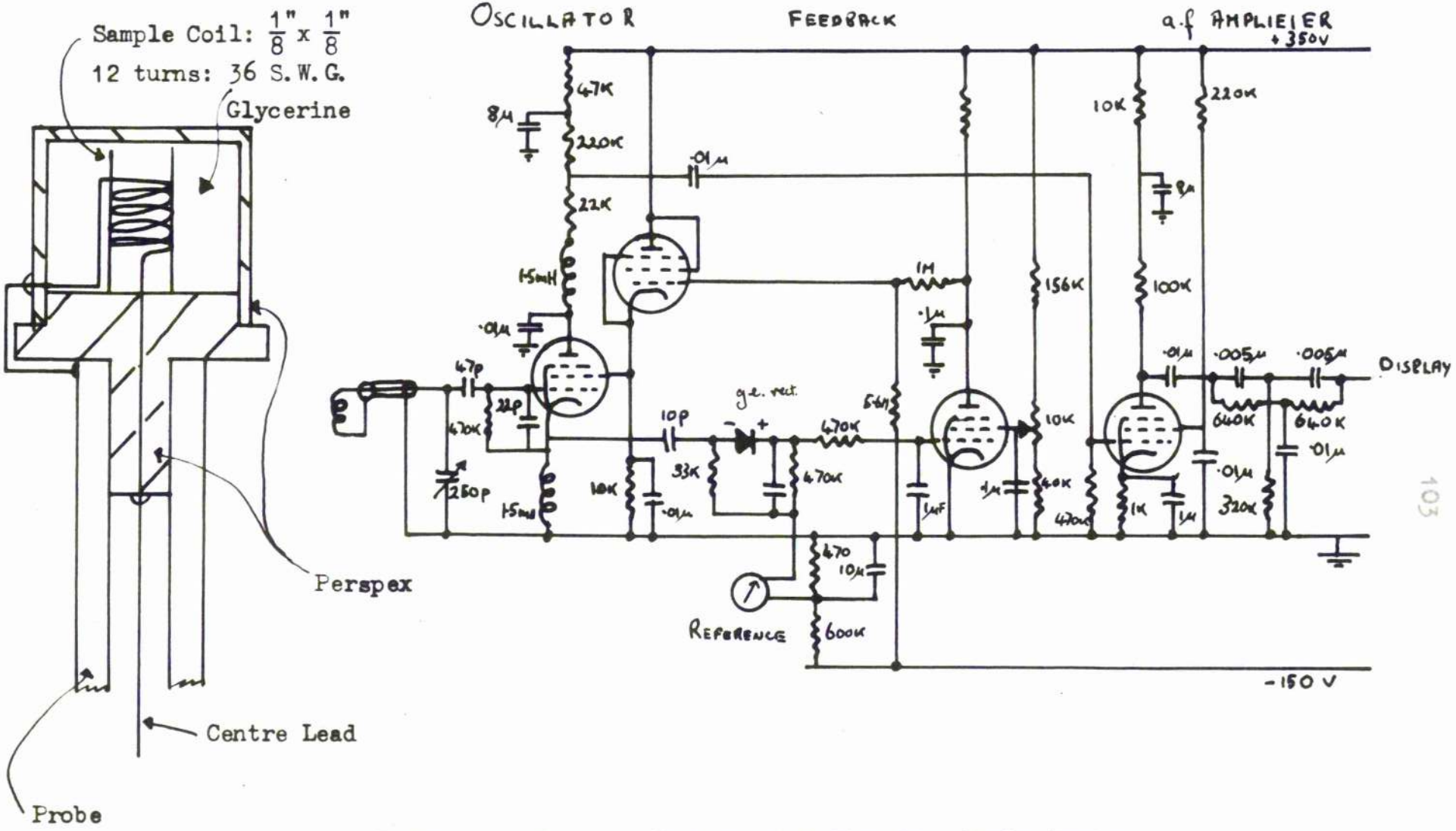

Figure 5.5 Magnetometer Circuit : Probe Design.

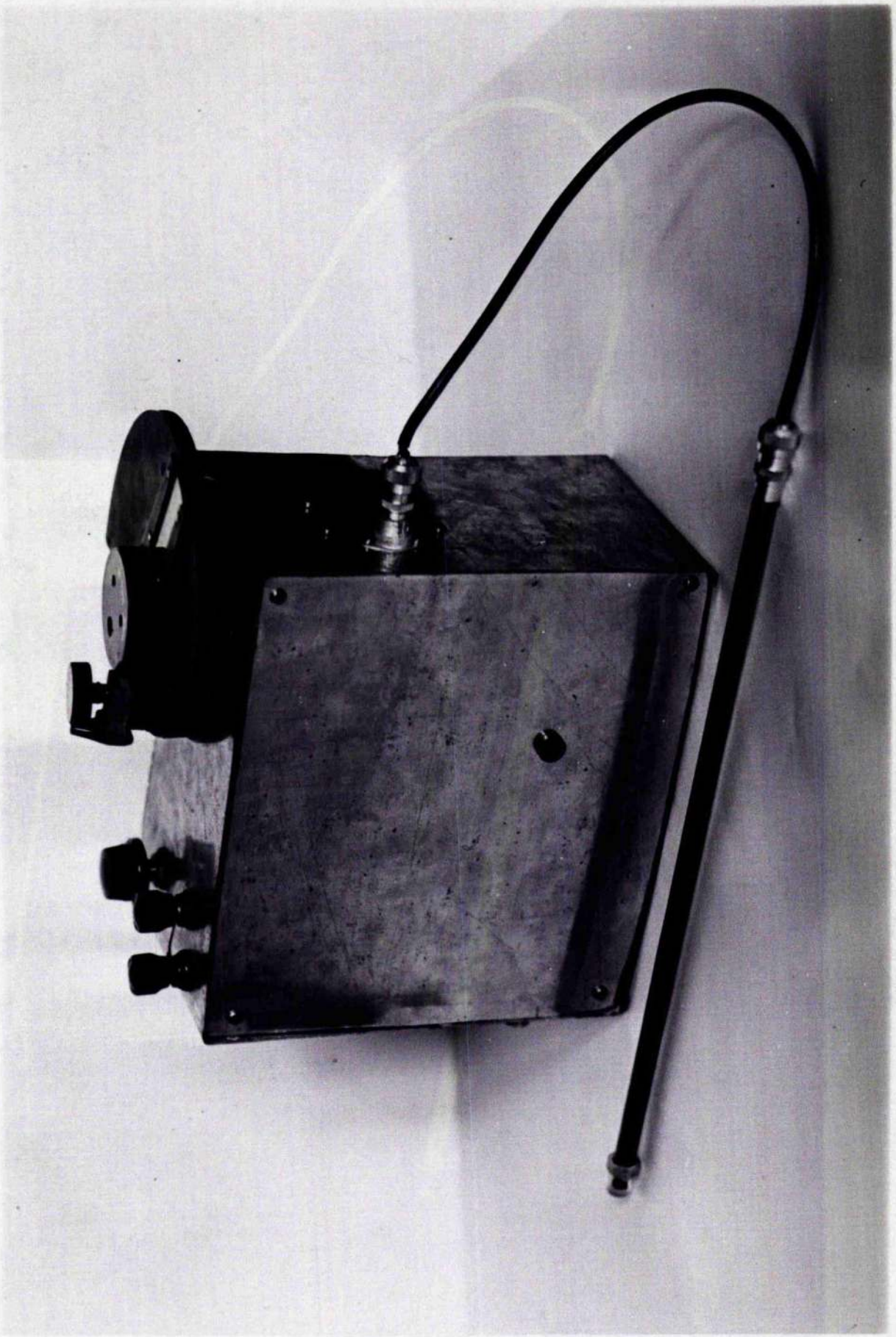

Figure 5.6 Photograph of N.M.R. Magnetometer

low dielectric loss, permits complete immersion of the coil in a cup of the liquid, Figure 5.5. Connections to the coil are made by using the probe as the outer sheath of a coaxial cable, the inner lead being an insulated wire stretched along the axis of the probe. The coil had dimensions $\frac{1}{8}$" x $\frac{1}{8}$" and covered the range 9.0 - 17.0 Mcs or 2100 - 4000 gauss.

Measurement of the magnetic field is carried out by sweeping the field through $\sim$ 5 gauss at 50 cs and tuning the oscillator frequency until resonance absorption of the protons is displayed. The frequency is adjusted to the steady field valve by displaying the resonance absorption with a 50 cs sweep applied to the X-plates of the oscilloscope, phase shifted by about 90° so that the two displayed absorption peaks are superimposed, and centering the absorption peak in the trace. The oscillator frequency is measured by a frequency meter (BCC.21), loosely coupled to the oscillator: the field is given by $\omega = \gamma_p H_o$ where γ_p is the magnetogyric ratio for protons. The accuracy of field measurements is determined largely by the accuracy of the frequency measurement which can be read to $\pm$ 0.5 kcs ($\simeq \pm$ 0.15 gauss). One criticism of the magnetometer is the large microphonic noise content in the output. This could have been almost completely avoided by building the unit into a more sturdy metal box.

Field measurements have been carried out on the magnet in

planes orthogonal and parallel to the field direction; field plots are shown in Figure 5.7. In the largest sample used in these studies, a disc of radius 8.75 mm, the maximum field variation over the sample is about 0.1 gauss. A field stability check has been carried out over a long period of time and the findings indicated that the stability is not better than the specified figure of 1 part in 10^4.

5.4 Electronic Circuits

The voltage waveforms required for the operation of the two-level maser will be discussed before the electronic circuits are considered. In one cycle of operation, the time sequence of the necessary waveforms for the cases of inversion by A.F.P. field and frequency sweep is shown in Figure 5.8: the microwave power and magnetic field modulation are also indicated in this Figure. The following remarks are to be considered with reference to Section 3.2 and also the block diagram of the electronic circuits in Figure 5.9.

Considering first the case of maser operation where the spin system is activated by A.F.P. field sweep, the cycle of operation is repetitive and the waveforms are timed and triggered by a free running multivibrator of variable cycling rate. The minimum period of this multivibrator is fixed at 2.1 msec, slightly less than T_1 for the colour centres of MgO, and the maximum period is 0.4 sec which will ensure complete thermalisation of the

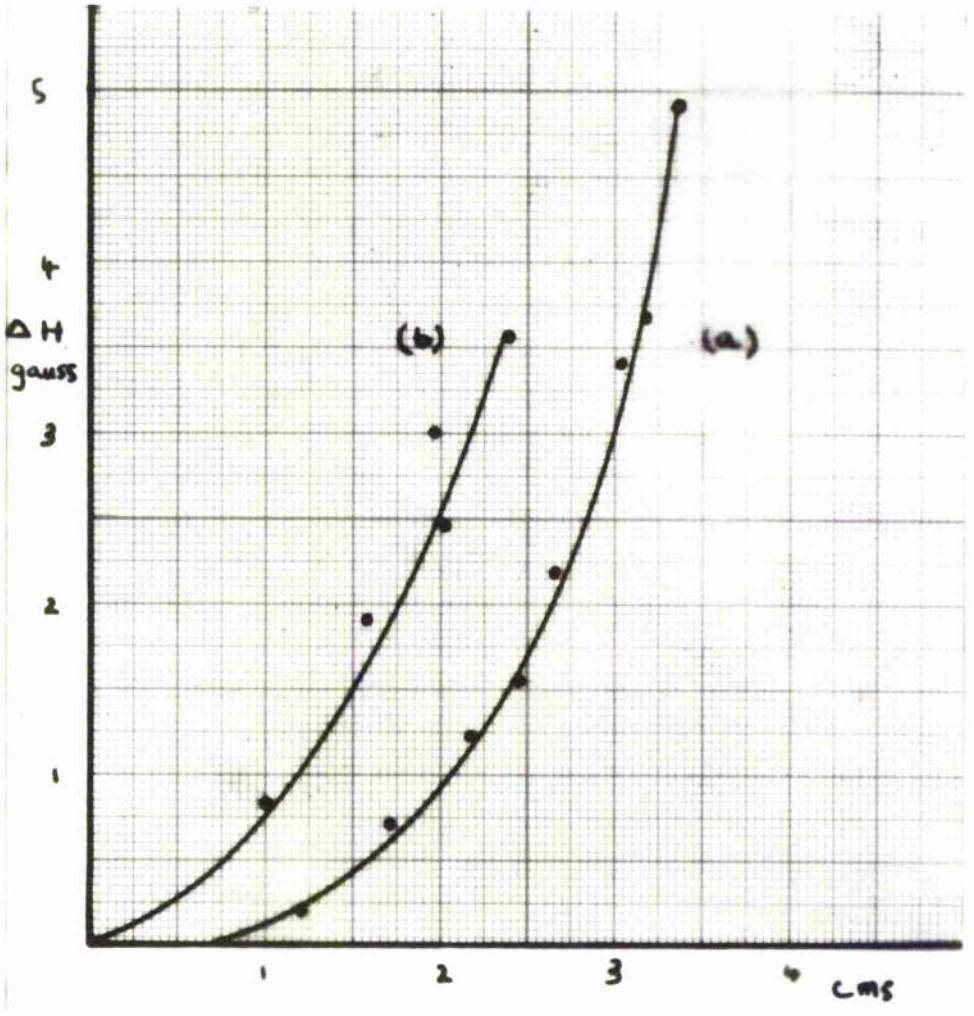

Figure 5.7 Field Plot of the Type E Magnet.
(a) Orthogonal to the field axis.
(b) Parallel to the field axis.

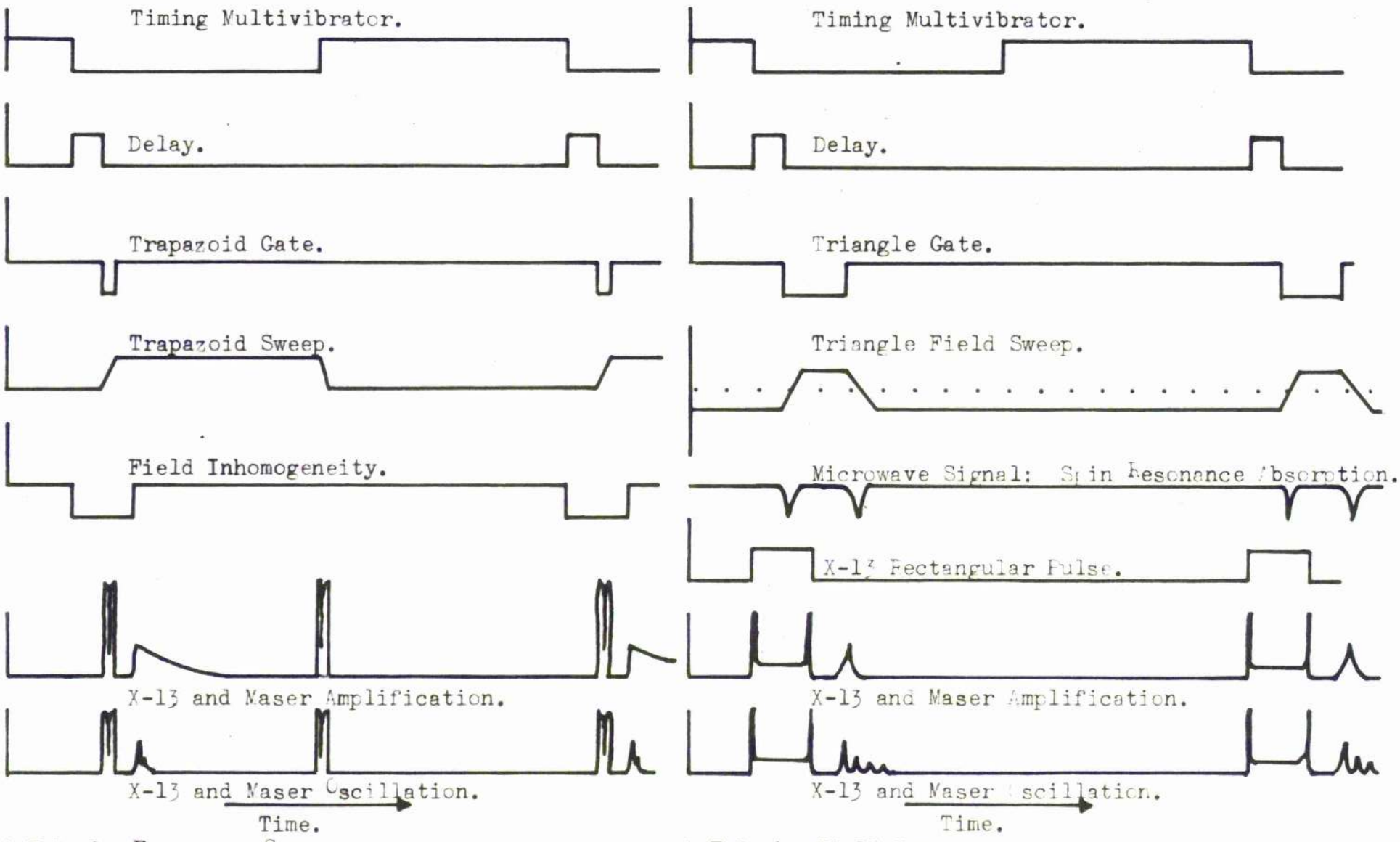

Figure 5.8 Time Sequence of A.F.P. Inversion and Maser Action.

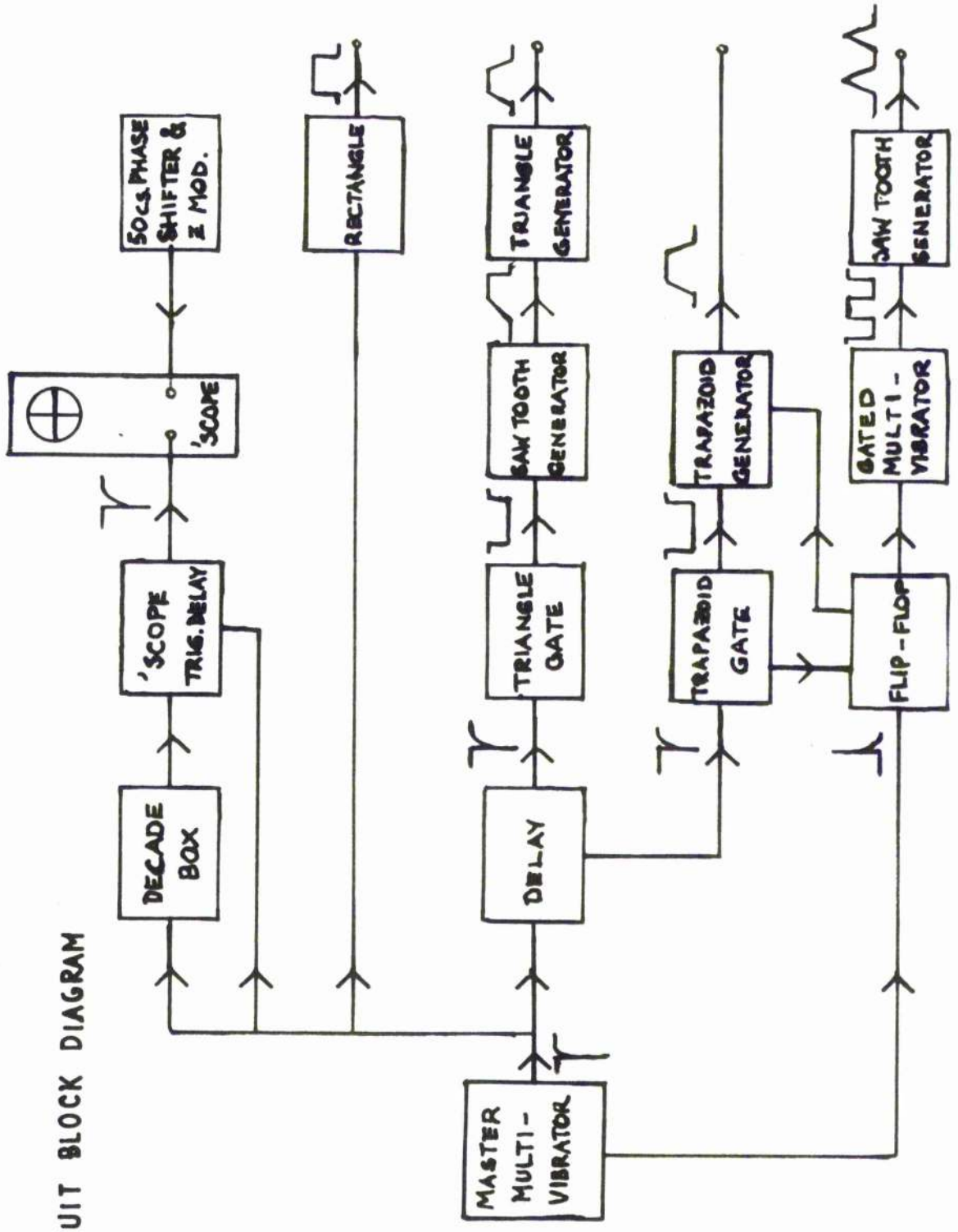

Figure 5.9 Pulse Circuit Block Diagram.

spin system at the end of each cycle. In inversion, the power klystron (Varian X-13) is momentarily tuned electronically to the cavity resonant frequency by applying a rectangular waveform to the reflector which takes the klystron from a biased position outside the $3\frac{3}{4}$ mode to the peak of the $3\frac{3}{4}$ mode, which is mechanically tuned to the microwave cavity frequency. After a short delay, but while the X-13 is tuned to the cavity, the magnetic field is swept through the paramagnetic resonance line from a position biased below resonance. The sweep is executed by applying a triangular waveform to the power amplifier that drives the field sweep coils. The rate of sweep on the first slope is such that the resonance line is traversed in a few microseconds, being the condition requisite for A.F.P. when T_1 = 4.0 msec. On the second sweep, the emissive or absorptive state of the spin system is monitored by a low power signal from the monitor klystron, and in this way transient decay of the spin system from an excited state to the thermal equilibrium can be observed by delaying the second sweep to later times.

When the spin system is activated by A.F.P. frequency sweep, the X-13 klystron is swept through the $3\frac{3}{4}$ mode from a quiescent point on the high frequency side of the mode by applying a trapezoid waveform to the reflector to be extinguished on the other side. The trapezoid is triggered by the same time delay as above. Half way through the cycle of the multivibrator, well after the maser cycle

has finished, the X-13 is returned to its quiescent point. To accomplish inversion by this means, a field inhomogeneity is introduced by the sweep coils by applying a rectangular pulse to the power amplifier for the duration of the X-13 sweep. After the inhomogeneity is removed, maser action, i.e. amplification or oscillation, can commence. The state of the spin system after inversion can be monitored in two ways, (1) by constant monitor klystron power and (2) by sweeping the monitor klystron through its mode repeatedly, by applying a sawtooth waveform to its reflector. Either method gives the transient relaxation to thermal equilibrium.

The delay introduced into the cycle of operation, described above, ensures that any initial transients caused by the application of the rectangular waveform to either the X-13 or the power amplifier have died away before field sweep, or frequency sweep, is commenced respectively.

The electronic circuits of the block diagram of Figure 5.9 are shown in Figures 5.10, 5.11, 5.12 and in Figure 5.13, oscillograms of the waveforms generated by these circuits are shown. The timing multivibrator, based on Valve 1 (V1) has twelve cycling rates between 2.5 cs and 480 cs by means of a switched condenser bank. The multivibrator triggers a rectangle pulse generator (V6, V2) and a one-shot multivibrator (V8) which introduces a trigger delay

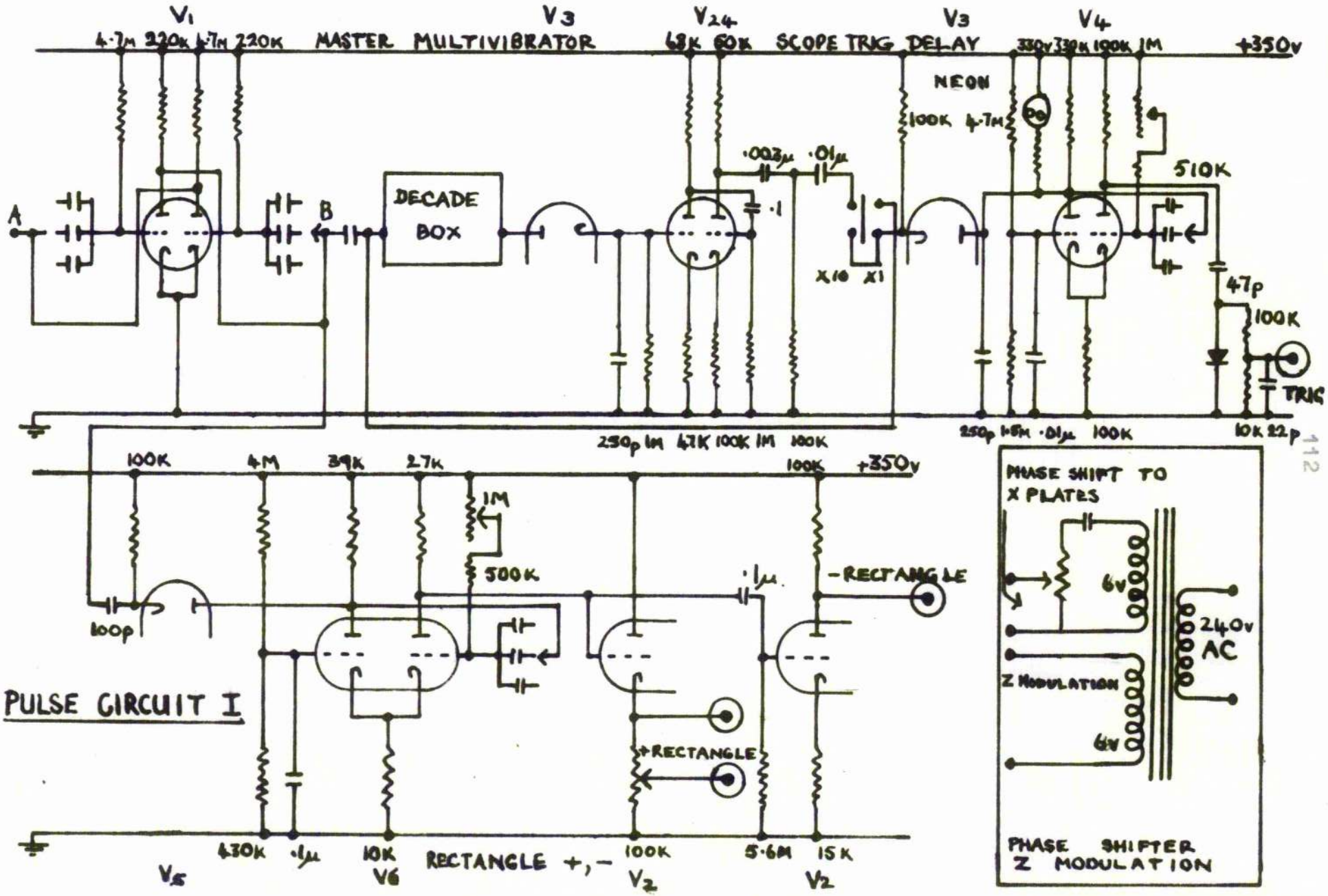

Figure 5.10 Pulse Circuit I.

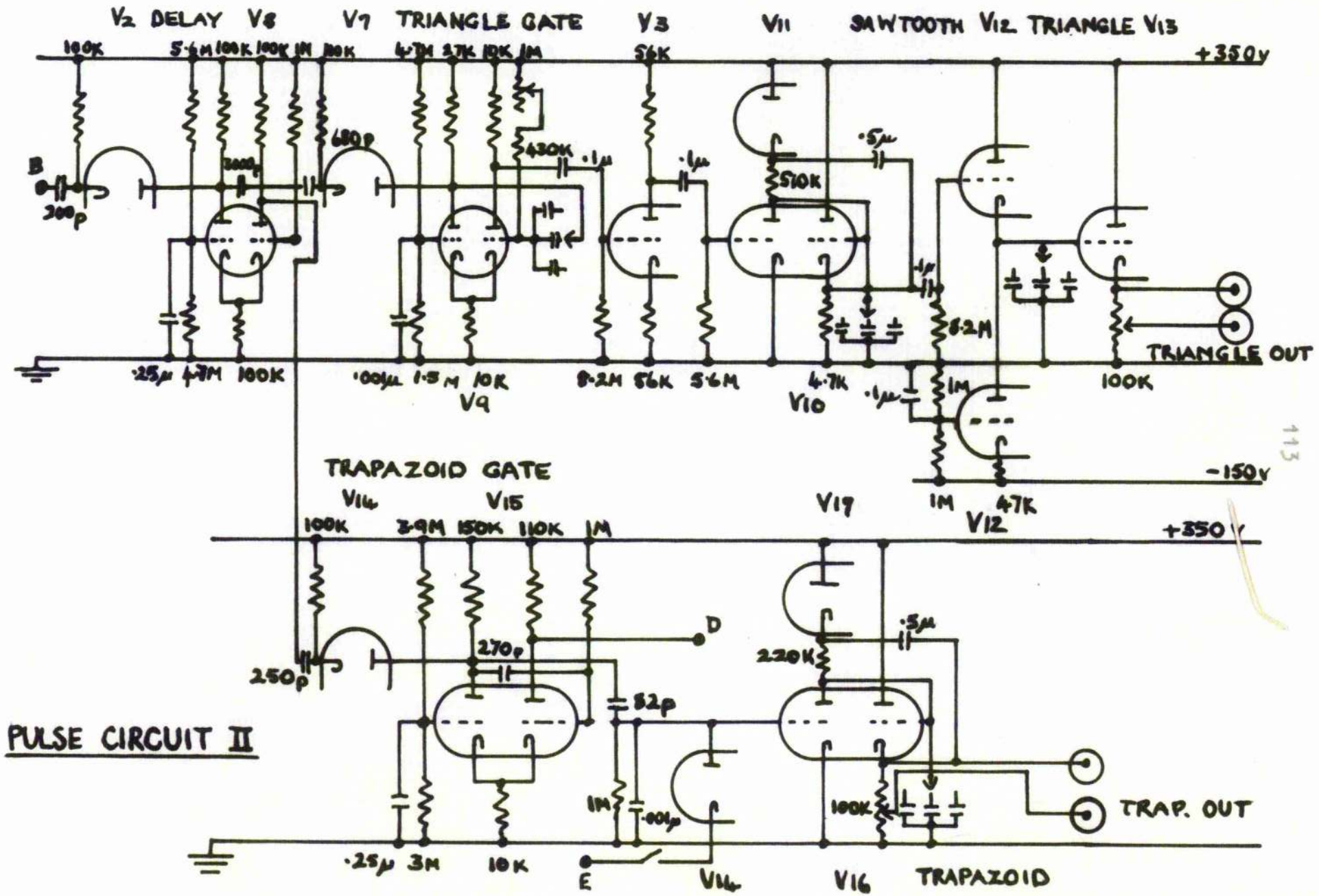

Figure 5.11 Pulse Circuit II.

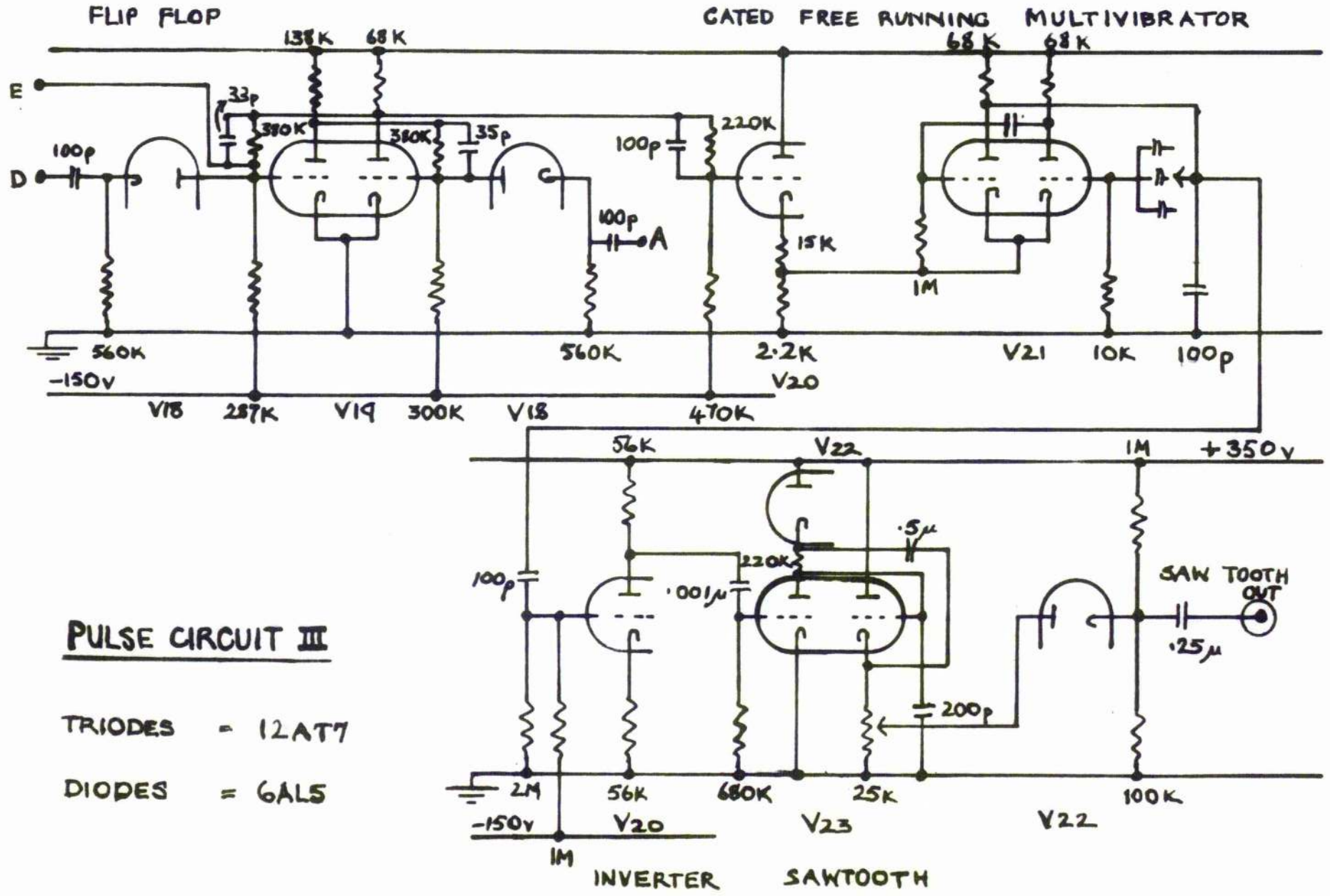

Figure 5.12 Pulse Circuit III.

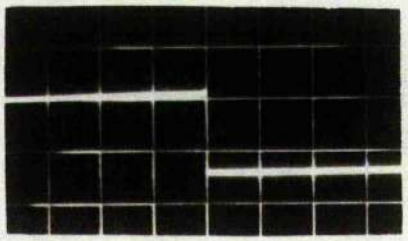

100 v

0.2 msec

Rectangle

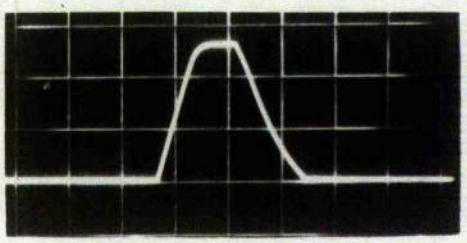

100 v

0.2 msec

Trapazoid

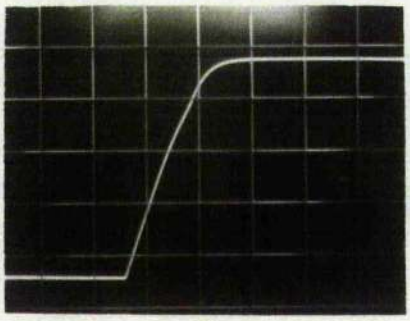

20 v

0.1 msec

Trapazoid, no return

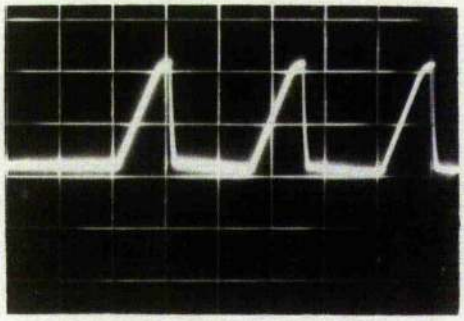

100 v

0.6 msec

Repetitive Sawtooth

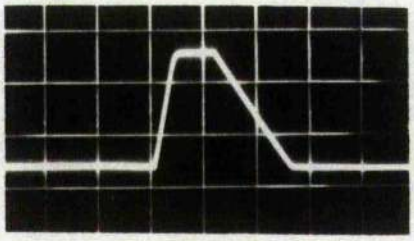

100 v

0.2 msec

Triangle

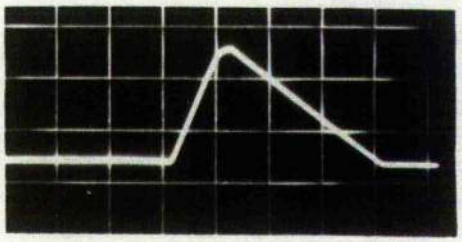

100 v

0.2 msec

Triangle

Figure 5.13 Series of Waveforms

of 600 μsec to the other waveforms. The positive rectangle from V6 is fed to the cathode follower clipper (V2) from which an essentially rectangular pulse of 170 volts of variable duration (0.4 - 1.2 msec) is obtained. In A.F.P. field sweep this pulse is applied to the X-13 reflector, and in frequency sweep the rectangle drives the power amplifier.

The triangle waveform is triggered by the delay circuit (V8). The triangle gate (V9) determines the time between the first and second slopes and is variable from 0.1 msec to 9 msec. The positive going gate of V9 is used because it is of better form, and after inversion at V13 is applied to the grid of a bootstrap sweep generator (V10, V11) which gives the linear first slope of the triangle, and a sharp second slope. This waveform is fed directly to the second slope generator (V12), which passes the first slope unimpeded, it being slowly varying, but as V12 (upper) is cut-off by the sharp second slope, the condenser between the cathode of this valve and ground, charged during the conduction period, discharges through the constant current tube (V12 lower). The discharge is essentially linear, giving a linear second sweep to the triangle waveform. The sweep is finally available from the cathode follower (V13). Each slope is variable in twelve steps with slopes in the ranges: first slope, $1.3\ 10^6$ to $9.0\ 10^6$ volts sec^{-1}; second slope, $1.6\ 10^4$ to $1.8\ 10^7$ volts sec^{-1}, the maximum output being 150 volts.

A general purpose waveform, the trapazoid, is generated by the bootstrap sweep generator with fixed gating time based on V15, V16 and V17. This waveform is used to sweep the X-13 repetitively through its mode, so as to display the power reflected from the cavity in experimental tests (See Section 5.6). Under the conditions of A.F.P. frequency sweep, the return sweep of the trapazoid is delayed until halfway through the timing cycle by introducing the clamping diode (V14). With this diode switched into the circuit, the grid of V16 is pulled down below cut-off whenever the bistable flip-flop (V18, V19) is triggered by the trapazoid gate. The flip-flop reverts to its initial state by a trigger from the timing multivibrator (V1) which occurs half way through the cycle. The first slope of the trapazoid is variable.

The bistable flip-flop also gates on an additional repetitive sweep for the monitor klystron. The sweep is derived from the gated free-running multivibrator circuit (V20, V21) and the bootstrap sweep circuit (V22, V23), and in this way the monitor klystron can be swept through its mode after inversion has taken place with a sweep interval 0.2 ms to 0.4 ms.

5.5 Field Sweep Unit

The two main considerations in the design of the power amplifier for magnetic field modulation are: (1) the sweep coils must be placed in the anode circuit of the amplifier valves

because transformer coupling of the coils would give considerable sag in the required waveform when there is a long delay ($\sim$ 9msec) between first and second sweeps, and (2) the current required to produce a field sweep of about 10 gauss is anticipated to be of the order of 4 amps for sweep coils of about 10 turns. The amplifier has been designed around a parallel arrangement of four Mullard 13E1 valves and the circuit is shown in Figure 4.14.

The 13E1 valves (maximum current 0.8 amps, maximum dissipation 95 watts), are permanently biased well below cut-off and are driven by the triangle or rectangle waveform into the conducting region. The amplifier is powered by a 225 volt accumulator bank with a tapping point for direct connection to the screen grid of the valves. The screen voltage is adjusted to give optimum linearity of the current waveform, the direct connection with the batteries ensuring that the screen voltage remains very nearly constant during the current pulse. The amplifier current is monitored at all times during operation by displaying the voltage appearing across a 10 ohm resistance in the anode circuit. Although the maximum current rating of the amplifier is 3.2 amps, with forced air cooling, peak currents of 4.5 amps have been obtained without damage to the valves.

The sweep coils are placed in series in the anode lead of the amplifier. Protection from damage to the valves is afforded

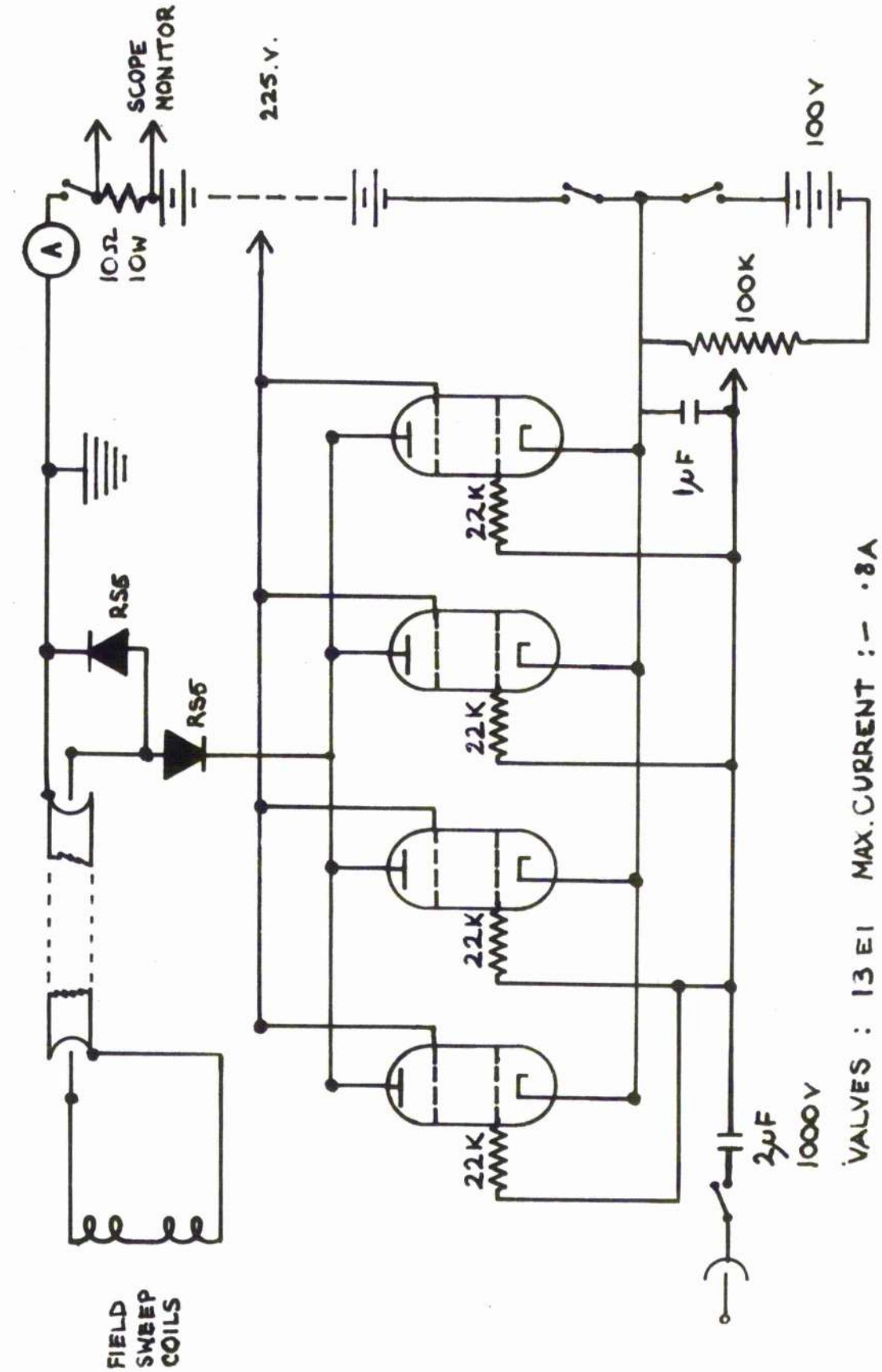

Figure 5.14. Power Amplifier.

by fuses, rated at 1 amp, in both the HT+ and HT- leads, and by earthing the HT+ lead, accidental shorting of the battery through the sweep coils is avoided: the sweep coils were immersed in liquid air in most experiments so that the possibility was particularly dangerous. However, this arrangement puts stringent requirements on the input condenser; a maximum of 450 volts appears across the condenser, so that a high quality paper foil condenser rated at 1000 volts working, has been used here.

No special precautions are taken, except for the inclusion of low value grid-stoppers, to prevent self-oscillations of the valves, due to their high mutual conductance and, in fact, no difficulty has been experienced in their designed operation. The precaution is taken, however, to include in the coil circuit two silicon junction rectifiers (S.T.C., RS5) which effectively prevent ringing oscillations in the coils after the current pulse. The series parallel arrangement of the diodes completely separates the valves from the sweep coils after a current pulse and the diode in parallel provides a damping path for any oscillations. The effectiveness of this arrangement has been checked by means of a pick-up coil placed between the two sweep coils and by viewing the line shape of the E.S.R. resonance line displayed by the repetitive sweep: no ringing has been observed.

Two designs for the sweep coils have been used in this

study, but they have the common feature that the coils are mounted as close to the sample cavity as possible, that is, as far from the magnet pole pieces as possible. In this way the eddy currents induced in the pole pieces are minimised and the effective field at the sample (total sweep field minus that due to eddy currents in the cavity) are maximised, so that the current required to sweep the field a given amount at a given rate, is as low as possible. A Helmholtz pair of coils mounted on the outer walls of the cavity was used in the earlier experiments but because of the heating of the coils, this system was replaced in later work by coils strapped to the outer wall of the helium dewar and immersed in liquid air. These coils are moulded to the cylindrical exterior of the helium dewar and are sufficiently thin to allow the liquid air dewar to be mounted without restriction: the clearance is 2 mm. To counteract differential contraction between the glass dewar, wall thickness 0.5 mm, and the copper wire coils, the coils are first wound and glued to the correct shape on to paper, then placed in position on the dewar and held under the tension of four springs joining opposing edges of the paper mounts. Further care is necessary over the insulation between windings for operation of the coil system in liquid air: liquid nitrogen is not available in large quantities. The coils are as near a Helmholtz pair as is possible on a cylindrical former and as far as can be seen, the inhomogeneity introduced into the steady field during sweep is negligible. A photograph of these coils is shown in Figure 5.15.

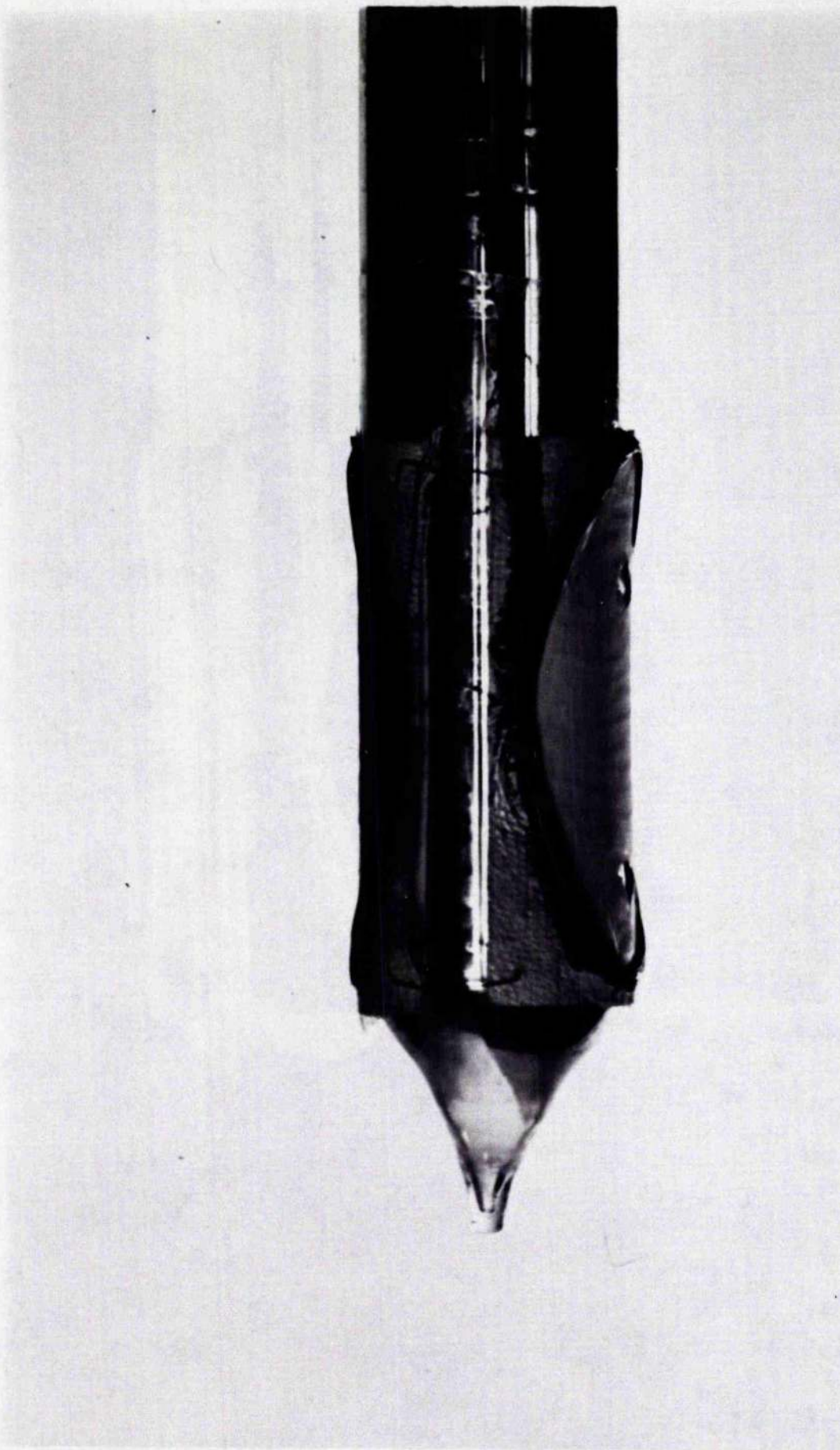

Figure 5.15 Photograph of Field Sweep Coils

With a pulsed current of 3.2 amps, a maximum field sweep of 5 gauss has been attained with the liquid air coils. The rates of sweep are measured by noting the time of sweep through the line width of the MgO sample (no saturation), the line width of the sample being previously measured by the N.M.R. magnetometer, see Table 6.2. The rates of sweep are noted in Table 5.1, for a current pulse of 3.2 amps: the rates are checked from run to run for the standard current pulse of 3.2 amps.

The inhomogeneity required in the steady magnetic field for inversion by A.F.P. frequency sweep is introduced by driving the power amplifier with the rectangle pulse. Only one of the coils is used here, the one on the earth side being shorted out by connecting the centre tap of the coils to earth, and the dipole field produced by a current of 2 amps broadens the resonance line sufficiently for inversion to be effected and spontaneous emission to be suppressed until after the X-13 sweep has been completed. It is noted, however, that the applied inhomogeneity took some 20 μsec to disappear.

5.6 Microwave Circuit

In the following discussion, reference is made to the photographs of Figures 5.3 and 5.4, and to the block diagram of the microwave circuit in Figure 5.16. The microwave system is operated at X-band with frequencies generally ± 100 Mcs about the centre

First Slope		Second Slope	
No.	Rate Gauss sec^{-1}	No.	Rate Gauss sec^{-1}
1	$4.1 \quad 10^4$	1	$1.25 \quad 10^4$
2	$3.85 \quad 10^4$	2	$1.0 \quad 10^4$
3	$3.65 \quad 10^4$	3	$7.7 \quad 10^3$
4	$3.3 \quad 10^4$	4	$6.25 \quad 10^3$
5	$2.94 \quad 10^4$	5	$5.56 \quad 10^3$
6	$2.78 \quad 10^4$	6	$5.0 \quad 10^3$
7	$2.5 \quad 10^4$	7	$4.0 \quad 10^3$
8	$2.4 \quad 10^4$	8	$3.3 \quad 10^3$
9	$1.95 \quad 10^4$	9	$2.86 \quad 10^3$
10	$1.75 \quad 10^4$	10	$2.5 \quad 10^3$
11	$1.3 \quad 10^4$	11	$2.0 \quad 10^3$
12	$9.5 \quad 10^3$	12	$1.67 \quad 10^3$

Maximum Sweep: 3.2 amp : ~ 4 gauss

Accuracy: $\pm$ 15%

Table 5.1 Rates of Field Sweep : Triangle Waveform.

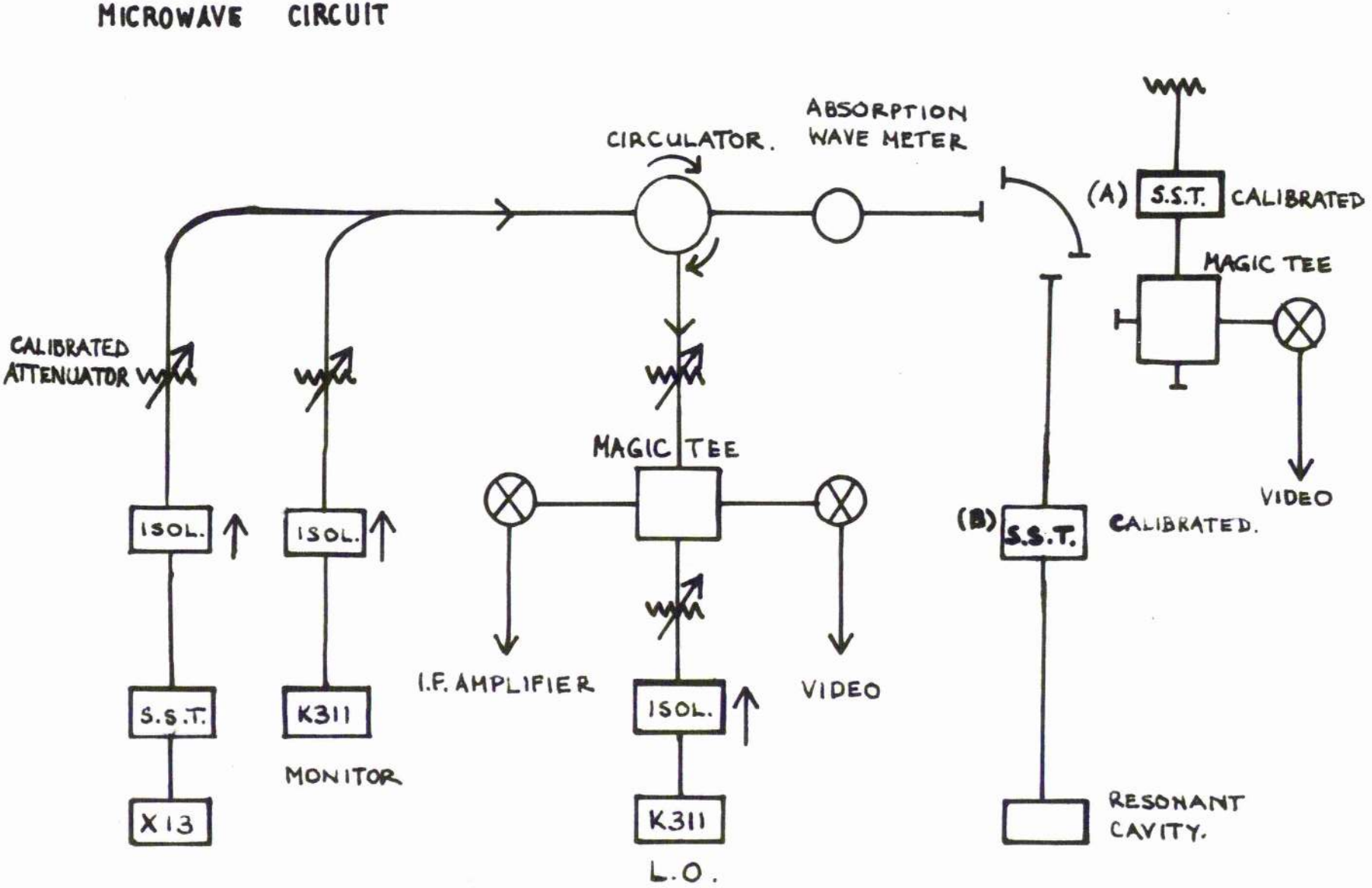

Figure 5.16 Microwave Circuit: Bridge for Q measurements is shown.

frequency of the circulator, 9.375 kMcs. The power supplies for the resonators of the klystron oscillators are voltage stabilised, and the reflector supplies are provided by dry cell batteries: the reflector controls are grouped together in the electronic rack and all leads to the klystrons are electrostatically screened.

The microwave circuit may be divided into three parts, the cavity input circuit, the monitor circuit and the detection arm: these will be considered in detail.

Cavity Input Circuit

During inversion either the rectangle or trapezoid waveform is applied to the reflector of the power klystron, Varian X-13, by means of a decoupling condenser, 2 μF (1000V working), attached to the reflector. For general purposes the X-13 is swept through its $\frac{3}{4}$ mode by the trapezoid waveform, and the reflected power from the cavity is displayed from one of the detector crystals. Provided the mode centre frequency has been adjusted close to that of the cavity, the display will show a dip as the frequency is swept through the cavity frequency. The frequency of any point in the sweep can be measured by adjusting the Philips PT4290X absorption-cavity type wavemeter to that frequency, as indicated by the wavemeter dip at the point in the oscilloscope trace. The frequency can be measured in this way to an accuracy of $\pm$ 1 Mcs.

For optimum power output, the X-13 is operated with the cavity dip at the top of its $3\frac{3}{4}$ mode, and operated also into an optimum load. The load is adjusted by a sliding stub tuner directly in front of the valve and a specified maximum output of 500 mw can be obtained in comparison to the matched output of 250 mw at 9.4 kMcs. The 30 db isolator used in this circuit, as with the other two klystrons, minimises frequency pulling of the klystron by the other circuit elements. An uncalibrated 30 db variable attenuator and a 40 db calibrated attenuator provide attenuation of the X-13 power and the attenuators can be calibrated against each other when it is necessary to know the total attenuation of any one setting. The X-13 is forced air cooled and once an ambient temperature is reached, the frequency stability is good.

The X-13 power is transmitted through the Ferranti 3-port circulator, 5M161A, to the cavity, and reflected power from the cavity is directed at the circulator into the detecting arm. The advantage of the circulator in separating the reflected power from the transmitted power is clear, but the small bandwidth of the circulator, $\pm$ 100 mc about 9.375 kMcs, means that for optimum working conditions, the cavity resonant frequency should be within this range at all temperatures. The decrease in cavity frequency of about 1% on cooling to helium temperatures could generally be allowed for by pre-tuning the cavity to a frequency higher than 9.375 kMcs by this amount; operation with the circulator was

found, however, to be quite possible at frequencies ± 250 Mcs of the centre frequency.

The additional bridge for measuring the cavity Q's, described in Section 5.9, is included in the cavity arm by removing a 90° bend and replacing this with a magic tee: quick release clamps are used. A second sliding-stub tuner, also in the cavity arm, is used for small coupling adjustments to the resonant cavity.

Monitor Circuit

The monitor klystron, an English Electric K311 of output power 45 mw, is coupled to the cavity arm by a 30 db directional coupler. A 30 db uncalibrated attenuator in the circuit allows powers as low as 45 milli-microwatts to be incident at the cavity. In general this klystron is operated at the cavity frequency, either as the signal in E.S.R. spectroscopy or as the probe signal in maser or E.S.R. relaxation experiments. With a 1 μF integrating condenser across the reflector, the overall frequency stability is good.

Detection Arm

Reflected power from the cavity is coupled into the detection arm by the circulator and mixing with the local oscillator power, takes place at a magic tee: straight detection or super-heterodyne detection is simultaneously possible from the two crystal

detectors of the tee. The L.O., a K311, is operated in a similar manner to the monitor klystron and its frequency stability is found to be as good.

The direct reading, calibrated attenuator in the detection arm, serves three purposes. Firstly, it is used to determine whether the I.F. amplifier is operating near saturation, for by decreasing the input to the amplifier, the output should drop by an equal amount if the amplifier is not saturated. Secondly, the attenuator is used to avoid saturation in the I.F. amplifier in preference to biasing the first stage towards cut-off, for as the valves have a sharp cut-off, considerable gain fluctuations occur in this region. Thirdly, the attenuator is used to compare two signals, e.g. maser oscillation pulses and the X-13 power, by reducing each to a chosen level: this measurement does not disturb the operation of the apparatus and being a null method is independent of any detecting crystal nonlinearities.

The klystron valves and all the electronic circuitry are run for a period of at least one hour before any experiment to ensure thermal stability from the beginning of a run. This practice has proved very satisfactory.

5.7 Cryogenics

The liquid air and liquid helium dewars are made of selected Monax Glass and tailed to fit the magnet Type 'E'. A detailed

description of the construction has already been given in Reference 8 and a diagram of the cryostat is shown in Figure 5.17. The approximate capacity of the helium dewar is one litre.

The main microwave circuit is attached to the cryostat section by a flexible connection and quick release clamps, so that the cryostat can be removed from the apparatus to be carried to the helium liquefier for transfer. A 0.005" mica window across the waveguide is located between the clamp and the cryostat, so that the cryostat can be evacuated. The window is located between a plain and choke waveguide flange, being sealed by placing oversize Cacc rubber rings in each of the flanges. Thence, the waveguide is coupled to the cryostat through an E-plane bend.

The waveguide in the cryostat is of 0.020" walled, nonmagnetic stainless steel, at the base of which is the cavity coupling flange. A $\frac{1}{8}$" diameter Quartz rod, mounted on the E-plane bend, passes down the centre of the waveguide and is used as a tuning system for external adjustments to the cavity resonant frequency. For simplicity of design, the waveguide is left open to liquid helium and $\frac{1}{8}$" holes drilled centrally in one broad face at the top and bottom of the waveguide allow free gas exit and liquid entry respectively.

Two low loss coaxial leads are brought into the cryostat and terminate at the base of the waveguide to which they are attached at several points. These cables feed current to the Helmholtz sweep

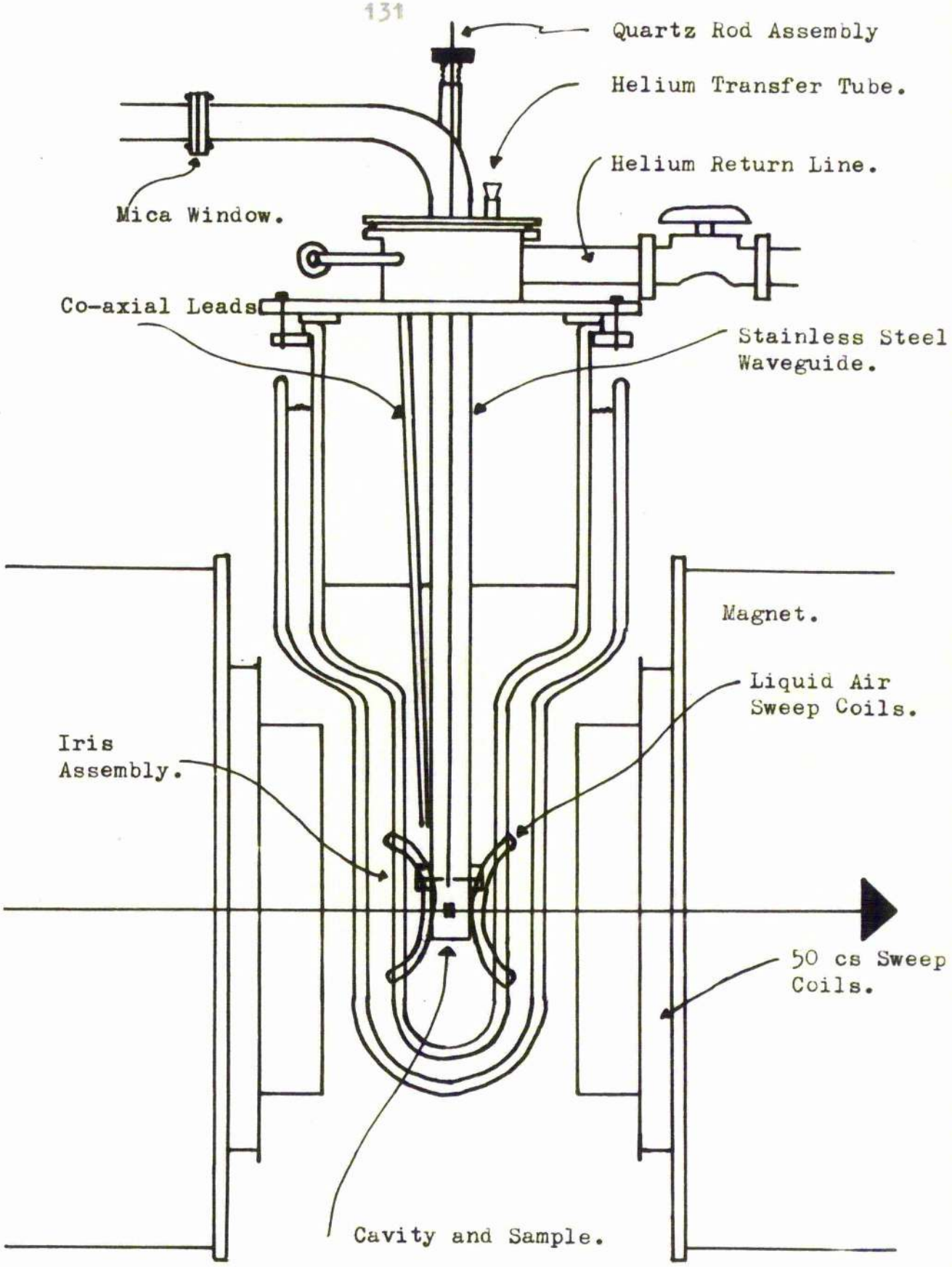

Figure 5.17 Cryostat Assembly. (not to scale)

coils mounted on the cavity and, in later experiments, serve as leads from the pick-up coils to recording instruments (See Sections 5.8 and 8.9). The outer sheaths of the leads are lengths of thin walled copper-nickel tubing and the inner cables 32 SWG enamelled copper wire with ceramic beads as spacers. The centre lead is brought out of the cryostat through a glass-to-metal Kovar seal, and an external tube gives complete shielding of the lead to a coaxial socket. Holes, similar to those in the waveguide section, are drilled in the outer sheaths to give free entry and exit of the helium. The capacity of the lines at low temperatures is 18 pF per foot and the heat leak of the two cables did not significantly increase that of the waveguide alone. In addition to these electrical leads, wires are brought into the cryostat via Kovar seals, to connect to the resistance wire heater (2 watts) wound about the waveguide at its lowest point.

In low temperature operation, helium gas at atmospheric pressure is returned to the main gas holder along a 1" return line. A 2½" pumping line, coupled to an Edwards rotary pump 18C3000, could be opened to the cryostat, the return line being closed, and the pressure of the helium gas in the cryostat adjusted by a needle valve. The pressure is monitored with a mercury manometer, Vacustat gauge and differential oil gauge (butylpthalate, density 1.046) connected by rubber tubing to the cryostat head. The lowest pressure recorded, with all pumping valves open, was 1.4 mm but a

pressure of 2.0 mm, 1.4°K, was attained on all runs. The average length of a run at 2.0 mm pressure was about six hours.

5.8 Microwave Cavities

Metal Cavities

The cavities used in the initial stages of this study are made from sections of rectangular copper-nickel waveguide, wall thickness 0.010", and are designed to resonate in the TE_{102} mode. The choice of the TE_{102} mode is made on the following considerations: simplicity of design; large central volume over which the maximum cavity field occurs giving effective coupling between large samples and the cavity radiation field; easy positioning of field sweep coils on the broad faces of the cavity.

The length of the cavity is such that the resonant frequency at room temperature is about 1% greater than that required at helium temperatures; the exact length is ascertained by trial with the sample mounted in the cavity. The resonator is completed by an end plate and a top flange for securing the cavity to the cryostat waveguide section by bolting this flange to a similar one soldered to the base of the waveguide. The coupling iris of the cavity, a hole reamed in copper foil, is located between the two flanges and positioned by four 8 BA securing screws. By bolting the cavity to the waveguide, good electrical contact is made between the iris and the top edge of the cavity. The cavity and iris are silver plated to reduce resistive losses. Figure 5.18 shows a

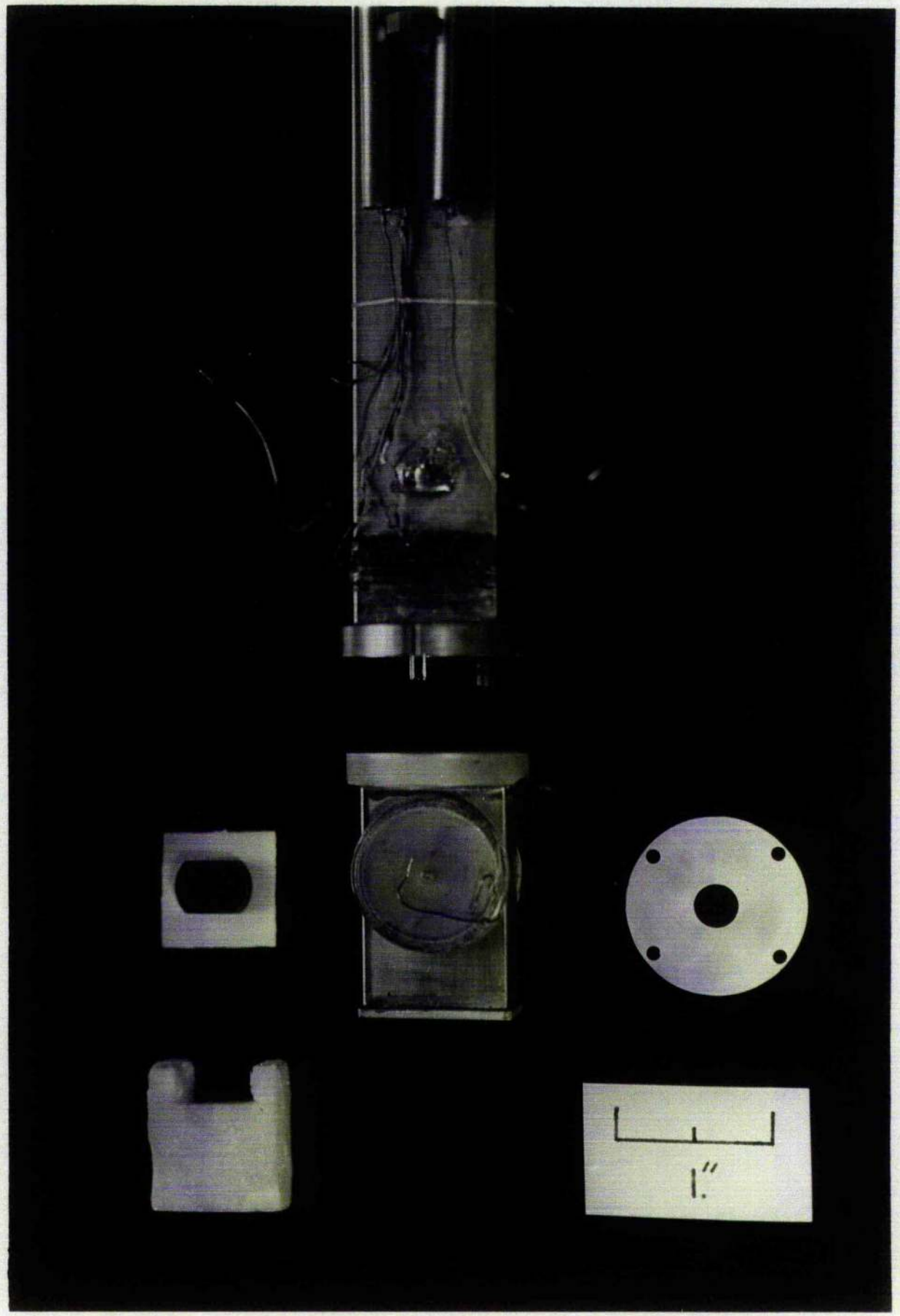

Figure 5.18 Metal Cavity Assembly. Samples (2,3), crystal mount, iris, sweep coils and coaxial leads are shown.

metal cavity, iris and waveguide assembly.

The unloaded Q is in the range 4000 - 6000 for these cavities. So long as care is taken in the assembly and tightening, no real change of the cavity unloaded Q or the coupling Q occurs from assembly to assembly.

The cavity is not tunable except for fine frequency adjustments by the Quartz rod unit already described in Section 5.7. The Quartz rod is constrained to enter the cavity centrally through a clearing hole in a thin mica plate (.002"), of the same dimensions as the iris, placed directly above the iris in the assembly. If this plate is absent, the lateral motion of the rod upon turning, alters erratically the coupling of the cavity.

In Section 3.3 it was indicated that the maser oscillation condition is very sensitive to the coupling condition of the cavity and that oscillations should be more easily obtained when the cavity is under-coupled. An attempt was made, therefore, to provide variable coupling at the cavity iris rather than at the sliding-stub tuner in the waveguide, by a manually controlled movable plate situated directly above the coupling iris. In this arrangement the plate is fixed to a spring loaded pin which is moved by a cam. The cam is in turn attached to a thin steel rod, running the length of the cryostat which is turned externally at the cryostat head. The coupling could be changed by large amounts by simply changing

the position of the plates, and also the effective coupling area, but the unit was not reliable and had to be abandoned. The failure is partly due to poor electrical contact between the plate and the waveguide caused by the large clearances that must be allowed at room temperature to obtain any movement of the pin at low temperatures, and partly due to the reduced efficiency of the spring at low temperatures in locating the pin.

Paramagnetic samples are mounted centrally in the cavities by embedding them in a plastic foam. Jabolite is used* because of its low microwave losses and because it does not collapse either under vacuum or in the presence of liquid helium. By careful design, the total volume of Jabolite in the mount is kept to a minimum.

Helmholtz sweep coils are mounted on the broad faces of the cavity. The coils, of 10 turns on 1" diameter perspex formers, are mounted by screwing the formers to brass screws soldered centrally to the broad faces (See Figure 5.18). In this arrangement the eddy current and coil heating losses were found to be large, but by removing the sweep coils to the outside of the helium dewar (Section 5.5) a significant reduction of these losses occurred, which was made apparent by extended time at helium temperatures.

---

* Footnote: Styrofoam, a more commonly reported mount, is found to collapse to half its volume in liquid helium.

Plastic Cavities

For the main part of the experimental work, plastic cavities have been used. There are four reasons for their development:

(1) the heating losses and opposing field losses of eddy currents in thick (0.010") walled cavities gives reduced experimental run times and non-uniform penetration of the sweep field into the cavity,

(2) the intention to attempt to detect nutations of $\underline{M}$ that might be present in amplitude modulated oscillation of the maser operated in this study. It was believed that nutations of $\underline{M}$, if present, could be detected by monitoring the changes in the magnetic dipole field of $\underline{M}$, which indicated that an induction experiment, possibly on lines similar to N.M.R. induction, should be performed. Note was taken of the move in this direction by Campbell[8], who showed that more than two turns of 46 SWG copper wire wound about the sample inside the cavity, destroyed the cavity Q. In this case the skin effect in a thin silver film might be used to advantage: in a plastic cavity, that is one where the microwave cavity is formed by a thin film of silver deposited on a plastic mould of the correct dimensions, the microwave fields will be confined within the cavity so long as the wall thickness is greater than the skin depth, whereas any variation in the dipole field of $\underline{M}$ occurring at the modulation frequency, found to be between 1.5 Kcs and 10 kcs in these studies, would not be totally confined. Pick-up coils could, therefore, be placed outside the cavity and, furthermore,

calculations predicted that the voltage induced in such an external coil of 800 turns, by nutations of $\underline{M}$ in the strongest sample available (Sample (1)), might be as large as one millivolt,

(3) the difficulties involved in making glass cavities[61]; the variations in Q of such cavities on successive reassemblies and a marked deterioration in Q as exposed surfaces are subjected to wear and chipping, and

(4) the interesting topic of finding a plastic manufactured in this country that could be used in this connection at helium temperatures, there being no previously reported case. The work of Chester et al[62] is, however, noted in this respect where a plastic manufactured in the U.S.A. has been used.

A recent laboratory note by the Author has been published in the Journal of Scientific Instruments[63] on the subject of plastic cavities: a copy of the article is contained in Appendix I.

Upon the tentative advice of Messrs. Ciba (A.R.L.) Limited, the epoxy casting resin Araldite CT200 and Hardner HT901 was tried initially, and in fact proved fully successful. French chalk was used as a filler to the resin, so reducing the thermal expansion and thereby reducing internal strains in the cavity and strains at the interface with the waveguide coupler, as the cavity is cooled to helium temperatures. Other inert fillers, e.g. silica flour, may be used with more effectiveness in this respect but the resin is then more difficult to machine due to its abrasive nature.

The brass mould used in casting the cavity is shown in Figure 5.19. The mould is in three parts: a central mandrel, a base and an outer shell. The solid mandrel has the required cross-sectional dimensions of the cavity but is longer than the cavity. The corners of the mandrel are rounded to facilitate cleaning, polishing and silvering the cavity, and to one end of the mandrel is brazed a disc which mates with an inset in the base. A central hole tapped 0 BA in the disc serves two purposes; to secure the mandrel to the base and as a means of attachment in extracting the mandrel from the cured casting. Cavities that have been made have had cross-sectional dimensions .9" x .4" and also .9" x .1". The shell, a length of $1\frac{3}{16}$" inside diameter tube, makes a tight push fit onto a lip on the base. In this way the mandrel is centred to the base and is coaxial with the outer shell.

Prior to assembly, the components are polished with Brasso and washed with detergent. The mould release agent, Releasil 7 silicone compound, is applied with a fine camel hair brush as a 20% solution in white spirit. After evaporation of the spirit, two further coats are similarly given.

After mixing the resin and hardner at 130°C, the French chalk is added to the liquid resin, the proportion by weight of filler to resin being 8 : 10. The mixture is vacuum treated to ensure a void-free casting and then poured into the preheated mould,

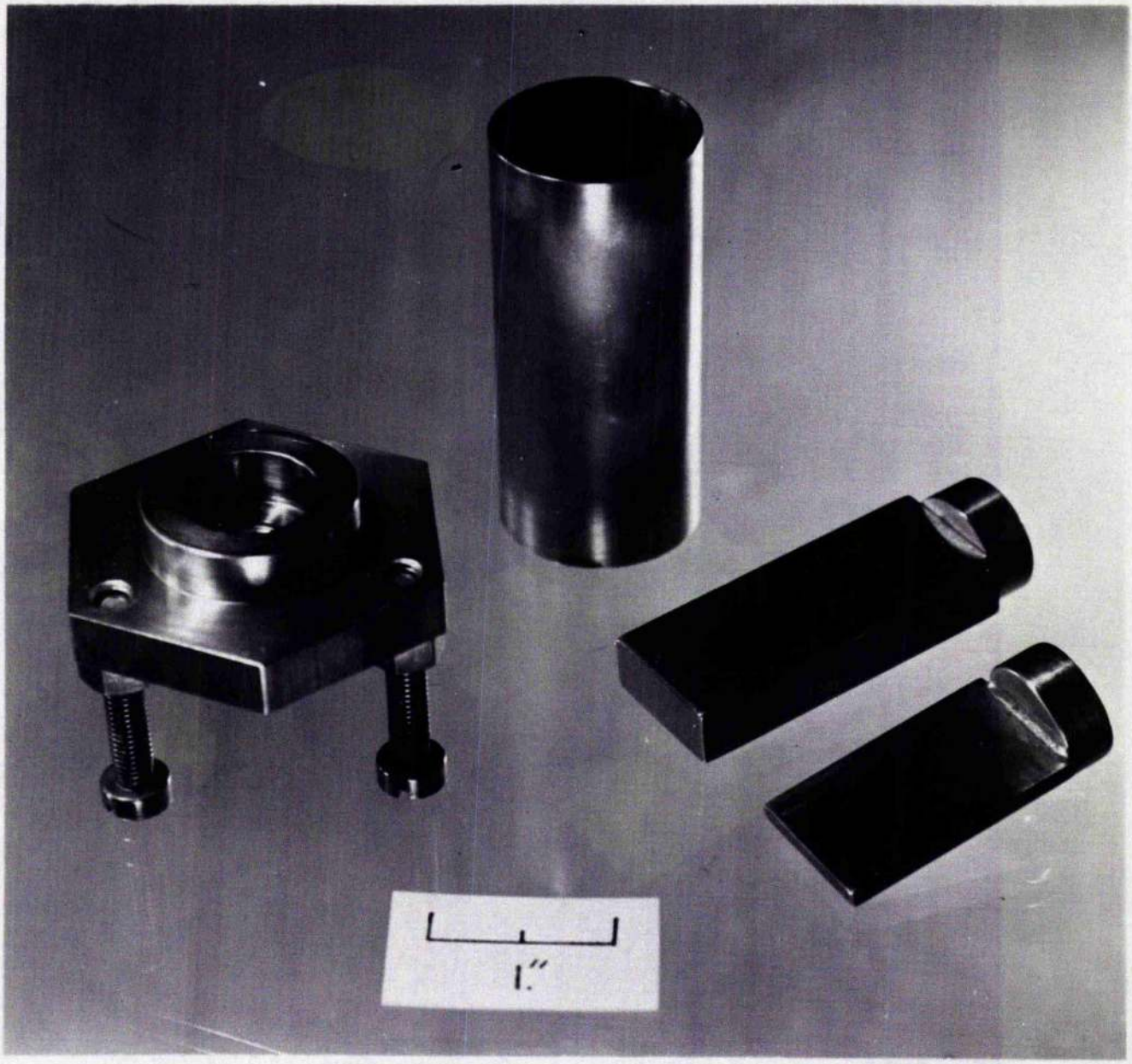

Figure 5.19 Brass Mould for Casting Plastic Cavities

and the casting cured at 200°C for two hours. Some difficulty is experienced in removing the mandrel from the cold casting, but this is accomplished with patience. A better design for the mould would be to taper the mandrel slightly on all four sides for ease of removal.

The cured casting is found to machine easily. By machining the cavity to lengths predetermined in experiments with metal cavities, a particular resonant frequency can be obtained. Further machining of inset holes in the sides of the casting allow either Helmholtz sweep coils of the same design described above, or pick-up coils, designed for the induction experiments, to be placed as close as possible to the sample. After polishing the inner walls and the top face with jeweller's rouge and then with Bresso, the cavity is washed in white spirit to remove the release agent, and finally with detergent.

The method described by Chester et al[62] is followed in the final cleansing and silvering but the ammoniacal silver nitrate and the reducing solution, however, are cooled to 12 - 15°C, thereby obtaining a slower rate of deposition. This facilitates mixing and decanting into the cavity and, furthermore, ensures a more uniform silvering. The cavity is placed in a beaker and the silvering solution is poured directly into the cavity thus excluding air bubbles, and is allowed to overflow until the casting is

completely immersed: three similar silverings are given. After drying, the silver coating is removed from the base and the cylindrical exterior. The cavity and iris assembly are attached to the waveguide flange by four 8 BA nylon screws which serve to locate the coupling iris. Finished cavities are shown in Figure 5.20 with iris and coils.

The success of the design has been good. Firstly, no cracking of any cavity cooled to helium temperatures, 4.2°K - 1.5°K, has occurred either in the casting or in the silver plating and, secondly, little deterioration or scratching of the plating, caused by repeated mounting of samples, has been seen. In the case of one .9" x .1" cavity, repeated use in 10 experimental runs is noted with the same silver plating but replating is, however, easily carried out by cleansing with concentrated nitric acid and silvering as above. The unloaded quality factor, Q_o, for the .9" x .4" cavity, length 42.5 mm, is at best between 4000 and 6000 and Q_o is maintained for repeated coolings, whereas for the .9" x .1" cavity, length 19.7 mm, in which the MgO sample completely fills the cavity,* Q_o is about 1500. The reduction in this latter case is attributed

---

* Footnote: The dielectric constant of MgO, measured at 9.4 kMcs, is 4.1, which explains the difference in length of the cavities, although they operate in the same mode.

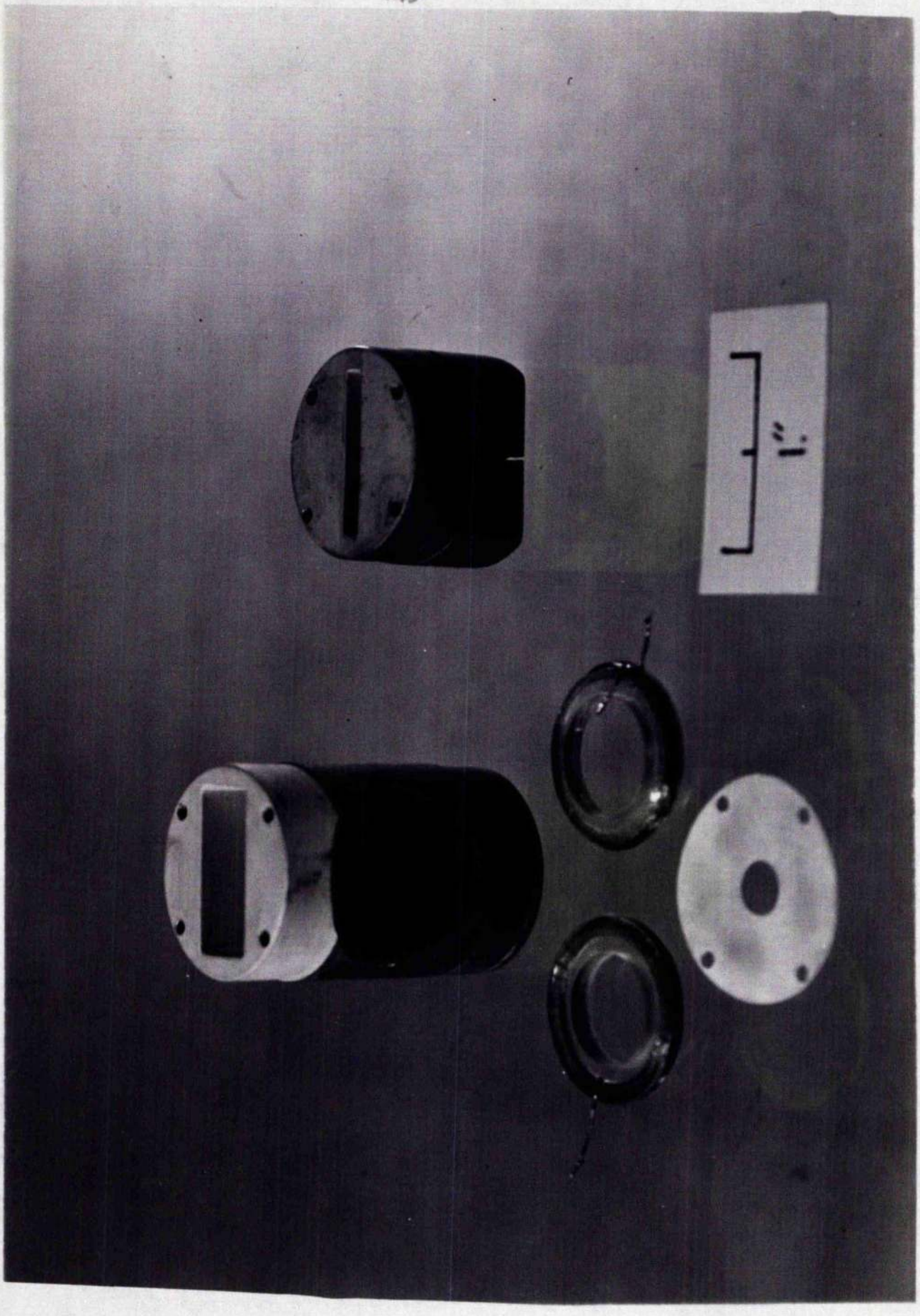

Figure 5.20 Plastic Cavities. A .9"x.4" and a .9"x.1" cavity are shown. Sweep coils and iris are shown

to the smaller energy stored in the cavity volume, the volume being only one eighth of the larger cavity, and also to the poor electrical contact between the iris and the lip of the cavity, for the waveguide flange is designed for the .9" x .4" case. Temperature variation of Q is indicated in Table 5.2 for the two types.

The technique described above could be used in other low temperature microwave components, e.g. tapered waveguide sections, or could be used generally in cryogenic techniques where a moulded plastic component is required.

5.9 Measurement of Cavity Q.

To a certain extent an idea of the loaded cavity Q, Q_L, can be obtained by measuring the half width of the cavity mode with the wavemeter when the cavity resonance is displayed as a dip in the X-13 mode. However, when Q_L approaches the Q of the wavemeter (10,000) great inaccuracies occur because of difficulties encountered in positioning the wavemeter dip across the cavity dip. The standard procedure[64] of measuring the V.S.W.R. of the waveguide terminated by the cavity at different frequencies across the cavity mode, is clearly impossible here in view of the time required for such measurements in the presence of non-stabilized frequency sources. The transient method, proposed by Yariv and Clapp[65], has been used, however, to measure the cavity Q's.

The microwave bridge required for Q measurements is

Cavity	1			2		
Cross-Section	.9" x .4"			.9" x .1"		
Temperature	Q_o	Q_L	ν k Mcs	Q_o	Q_L	ν k Mcs
300°K	1120	705	9.5084	1080	630	9.5545
77°K	1320	517	9.5673	1450	725	9.6262
4.2°K	1700	606	9.4337	1760	450	9.4750
1.5°K	2210	792	9.3481	2100	1190	9.4424

Table 5.2 Temperature Variation of Q_o, Q_L, ν

included in the microwave system by replacing a bend by two arms of the bridge, see Figures 5.4 and 5.16. This modification can be effected quickly and does not disturb the operation of the cavity. Sliding-stub tuners, A and B, in the arms of the bridge are calibrated against V.S.W.R.[66] and reflections from the bridge are monitored at the crystal detector of the bridge circuit. The exact procedure for measuring Q_o and Q_c is detailed by Yariv and Clapp and will not be repeated here, but the general outline of the method will be mentioned.

The cavity mode is displayed at the bridge crystal detector by repeatedly sweeping the X-13 through its mode by applying the trapezoid waveform to the X-13 reflector. Probe A is moved along the waveguide and its penetration varied until a match occurs at the cavity frequency: the V.S.W.R. of the cavity is then equal to that introduced by probe A. This measurement gives the ratio of Q_o to Q_c or vice versa depending upon the coupling condition. The coupling condition is determined by introducing a small reflection from A, varying the position of A and observing the relative motion of the shoulders of the mode and the dip of the cavity: if the shoulders and dip move in synchronism the cavity is undercoupled, and overcoupled if they move in opposite directions. Further detailed measurements with B gives Q_c. The quick determination of the coupling condition is most useful in studying maser action, for maser amplification can be confused with resonance

absorption if the cavity is taken through match by the action of the spin system[43]. The accuracy in determining Q_o and Q_c depends largely upon the accuracy with which a small frequency difference, necessitated by the method, can be measured by the wavemeter: the overall accuracy is estimated to be ± 10%.

The bridge is useful in setting up the microwave cavity previous to a low temperature run. Its use here is chiefly to determine the coupling condition and also to optimise Q_o by small adjustments to the bolting screws in the cavity assembly. The preferred coupling condition at room temperature is slight over-coupling because there is a tendency to undercoupling as the cavity is cooled: this condition can always be obtained by small adjustments to the hole area of the coupling iris.

5.10 Display

For video presentation of any signal the Solartron oscilloscopes CD 513.2 (general purpose), CD 643.2 (measuring) and CD 1014 (double beam) are available. The high sensitivity ranges on the CD 513.2, 1 mv/cm and 10 mv/cm, had to be used with care because the bandwidth of these ranges is only 100 kcs and 2 Mcs respectively, whereas on the lower sensitivity scales, the bandwidth is upwards of 5 Mcs. A similar argument applies to the use of the CD 1014. Generally, however, when the signal to be displayed is greater than 50 mv the measuring oscilloscope, CD 643.2, is used

because the bandwidth on all scales (100 mv/cm upwards) is 12 Mcs.

The I.F. amplifier is a 'war surplus Pye-strip' with a total bandwidth of ± 5 Mcs about a centre frequency of 30 Mcs. The base of this amplifier is mounted in styrofoam for thermal insulation purposes and that mounted on rubber feet to minimise mechanical vibrations; all leads to the amplifier are electrostatically shielded. To reduce the high frequency noise that appeared initially in the amplifier, the first stage has been bypassed, giving a somewhat reduced gain of 1860 and a high frequency noise component of 50 mv r.m.s. As mentioned in Section 5.6, the amplifier is operated with little grid bias due to the gain instabilities that appear near cut-off. The output level is monitored by means of a milliameter connected into the second detector circuit, and provision is made to connect a variable condenser bank, up to 4000 pF, across the output to reduce background noise. The amount of integration that can be introduced is, of course, dependent on the waveform under investigation.

5.11 Photography

Transient measurements have necessarily been made on film. The Langham Thompson oscilloscope camera, Series 105, with direct viewing hood, has been used and in its operation the following points have been considered: (1) the camera is focussed onto the cathode ray tube screen with maximum aperture for maximum

transmission, but no attempt is made to obtain any particular magnification ratio; (2) optimum trace brilliance at slow trace speeds is found to occur when the whole trace can just be seen through the amber direct viewing screen; (3) graticule lighting is always considerably less than that of the trace; (4) exposures are monitored through the viewing hood. Ilford 5091 film is used for all recordings but where the trace speed is in excess of 10 μsec/cm poor contrast is obtained.

Due to small instabilities in the apparatus, transient waveforms in maser operation are not repeated exactly from cycle to cycle so that the resultant negative of a simple exposure of a number of traces, is blurred. This defect is overcome by use of the oscilloscope trigger circuit shown in Figure 5.10. Here, the oscilloscope is triggered by a variable delay multivibrator (V4) which is driven by the timing multivibrator, the delay being incorporated so that the waveform to be recorded can be brought close to the origin of the trace in order that the full expansion facilities of the oscilloscope can be used. Provision is included to trigger the oscilloscope on only every tenth, or even every hundredth, cycle of the timing multivibrator by switching in a Decatron pulse counter and associated shaping circuit (V24). Hence, oscillograms of single traces can be made by opening the camera shutter between oscilloscope triggers, as seen from the neon counters, or from viewing the traces directly. This selective

recording has been used in transient relaxation experiments and maser experiments and has proved successful.

The oscillogram negatives are mounted between glass and measurements from the trace are taken either by viewing the assembly with a travelling microscope, or by projecting the trace onto a screen of inch graph paper. The methods have been compared and give consistent results: the latter method has been used in the majority of oscillograms because of the ease of taking measurements.

CHAPTER 6

SPIN RESONANCE SPECTRUM OF NEUTRON-IRRADIATED MgO

6.1 Introduction

The three important properties of a paramagnetic sample to be used as the working material in a two-level maser have been discussed in Chapter 3. They are: (1) a single, narrow intense resonance line, (2) long spin-lattice relaxation time T_1, and (3) high spin concentration in a sample large enough to give a large filling factor. Of these, the first determines the ease with which the spin populations may be inverted, the second, the cycling rate of the maser, and the third, the presence of maser oscillations and the power that may be released in such oscillations.

These studies have been confined to investigations into neutron-irradiated MgO. Previous E.S.R. studies of the colour centres in this material by Weeks et al[57] have indicated that the first and third of the above properties occur in this material: the colour centre resonance consists of an intense line at $g = 2.002$, $\Delta H_L = 0.7 - 1.0$ gauss and possible spin densities of about 10^{19} cm^{-3}. Measurements of T_1 for this line[8,47] show that, at helium temperatures, T_1 is about 4 msec, so that the second requisite property obtains. Furthermore, the success of Chester et al[47] and Campbell[8] in obtaining two-level maser action in this material indicated that this material would be a useful one with which to study

maser action in general and, in particular, amplitude modulated oscillation.

In addition to the above arguments in favour of using neutron-irradiated MgO, a good supply of the material (Samples 1,2,3) was immediately available and further supplies were easily forthcoming. Slices of single crystals, supplied by Infra-Red Development Company Limited, were irradiated with fast neutrons by courtesy of the United Kingdom Atomic Energy Authority at Harwell and Dounreay.

In this chapter relevant data on the samples will be listed and the spectrum of the material at low temperature discussed. The total spectrum consists of a main line, with associated hyperfine structure, and many other lines space nearly symmetrically about the main line. These other lines are present in non-irradiated samples and are caused, most probably, by chemical impurities in the MgO crystals, e.g. manganese, chromium and iron. In this connection, no data on the purity of the MgO is available from the suppliers, nor has any chemical analysis been carried out. As the main line, a colour centre line, has been used only in the maser studies, the chemical purity of the MgO is relatively unimportant.

6.2 Sample Data

Seven specimens of MgO have been irradiated to different specifications to obtain varying colour centre concentrations.

Relevant data on the specimens is listed in Table 6.1. The specimens are dark blue or black in strong specimens to tinted blue in weak specimens, the original MgO crystals being translucent white. Two of the samples are shown in Figures 5.18 and 8.19.

The E.S.R. spectrum of irradiated MgO at 300°K is already well known from the work of Weeks et al[57], and the main central line has been interpreted as arising from F-centre. Weeks postulates that the F-centre occurs when an oxide ion is displaced from its normal position during irradiation, and an electron, donated by ever present divalent impurities, becomes trapped at the vacancy. F-centres which have only Mg^{24} and Mg^{26} neighbours give a single resonance line with g = 2.002, but those with one or two Mg^{25} neighbours (nuclear spin 5/2) give hyperfine patterns of six or eleven lines respectively. As the abundance of centres with one Mg^{25} neighbour is 36% of the total, Weeks shows that the sextet should be only 0.11 times as intense as the central line. The isotopic and anisotopic parts of the hyperfine structure, particularly of the sextet, have also been investigated by these authors.

The determination of the spin concentration of specimens, listed in Table 6.1, has been kindly carried out by D. Forke of this department, using the E.S.R. spectrometer (superhetrodyne spectrometer with frequency stabilization, at 300°K) described in Reference 59. This equipment is used in order to obtain greater accuracy in the determination: the sensitivity of this spectrometer,

No.	Weight gms	Dimensions mm	Volume cm^3	Dosage 1 Mev neutrons	Place	Date	Total Spins ± 20%	Spin Density N
1	1.72	17.5 x 2	.47	$10^{18} - 10^{19}$	Dounreay	Aug.1959	$2.0\ 10^{18}$	$4.3\ 10^{18}$
2	.75	12.7 x 2x9.3	.21	$2.4\ 10^{18}$	Harwell	Aug.1959	$1.1\ 10^{18}$	$5.2\ 10^{18}$
3	.75	12.7 x 2x9.3	.21	$2.4\ 10^{18}$	Harwell	Aug.1959	$1.1\ 10^{18}$	$5.2\ 10^{18}$
4	.37	13 x 2 x 4	.1	unknown	Dounreay	Jun.1961	$1.0\ 10^{18}$	$1.0\ 10^{19}$
5	.37	13 x 2 x 4	.1	"	"	"	$6.0\ 10^{17}$	$6.0\ 10^{18}$
6	.37	13 x 2 x 4	.1	"	"	"	$1.3\ 10^{17}$	$1.3\ 10^{18}$
7	.30	13 x 2 x 4	.08	"	"	"	$5.0\ 10^{16}$	$6.25\ 10^{17}$

Table 6.1 Sample Data of Neutron-Irradiated MgO Crystals

10^{14} spins, is to be compared to 10^{17} spins obtained for the apparatus used in this Thesis. The spin concentrations are obtained by comparing the area under the absorption curve of the F-centres to that of standard weights of the free radical diphenylpicrylhydrazl (DPPH). Recordings of the absorption curves for each are taken on successive runs under the same experimental conditions. The error in the comparison has been calculated to be about 15 - 20%. For samples where the neutron dosage is known, the spin concentration is to be compared to the F-centre production of 5.7 fast neutron per centre reported by Weeks.

6.3 Spectrum

The apparatus described in Chapter 5 can be operated as an E.S.R. superhetrodyne spectrometer. The apparatus is set up for use in the following manner:

(1) The X-13 is swept through its mode by the trapezoid waveform and its output video detected. The X-13 is manually tuned to display the cavity dip at the centre of the mode.

(2) The L.O. is manually tuned to present beats on the low frequency side of the cavity dip. In order to do this the L.O. is located by tuning the X-13 over its range and then "homed in" to the required frequency by the X-13.

(3) The L.O. is adjusted so that the I.F. response, unsaturated, is displayed with the cavity dip central.

(4) The monitor klystron is manually tuned or "homed in" until the

I.F. second detector indicates an output. Further fine adjustment of the reflector voltage is made until the cavity dip is indicated on the second detector. The integrating condenser is connected to the reflector of the valve. The X-13 is fully attenuated. Only infrequent, small adjustments of the reflector voltages of the two operating klystrons are required during operation.

The N.S.R. spectrum is located and displayed by modulating the magnetic field at 50 cs by about 50 gauss, and tuning the steady field over its range. The resonance signal is fed to the Y_1 plates of the double beam oscilloscope and to the X plates a 50 cs sweep is applied, phase shifted by 90°, for synchronous display. In order to measure the g values of the various lines in the spectrum, the magnetometer output is applied to the Y_2 plates and is set for use in the following way:

(1) The N.S.R. output is adjusted to show absorption only, by tuning the sliding-stub tuner in the cavity arm.

(2) The displayed absorption peak is centred in the trace by adjusting the magnetic field.

(3) The magnet is wheeled forward and the magnetometer sample coil inserted in the field to the former position of the crystal (predetermined) and the N.M.R. signal adjusted to a similar position in the trace by adjusting the oscillator frequency.

(4) The N.M.R. oscillator frequency is measured by the BC021.

(5) The microwave frequency is measured by the wavemeter. In the

same way the magnetic field at any point in the spectrum can be measured in order to obtain the widths of the component lines. The study of the MgO spectrum has been confined to measurements of the g values, widths and relative intensities of the various lines. No study of the anisotropy of the spectrum has been carried out.

The spectrum of irradiated MgO is shown in Figure 6.1 and oscillograms of the F-centre line and line I are shown in Figure 6.2. The spectrum has been recorded for Sample 2 at 9.3255 kMcs and 1.5°K: Table 6.2 gives the g values, widths and relative intensities of the lines. Hyperfine structure about the main line is resolved and seems to be a sextet. At low temperatures all the lines are easily saturated so that spectroscopic measurements have been taken with 15 db attenuation in the monitor klystron arm.

The line width of the F-centre line decreases at low spin densities and the associated hyperfine structure is not resolved in Samples 6 and 7. The intensities and line widths of the other lines remain unaltered for all samples.

6.4 Spectrometer Sensitivity

The sensitivity of the spectrometer was evaluated at room temperature by measuring the resonance absorption signal of standardised weights of DPPH (ΔH_L = 2.7 gauss) with a monitor power level of 45 μw at the cavity. The standards had been freshly made up. The signal to noise ratio was optimised by fine adjustments of the reflector voltages of the monitor and L.O. klystrons, and of

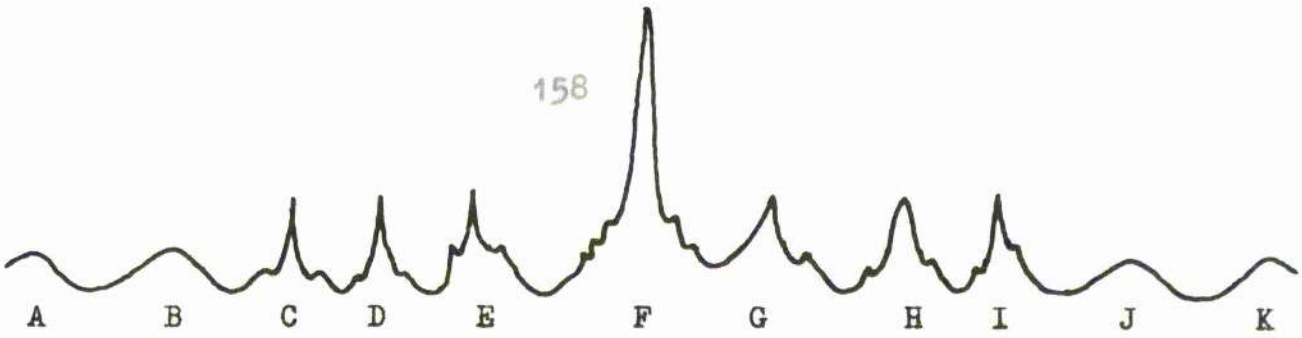

Figure 6.1 Spectrum of Neutron-Irradiated MgO. (not to scale)

Line	g value [± .02]	Linewidth (gauss)	Relative Intensity
A	1.65	50	0.024
B	1.75	40	0.016
C	1.87	1.2	0.12
D	1.92	0.6	0.1
E	1.92	0.5	0.12
F	2.00	1.0	1.0
G	2.03	0.5	0.16
H	2.09	0.7	0.12
I	2.15	1.3	0.11
J	2.35	40	0.016
K	2.42	60	0.016

γ = 9.3255 kMcs : T = 1.5°K

Sample 2 : Input power 4.510^{-8} Watts.

Table 6.2 Spectrum Data.

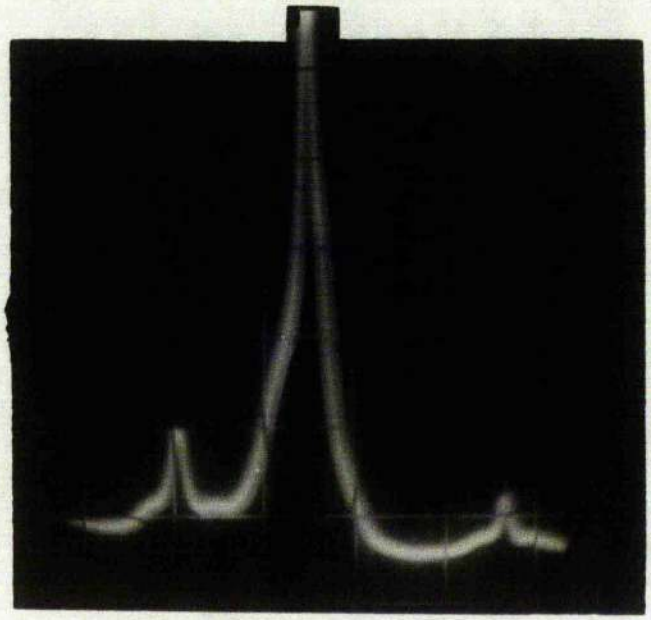

F-Centre Line with Two Impurity Lines

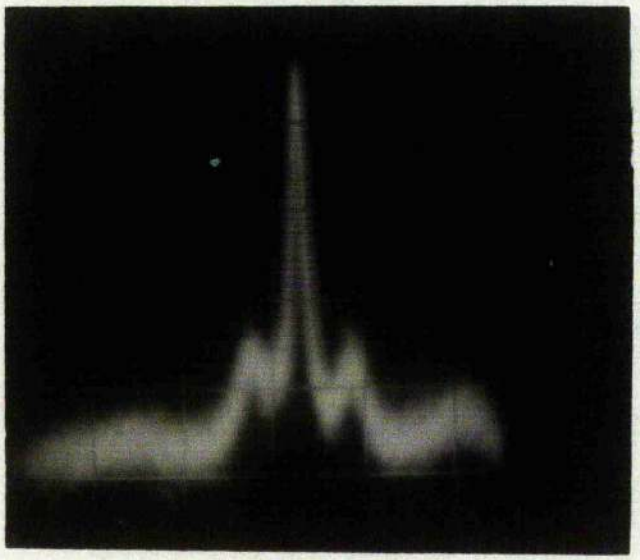

Line I of Spectrum. An Impurity Line

Figure 6.2 Oscillograms of the F-Centre Line and Line I

the sliding-stub tuner in the cavity arm.

With a standard containing about 10^{18} spins, the absorption signal was 300 mv with a noise level of 50 mv. Hence the sensitivity for DPPH is

$1.65\ 10^{17}$ spins at $300^{\circ}K$: 45 μw power input

and for samples other than DPPH

$6.1\ 10^{16}\ \Delta H_L$ spins at $300^{\circ}K$: 45 μw input

where ΔH_L is the sample line width in gauss. At low temperatures the sensitivity is increased to

$8.5\ 10^{14}\ \Delta H_L$ spins at $4.2^{\circ}K$: 45 μw

$3.0\ 10^{14}\ \Delta H_L$ spins at $1.5^{\circ}K$: 45 μw.

CHAPTER 7

RESULTS OF SPIN-LATTICE RELAXATION EXPERIMENTS

7.1 Introduction

There are three widely used methods of measuring spin-lattice relaxation times by microwave techniques: the cw saturation method; the "saturation-recovery" method, and the "inversion-recovery" method. The first method has been used in these experiments.

In inversion-recovery the line is inverted by A.F.P. field sweep, and the relaxation of the line to its thermal equilibrium value is observed as a function of time, by monitoring the whole line by a second field sweep through the line. The cycle is repetitive, the period of each cycle being much longer than T_1. In this method spin-lattice relaxation proceeds unimpaired by any interaction with the monitor microwave field, the Zeeman and cavity frequencies being different (Figure 7.1), until the second sweep occurs, so that a true T_1 may be obtained. A further advantage of this technique is that a phonon-bath bottleneck may be detected[29] as a marked decrease in the rate of recovery at the point of saturation. Results obtained by this method are independent of the broadening mechanism of the line, and as the recovery of the whole line is observed, any large cross-relaxation or spin-diffusion within the line may be detected by a change of shape.

The spin-lattice relaxation times of Samples 1 - 7 have been measured at varying temperatures in the range 1.4 - 4.2°K. The results of these measurements will now be presented.

7.2 Inversion-Recovery Method

The experimental technique in this method is the same as that used in field-swept maser oscillation experiments. The sequence of events in a measurement of T_1 is shown in Figure 7.1 and is as follows:

(1) Apparatus is set up as a spectrometer with the monitor and L.O. klystrons.

(2) The magnetic field is swept by the coils mounted on the helium dewar by driving the power amplifier with the triangle waveform.

(3) The X-13 is pulsed to the cavity frequency by applying the rectangle waveform to the reflector. The power output is optimised by adjusting the sliding-stub tuner in front of the X-13 and the X-13 is tuned so that the peak of its mode is coincident with the cavity frequency; exact tuning to the cavity is made by fine adjustments to the rectangle voltage. The length of the rectangle is adjusted to completely overlap the first field sweep and the rate of the first sweep is adjusted to give maximum inversion.

(4) Recovery of emission to absorption is recorded as a function of time by delaying the second sweep to later times. The measurement of interest is the difference between the emission and absorption peaks from the thermal equilibrium value of the absorption, and by

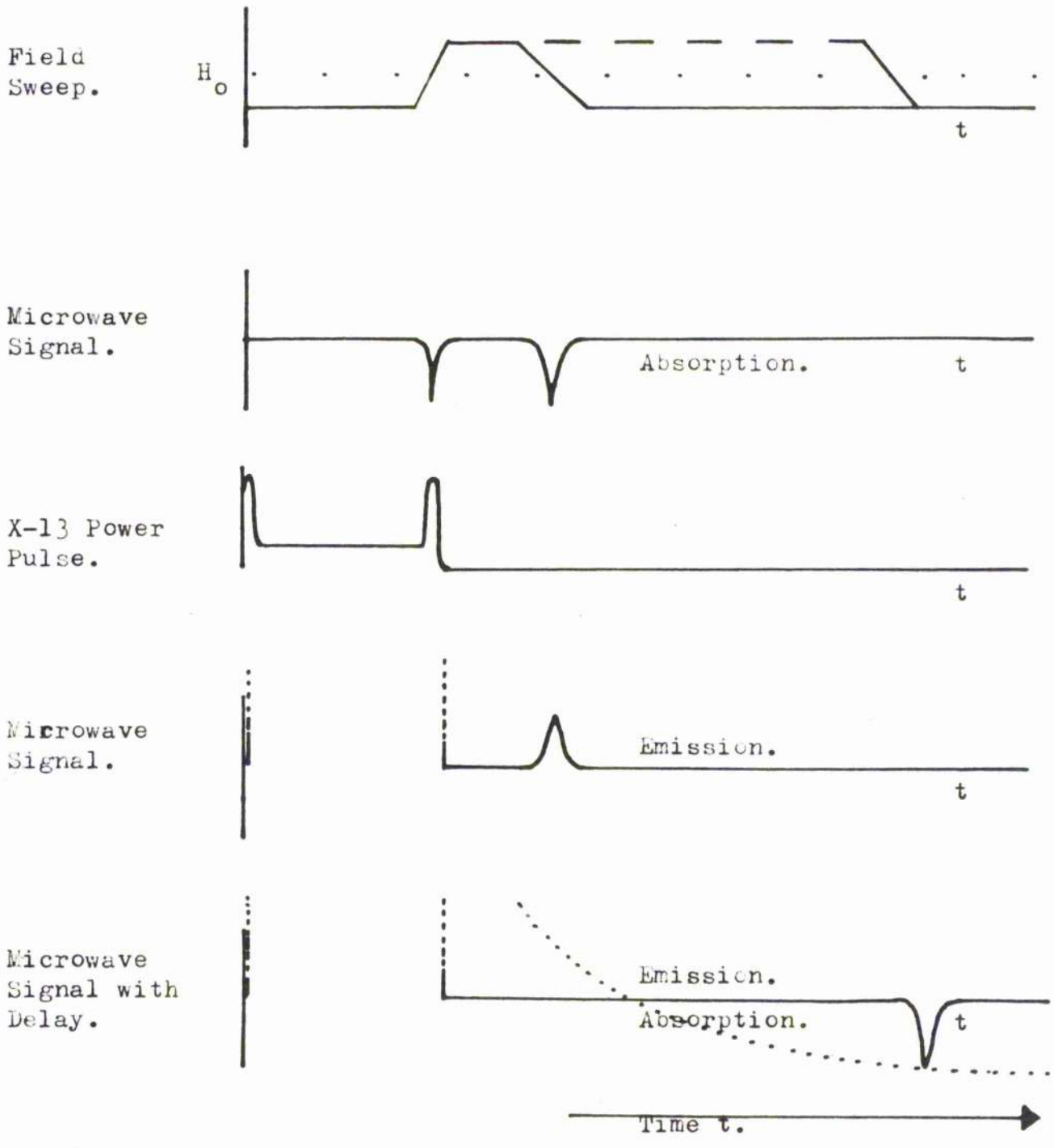

Figure 7.1 Inversion-Recovery Technique.

noting the equilibrium value of absorption when the X-13 is fully attenuated, this difference can be recorded. The linearity of the detector crystal characteristic has been checked at the power levels used in these experiments, so that a simple addition of the signals recorded is possible.

The monitor power to the cavity is kept as low as possible, $\sim 5\ 10^{-8}$ watts, but small increases in this figure are found not to alter the recovery rate. The cavity is tuned by the sliding-stub tuner, in the cavity arm, so that only resonance absorption is displayed and by using slight overcoupling, the cavity is not taken through match during the recovery by the absorption of the spin system. In order that the shape of the line is displayed in full, the second sweep is made slower than the first, so that the whole line will get through the I.F. amplifier (bandwidth 10 Mc). A typical series of photographs of the relaxation from an inverted line is shown in Figure 7.2.

7.3 F-Centre Line

The measured line width of the F-centre absorption line is 1 gauss in Sample (1) but it decreases as the spin concentration decreases to $\sim$ 0.4 gauss in Sample (7). The broadening is not a strong function of concentration. The nature of the broadening has been investigated by attempting to burn or invert a hole in the line. By applying the X-13 power pulse to the first half of

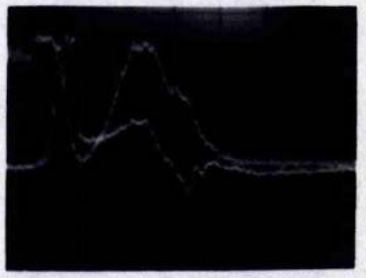

Inverted hole in Sample (5)

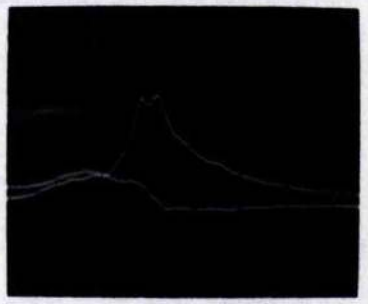

Inverted hole in Sample (1)

Figure 7.3 "Hole Burning" in the F-Centre Line

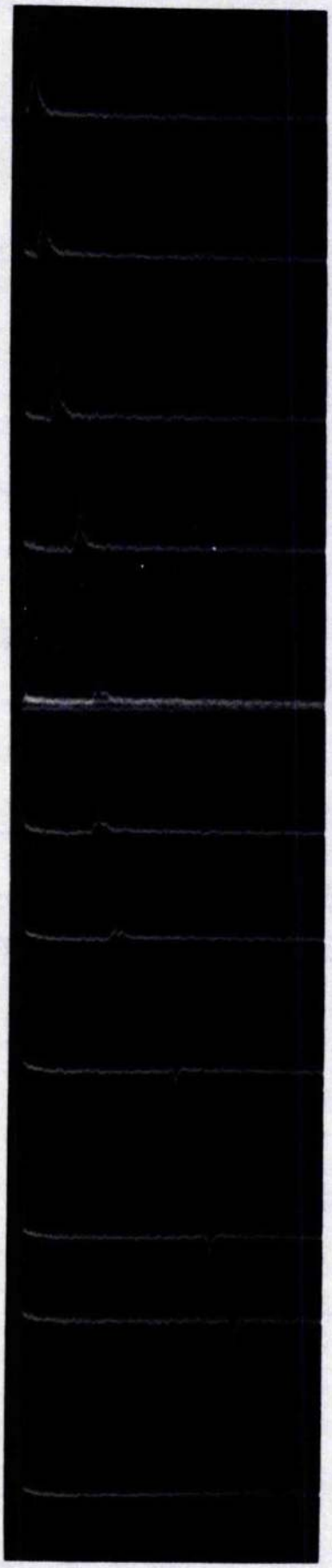

Figure 7.2 Oscillogram of Recovery of the F-Centre Line from Inversion

the first passage through the line, that is, slightly shortening the rectangle pulse, it is possible to invert a hole in all samples. The degree of inversion that is obtained is significantly greater in weak samples. Inverted holes are shown in Figure 7.3 for Samples (1) and (5): holes remain inverted up to 0.5 msec after inversion. The broadening of the F-centre line in MgO is inhomogeneous at the spin densities used here, and at the lower spin densities this type of broadening becomes even more pronounced.

7.4 Relaxation

Relaxation Rates

The recovery is measured up to 9 msec from inversion and the recovery is adjusted to take place from $\sim 40\%$ of inversion. The repetition cycle rate is 2.5 cs which ensures complete recovery to thermal equilibrium in all samples. The samples, except Sample (1), are mounted in a .9" x .4" plastic cavity. By the nature of the size of the MgO samples the resonance loss is quite large in comparison with the total cavity loss, so that radiation damping may contribute to some extent during the second sweep in the relaxation process.

The recovery can be described by a single exponential at all spin temperatures in only Sample (7). At higher concentrations the nature of the recovery changes: recovery of Samples (5) and (6) is of the form of Figure 7.4, the recovery curve of Sample (5)

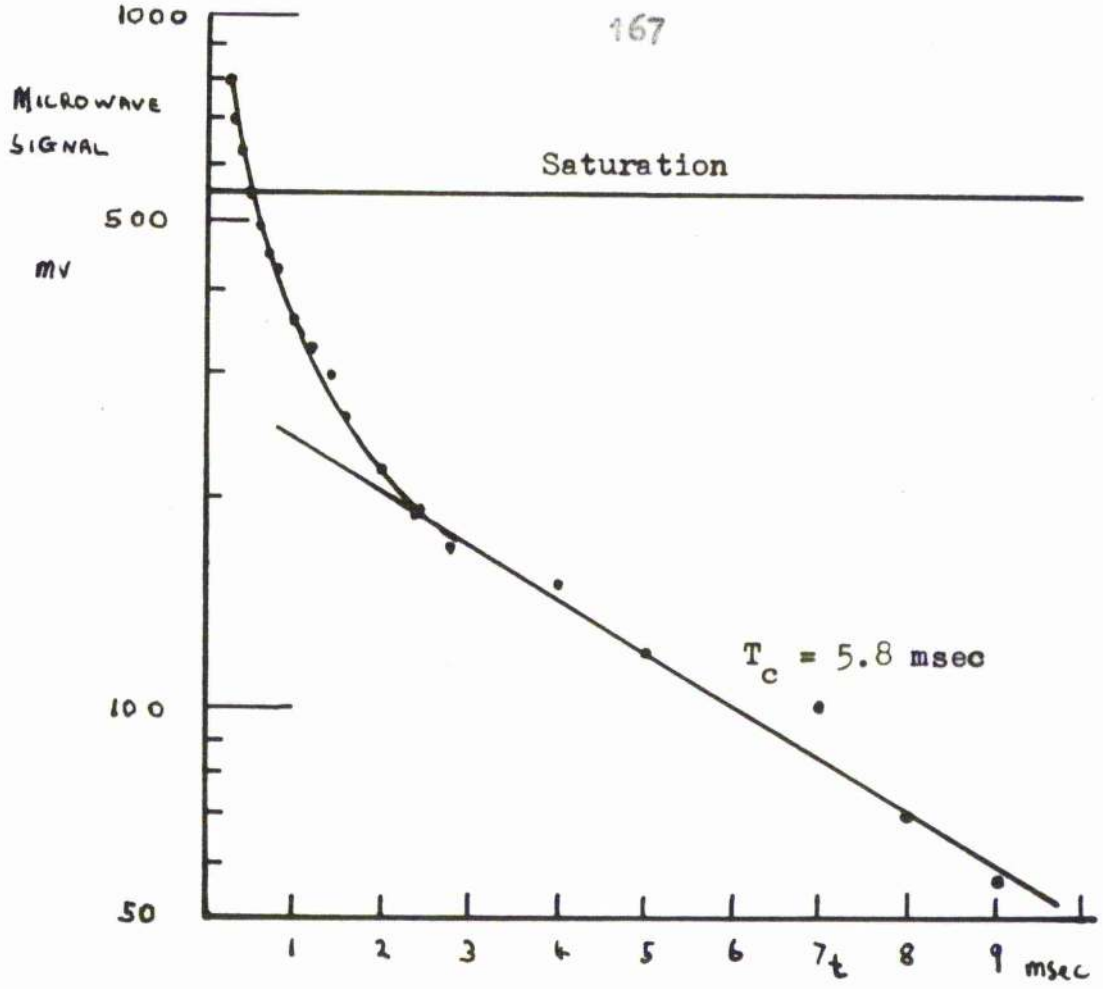

Figure 7.4 Relaxation of Sample (5) at T = 2.89°K

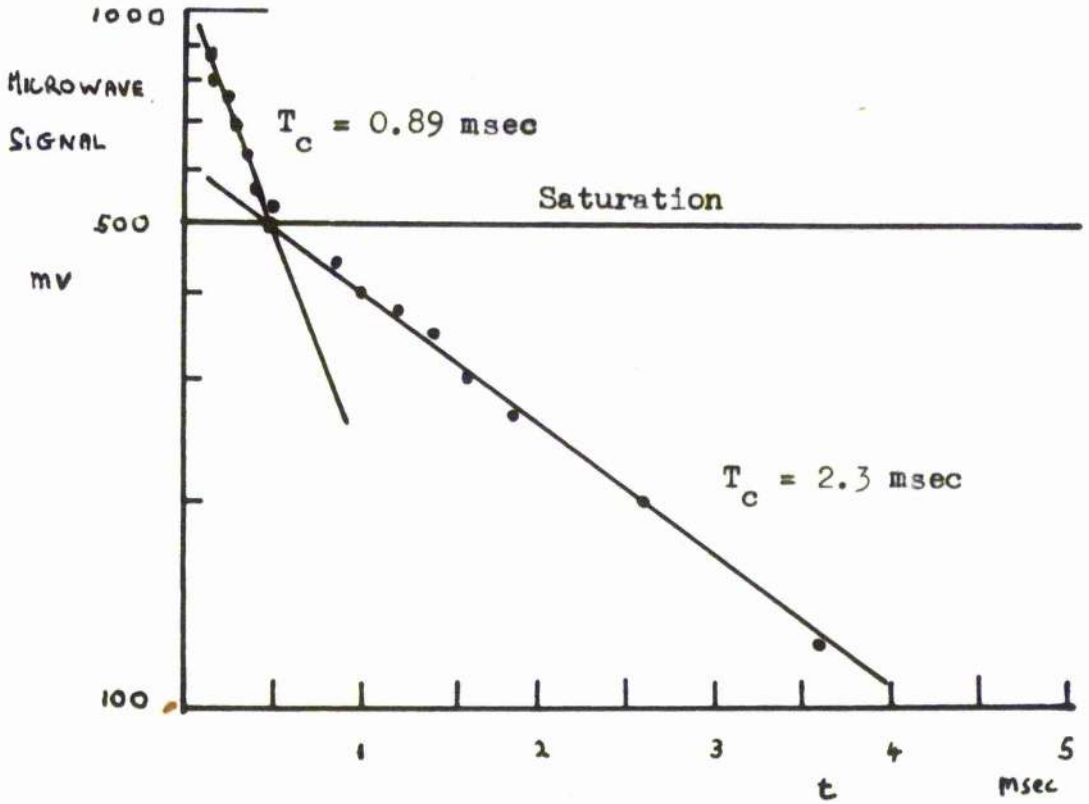

Figure 7.5 Relaxation of Sample (1) at T = 2.5°K

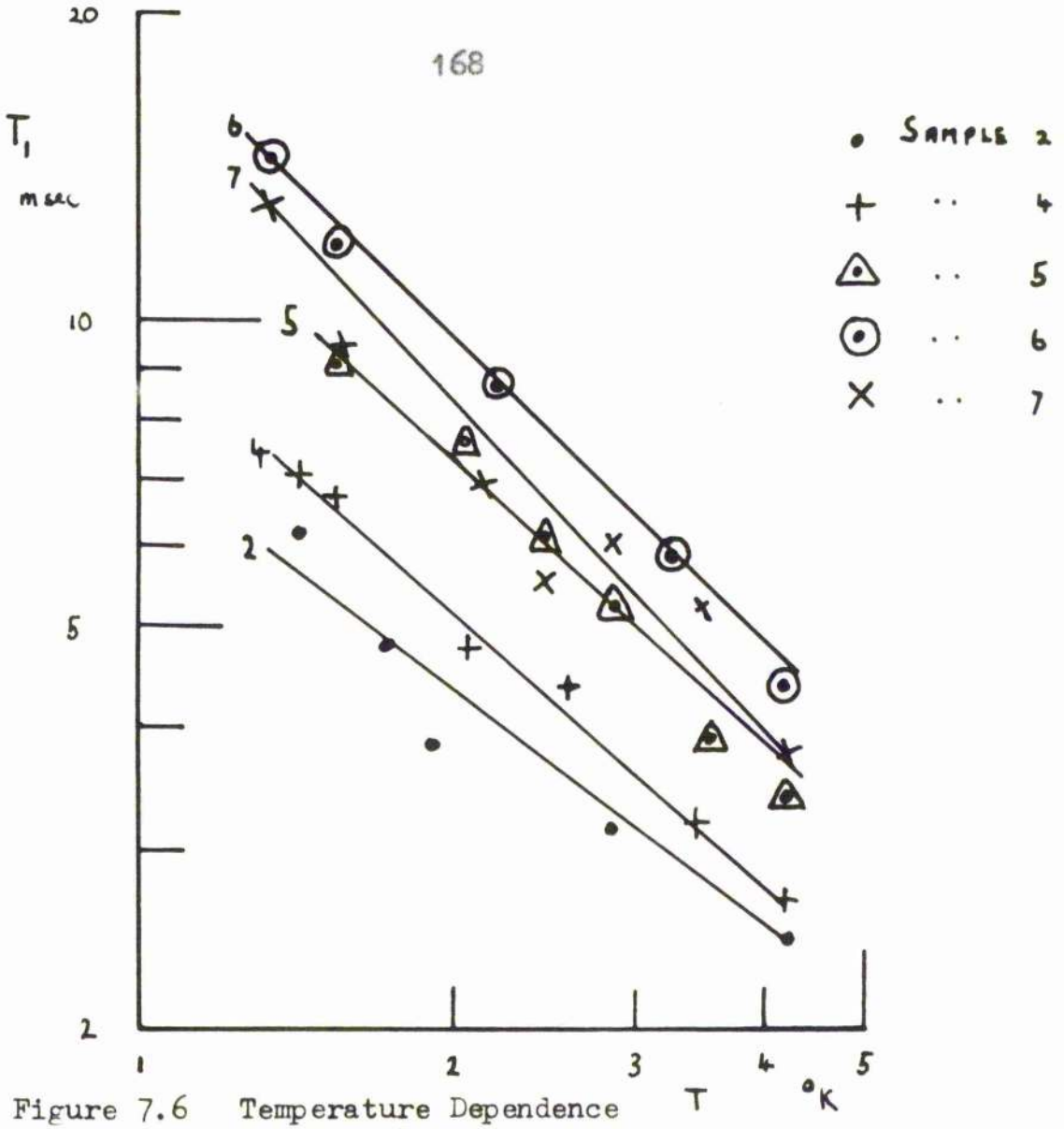

Figure 7.6 Temperature Dependence of T_1

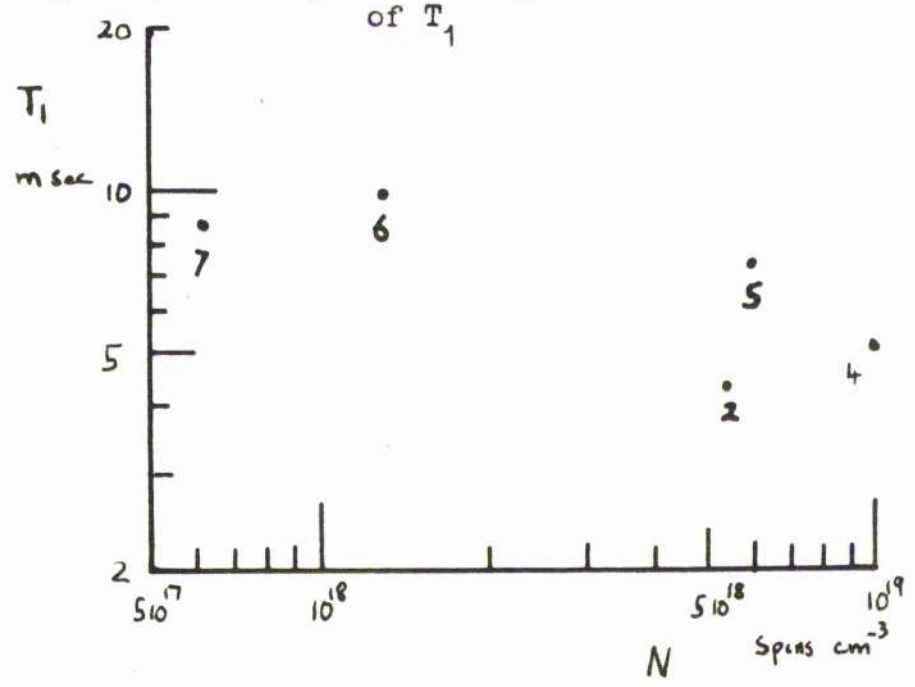

Figure 7.7 Concentration Dependence of T_1 at T = 2°K

at 2.89°K, whereas the recovery of Samples (1), (2) and (4) is similar to Figure 7.5, the recovery of Sample (1) at 2.5°K. The recovery of Samples (5) and (6) will be discussed here and that of Samples (1), (2) and (4) under the heading Phonon-Bath Bottleneck.

In Samples (5) and (6) the initial recovery is fast but the asymptotic time constant is only a little smaller than that of Sample (7), see Figure 7.6. In general the concave nature of the recovery becomes more pronounced at lower temperature in any one sample and also at a given temperature, in Sample (5) over Sample (6). In Reference 29 a similar effect has been observed by Chester et al in the relaxation of Cr^{+++} in $K_2Co(CN)_6$. At high Cr^{+++} concentrations the linewidth of the 1 ↔ 2 transition increases and overlap between neighbouring lines of the Cr^{+++} spectrum occurs. The cross-coupling that arises gives a fast component in the relaxation over the first few percent of the recovery so that a similar recovery curve to Figure 7.4 is obtained. In MgO the situation is similar. At low spin densities the F-centre line is narrow and essentially no overlap is seen with the nearest members of the sextet of the impurity lines, whereas at high concentrations some overlap is observed, the F-centre line being more spread out in the wings of the line in particular. Hence, it is possible that the shape of the recovery of Samples (5) and (6) is caused by cross-relaxation between the F-centre line and the impurity lines.

Phonon-Bath Bottleneck

In Samples (1), (2) and (4) a discontinuity is noted in the recovery at saturation, such that the recovery is exponential but proceeds with two time constants; the time constant at negative spin temperatures is smaller than that at positive temperatures. The discontinuity is not marked in Samples (2) and (4). For example, in Sample (4) at 2.85°K the time constants are 2.3 msec and 3.8 msec respectively, but in Sample (1) the change in slope is large; at 2.5°K the time constants are 0.89 msec and 2.3 msec respectively. The recovery of Sample (1) is shown in Figure 7.5.

There is no evidence that the relaxation of these samples is just a limiting case of the concave recovery of Samples (5) and (6) for at all temperatures the discontinuity is sharp and the recovery can be fully described by two single time constants. As the discontinuity always appears at the point of saturation, a phonon-bath bottleneck would seem to be responsible for this type of recovery. The recovery seems also to be caused by phonon imprisonment for two reasons. Firstly, the bottleneck increases, as expected for true phonon imprisonment, with sample dimensions the same as those of Samples (1) and (4), and secondly, the discontinuity does not appear in weak samples.

In maser oscillation experiments with Sample (1), see Section 8.5, the decay of the oscillator output with time is exponential and at 1.5°K takes place with a time constant of 0.6 msec.

This result agrees well with the spin-lattice relaxation time during inversion measured by the Inversion-Recovery method and indicates also the presence of a phonon bottleneck.

Temperature Dependence

The temperature dependence of T_1 has been checked in the range 1.4 - 4.2°K. Temperatures are measured from the vapour pressure of the helium bath with the mercury manometer, or the Vacustat gauge, to an accuracy of ± 0.04°K. In Sample (1) no consistent results have been obtained for the temperature variation but at 2.5°K a reproducible value of T_1 is 2.3 msec. The dependence of T_1 on temperature is shown in Figure 7.6: the accuracy of T_1 measurements is estimated to be ± 15%. In Figure 7.6 only the time constant at positive spin temperatures is plotted for Samples (2) and (4), and for Samples (5) and (6) the asymptotic part of the recovery has been used.

In strong samples, Samples (2) and (4), the dependence seems to follow a $T^{-0.7}$ law but in Sample (7) there is a T^{-1} relationship. Although this shows that the direct phonon process is dominant in the relaxation, the deviation from the expected T^{-1} law is marked.

Concentration Dependence

In Figure 7.7 the dependence of T_1 on the F-centre concentration is shown; the points are taken directly from

Figure 7.6 at 2°K. Of these points, Sample (2) seems to give a too low value for T_1, so that it is possible that radiation damping effects in this large sample contribute to the rate of recovery. At low concentrations it seems as if T_1 is tending to become independent of concentration.

In conclusion it is noted that the present study of the relaxation of F-centres in MgO is in no way a complete one, the orientation being quite arbitrary for any sample and the samples may in any case not be single crystals. The single phonon process is shown to be dominant but in weak samples the recovery from the inverted state is not described by a single exponential and seems to be determined by cross-relaxation with nearby impurity lines. In strong samples, however, the relaxation takes place with two exponentials which show a discontinuity at saturation. It is concluded, therefore, that a phonon-bath bottleneck quite likely appears in samples of large dimensions, and that radiation damping is not responsible for this effect.

CHAPTER 8

RESULTS OF MASER OSCILLATION EXPERIMENTS

8.1 Introduction

Maser oscillations have been obtained by activating the spin system of the F-centres in irradiated MgO by either A.F.P. field or frequency sweep: the two types of oscillations that occur after these methods of activation will be called for clarity, "field-swept" and "frequency-swept" oscillations respectively. Experiments have been carried out with Sample (1) mounted in a .9" x .1" cross section plastic cavity, length 19.7 mm, and with Samples (2) and (3) stuck together with nail varnish, mounted in a .9" x .4" plastic cavity, length 42.5 mm, where each cavity is operating in the TE_{102} mode.

Oscillations are obtained quite readily in the temperature range 1.4 - 4.2°K, and large output powers have been detected, the maximum power recorded being 220 mw (Sample (1), "field-swept" oscillation, 1.5°K, 9.464 kMcs). The structure of all oscillation pulses is characterised by amplitude modulation, which in the extremes of high and low powers, takes the limiting form of many well separated pulses with superimposed high frequency modulation, Figure 8.1, or one pulse with high frequency "wiggle" modulation Figure 8.2, respectively: the single low power pulse corresponds to the first pulse of the high power complex. It has proved

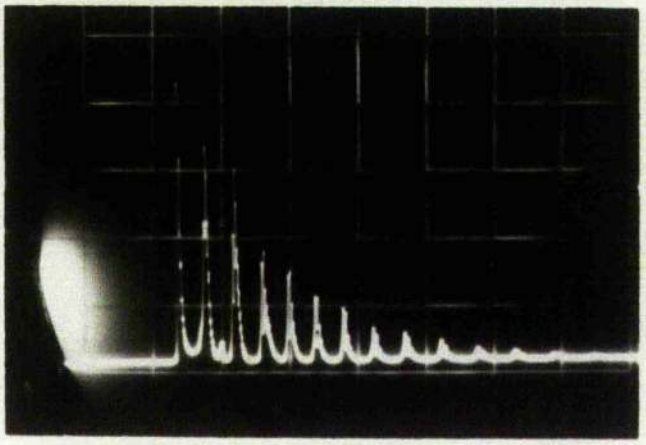

100 μsec

Oscillation pulses of the separated type.

Figure 8.1 Oscillograms of Maser Oscillation Pulses.

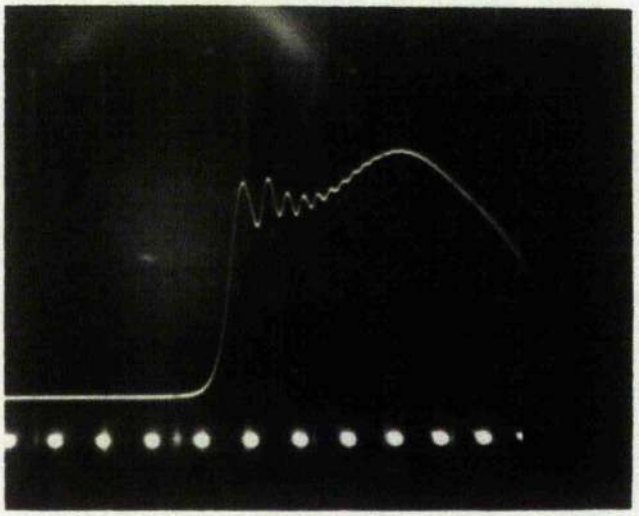

1 μsec markers

Oscillation pulse with "wiggle" structure.

impossible to obtain oscillations where field sweep is absent, for the very method of activation and display of field-swept oscillations entails large magnetic field sweeps, and in frequency-swept oscillation, the establishment and removal of the required field inhomogeneity introduces field variation.

The characteristics of maser oscillations and the structure of the pulses have been investigated. Results are presented and compared to the theoretical work carried out in Chapter 4. Comparisons of the frequency of modulation and depth of modulation in pulses of low powers are made with predictions for purely field-swept oscillations.

In Section 8.8, the experiment designed to detect variations of $\underline{M}$ during maser oscillation is described, and evidence in verification of $\underline{M}$ nutating during oscillation is presented. Variations of $\underline{M}$ during inversion and oscillation, field or frequency-swept case, have been detected by a simple induction experiment but no detailed comparison to the work of Chapter 4 is possible.

Oscillation pulses have been studied by crystal-video detection. The I.F. amplifier is not used to study the structure of pulses because the total bandwidth, $\pm$ 5 Mcs, with a linear response over only $\pm$ 1.5 Mcs, proved in some cases to be three times smaller than that of the total frequency spectrum of oscillation pulses, see Section 8.7. Oscillation pulses are in

general sufficiently large to allow simple crystal-video detection, the CD 643.2 oscilloscope, linear bandwidth 12 Mcs, being used for display. A direct comparison of the I.F. signal and crystal signal of oscillation pulses shows that crystal-video detection gives a more valid recording. It is stressed, however, that this system of detection is not optimum and some proportion of the high frequency detail of pulses will remain unresolved. A better detection system to study the structure of oscillation pulses would be superheterodyne detection, I.F. $\sim$ 40 Mcs and bandwidth $\pm$ 20 Mcs, and display oscilloscope of similar bandwidth: such equipment, however, was not available.

8.2 Inversion Techniques

The methods of activation, A.F.P. field and frequency sweep, have already been described in Section 5.4, the sequence of events in either method being illustrated in Figure 5.8. The methods of obtaining oscillation will be considered.

Field-Swept Oscillation

In the field-swept case the procedure for setting up the apparatus is a facsimile of that described in Section 7.2, as used in Inversion-Recovery measurements, but further fine adjustments of the X-13 frequency (rectangle waveform voltage and micrometer adjustment) and output power (load sliding-stub tuner), and careful adjustment of the cavity coupling to the waveguide (sliding-

stub tuner in the cavity arm) is necessary before maser oscillation is obtained. Most efficient inversion is ensured by adjusting the first slope of the triangle waveform so that the rate of sweep through the line is optimum: a rate of $2.87\ 10^4$ gauss sec^{-1} was found to give maximum inversion although good inversion is obtained at all available sweep rates. The presence of oscillations is checked by switching off the monitor klystron and both the monitor and L.O. klystrons are switched off during oscillation pulse measurements. A typical oscillogram of the X-13 inverting pulse followed by oscillation, is shown in Figure 8.3: the spin system absorption is clearly seen in the X-13 pulse as the line is traversed.

A large remnant inverted magnetization occurs after field-swept oscillation and its presence has been demonstrated by repeatedly sweeping the field back and forth through the line, by applying the gated repetitive saw tooth to the power amplifier after the triangle waveform by means of a mixing circuit and so observing the decay from emission to absorption. No recording of this effect is available but with a monitoring power of 10^{-7} w, a gain of 6 db occurred 250 μsec after oscillation.

It should be further noted that the oscillation pulse is narrower than the resonance absorption line, Figure 8.4, although the whole line is inverted. Amplification in the wings of the line

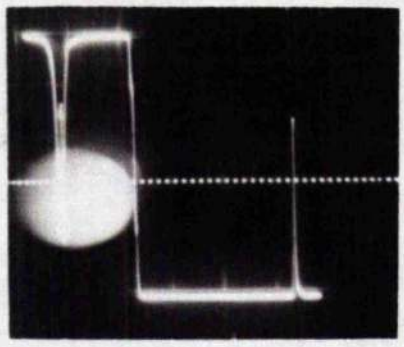

1 μsec markers

Figure 8.3 Field-Swept Oscillation: X-13 and Oscillation Pulse.

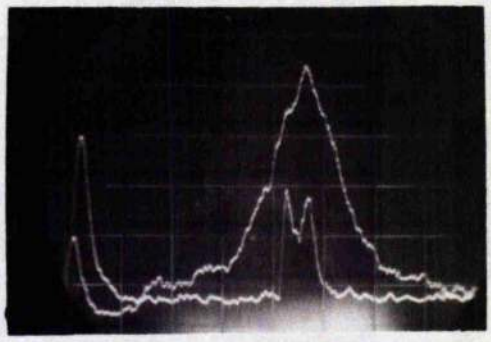

100 μsec

Figure 8.4 Maser Oscillation Narrower than the Resonance Line.

40 μsec

Figure 8.5 Maser Oscillation Alone.

40 μsec

Figure 8.6 Maser Oscillation with Maser Amplification in the Wings of the Line

is possible, therefore, while oscillation occurs in the centre. This is demonstrated in Figures 8.5 and 8.6: amplification of the monitor signal, tuned to one side of the line, is seen in Figure 8.6.

Frequency-Swept Oscillation

Less care is necessary in setting up oscillation by frequency sweep inversion. The trapezoid waveform, with delayed return sweep, is used to sweep the X-13 through the $3\frac{3}{4}$ mode, pretuned to the cavity frequency. When the magnetic field is adjusted to resonance, spontaneous oscillations occur after the sweep through the cavity frequency, as a series of bursts of radiation beating with the X-13 power. Oscillations are suppressed, for the duration of the X-13 sweep, by adding an inhomogeneity to the field by applying the rectangular waveform to the power amplifier which here drives one sweep coil only. As the inhomogeneity is removed maser oscillation commences. The X-13 sweep, followed by oscillation, is shown in Figure 8.7.

The rate of sweep of the X-13, most efficient in inverting the spin populations, is $8\ 10^5$ Mcs sec^{-1} in the presence of the inhomogeneity (optimum) due to a 2 amp current pulse. This current pulse gives rise to a 0.7 gauss displacement of the steady field and introduces an estimated inhomogeneity[67] at the sample of 0.9 gauss cm^{-1} due to the dipole field of the single coil. The F-centre line is, therefore, broadened to 2.8 gauss in Sample (1) and 2.1 gauss in Samples (2,3). These widths are to be compared

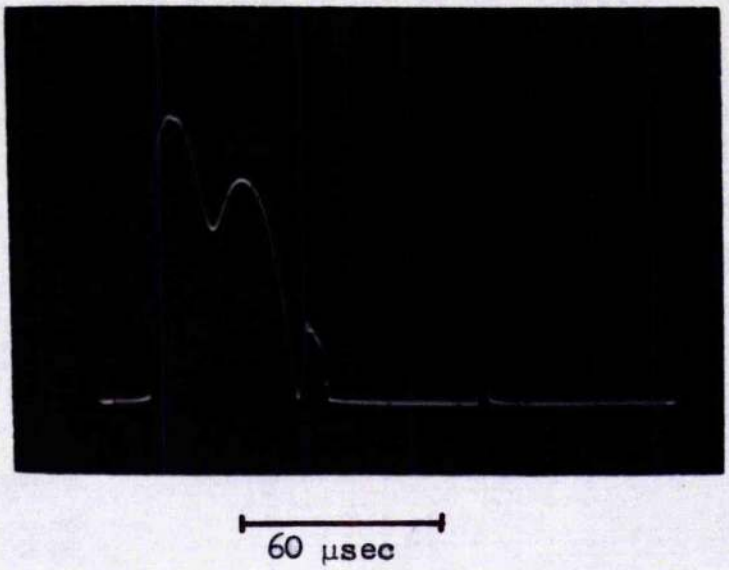

Figure 8.7 Frequency-Swept Oscillation: X-13 and Oscillation Pulse

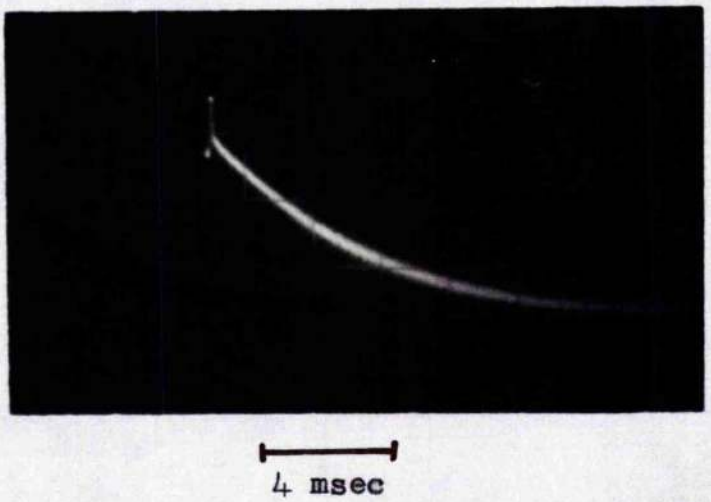

Figure 8.8 Frequency-Swept Oscillation and Relaxation.

to those of the cavities in which the samples are mounted, Table 5.2, which are respectively 11.8 Mcs (4.0 gauss), 7.9 Mcs (2.7 gauss) at 1.5°K, showing that the F-centre line is fully traversed during the inversion sweep.

A remnant inverted magnetization is also present after frequency-swept oscillation. Figure 8.8 shows amplification, after oscillation, of a monitor signal, 10^{-7} w, in a steady magnetic field: the decay is due to T_1 relaxation. This phenomenon may be due to self damping in both field and frequency-swept oscillation but in Section 8.7 this effect will be further discussed.

Frequency-swept oscillations in these studies do not take place completely in a steady magnetic field. Oscillations commence, rather, during the field sweep introduced as the inhomogeneity is removed and continue to extinction in the steady field. Hence, in detailed measurements of the structure of oscillations only the field-swept type have been studied where all the parameters of oscillation are well known and can be measured: it would be impossible to measure the time variation of the homogeneity or variation of the field during frequency-swept oscillation. The general characteristics of both types of oscillation have, however, been investigated.

8.3 Efficiency of Inversion

The fact that maser oscillation has been achieved is

evidence of the efficiency of the inversion of the spin populations of Samples (1) and (2,3) to a degree to satisfy $T_r < T_2^x$. However, the conditions of A.F.P. leading to oscillation are worthy of consideration.

The microwave field in the cavity at incident power P of the X-13, P being taken from the specification of the valve because no power measuring equipment is available,* can be calculated from measurements of Q_o and the V.S.W.R. in the cavity arm. The power reflector coefficient is

$$\Gamma^2 = \left(\frac{a-1}{a+1}\right)^2 \qquad 8.1$$

where V.S.W.R. a is equal to either Q_c/Q_o or Q_o/Q_c depending whether the cavity is under or over-coupled. The power dissipated in the cavity is, therefore, $P(1-\Gamma^2)$, and it can be shown[68] that the maximum cavity field ($2H_1$) for a rectangular TE_{102} cavity is given by

$$(2H_1)^2 = 8\,\mu_o\,Q_o\,P(1-\Gamma^2)/\omega V_c \qquad 8.2$$

---

* Footnote: A Wayne Kerr X-Band Milliwattmeter, U281, became available at the end of these experiments so that a power calibration of the X-13 output was possible. Powers quoted in this Thesis have been found to be correct to ± 15%.

in rationalised MKS units, where $\mu_o = 4\pi\ 10^{-7}$ henry m^{-1}. A conversion to Gaussian units gives

$$(2H_1)^2 = 32\pi\ 10^7\ Q_o\ P(1-\Gamma^2)/\omega V_c \qquad 8.3$$

where H_1, P, V_c are expressed in gauss, watts and cm^3 respectively.

For the two cavities mentioned in Table 5.2, which have Q's typical of all experimental runs, the A.F.P. inversion condition, Section 3.2, is evaluated at 1.5°K in Table 8.1 for the cases of field and frequency sweep inversion. Δ T in this table is the time to sweep through the resonance width and is here evaluated at the optimum rates of sweep already quoted. At maximum X-13 powers the condition $(\gamma H_1)^{-1} \ll \Delta$ T is clearly satisfied by a large margin and although $\Delta T \ll T_1$ for these samples, Δ T is larger than T_2^x and so the condition seems to fit the Redfield condition[41] for A.F.P. more closely than the Bloch condition[17]. Inversion will be shown in Section 8.5 to be completely successful for X-13 powers slightly less than maximum.

Estimates of the radiation damping time $T_r = (2\pi\gamma Q_L |\gamma H_o|)^{-1}$ at 1.5°K for the same cavities, from the data of Table 6.1 for Samples (1) and (2,3), are also made in Table 8.1. The oscillation condition $T_r \ll T_2^x$, $T_2^x = 2/|\gamma| \Delta H_L$, for an inhomogeneously broadened line, is well satisfied, the oscillation threshold being exceeded by a factor 71 for Cavity 1 and by 14.4 for Cavity 2. Similar figures have held in all experimental runs. As the spin

Sample	1	2, 3
Cavity	1	2
ν	9.3481 kMcs	9.4424 kMcs
Q_L	792	1190
Q_o	2210	2100
VSWR	1.8	1.19
Γ^2	0.817	0.57
P	490 mw	500 mw
V_c	1.12 cm^3	9.9 cm^3
η	1.0	0.13
H_1	0.87 gauss	0.51 gauss
$(\gamma H_1)^{-1}$	$6.54\ 10^{-8}$ sec	$1.12\ 10^{-7}$ sec
ΔT (field sweep)	$3.6\ 10^{-5}$ sec	$3.6\ 10^{-5}$ sec
ΔT (frequency sweep)	$3.5\ 10^{-6}$ sec	$3.5\ 10^{-6}$ sec
T_2^x	$1.14\ 10^{-7}$ sec	$1.14\ 10^{-7}$ sec
N	$4.3\ 10^{18}$	$5.2\ 10^{18}$
M_o [$T = 1.5^oK$]	$6.8\ 10^{-3}$ gauss	$7.7\ 10^{-3}$ gauss
T_r	$1.6\ 10^{-9}$ sec	$7.6\ 10^{-9}$ sec
$M_z(o)$ Threshold	$1.0\ 10^{-4}$ gauss	$5.1\ 10^{-4}$ gauss

Table 8.1 Inversion and Oscillation Conditions for Sample (1) and (2, 3) at 1.5^oK

densities, N, of Samples (1) and (2,3) are about equal, the superiority of Cavity 1 in producing maser oscillations is due to the large filling factor of this cavity. This conclusion is to be compared to remarks in Section 4.7 on the advantage of large η. The exact figure by which threshold is exceeded may, however, vary from the calculated figure because Q_L can be altered by the sliding-stub tuner in the cavity arm.

The X-13 pulse is extinguished after inversion as the rectangle or trapazoid waveform is removed from the reflector, but the cavity power will remain for a few times the cavity ringing time, Q_L/ω. For Cavities 1 and 2, Q_L/ω is $8\ 10^{-8}$ sec and $1.2\ 10^{-7}$ sec respectively, so that as oscillation is triggered a few microseconds after the extinction of the X-13, the cavity power will have decayed to a very small level. Oscillations are not triggered, therefore, by X-13 power.

The rates of sweep involved in this study would have been difficult to achieve without the use of plastic cavities. Large, opposing eddy currents would have been set up in normal metal cavities, say, Cu Ni of 0.010" wall thickness, and would have introduced limitations on the rate of sweep achievable with the available maximum sweep current (4.5 amps): the work of Hayward[69] is noted in this respect in estimating the magnitude of eddy currents. Large eddy currents in the walls of the cavity may, furthermore, introduce transient inhomogeneities to the steady

magnetic field at the sample, so broadening the resonance line and making inversion more difficult. No transient broadening is apparent in the MgO line at the highest sweep rate available.

The independence of the first slope of the triangle waveform from the second slope, has been checked by observing the constancy in width of the MgO line on the first field sweep, while the second rate is varied, the maximum field sweep being constant. Hence, in studying oscillation pulses for different rates of field sweep, the constancy of the degree of inversion can be assumed for any particular X-13 power setting.

8.4 Varying the Degree of Inversion

Three methods are available to control the inversion of the spin system. Of these, two rely on T_1 relaxation, and the third upon the condition of A.F.P. The three techniques will be discussed.

Firstly, by increasing the cycling rate of the maser, the spin system is prevented from fully reaching thermal equilibrium so that the net number of spins available for inversion, at the end of any cycle, is less than the thermally available number. This method was introduced in Section 3.3. One technical drawback here is the maximum repetition rate set by the maximum dissipation of the power amplifier valves (95 watts). For instance, with a current pulse of 3.2 amps of duration 0.3 msec, the maximum rate

is 440 cs, and at maximum X-13 power this rate is generally not sufficiently high to reduce oscillations to zero.

In the second method, the spin system is inverted at high X-13 power but at a low cycling rate, $\sim$ 13 cs. High power oscillations ensue immediately after the X-13 pulse, but by delaying the oscillation trigger to later times, as in the Inversion-Recovery experiments, and allowing T_1 relaxation to act, controlled oscillation heights can be obtained. The long delays required to obtain oscillations of a few milliwatts, up to 3 msec in some cases, proved troublesome in photographing oscillation pulses, when well expanded, due to apparatus instabilities.

Thirdly, the degree of inversion is controlled by varying the output power of the X-13 by the calibrated attenuator, so affecting the efficiency of inversion. It was thought initially that with weak inverting powers, the radiation damping field of the spins in the centre of the line may be large enough to inhibit inversion of these spins, the result being a broadening of the line and consequent change in the oscillation behaviour. Comparisons of oscillograms of pulses of the same power, under similar apparatus settings in the same experimental run showed, however, no difference in oscillation structure for inversion by any of the methods. The latter method has been used, therefore, throughout these studies for it proves to be the simplest to operate and allows most fine

control over the degree of inversion.

8.5 General Characteristics of Oscillation: Estimation of the Degree of Inversion

Oscillation powers are estimated either directly from the signal of the crystal detector, or from a comparison of the oscillation pulse power and the X-13 power by reducing the X-13 signal to that of the pulse by the direct reading attenuator in the detection arm. In the former, the calibration of the crystal detector voltage is carried out by introducing a reflection coefficient of unity into the cavity arm, and varying the X-13 power arriving at the crystal detector by the direct reading attenuator. The X-13 output is again ascertained from the valve specifications and a small correction for the transmission losses at the ferrite circulator is applied; the loss at the 30 db coupler in the monitor klystron arm is only 0.5 mw at an output of 500 mw. In the second method, the pulse power is obtained in decibels of the X-13 power: both methods prove to be equivalent, and powers accurate to $\pm$ 15% are obtained.

Useful information is obtained on the general operation of the maser oscillator from the characteristic curve of the oscillation peak power against inverting power. Figures 8.9 and 8.10 show the characteristics of oscillation (field-swept) at 1.5°K for operation with Cavities 1 and 2 respectively, under the conditions listed in Table 5.2. These curves are typical of field and frequency-swept

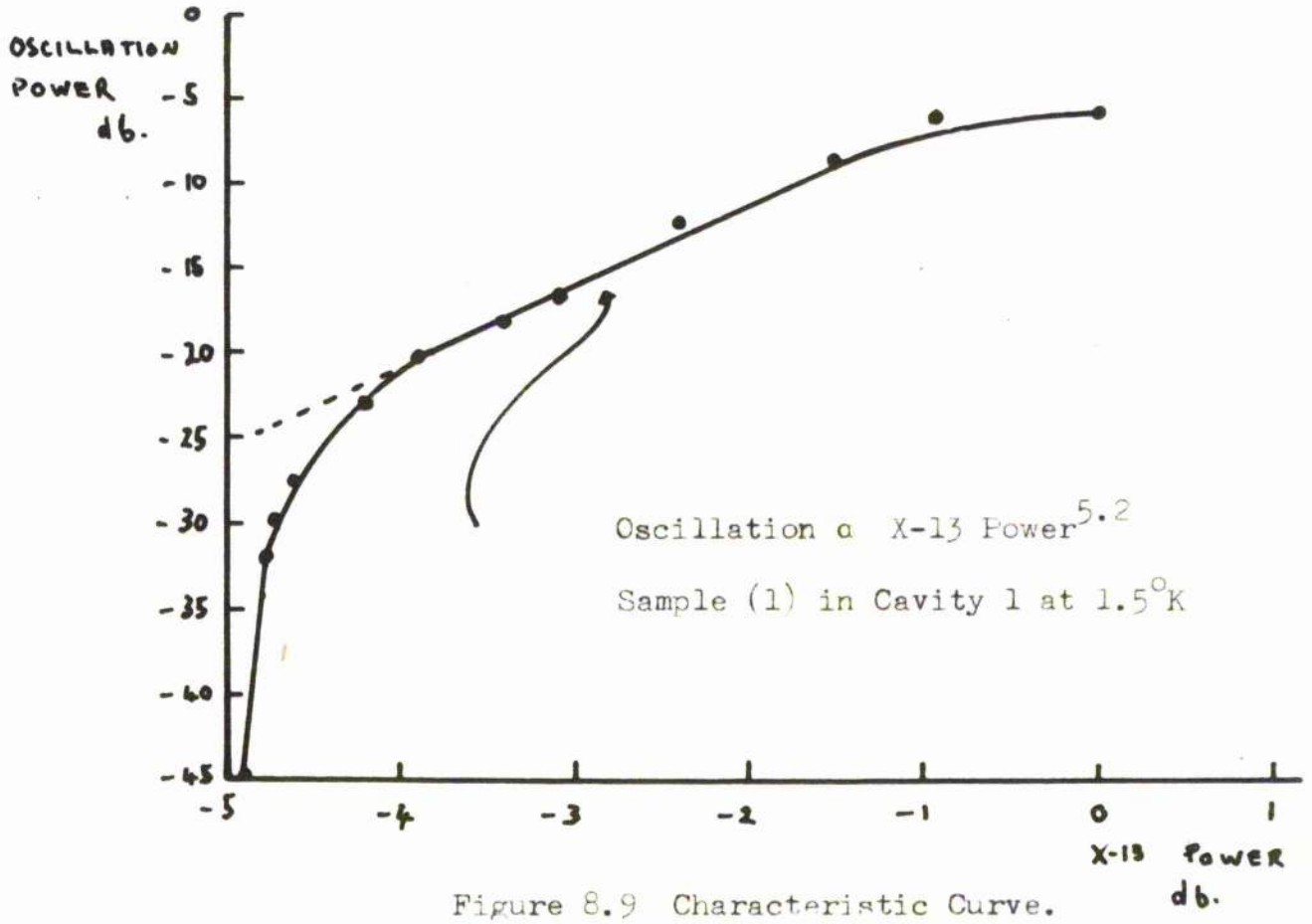

Figure 8.9 Characteristic Curve.
0 db = 500 mw.

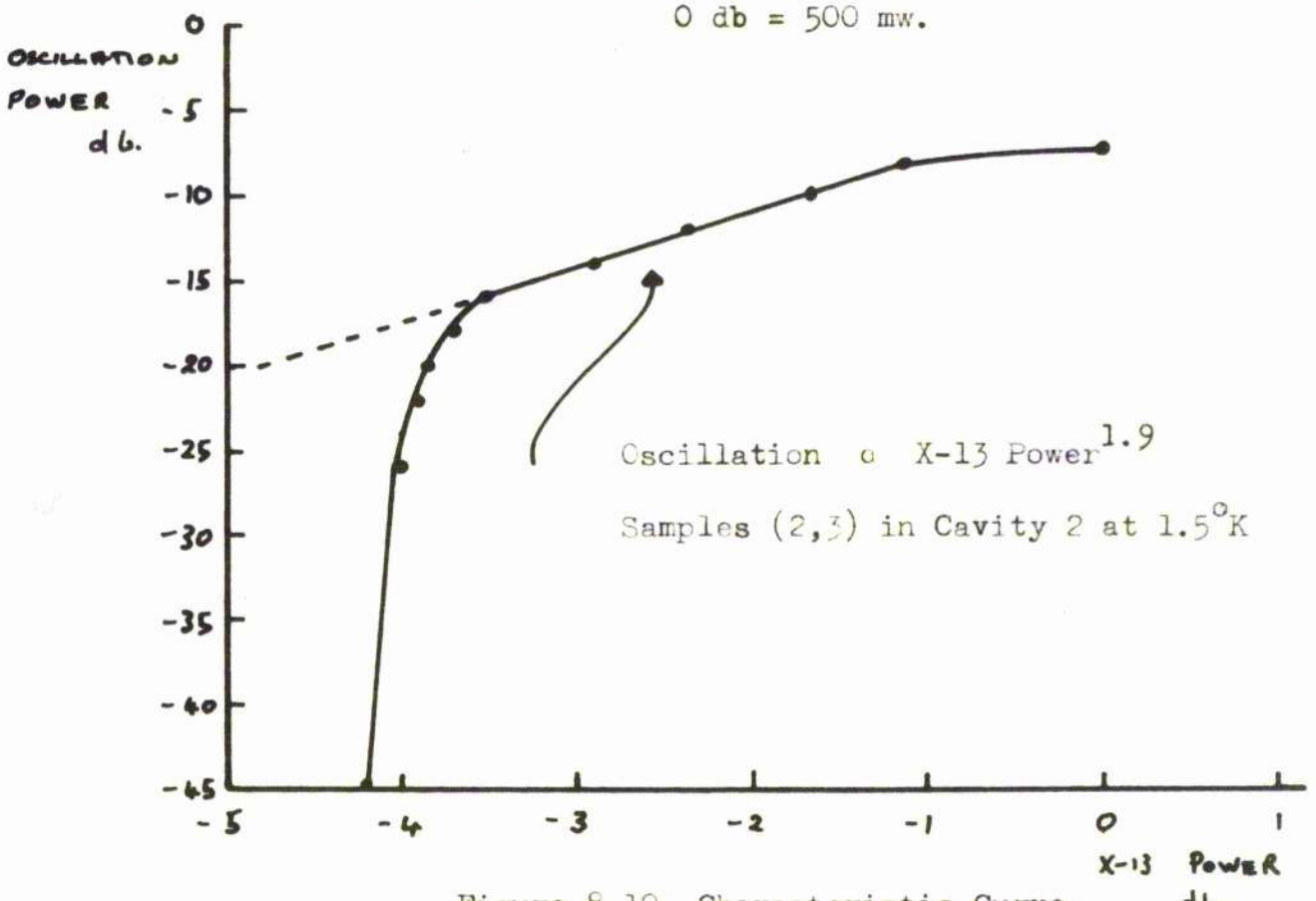

Figure 8.10 Characteristic Curve.
0 db = 500 mw.

oscillations obtained throughout the experiments, differing only slightly from run to run. The following conclusions, reached from these curves apply equally to field or frequency-swept oscillations.

At high X-13 powers, oscillations become constant, indicating that inversion of the spin population is complete. Further increase in inverting power would not increase the oscillator output. For lower X-13 powers, the linear portion of these figures, inversion is very efficient with inverting power, the dependence in this region being,

oscillation power α (X-13 power)^{3} to (X-13 power)^{6} for Sample (1)

oscillation power α (X-13 power)$^{1.5}$ to (X-13 power)^{4} for Sample (2,3)

where the exact dependence on X-13 power seems to be related to Q_o and to the cavity coupling condition. It has been noted that where saturated oscillation is weak, due to poor cavity coupling, the dependence is weaker then cases where oscillation is strong. The increased dependence on X-13 power of Sample (1) must be related to the large filling factor, η = 1 in this case. This is a situation analogous to that discussed in Chapter 4 where it was shown that large η favours strong oscillation.

In considering the sharp cut-off in the characteristic curve, it is noted that cut-off occurs in both cases for a reduction of X-13 power, from maximum, of only a few decibels. Re-evaluation of the A.F.P. condition at cut-off shows that the

inversion condition $(\gamma H_1)^{-1} \ll \Delta T$, is still satisfied. Hence, it is concluded that cut-off of oscillation is caused by failure to satisfy the condition $T_r < T_2^*$ alone: the sharp nature of the cut-off is, therefore, the experimental equivalent of the sharp threshold of oscillation predicted in Section 3.3 from very simple arguments and in Section 4.8 from the classical treatment of the oscillator.

A further conclusion of practical importance may be drawn from the characteristic curve in the region of the threshold of oscillation. Where oscillations are well established, the linear and saturated portions of Figures 8.9 and 8.10, the reasonable assumption can be made that

$$\text{peak oscillation power} \propto M_z(o)$$

where $M_z(o)$ is, in the notation of Chapter 4, the magnitude of the magnetization at the beginning of oscillation: this is based on the finding

$$(H_u^2 + H_v^2)_{max} \propto M_z(o)$$

of Section 4.7. This assumption when considered with the fact that A.F.P. inversion is maintained at threshold, indicates that an extrapolation of the linear portion of the characteristic curve towards lower X-ray powers gives the magnitude of the inverted magnetization down to cut-off. The degree of inversion k, where k is defined by

$$M_z(o) = - k M_o \qquad 8.4$$

$M_o = N \mu_\beta^2 H_o/kT$ being the thermally available magnetization, can be estimated from the characteristic curve by taking the ratio of the oscillation height, or near threshold the height of the extrapolated line corresponding to a given oscillation power, to the saturated oscillation height.

The validity of this method of evaluating k is substantiated by numerical calculation on Figures 8.9 and 8.10. Taking the height ratio of saturated oscillation, representing M_o, to the extrapolated line at cut-off, representing $M_z(o)_{Threshold}$, remembering the plots are logarithmic, gives a value of 120 and 12.5 for Cavities 1 and 2 respectively. These values are to be compared with the calculated figures of 70 and 14.4 respectively by which the oscillation threshold is exceeded, Section 8.3. The discrepancy between the measured and calculated values is resolved if Q_L during oscillation is larger than that listed in Table 5.2, that is, in the adjustment of the sliding-stub tuner in the cavity arm to give maximum oscillation output the cavity coupling has been made weaker. This situation compares favourably with the prediction in Section 3.3 that an undercoupled cavity should favour the production of strong maser oscillations.

The experimental procedure for estimating k in an experimental run is, therefore, as follows:

(1) The characteristic curve of oscillation power against X-13 power is taken for a particular apparatus setting and the extrapolated line drawn.

(2) The operating point on the straight line portion of the characteristic curve is found by noting the oscillation power.

(3) The ratio of the two heights is taken ($k < 1$).

The nature of the threshold of oscillation can be demonstrated also by viewing the time decay of oscillation as the oscillation trigger is delayed. The decay is exponential, the exponent having a single time constant, up to a certain time after inversion at which oscillation falls sharply to zero, Figure 8.11. The mechanism of the threshold can only be due here to the loss of the oscillation condition $T_r < T_2^x$. The time constant of decay in this figure is 0.6 msec for Sample (1) and 1.0 msec for Sample (2,3), both at 1.5°K (field or frequency-swept oscillations), which are smaller than T_1 measured by the Inversion-Recovery method for these samples at a negative spin temperature. The decrease must be due to an increased phonon-bath bottleneck that has been demonstrated to occur in these samples, for the negative temperature is "hotter" here than that allowed in Inversion-Recovery measurements.

The degree of inversion at any oscillation level can be determined from Figure 8.11 by the simple procedure of taking height ratios. For Sample (1) the threshold of oscillation is

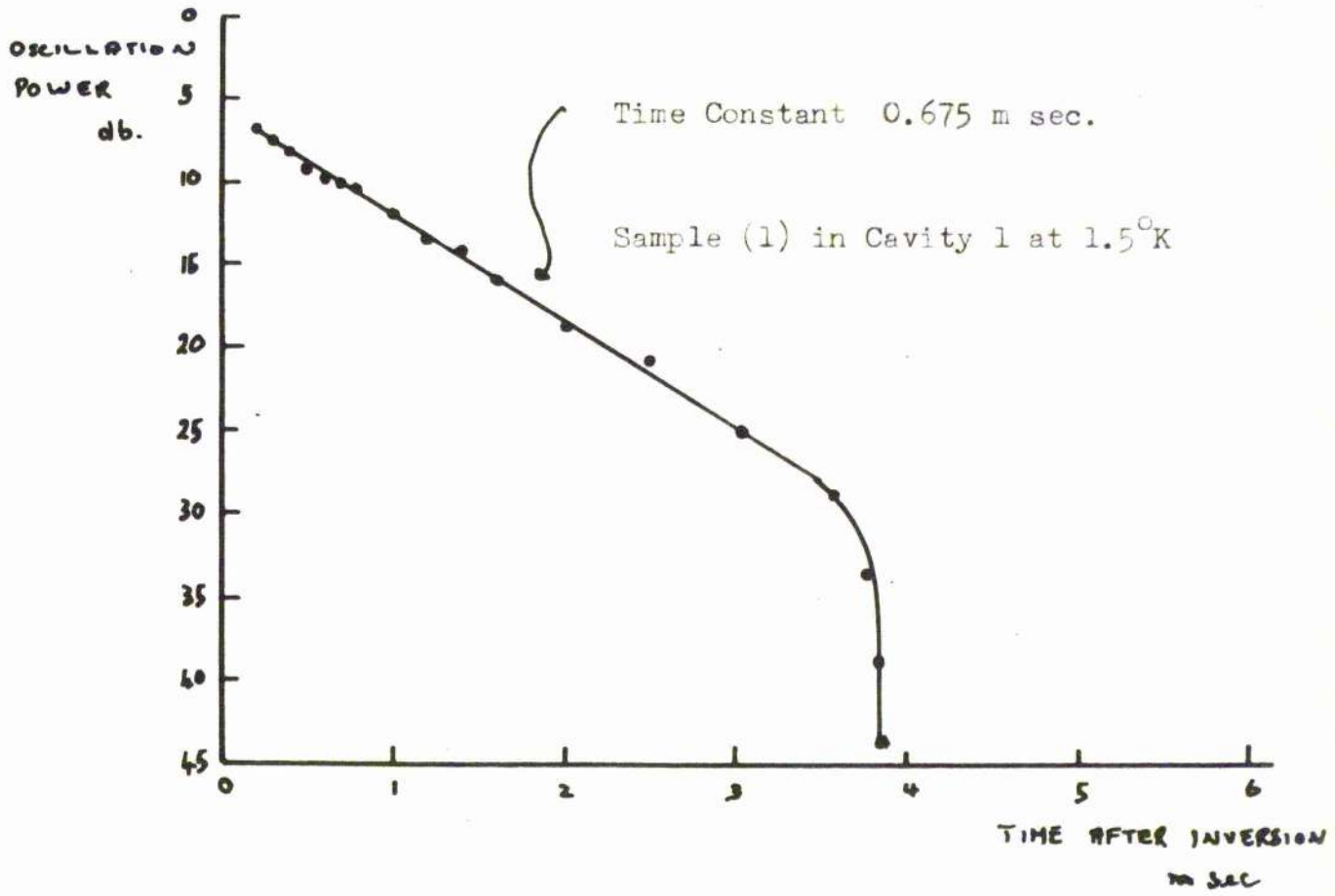

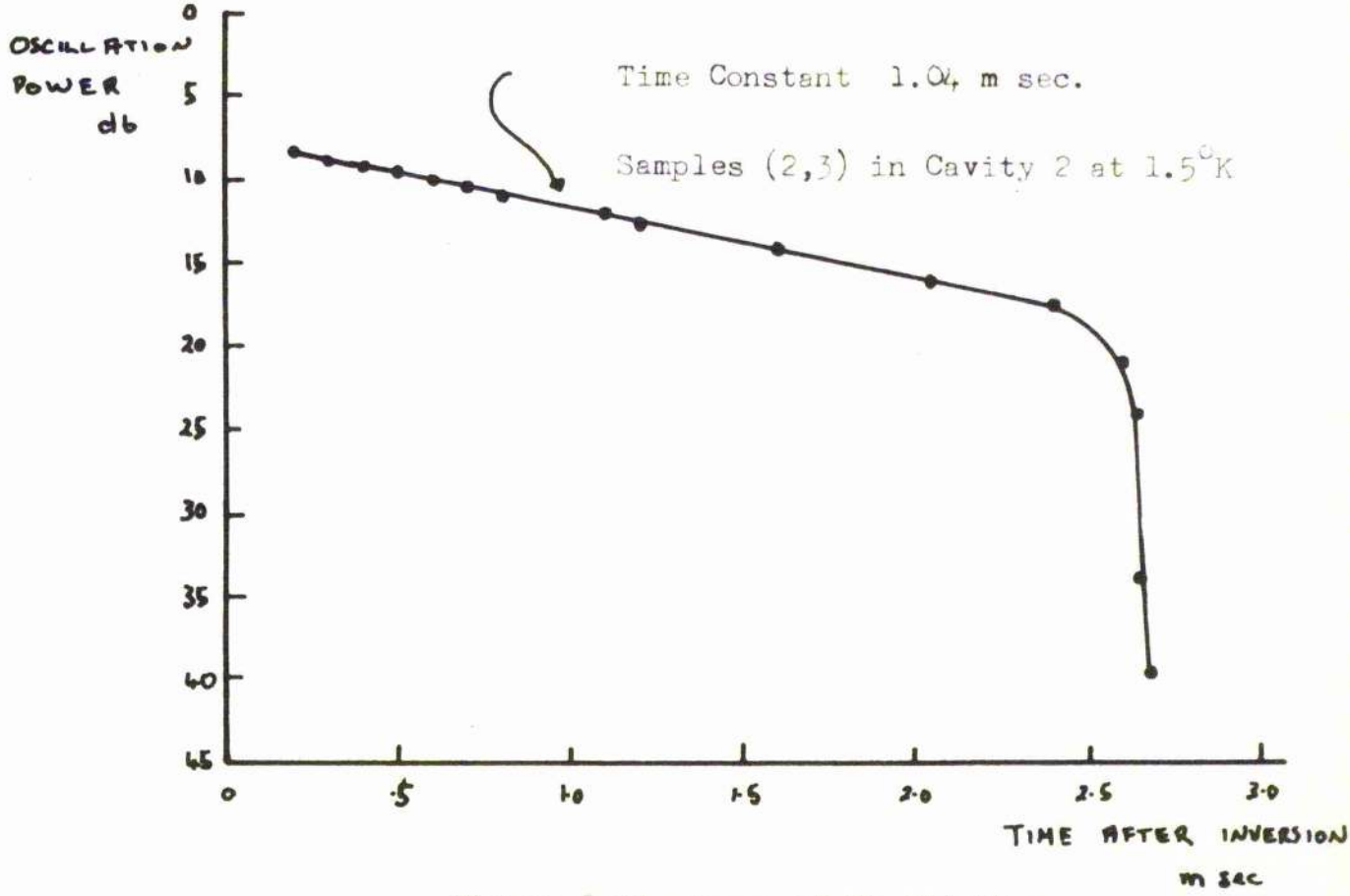

Figure 8.11 Decay of Oscillation.
0 db = 500 mw.

exceeded by a factor of 110 immediately after inversion and for Sample (2,3) by a factor of 13. These values are again in agreement with figures that are obtained by calculation.

The maximum oscillation powers that have been noted in these experiments are

Sample (1) : 220 mw

Sample (2,3) : 150 mw

being obtained in field-swept oscillation at 1.5°K. Smaller powers, by about 5 db, have been obtained in the frequency-swept case. In Sample (1) oscillations are possible up to 3.8 msec after inversion.

8.6 Energy Released in Oscillation

The total Zeeman energy of the spin system is given by

$$W_z = 2 M_z(o) H_o V_s = 2 (M_o k) H_o V_s \qquad 8.5$$

where k is the degree of inversion defined previously, and V_s the sample volume. At 1.5°K, for k = 1, W_z is 21.4 ergs for Sample (1) and 21.6 ergs for Sample (2,3). The energy W detected during oscillation is estimated from oscillograms of the pulse (see Section 5.11): a small correction factor is applied to the area of the pulse envelope to take into account the non-linear response of the detecting crystal. The total energy released is, therefore,

WQ_c/Q_L.

Evaluation of W allows the remnant magnetization $M_z(\infty)$ after oscillation to be evaluated from Equation 4.19, giving in this case

$$M_z(\infty)\, H_o V_s = -(V_z/2 - WQ_c/Q_L) \qquad 8.6$$

Equation 8.6 will be used in Section 8.7 where the structure of oscillation pulses is investigated.

8.7 Structure of Oscillation Pulses

Measurements on field-swept oscillations that will be presented and discussed in this section have been obtained in one experimental run: Cavity 2 with Samples (2,3) at 1.5°K, ν = 9.343 kMcs. The results are typical of ten other experimental runs with Samples (1) and (2,3) and conclusions drawn from this single run may also be made elsewhere. In brief this run took the following course: oscillation pulses of varying power were photographed for different rates of field sweep; the degree of inversion of a particular pulse was obtained at each field sweep setting by plotting the characteristic curve of the oscillator.*

---

* Footnote: This step is necessary for at fixed gating time for the triangle waveform, oscillations occur at later times at slow sweeps. The characteristic curve is, therefore, slightly lower due to spin-lattice relaxation.

Figure 8.12 shows a series of recordings of field-swept oscillations for various power outputs when the rate of field sweep is $4.0\ 10^{3}$ gauss sec^{-1}. Measurements from this figure are listed in Table 8.2: the threshold value of k is here 0.071.

The discussion of the results will concern the following points: (1) the general structure of oscillation pulses, in particular presenting comparisons between these experimental studies and the theoretical studies of Chapter 4, (2) the structure of the high frequency "wiggle", and (3) the structure of the well separated pulses.

Frequency Spectrum

The frequency spectrum of oscillation pulses is measured by using the wavemeter on the transmission principle, displaying the signal from the transmission crystal detector. Measurements of the signal height, assumed proportional to the power transmitted in the waveguide, with frequency, allow the spectrum of oscillation pulses to be plotted. The shape of the spectrum is Gaussian where the width at half height and the full width are 0.7 gauss and 7.0 gauss at high powers, and 0.2 gauss and 0.74 gauss at low powers respectively. These figures are to be compared to the F-centre line width of 1 gauss and the cavity bandwidth which for $Q_L = 1420$ is about 7 Mcs or 2.5 gauss. Oscillations are always narrower than the line width, see Figure 8.4, the narrowing being significant at weak powers, indicating that oscillations are confined mainly to

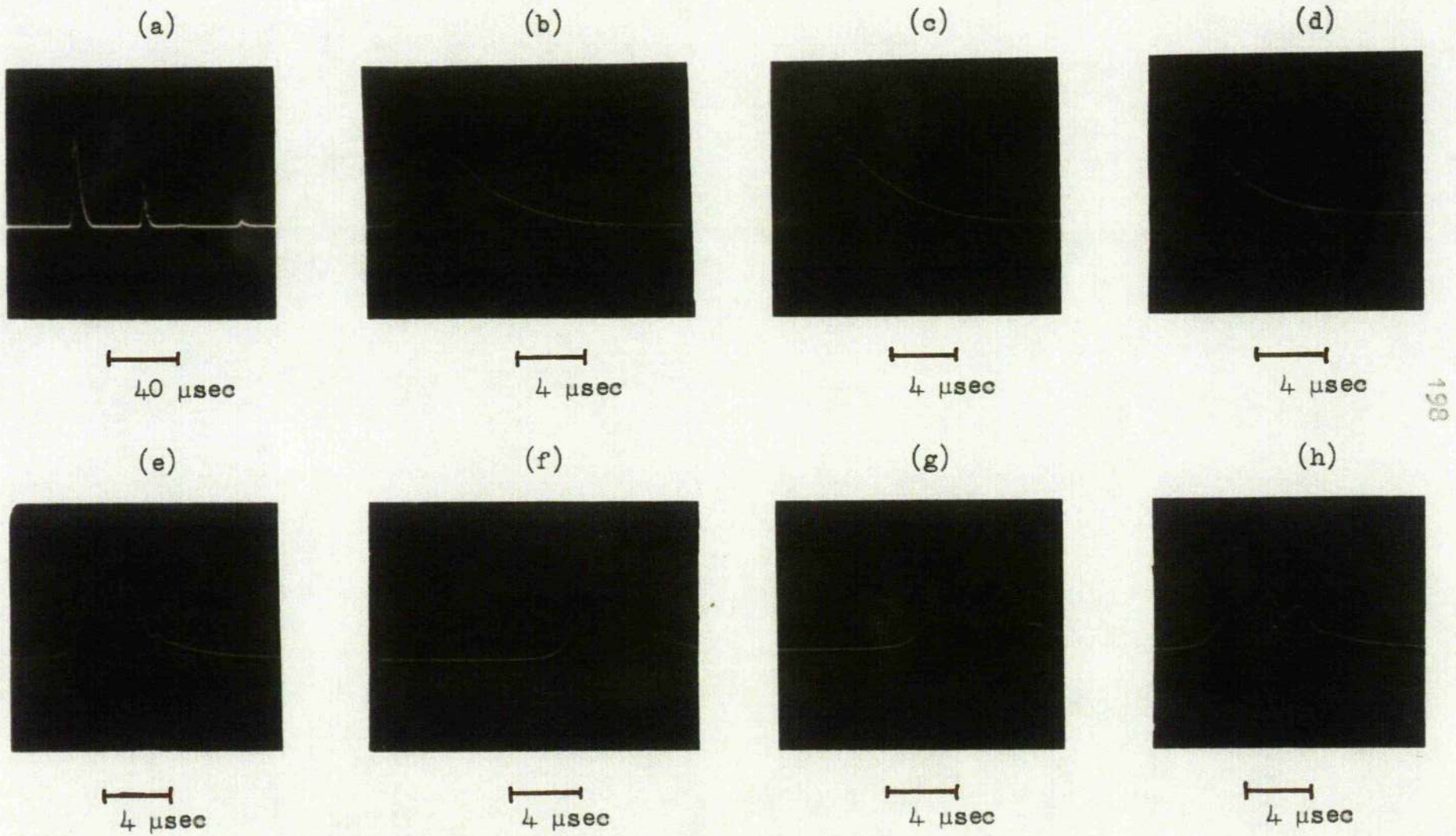

Figure 8.12 Oscillograms of Field-Swept Oscillation Pulses.

No.	k	T_I μsec	β Mcs	P M W	W_Z erg	W erg	$-M_z(\infty)$ 10^{-4} gauss	$-M_z(o)$ 10^{-4} gauss	$\frac{M_z(\infty)}{M_z(o)}$
a	1	7	2.3	26	21.6	1.25 .3 .04	59 55 54	77	.76 .71 .7
b	.38	11	1.35	10	8.0	.51	21.6	29	.74
c	.26	15	1.1	6.7	5.5	.40	14.2	20	.71
d	.17	19	0.97	4.5	3.6	.23	9.6	13	.74
e	.12	22	0.73	2.9	2.45	.16	6.5	8.9	.74
f	.084	29	0.54	1.1	1.8	.083	5.3	6.5	.82
g	.08	33	0.44	0.71	1.71	.065	5.2	6.2	.84
h	.079	38	0.40	0.56	1.70	.049	5.4	6.1	.89

Samples (2, 3): $1.5^{\circ}K$: 9.343 kMcs: $Q_o = 2840$: $Q_L = 1420$: $M_z(o)_{Threshold} = -4.3\ 10^{-4}$ gauss:

Field Sweep = $4.0\ 10^3$ gauss sec^{-1}

Table 8.2 Data on Figure 8.12

the F-centre line so that the hyperfine structure in the wings of this line take little part in oscillation.

The frequency of individual pulses is higher at the beginning of the pulse than in the tail, and in high power pulses the frequency of the maximum power in each pulse is lower in successive pulses, in agreement with the direction of field sweep, high to low fields. The frequencies of the peak powers in separated pulses occur within the halfwidth of the spectrum.

The widths of frequency-swept oscillations, under similar apparatus settings, are generally three times the above figures for field-swept oscillations. This increase is caused by the field inhomogeneity that is still present during frequency-swept oscillation.

Incubation Time

The incubation time T_I, defined in Chapter 4, cannot be measured directly, for the exact time of triggering of oscillation is unknown. It is possible, however, to infer its magnitude for pulses of varying k from other considerations.

The value of k at threshold is smaller at low sweep rates than at high, showing that very weak oscillations with long T_I can appear only at low rates of field sweep. It has proved impossible to suppress field-swept oscillation at maximum output by simply increasing the rate of field sweep, with the rates available.

However, the effect has been demonstrated by suppressing weak oscillations at slow rates of sweep, $2\ 10^{3}$ gauss sec^{-1}, by switching to maximum sweep, $1.25\ 10^{4}$ gauss sec^{-1}. Oscillations, when $k = .08$ can just be suppressed in this way, suggesting that to first approximation a sweep rate $1/.08$ times in excess of maximum would be required to suppress maximum oscillation. Hence T_I at maximum oscillation power $k = 1$, is of the order of 7 μsec, the time to sweep through the line width of the F-centre resonance at this higher rate of sweep. By noting the time delay of pulses for varying k from the first peak of oscillation for $k = 1$, T_I is obtained by adding 7 μsec to the readings.

It has proved impossible to check the predicted logarithmic dependence of T_I on signal power incident at the cavity, Equation 4.16, because at incident power levels below 10^{-6} watts, supplied by the monitor klystron tuned to the cavity frequency, the whole shape of the oscillation pulse is changed. Beating occurs between the signal power and the oscillation power to such an extent that the oscillation pulse is broadened, cf. Figure 8.6, and no reliable measurements are possible. There does not seem to be any tendency for T_I to be shortened at high signal powers.

The variation of T_I with k has, however, been checked: T_I, for oscillation alone, is listed in Table 8.2 for the cases of Figure 8.12. This data is plotted in Figure 8.13 and shows that where oscillation is well established $k \rangle .1$, $T_I \propto k^{-.51}$ or

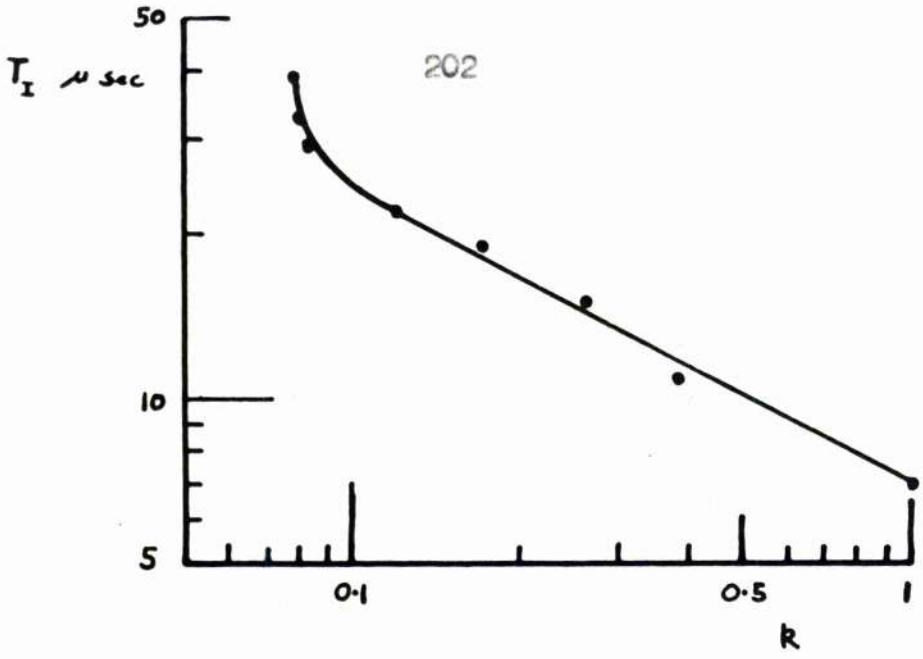

Figure 8.13 Incubation Time versus Degree of Inversion

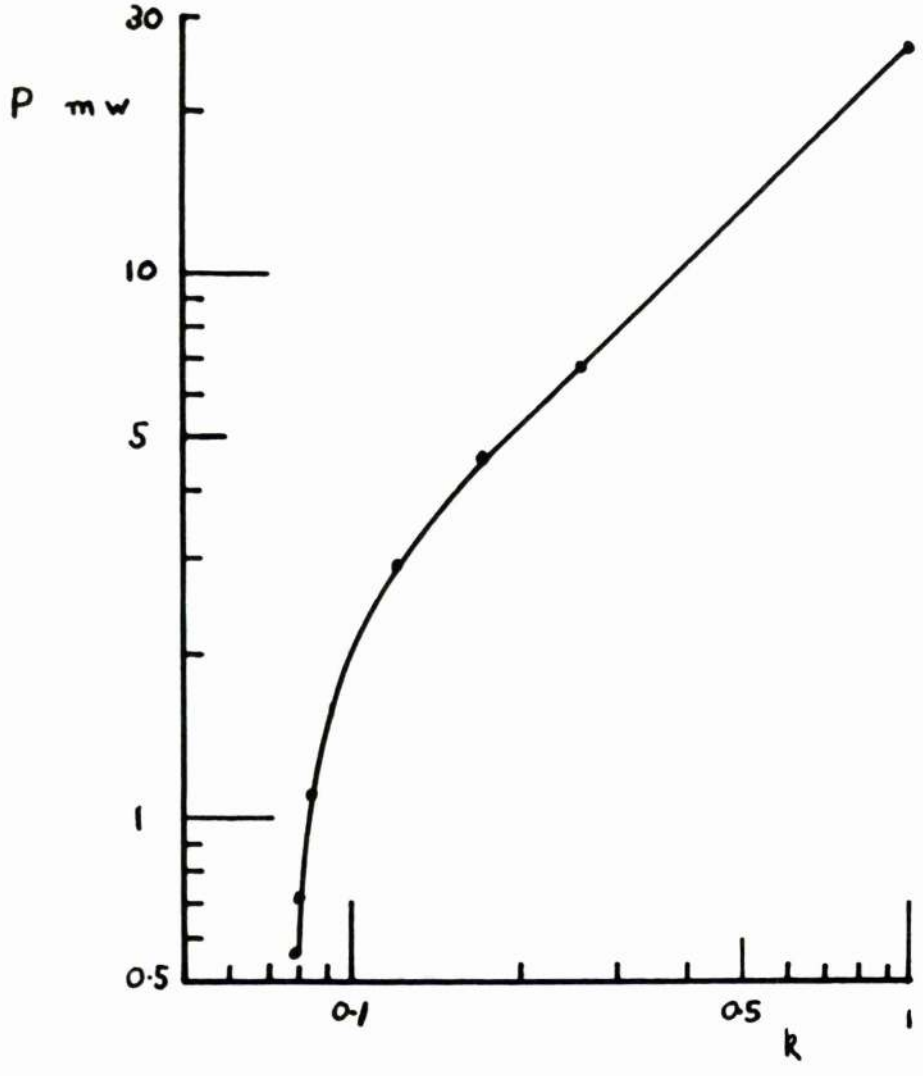

Figure 8.14 Oscillator Power Output versus Degree of Inversion

from Equation 8.5

$$T_I \propto H_z(o)^{-.51} \qquad 8.7$$

in direct confirmation of the prediction of Equation 4.17. The increase of T_I near k = .071 shows the onset of the threshold of oscillation. In general, at all rates of sweep, Equation 8.7 holds, but the increase of T_I at threshold is more acute at high rates of sweep: it is expected that if field sweeps in excess of $1.25\ 10^4$ gauss sec^{-1} were available, the increase in T_I would be more sharp and occur at a higher value of k than has been observed in these studies.

Power and Energy Output

The detected peak power P and energy W of oscillation for Figure 8.12 are listed also in Table 8.2. The energy released from the cavity W, compared to the available Zeeman energy W_z is .07 at k = 1, but drops to .03 at k = .08. In Figures 8.14 and 8.15(a) the peak power P and total oscillation energy $W\ Q_c/Q_L$ respectively, are plotted against k. These curves correspond very closely to Figures 4.9 and 4.11 in which similar parameters are plotted from computed solutions. Where oscillations are well established, $k > .1$,

$$P \propto k$$

$$W \propto k$$

which corresponds to theoretical findings, see Section 4.7. Near

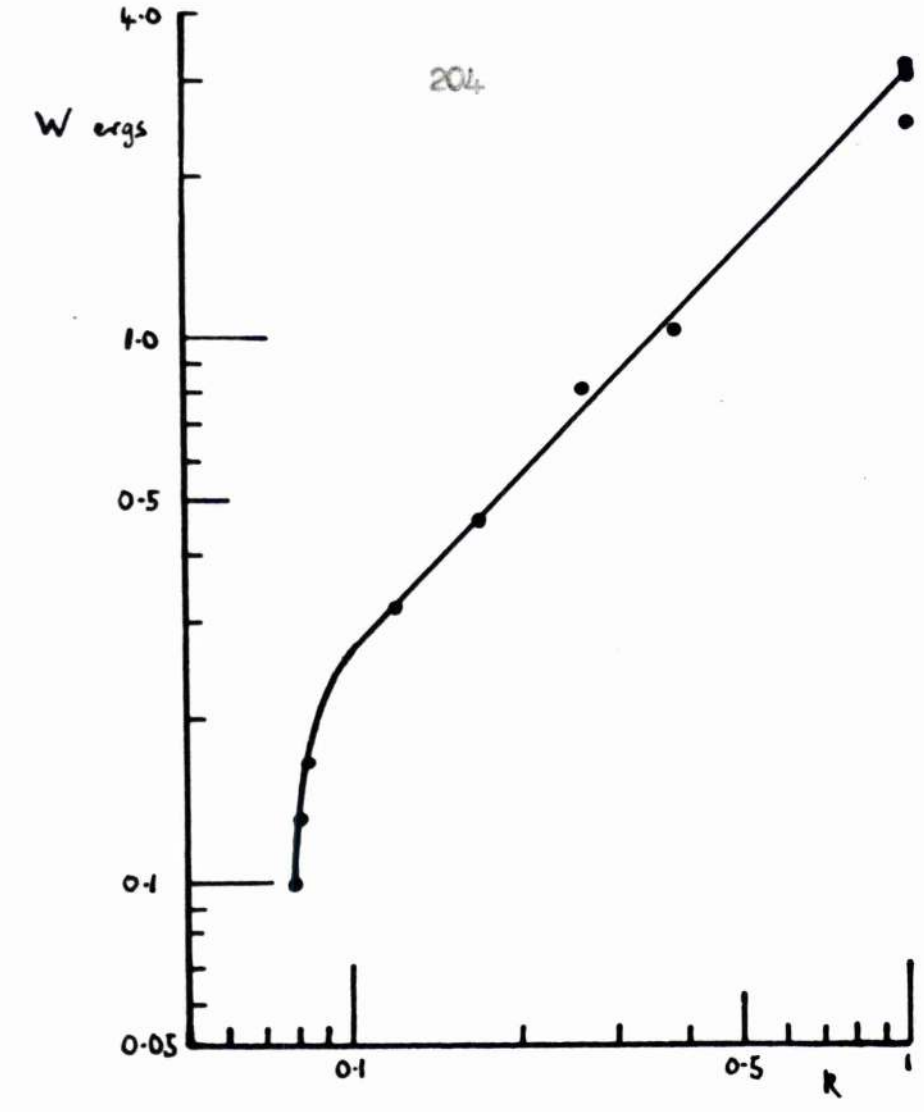

Figure 8.15(a) Total Energy Output versus Degree of Inversion

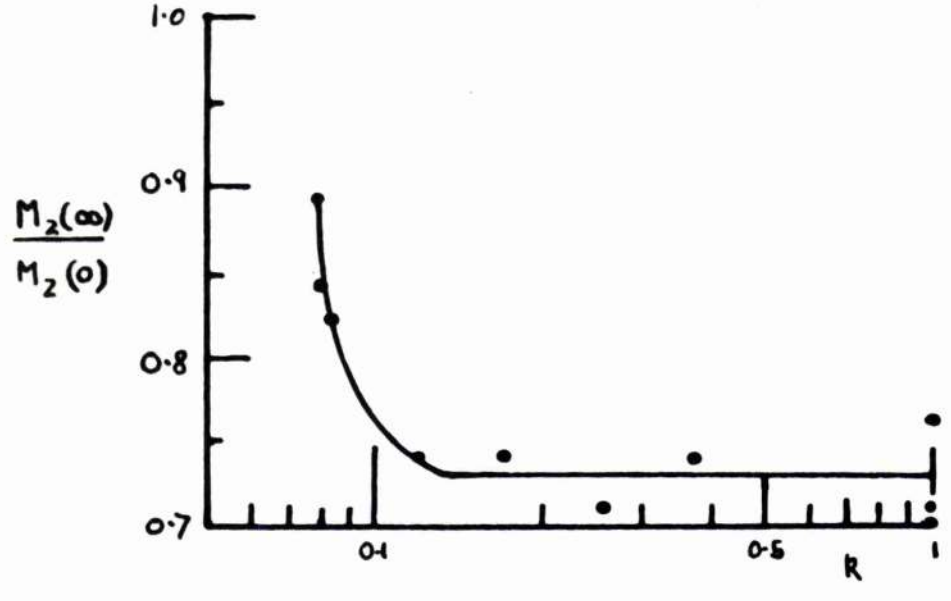

Figure 8.15(b) $\frac{M_z(\infty)}{M_z(0)}$ versus Degree of Inversion

threshold, k = 0.71, P and W fall rapidly to zero indicating the sharp threshold of oscillation. Figure 8.14, although similar in shape, is not the same curve as the characteristic curve of the oscillation, Figures 8.9 and 8.10.

From the measured value of W, $M_z(\infty)$ is calculated from Equation 8.6, and the ratio $M_z(\infty)/M_z(o)$ is listed in Table 8.2. In all cases the remnant magnetization is negative and is sufficiently large to satisfy the oscillation condition $T_r < T_2^x$, so that oscillations are quenched by the removal of the Zeeman frequency from the cavity frequency as the field sweep progresses, rather than by self-damping of the spin system to the condition $T_r = T_2^x$. In Figure 8.15(b), $M_z(\infty)/M_z(o)$ is plotted against k. This figure is to be compared with Figure 4.11 which also shows a sharp rise in $M_z(\infty)/M_z(o)$ at threshold to the sub-threshold value +1. Although $M_z(\infty)/M_z(o)$ is fairly constant for $k > 0.1$, that is oscillation well established, the value is positive whereas in the theoretical case, Figure 4.11, the corresponding value in this region is negative. The two cases are not completely analogous, for, in the steady-field case, oscillations continue until a self-damping action takes place, whereas in this case, oscillations are forcibly extinguished by the swept field passing through the resonance line: the steady value of $M_z(\infty)/M_z(o)$ is, therefore, expected to be larger in the field-swept case. Figure 8.15 suggests that for $k > 0.1$, large nutations of $\underline{M}$ may take place, but

for $k < 0.1$, $M_z(\infty)/M_z(o) \simeq 1$ so that little movement of $\underline{M}$ from the z direction is expected.

"Wiggle" Structure

The frequency of the "wiggle" structure is measured directly from oscillograms: the results of this run are based on measurements from about ninety photographs, taken at different sweep rates and varying oscillation powers. Similar structure has been observed by Kemp[50] in oscillations where only a small fraction of the Zeeman energy is released and have been described as "parametric modulation" of the oscillation by the swept magnetic field, resulting in modulation at a frequency proportional to the difference between the Zeeman and cavity frequencies. The linear dependence of the modulation frequency on time suggested by this description is seen to hold in Figure 8.12.

For the oscillograms of Figure 8.12, the frequency of modulation β, measured for the first period of modulation, is plotted against k in Figure 8.16, sweep rate $a = 4\ 10^3$ gauss sec^{-1}. The dependence of the linear portion of the figure is $\beta \propto k^{0.51}$ or $\beta = 2.7\ 10^6\ M_z(o)^{0.51}$; for other sweep rates the power dependence is similar, being 0.43 for $a = 1.25\ 10^4$ and 0.61 for $a = 1.67\ 10^3$, with constants of proportionality $3.4\ 10^6$ and $2.4\ 10^6$ respectively. The similarity between this curve and Figure 4.8 is marked and the power dependence of β on $M_z(o)$, Table 4.3, agrees nearly exactly.

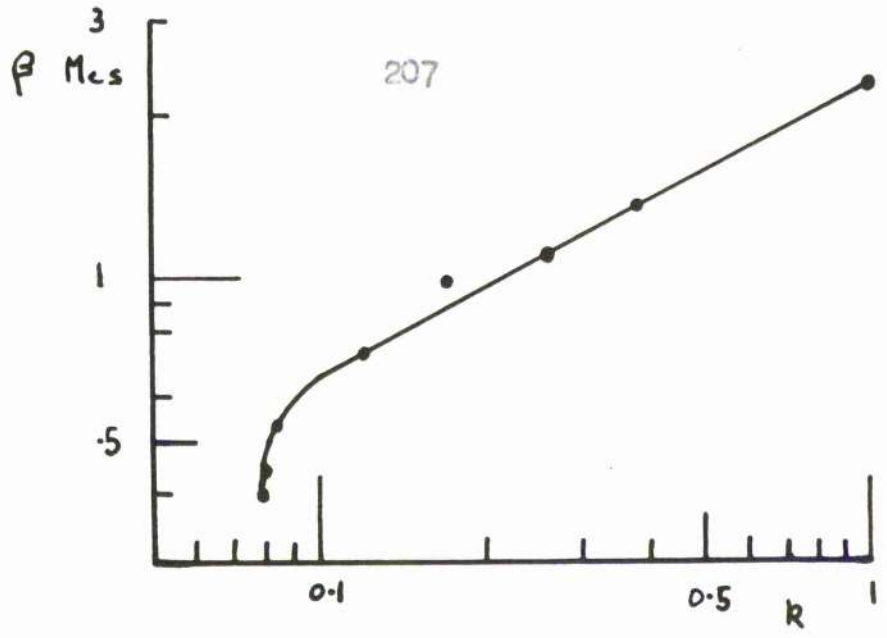

Figure 8.16 Modulation Frequency versus Degree of Inversion

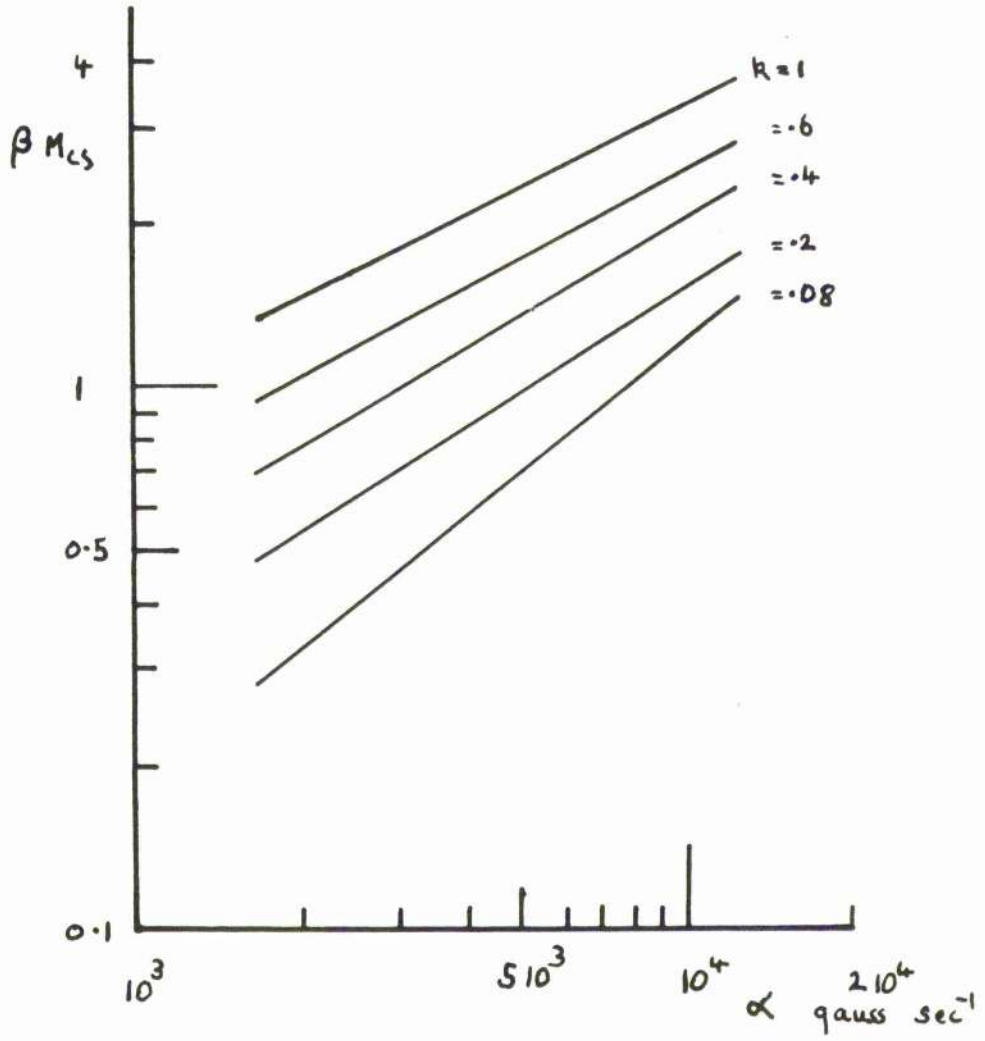

Figure 8.17 Modulation Frequency versus Rate of Field Sweep

However, no comparison between the constants of proportionality or the factor $(2\pi\omega\eta|\gamma|)^{\frac{1}{2}}$ in that table exist.

The variation of β with the rate of sweep a is shown in Figure 8.17 as a family of curves for the parameter k. Again a simple power relation seems to describe the relation when oscillations are well established: $\beta \propto a^{.49}$ when $k = 1$ and $\beta \propto a^{0.9}$ when $k = .08$ (very close to threshold).

No quantitative comparison can be made between this work and the theoretical predictions of Kemp[50] for field-swept oscillations with $M_z(o) \simeq M_z(\infty)$. This occurs because most of Kemp's work is based upon a dimensionless constant $K = a/\pi\omega\eta\, kM_o$, in the present notation, being greater than 0.04. In this experimental run for instance, at maximum field sweep k has to be less than $2\ 10^{-3}$ for this requirement to hold; this is not attainable in these experiments mainly because Q_L and T_2^* are too small in comparison to the values of these parameters in Kemp's work.

Qualitatively, however, the comparison with Kemp's predictions are good. In the region of threshold, the region to which the predictions apply, $\beta \propto (a\ t)$ agrees with the above findings. Furthermore, the depth of modulation is predicted as being nearly 100% at threshold showing an inverse time dependence which is seen to be the case in Figure 8.12, particularly trace (e). Kemp also suggests that for $K < 0.04$, that is, strong oscillations,

the modulation depth should be constant at only a few percent of the total height, a sudden change to the large depth of modulation taking place at K = 0.04. There is, in fact, a sudden transition in the modulation structure between these two extremes as seen in Figures 8.12(c) and (d), when $k \simeq 0.2$.

Separated Pulses

The appearance of many well separated pulses within the total maser output is not expected. This structure is only pronounced for $k > 0.5$ and below this value the oscillation output is a single pulse. Considering the motion of the magnetisation vector $\underline{M}$, it would seem that $\underline{M}$ might undergo a series of 360° nutations from the inverted state during each pulse after each of which there is a dead time when $\underline{M}$ remains totally in the -z direction until oscillations are again triggered. The work of Chapter 4 has, however, shown no tendency for $\underline{M}$ to nutate through exactly 360°, although when $T_r \simeq T_2$ $\underline{M}$ remains inverted after oscillation, but this is a case of weak oscillation and does not apply here, for when k = 1, Figure 8.12(a), $T_r = T_2^{\pi}/14$.

Two possible explanations of the structure arise but these can be shown to be irrelevant.

(1) The total frequency width of the pulse is sufficiently large to indicate that the hyperfine lines associated with the F-centre line take part to a very small degree in oscillation, and these

lines could be responsible for the separated pulses. By reducing the sweep to about 0.8 amp only the F-centre line is inverted and the frequency halfwidth of the oscillation spectrum becomes correspondingly smaller but oscillations occur with about the same maximum power as with full sweep and with similar structure. It is concluded that the hyperfine structure of the MgO line is not a cause of the effect.

(2) Any ringing of the sweep coils during passage would produce sinusoidal variation of the swept field. This might cause the F-centre line to be traversed many times during oscillation, so giving individual pulses. The absence of ringing has been checked, as described in Section 5.5, both by means of a pick-up coil placed between the sweep coils and by viewing spin resonance absorption in the swept field.

The mechanism underlying the structure is not fully understood but it is likely to lie in the coupling of the radiation damping field of the spin system and the cavity field. The inhomogeneous broadening of the F-centre line will probably determine to some extent the shape of the pulse and other processes, such as cross-relaxation, and spin diffusion may also play some part. The similarity between the structure of separated pulses and the discontinuous output from 3-level maser oscillators[73] operating under certain conditions is noted.

In Table 8.2, $M_z(\infty)$ is evaluated after each pulse of Figure 8.12(a). The remnent magnetisation is in the -z direction and is of such magnitude that oscillation conditions hold between pulses. It would seem, therefore, that $\underline{M}$ does nutate in some way during each pulse to return at the end of the pulse to the -z direction. In the next section the detection of the nutations of $\underline{M}$ in separated pulses is described but it is impossible to tell whether $\underline{M}$ nutates through 360° or through a few degrees from the z direction. The variation of the wiggle structure on the three pulses of Figure 8.12(a) is just that of the first pulse for smaller k, i.e. depth of modulation increasing to 100%, for the structure of the second and third pulses compares well with Figures 8.12(d) and (f) respectively. Hence, it would seem that in high power oscillations, the first pulse is repeated at certain fixed points along the characteristic curve of the oscillator, the structure of the pulse being determined by the value of k at the points. In opposition to this argument, the period between successive pulses decreases with time where T_1 has already been shown to increase as the oscillation power is lowered. Hence individual pulses cannot be completely independent and each pulse must trigger the next in some way.

It should be mentioned that a simple relation, $\nu \propto t \propto a^{1.1}$ holds between the frequency ν of the separated pulses, the rate of field sweep a and the time t from some arbitrary zero of time.

ν varies from 58 kcs at $a = 1.25\ 10^4$ gauss sec^{-1} to 7.5 kcs at $a = 1.67\ 10^3$ gauss sec^{-1}.

8.8 Detection of Magnetisation Variation During Oscillation

The theoretical discussions in Chapter 4 and those in References 46 48 49 56, on the subject of amplitude modulated output from two-level maser oscillators, indicate that $\underline{M}$ should undergo damped "pendulum-like" nutations, correlated to the modulation of the output, from the inverted state, $\underline{M}$ anti-parallel to the steady magnetic field. These discussions are concerned mainly with oscillations in a steady field but in the present case, nutations of $\underline{M}$ should almost certainly be present in strong field-swept oscillations although this may not be the case at low powers, see Section 8.7 (Figure 8.15).

These predictions have not been put to the test, however, nutations of $\underline{M}$ being inferred only from measurements of the cavity power. Stevens[46] has suggested that an instructive test of these theories would be to observe directly the variation of M_z during maser oscillations. Evidence confirming the suggested behaviour of $\underline{M}$ has been obtained in an induction experiment designed to detect the "dipole" field of M_z. The findings of this experiment have been published recently by the Author and D. Bijl in Nature[70]: a copy of this article is contained in Appendix II.

The method used in this experiment has already been introduced in Section 5.8 where it was argued that the variation of the dipole field of M_s would not be confined within the plastic microwave cavity. At the highest rates of variation of the "dipole" field that may be involved, for instance, M may mutate through 360° in a few microseconds in pulses of the separated type, the skin depth in silver at 1.5°K is about $3.0\ 10^{-3}$ cms, whereas the estimated silver plating thickness of plastic cavities (3 silver coatings) is only $5.0\ 10^{-4}$ cms (0.0002"). Hence the necessary criterion for detecting variations of the field of M_s outside the cavity would seem to be satisfied.

The optimum conditions for detecting the field of M_s seem to lie in field-swept oscillation experiments on Sample (1) in a cavity of cross-section .9" x .1" for two reasons. Firstly, maximum oscillation powers are observed from this sample suggesting maximum flux variation of the field of M_s and, secondly, external pick-up coils can be placed very close to this sample in the smaller cavity. In this situation, calculations[71] predict the induced voltage in a pair of coils, one on either side of the cavity, each of 400 turns, to be of the order of a millivolt.

The coil system should be balanced against pick-up from the swept field. This requirement is satisfied to a sufficient extent by the four coil system shown in Figures 8.18 and 8.19.

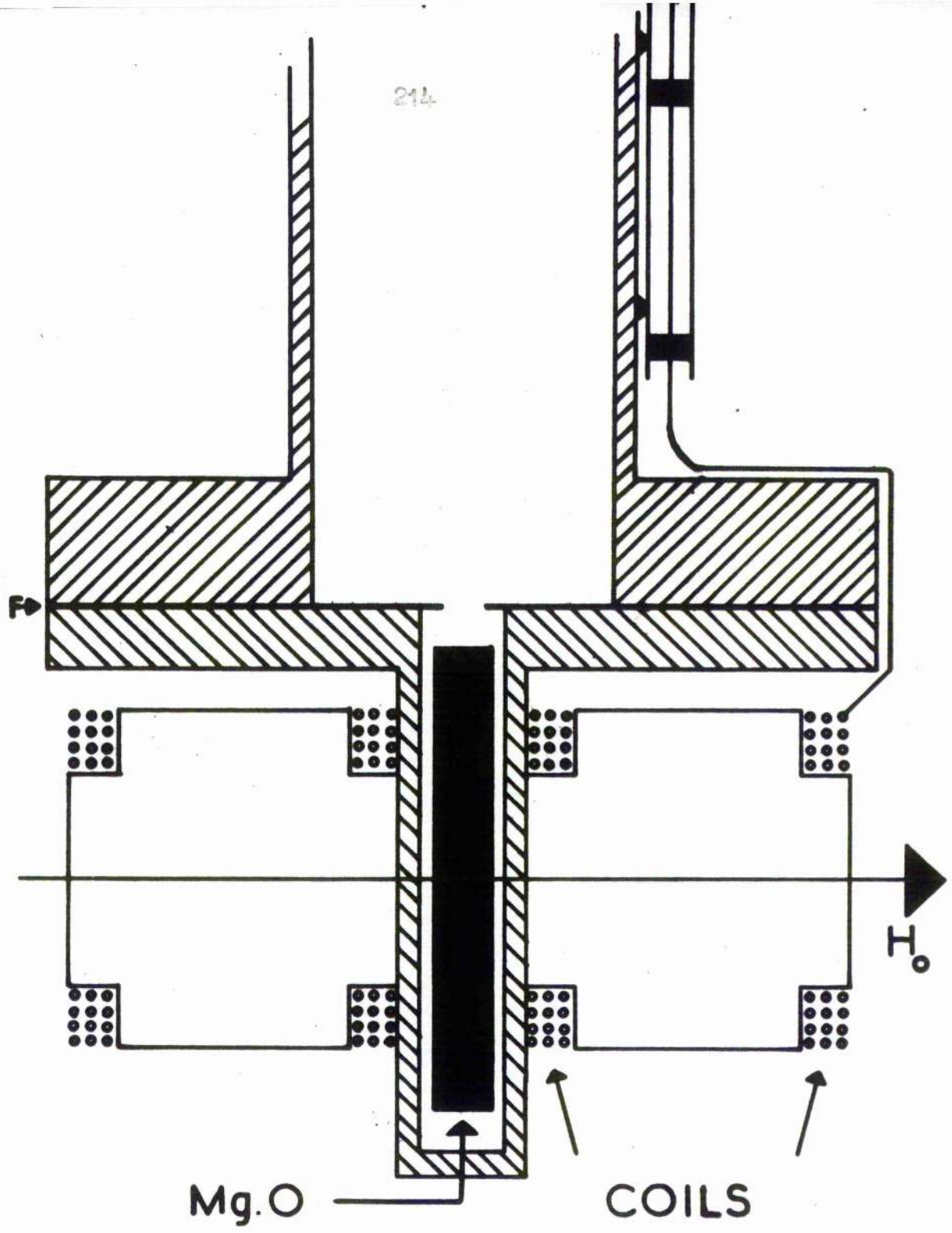

Figure 8.18 Pick-Up Coil System.

The coaxial lead for the coils is shown.

F: Coupling iris made from silver plated copper foil.

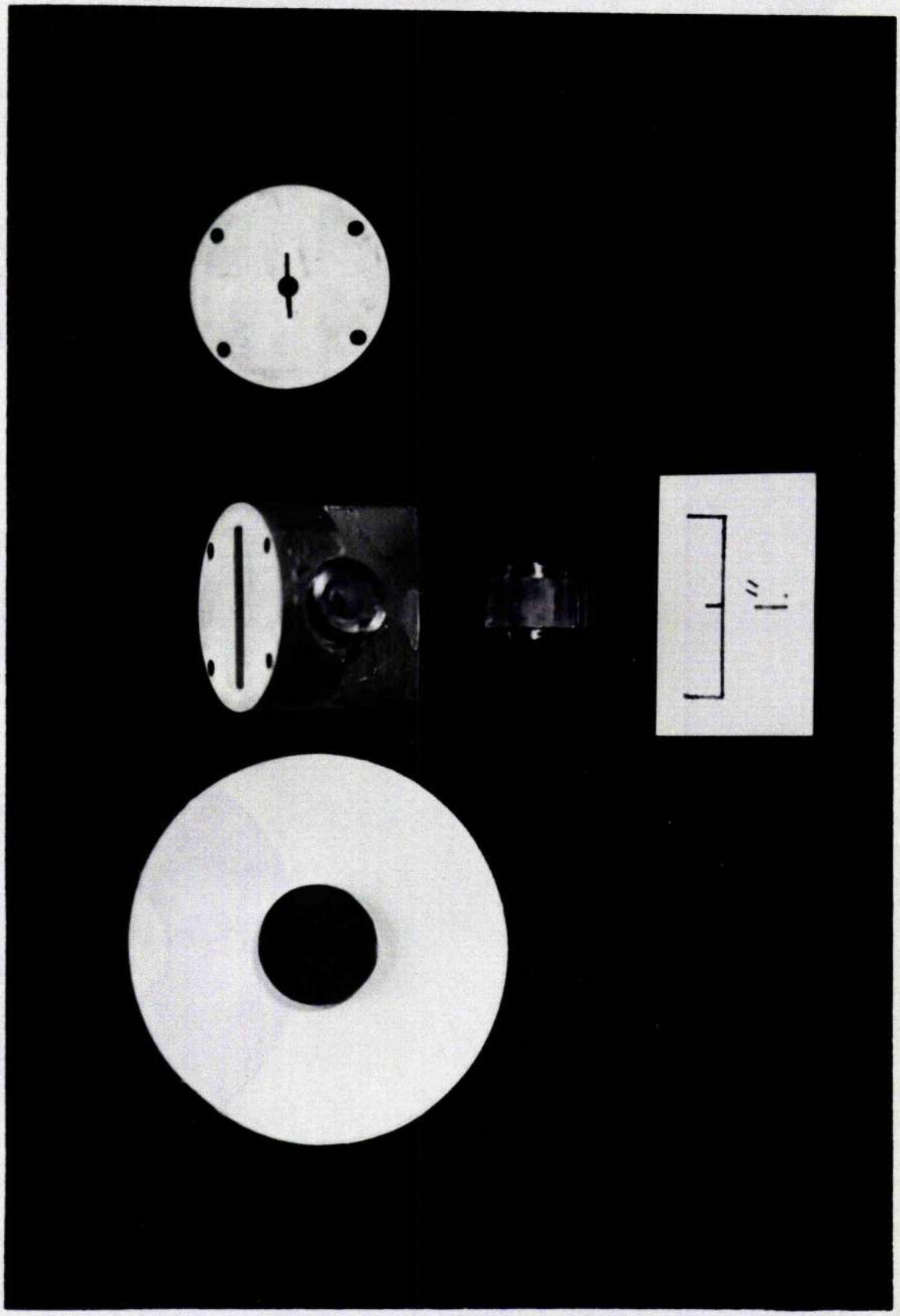

Figure 8.19 Photograph of the Pick-Up Coils and Cavity.

The .9"x.1" cavity, pick-up coils and Sample(1) are shown.

The outer coils (reversed) compensate for pick-up of the swept field in the inner coils, whereas the field of H_z should couple only to the inner coils. Connections to the coils are made through one of the coaxial leads in the cryostat. At 1.5°K, with an external coaxial lead connected, the coils have a resonance frequency of 150 kcs, Q = 4 and a damping time constant of 60 μsec.

Maser oscillations and the corresponding pick-up voltage in the coils are simultaneously monitored on two oscilloscopes; the double beam oscilloscope is used only to check coincidence of the signals because of its small bandwidth on the 1 mv/cm range. Typical oscillograms of these recordings are shown in Figure 8.20 and coincidence, in another case, is shown in Figure 8.21. The separated structure of oscillation in Figure 8.20(a) proved advantageous for two reasons. Firstly, variations of H_z should occur only during each pulse leading to shock excitation of the coils and, secondly, the response time of the coils is too long to record completely the variation of the field of H_z in each pulse but the coils recover sufficiently between pulses to respond to some variation in following pulses. In Figure 8.20(b) there are shock excitations coincident with the first three pulses. The negative signal from each pulse corresponds to a net increase in the local magnetic field indicating that the coils respond to a nutation

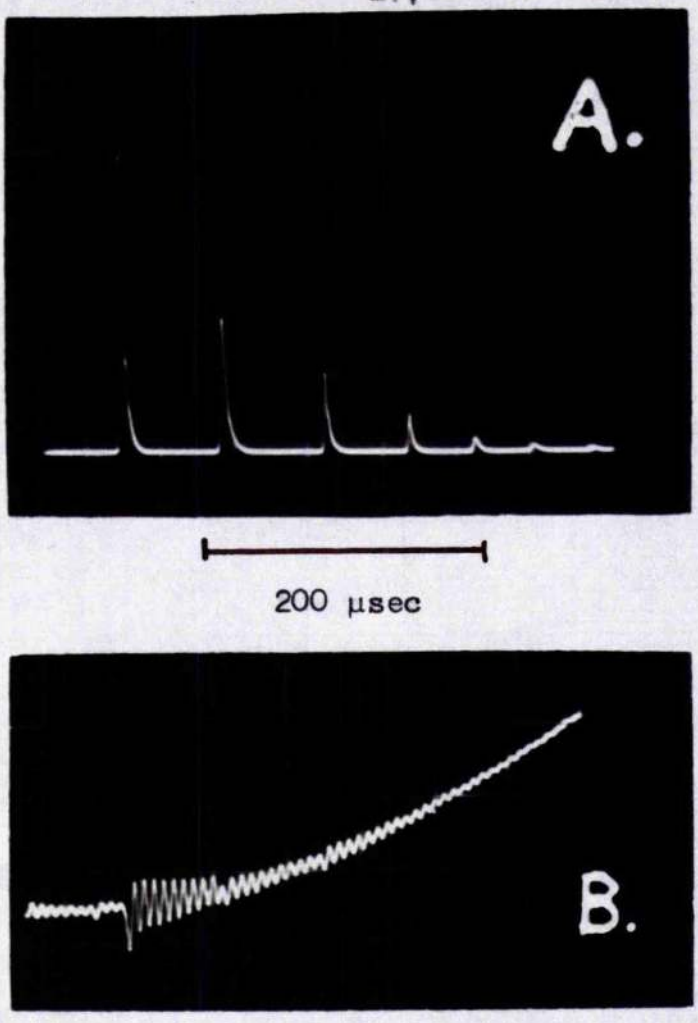

Figure 8.20 Field-Swept Oscillation and Pick-Up.

A, Modulated emission from oscillator.
B, Shock excitation of pick-up coils; maximum pick-up voltage, 0.5 mv.

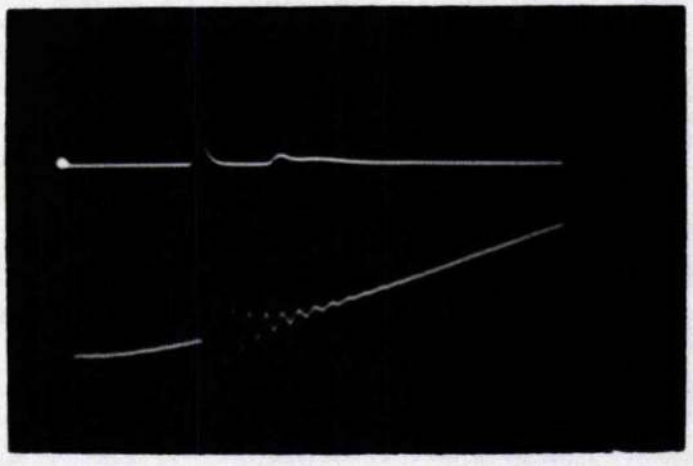

Figure 8.21 Coincidence of Oscillation and Pick-Up.

of M_z from a -z to +z direction.* The rising base line of this figure is caused by residual pick-up from the swept field. This evidence in support of the mutating character of $\vec{M}$ is further substantiated by the fact that pick-up disappears completely when the X-13 power is reduced below the threshold level, and only the residual voltage is observed.

A similar effect has been observed in frequency-swept oscillations. In this case the same sweep coils are not fully balanced and shock excitation by the applied field inhomogeneity occurs easily. Where no inhomogeneity is applied, i.e. oscillation follows inversion immediately, inversion by A.F.P. can be detected easily, Figure 8.22. The mean pick-up voltage indicated in this figure, shows the slow reversal of M_z from the +z to the -z direction. The pick-up is monotonically increasing to a maximum coincident with frequency sweep through the cavity, and so the line centre, followed by a decrease showing that M_z changes most rapidly at the line centre. The decrease after passage through the

---

* Footnote: The sign of the coil response is calibrated against increasing or decreasing field by noting the induced voltage from the swept field with the inner coils in place. The direction of sweep is determined from a display of the R.S.F. signal.

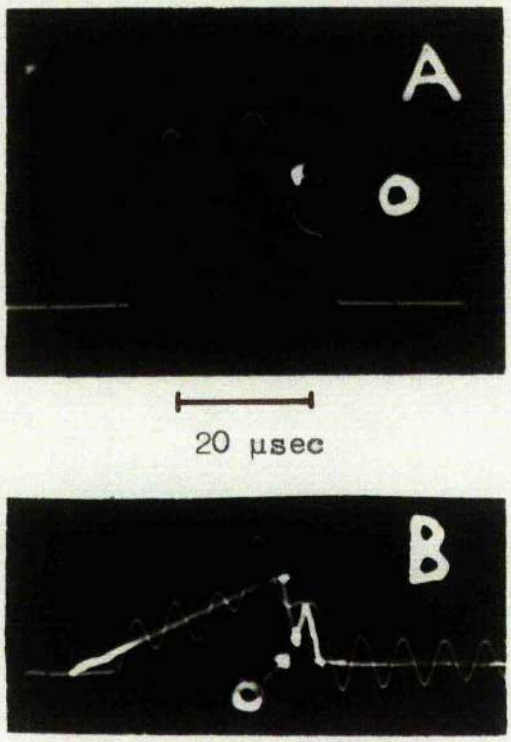

Figure 8.22 Frequency Sweep Inversion and Pick-Up.

A, X-13 sweep with spontaneous oscillations at O.
B, Pick-up showing slow variation as M is inverted and a negative spike at O corresponding to oscillations.

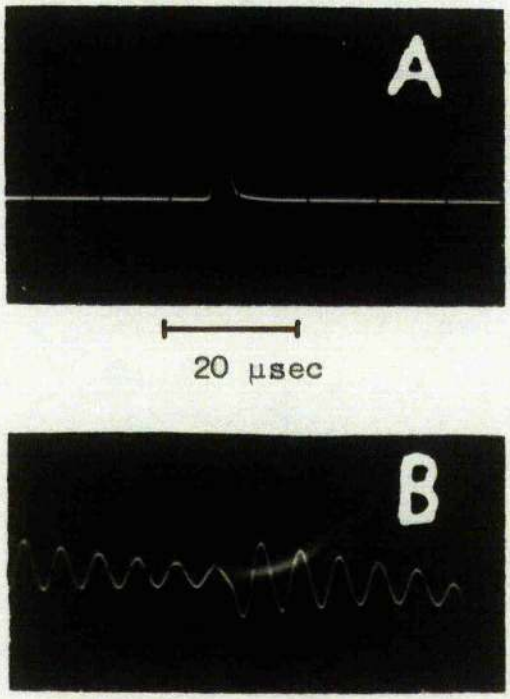

Figure 8.23 Frequency-Swept Oscillation and Pick-Up.
A, Oscillation pulse.
B, Pick-up superimposed on coil ringing.

line centre contains a negative spike (O), coincident with spontaneous oscillations that follow inversion, which interferes with the positive going self oscillation of the coils. Figure 8.23 shows pick-up from frequency-swept oscillation, superimposed on the coil ringing voltage produced as the field inhomogeneity is removed.

A review of points noted in these pick-up experiments follows.

(1) Maximum pick-up voltage recorded is 5.0 mv for a peak power of 54 mw frequency-swept oscillation.

(2) No pick-up is detected for oscillations less than 0.5 mw. The decrease in pick-up is gradual as oscillation power is reduced, suggesting this effect may be due to the low sensitivity of the system. Detection of the behaviour of $\underline{M}$ at low powers is, therefore, not possible, but in any case, little information could be gained with this coil system because the ringing frequency is ten times lower than the wiggle frequency.

(3) Full response to the variation of M_z is not possible due to the long coil response time. Only when M_z is slowly varying, as during inversion, can the motion of M_z be followed. In separated pulses, it is impossible to tell whether $\underline{M}$ nutates by 180° or 360° during each pulse, because only the first 180° nutation is detected.

(4) The sign of the signal from oscillation is opposite to that from inversion, showing that the variation of M_z is, as expected,

opposite in the two cases.

In an attempt to increase the sensitivity of the pick-up arrangement, a radio frequency bridge circuit was added modifying the system to respond to nutations of $\underline{M}$ as modulations of a high frequency carrier wave fed to the coils. An asymmetrical bridge, first used by Anderson[72], was fitted at the cryostat head, the rf input from an Advance Signal Generator being detected by an R.C.A. Communication Receiver.

Clearly the radio frequency should be as high as possible for maximum bandwidth response but difficulties are encountered in raising the operating frequency even to 4 Mcs, the resonant frequency of the coils, each of ten turns, being 3.2 Mcs at 1.5°K. The difficulties are caused by the fixed capacity of the coaxial cable, about 40 pF at low temperatures. The resonant frequency of the coils can, therefore, only be raised by lowering the coil inductance, i.e. reducing the number of turns of each coil. As the system consists of four coils, a substantial reduction in inductance can only be made by reducing the number of turns by a large figure which, in turn, drastically reduces the sensitivity to variations of M_z.

The bridge could be well balanced. The input to the bridge had to be restricted to below 100 mv, for above this level modulation of the oscillation output occurred due to sinusoidal

variation of the swept field at the rf frequency. No pick-up was observed, however, and it is believed that this is due to the low sensitivity of the pick-up system when the number of turns is so small. It should be possible, nevertheless, to carry out detailed measurements on M_s during oscillation by similar means, so long as the resonant frequency of the coils can be made large without reduction of sensitivity.

CHAPTER 9

CONCLUDING REMARKS

The problem of the two-level maser oscillator in a steady field, i.e. frequency-swept oscillations, has been treated for a spin system that is assumed to obey the Bloch equations. Modulation of the microwave cavity energy is shown to occur and arises because of an oscillatory transfer of energy between the spin system and the cavity mode. Correlated with this transfer the spin magnetization undergoes damped, pendulum-like nutations from the inverted state. Although this treatment does not take into account all factors that must take part in practice, in determining the oscillator output, e.g. inhomogeneous broadening, cross-relaxation and spin diffusion, the original aims of the study have been fulfilled, relations between measurable variables and an appraisal of the overall use of the equations under strong and weak oscillation conditions being the main accomplishments. However, the comparison with observations by Chester et al is poor. It is concluded, therefore, that a convincing qualitative check with experiment will not be possible unless fewer simplifying assumptions than used here (e.g. homogeneous broadening, H_o constant), are made in the treatment: such a mathematical task would be extremely difficult.

Observations on maser oscillations have necessarily been made on a field-swept oscillator. The comparisons between

experimental observations and theoretical results have been, therefore, mainly qualitative, but the measured dependence in strong field-swept oscillations of the frequency of modulation, the power output, the energy output and the incubation time on $M_z(o)$ and the behaviour of the oscillator in the region of threshold, show remarkable agreement with computed results. The method that has been used to determine the degree of inversion of the spin system in the oscillator is novel.

Experimental verification of the mechanism underlying amplitude modulated oscillation, i.e. large nutations of $\underline{M}$, has been obtained in a simple induction experiment. The development of this technique has been possible by the use of plastic microwave cavities, but in order to obtain detailed measurements of the motion of $\underline{M}$, or to detect small variations of $\underline{M}$ that should be present in weak maser oscillations, the sensitivity and the response time of the pick-up system should be increased. An attempt in this direction has been made, but further progress may be made by using techniques particularly familiar to double resonance[74] (E.N.D.O.R. techniques) and it should be possible to place a small coil inside the cavity, so obtaining a larger filling factor between coil and sample. An application of this induction experiment might be to 3-level maser oscillators; there is still doubt as to the exact mechanism of the discontinuous output from 3-level maser oscillators[75].

Experimental results show that the F-centre line in MgO should be particularly suited to pulsed-field maser experiments. The limitations on the shape of the pulsed-field are not too strict: inversion can be effected by A.F.P. for a large range of sweep rates and so long as the rate of field sweep during oscillation is less than $\sim 1.6\ 10^5$ gauss sec^{-1} large output powers should be obtained up to ~ 3 msec after inversion. Both theoretical and experimental results indicate, however, that a large filling factor should be used to ensure maximum inversion and to obtain maximum output powers.

The technical use of the two-level maser in spin-lattice relaxation measurements has been demonstrated. Two points arise in the experiments on the F-centre line in MgO: firstly, a phonon-bath bottleneck appears in samples of high spin concentration and large dimensions, and secondly, a deviation from the expected inverse temperature dependence of T_1 is noted in most samples. However, further experiments are required to complete these studies. In these, much smaller samples should be used to reduce radiation damping loss to a small fraction of the total cavity loss and the crystal orientations of the samples should be known.

J. SCI. INSTRUM., 1962, VOL. 39 226

On casting plastic microwave cavities

I. M. FIRTH
The School of Natural Philosophy, The University of St. Andrews, Fife
MS. received 20th November 1961

A simple mould is described for casting epoxy resin microwave cavities at X-band. The cured casting is machined to size, polished and silvered-plated. By cooling the silvering solution to 12–15° C a more uniform plating is applied. Finished cavities have been repeatedly cooled to 1·2° K maintaining a low temperature $Q \simeq 6000$. No cracking of the casting or of the silver-plating is reported.

To ensure the uniform penetration of a rapid magnetic field sweep into a microwave cavity it is necessary for the cavity to have very thin walls. Many experimental situations arise in which this is essential, among these being high frequency field modulation, adiabatic rapid passage and pulsed field Maser experiments. The performance of silver plated glass and plastic cavities has been reported by Bennett *et al.* (1958) and Chester *et al.* (1959), respectively, but no description of the cavity construction has been given. This note describes a simple technique for casting plastic microwave cavities, of various designs, at X-band.

The brass mould shown in figure 1 was in three parts: a central mandrel, a base and an outer shell. The solid

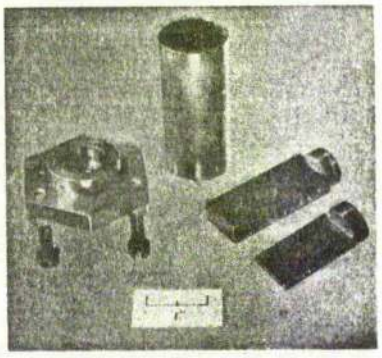

Figure 1. The mould shown with two mandrels.

mandrel had the required cross-sectional dimensions of the cavity but was longer than the cavity. The corners of the mandrel were rounded to facilitate cleaning, polishing and silvering the cavity. A disk was brazed to one end of the mandrel and this mated with an inset in the base. A central hole, tapped 0 B.A., in the disk served two purposes: to secure the mandrel to the base by a screw passing through a clearing hole in the base; secondly, as a means of attachment in extracting the mandrel from the cured casting. Cavities made so far have been rectangular TE_{102} for which the mandrel had cross section 0·9 in. × 0·4 in. and in a second case 0·9 in. × 0·1 in. The shell, a length of $1\frac{3}{16}$ in. inside diameter tube, made a tight push fit on to a lip on the base. In this way the mandrel was centred to the base and was coaxial with the outer shell. Prior to assembly, the components were polished with Brasso and washed with detergent. The mould release agent, Releasil 7 Silicone Compound (Midland Silicones Ltd.), was applied with a fine camel hair brush as a 20% solution in white spirit. After evaporation of the spirit, two further coats were similarly given.

The epoxy casting resin, Araldite CT200 with Hardner HT901 (Ciba (A.R.L.)), was used. To reduce thermal expansion French chalk was used as a filler; the proportion of filler to resin was 8 : 10 by weight. Other inert fillers, e.g. silica flour, may be used with more effectiveness in this respect but the casting is then more difficult to machine due to its abrasive nature. After mixing at 130° C, the mixture was vacuum-treated to ensure a void free casting and poured into the preheated mould. The casting was cured at 200° C for two hours.

The cured resin was found to machine easily. By machining the cavity to a predetermined length a particular resonant frequency could be obtained. Further machining of inset holes in the sides of the casting allow Helmholtz sweep coils to be placed close to the paramagnetic sample contained in the cavity. After polishing the inner walls and the top face with jeweller's rouge and then with Brasso, the cavity was washed in white spirit, to remove the release agent, and finally with detergent.

The method described by Chester *et al.* (1959) was followed for the final cleansing and silvering. However, by cooling the ammoniacal silver nitrate and the reducing solution to 12–15° C a slower rate of deposition was obtained. This facilitates mixing and decanting into the cavity and further-

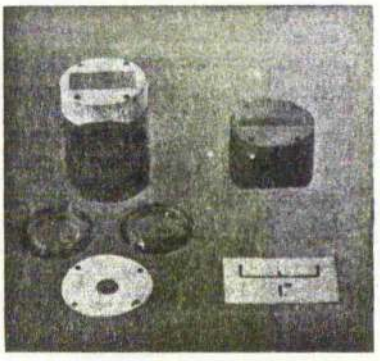

Figure 2. Finished cavities. Field sweep coils and coupling iris are shown.

more ensures a more uniform silvering. The solution was poured into the cavity, thereby excluding air bubbles, and was allowed to overflow until the casting was completely immersed. Three such silverings were applied. The silver coating was removed from the base and the cylindrical exterior.

The cavity was attached to the waveguide flange by four 8 B.A. nylon screws which serve to locate the coupling iris, formed by reaming a hole in silver-plated copper foil. By bolting this assembly tight, the foil made good electrical contact with the waveguide and the silvered top face of the cavity.

Finished cavities with the aforenoted dimensions are shown in figure 2. These have been cooled many times to 1·2° K and have maintained $Q \simeq 4000$ at room temperature and $Q \simeq 6000$ at low temperatures. Neither cracking of the cavity nor deterioration of the plating has occurred.

Thanks are due to Mr. J. McNab of this Department for the fabrication of the mould. Helpful discussions with Mr. B. B. Molloy, Chemistry Department, concerning the silvering technique are acknowledged.

References

BENNETT, R. G., HOEL, P. C., and SCHWENKER, R. P., 1958, *Rev. Sci. Instrum.*, **29**, 659.

CHESTER, P. F., WAGNER, P. E., CASTLE, J. G., and CONN, G., 1959, *Rev. Sci. Instrum.*, **30**, 1127.

(*Reprinted from Nature, Vol.* 192, *No.* 4805, *pp.* 860–861, *December* 2, 1961)

Detection of Spin Magnetization Variation in a Two-level Maser Oscillator

THE phenomenon of amplitude modulation in the spontaneous emission of two-level masers has been observed by several investigators[1–3], and has been the subject of a number of theoretical discussions[3–5]. The basic mechanism underlying most of the semi-classical treatments is an oscillatory transfer of energy between the spin system, in the working substance, and the cavity radiation field. In such a process the spin magnetization vector M should undergo damped, pendulum-like nutations, correlated to the modulation of the emission, between the inverted state, M anti-parallel to the steady magnetic field in the z direction, and the thermal equilibrium state, M parallel to the steady field. The quantum mechanical treatment[6] of the interaction between the spin system and the radiation field in the cavity also suggests the oscillatory behaviour of M_z. Stevens[6] further suggested that the direct observation of the variation of M_z, during an oscillation pulse, would be a more instructive test of the theories mentioned than monitoring the modulated cavity energy. Evidence confirming the suggested behaviour of M has been obtained in an induction experiment designed to detect the variations in the 'dipole' field of M_z.

The maser operated in this laboratory[7] is of the field-swept type. The sample, neutron-irradiated magnesium oxide containing about 5×10^{18} spins, was mounted in a rectangular 'TE_{102}' plastic cavity resonator[8]. Oscillation pulses have been observed in which the amplitude modulation frequency was dependent upon the rate of field sweep. It was estimated that the skin-depth at these frequencies was greater, by orders of magnitude, than the cavity silver plating, so that variations of the field of M_z would not be totally confined within the cavity. Furthermore, calculations predicted that the voltage induced by this flux in an external coil, of 800 turns, surrounding the sample would be of the order of a millivolt.

Such a coil system should be balanced against pick-up from the swept field. The coil assembly used in this experiment satisfies this requirement, to a

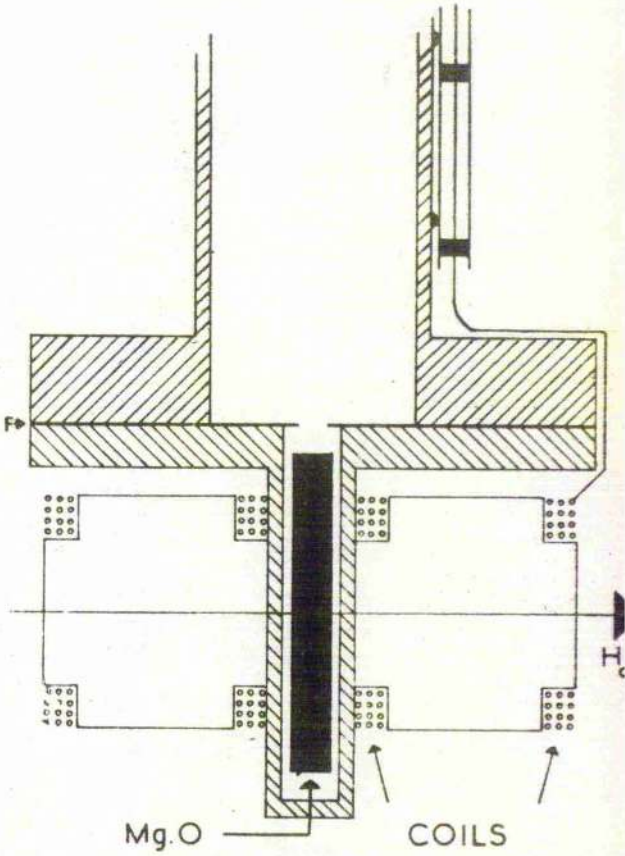

Fig. 1. Cavity with sample, pick-up coils and co-axial lead. Cavity, 0·9 × 0·1 × 0·8 in., sample, 17·5 × 2·0 mm. *F*, Silver-plated copper foil with iris to wave-guide

sufficient extent, and is shown in Fig. 1. The field M_z would couple only to the inner coils, whereas t outer coils compensate for the pick-up of the swe field in the inner coils. At 1·2° K. the coils had resonant frequency of 150 kc./s.; $Q = 4$ and damping time constant of 60 μsec.

Maser oscillations and the corresponding pick-u voltage in the coils were simultaneously recorded two oscilloscopes. Typical oscillograms of the recordings are shown in Figs. 2*A* and 2*B* respectivel The oscillation envelope, shown in Fig. 2*A*, is n continuous so that variations of M_z should occur on during the intermittent pulses, leading to sho excitation of the pick-up coils. This was found to advantageous because the response time of the syste is too long to record completely the variations of M In Fig. 2*B* there are shock excitations coincident wi the first three oscillation pulses. This coinciden

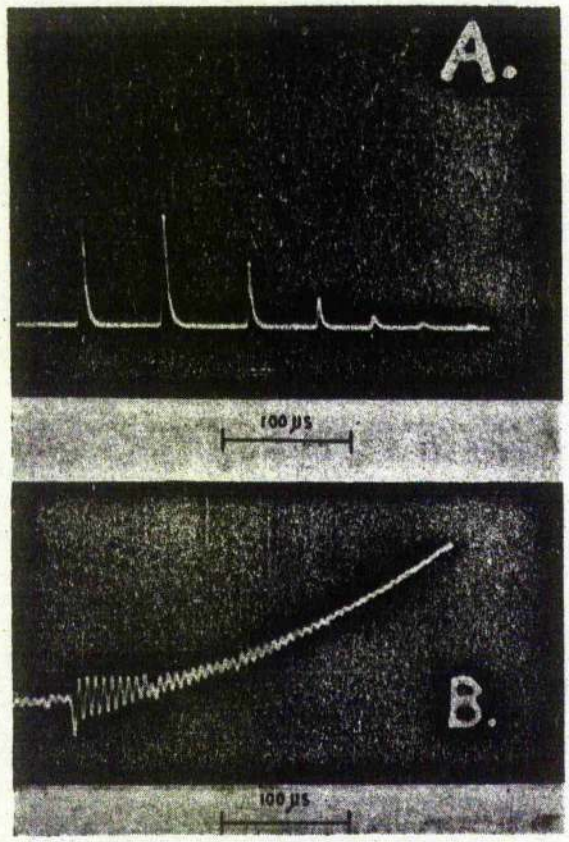

Fig. 2. *A*, Modulated emission from field-swept two-level maser: maximum power, 17 mW. *B*, Shock excitation of pick-up coils due to nutation of magnetic moment of the spin system; maximum pick-up voltage, 0·5 mV.

was checked in a special experiment. The rising baseline is due to the residual pick-up from the swept field. This evidence, in support of the nutating character of M, is further substantiated by the fact that no effect was observed when the inverting microwave power was reduced below the level necessary to sustain maser oscillations so that only the residual pick-up was observed.

This experiment establishes the existence of variations of M_z and therefore of the nutations of M during emission. Further measurements of M_z will, very likely, provide useful information on the mode of operation of maser oscillators. The technique described could be improved, to give detailed measurements of M_z, either by using critical damping in the pick-up coils, or by modifying the system to respond to the nutations of M as modulations of a high-frequency carrier wave fed to the coils.

We are indebted to Prof. J. F. Allen for placing low-temperature facilities at our disposal and to the Royal Naval Scientific Service for the interest shown in this work.

I. M. Firth
D. Bijl

School of Natural Philosophy,
University of St. Andrews.

[1] Feher, G., Gordon, J. P., Buehler, E., Gere, E. A., and Thormund, C. D., *Phys. Rev.*, **109**, 221 (1958).
[2] Chester, P. F., Wagner, P. E., and Castle, jun., J. G., *Phys. Rev.*, **110**, 281 (1958).
[3] Kemp, J. C., *J. App. Phys.*, **30**, 1451 (1959).
[4] Wang, S., and Singer, J. R., *J. App. Phys.*, **32**, 1371 (1961).
[5] Yariv, A., *J. App. Phys.*, **31**, 740 (1960).
[6] Stevens, K. W. H., and Josephson, jun., B., *Proc. Phys. Soc.*, **74**, 561 (1959).
[7] Campbell, C. K., and Bijl, D. (to be published).
[8] Firth, I. M. (to be published).

REFERENCES

1 J.Weber, Proc. I.R.E., P.G.E.D.-3 (June 1953)

2 J.P.Gordon, H.J.Zeiger and C.H.Townes, Phys.Rev. 95, 282 (1954)

3 N.G.Basov and A.M.Prokhorov, J.E.T.P. 27, 431 (1954)

4 N.Bloembergen, Phys.Rev. 104, 324 (1956)

5 J.Combrisson, A.Honig and C.H.Townes, Compt.Rend. 242, 2451 (1956)

6 G.Feher, J.P.Gordon, E.Buehler, E.Gere and C.D.Thurmund, Phys.Rev. 109, 221 (1958)

7 P.F.Chester, P.E.Wagner and J.G.Castle,Jr., Phys.Rev. 110, 281 (1958)

8 C.K.Campbell, "The Design of a Two-Level Solid-State Maser", Ph.D. Thesis, University of St. Andrews (1960)

9 J.R.Reitz and F.J.Milford, "Foundations of Electro-Magnetic Theory", Addison-Wesley Publishing Co.Inc. (1959)

10 A.R.Von Hipple, "Dielectrics and Waves", Wiley and Sons Inc. (1954)

11 J.H.Van Vleck, "Theory of Electric and Magnetic Susceptibilities", Oxford Press (1932)

12 B.Bleaney & K.W.H.Stevens, Rep.Progr.Phys. 16, 108 (1953)

13 K.D.Bowers and J.Owen, Rep.Progr.Phys. 18, 304 (1955)

14 J.W.Orton, Rep.Progr.Phys. 22, 204 (1959)

15 P.Grivet, "La Résonance Paramagnétique Nucleaire", C.N.R.S. (1955)

16 A.Abragam, "Principles of Nuclear Magnetism", Oxford Press (1961)

17 F.Bloch, Phys.Rev. 70, 460 (1946)

18 N.Bloembergen, E.M.Purcell and R.V.Pound, Phys.Rev. 73, 679 (1948)

19 W.Heitler, "Quantum Theory of Radiation", Oxford Press (1954)

20 E. M. Purcell, Phys. Rev. 69, 681 (1946)

21 A. Einstein, Phys. Zeit. 18, 121 (1917)

22 I. I. Rabi, N. F. Ramsey and J. Schwinger, Rev. Mod. Phys. 26, 167 (1954)

23 F. Bloch and A. Siegert, Phys. Rev. 57, 522 (1940)

24 I. Waller, Z. Physik 79, 370 (1932)

25 R. De L. Konig, Physica 6, 33 (1936)

26 J. H. Van Vleck, Phys. Rev. 57, 426 (1940)

27 A. H. Cooke, Rep. Progr. Phys. 13, 276 (1950)

28 S. Foner, L. R. Momo and A. Mayer, Phys. Rev. Lett. 3, 36 (1959)

29 J. C. Castle, P. F. Chester and P. E. Wagner, Phys. Rev. 119, 953 (1960)

30 A. Abragam and W. G. Proctor, Phys. Rev. 109, 1441 (1958)

31 J. A. Giordmaine, L. E. Alsop, F. R. Nash and C. H. Townes, Phys. Rev. 109, 302 (1958)

32 P. W. Anderson, Phys. Rev. 114, 1002 (1959)

33 N. Bloembergen, S. Shapiro, P. S. Pershan and J. O. Artman, Phys. Rev. 114, 445 (1959)

34 A. M. Portis, Phys. Rev. 104, 584 (1956)

35 A. M. Portis, Phys. Rev. 91, 1071 (1953)

36 F. Bloch, W. W. Hansen and M. Packard, Phys. Rev. 70, 474 (1946)

37 H. C. Torrey, Phys. Rev. 76, 1059 (1949)

38 E. L. Hahn, Phys. Rev. 80, 580 (1950)

39 E. M. Purcell and R. V. Pound, Phys. Rev. 81, 279 (1951)

40 D. I. Bolef and P. F. Chester, Proc. I. R. E. MTT-6, 47 (1957)

41 A. G. Redfield, Phys. Rev. 98, 1787 (1955)

42 A. E. Siegman, Proc. I. R. E. 45, 1737 (1957)

43 I.Feher, Bell System Tech.Jour. 36, 44 (1957)

44 N.Bloembergen and R.V.Pound, Phys.Rev. 95, 8 (1954)

45 R.H.Dicke, Phys.Rev. 93, 99 (1954)

46 K.W.H.Stevens and B.Josephson, Proc.Phys.Soc. 74, 561 (1959)

47 P.F.Chester, P.E.Wagner and J.G.Castle Jr., Westinghouse Research Laboratories Scientific Paper 6-94439-8-P4, and Wright Development Centre Research Paper AF23(616)5258-R3

48 A.Yariv, J.App.Phys. 31, 740 (1960)

49 S.Weng and J.R.Singer, J.App.Phys. 32, 1371 (1961)

50 J.C.Kemp, University of California, AFSOR-TN-60-509, Issue 275, E.R.L.Berkeley, 1960 (Unpublished)

51 C.K.Campbell, Canad.J.Phys. 39, 1514 (1961)

52 A.S.Jackson, "Analog Computing", McGraw Hill (1960)

53 G.A.Korn and T.M.Korn, "Electronic Analog Computers", McGraw Hill (1956)

54 R.A.Weeks, J.App.Phys. 27, 1376 (1956)

55 J.P.Gordon and K.D.Bowers, Phys.Rev.Lett. 1, 368 (1958)

56 J.C.Kemp, J.App.Phys. 30, 1451 (1959)

57 R.A.Weeks, R.H.Silsbee, J.E.Wertz and P.Auzins, Phys.Rev. 107, 1535 (1957)

58 C.J.Grebenkemper and J.P.Hagen, Phys.Rev. 80, 89 (1950)

59 I.M.Brown, "The Electron Spin Resonance Studies of Some Free Radicals", Ph.D. Thesis, University of St. Andrews (1961)

60 G.C.Lowe, Electronic Engineering 31, 138 (1959)

61 R.G.Bennet, P.C.Hoell and R.P.Schwenker, Rev.Sci.Instr. 29, 659 (1958)

62 P.F.Chester, P.E.Wagner, J.G.Castle, Jr. and G.Conn, Rev.Sci.Instr. 30, 1127 (1959)

63 I.M.Firth, J.Sci.Instr. 39, 131 (1962)

64 L.Malter and G.R.Brewer, J.App.Phys. 20, 918 (1949)

65 A.Yariv and F.D.Clapp, Rev.Sci.Instr. 30, 684 (1959)

66 G.B.Collins, "Microwave Magnetrons", Radiation Laboratories Series, McGraw Hill (1958)

67 K.S.W.Champion, Proc.Phys.Soc. 63B, 795 (1950)

68 J.F.Reintjes and G.M.T.Coate, "Principles of Radar", McGraw Hill (1953)

69 R.D.Hayward, Ministry of Aviation, S.R.D.E. Technical Memorandum No Res 230 (1959)

70 I.M.Firth and D.Bijl, Nature 192, 860 (1961)

71 E.R.Andrew, "Nuclear Magnetic Resonance", Cambridge Press (1958)

72 H.L.Anderson, Phys.Rev. 76, 1460 (1949)

73 C.Kikuchi, J.Lambe, G.Makhov and R.W.Terhune, J.Appl.Phys. 30, 1061 (1959)

74 J.Combrisson and I.Solomon, J.Physique Rad. 20, 683 (1959)

75 G.Makhov, J.Appl.Phys. 33, 202 (1962)